LANGLEY

Aerospace Test Highlights 89

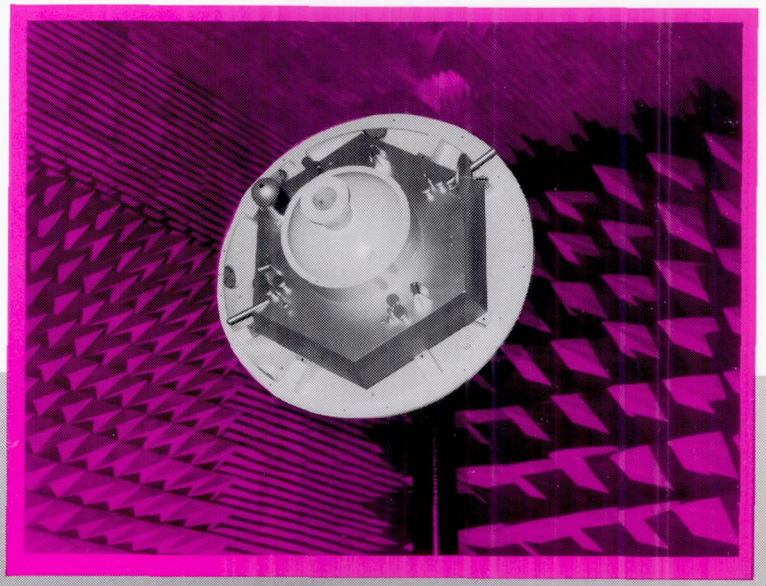

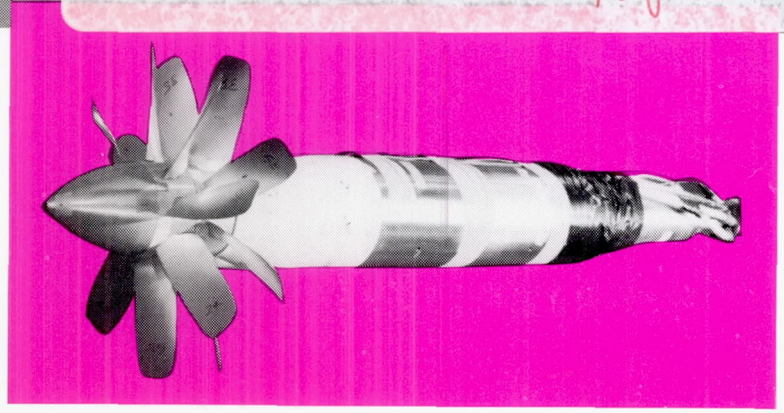

Langley Research Center

NASA Technical Memorandum 102631

1989

LANGLEY Aerospace Test Highlights 1989

Langley Research Center

NASA Technical Memorandum 102631

NASA
National Aeronautics and
Space Administration

Langley Research Center
Hampton, Virginia 23665-5225

Foreword

The role of the NASA Langley Research Center is to perform basic and applied research necessary for the advancement of aeronautics and spaceflight, to generate new and advanced concepts for the accomplishment of related national goals, and to provide research advice, technological support, and assistance to other NASA installations, other government agencies, and industry. This report highlights some of the significant tests that were performed during calendar year 1989 in the NASA Langley Research Center test facilities, a number of which are unique in the world. The report illustrates both the broad range of the research and technology activities at the NASA Langley Research Center and the contributions of this work toward maintaining United States leadership in aeronautics and space research. Other highlights of Langley research and technology for 1989 are described in *Research and Technology 1989—Langley Research Center*. Further information concerning both reports is available from the Office of the Chief Scientist, Mail Stop 105-A, NASA Langley Research Center, Hampton, Virginia 23665 (804-864-6062).

Richard H. Petersen
Director

Availability Information

For additional information on any highlight, contact one of the individuals identified with the highlight. This individual is either a member or a leader of the research group. Commercial telephone users may dial the listed extension preceded by (804) 86. Telephone users with access to the Federal Telecommunications System (FTS) may dial the extension preceded by 928.

Contents

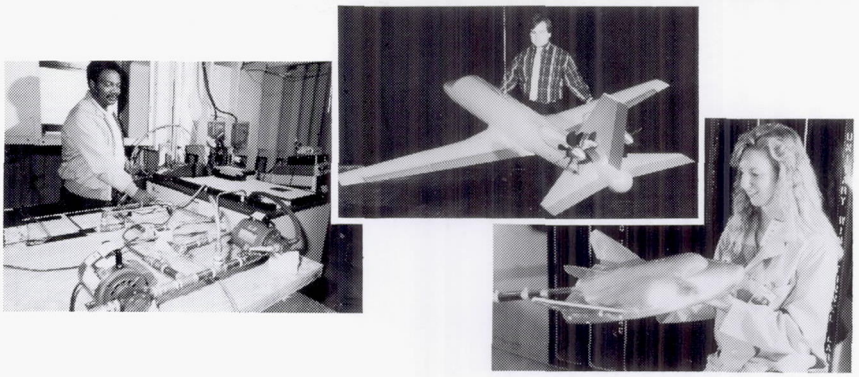

30- by 60-Foot Tunnel

The Langley 30- by 60-Foot Tunnel is a continuous-flow open-throat double-return tunnel powered by two 4000-hp electric motors, each driving a four-blade 35.5-ft-diameter fan. The tunnel test section is 30 ft high and 60 ft wide and is capable of speeds up to 100 mph. The tunnel was first put into operation in 1931 and has been used continuously since then to study the low-speed aerodynamics of commercial and military aircraft. The large open-throat test section lends itself readily to tests of large-scale models and to unique test methods with small-scale models.

Large-scale and full-scale aircraft tests are conducted with the strut mounting system. This test method can handle airplanes up to the size of present-day light twin-engine airplanes. Such tests provide static aerodynamic performance and stability and control data, including the measurement of power effects, wing pressure distributions, and flow visualization.

Small-scale models can be tested to determine both static and dynamic aerodynamics. For all captive tests, the models are sting mounted with internal strain-gauge balances. The captive test methods include conventional static tests for performance and stability and control, forced-oscillation tests for aerodynamic damping, and rotary tests for spin aerodynamics. Dynamically scaled subscale models, properly instrumented, are also freely flown in the large test section with a simple tether to study their dynamic stability characteristics at low speed and at high angles of attack. A small computer is used in this free-flight test technique to represent the important characteristics of the airplane flight control system.

The Langley 12-Foot Low-Speed Tunnel, which is used extensively for static tests prior to entry in the 30- by 60-Foot Tunnel, is an atmospheric wind tunnel with a 12-ft octagonal cross section for model testing. The tunnel serves as a diagnostic facility for exploratory research primarily in the area of high-angle-of-attack stability and control studies of various airplane and spacecraft configurations. Preliminary tests are conducted in the 12-Foot Low-Speed Tunnel on simple models prior to testing in higher speed facilities on more sophisticated models to obtain more efficient test planning and effective use of occupancy time in such facilities.

Laser Light Sheet Flow Visualization of High-Alpha Research Vehicle

A laser light sheet system was installed in the Langley 30- by 60-Foot Tunnel to support the High-Alpha Research Vehicle (HARV) test. The system was used to visualize the flow over an F-18 forebody model at angles of attack up to 80° and sideslip angles up to 10°.

The laser light sheet system utilized a 6-W argon-ion laser coupled to an X-Y galvanometer mirror scanner mounted over the exit cone of the tunnel plenum. The X-Y scanner generated a time-averaged laser sheet that was capable of being positioned at any location over the model. An electronic control system located in the upper observation room permitted remote control of the mirror scanners. From this location, the operator was able to generate the proper X and Y drive signals necessary

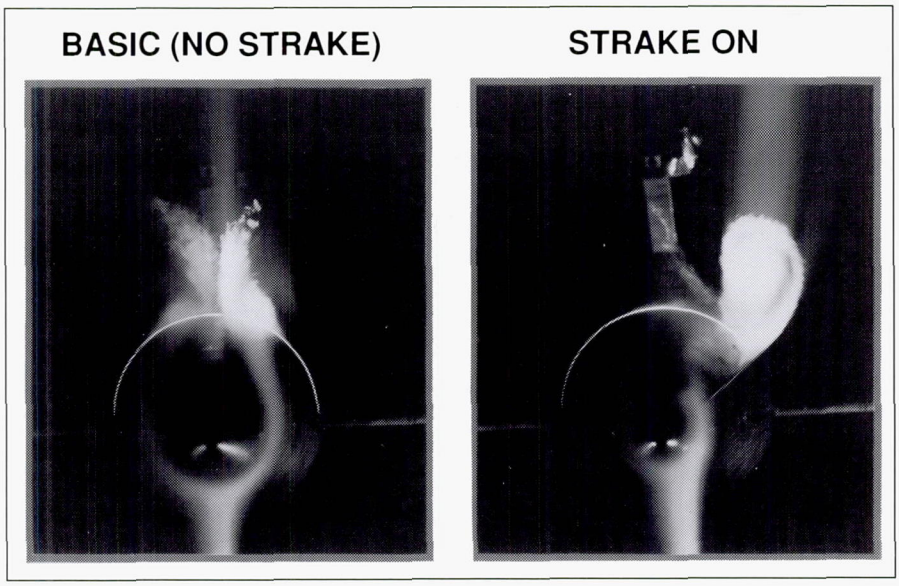

Full-scale F-18 forebody laser sheet flow visualization ($\alpha = 50°$). L-90-977

to position the sheet along the model as well as rotate the sheet to be perpendicular or parallel to the model axis.

Both video and photographic data were obtained of flow over the F-18 forebody with and without a strake. The interaction of the strake and forebody vortices was studied and compared to oil-flow studies.
(David B. Rhodes, John M. Franke, Stephen B. Jones, and Bradley D. Leighty, 44622)

X-31 Static and Dynamic Wind Tunnel Tests

The Defense Advanced Research Projects Agency (DARPA) is currently sponsoring a joint U.S./Federal Republic of Germany X-31 experimental aircraft program that will focus on flight demonstration of the tactical usefulness of a poststall capable fighter airplane. The principal element in the program is the Rockwell International Corporation/Messerschmitt-Bölkow-Blohm-designed configuration that incorporates an all-movable canard, a cranked delta-wing planform, and thrust vectoring to augment pitch and yaw control.

In support of the development of this airplane, a series of tests were conducted in the Langley 30- by 60-Foot Tunnel on a 19-percent scale model of the X-31. The wind tunnel studies included static force and moment testing and dynamic free-to-roll and forced-oscillation experiments. The results from these tests indicated that the configuration possesses good levels of static stability over most of the angle-of-attack range. However, the dynamic test results revealed weak to unstable damping characteristics, especially near maximum lift. These data are being used to develop suitable flight control laws to provide desired flight dynamic characteristics and to define an aerodynamic model for use in analytical and piloted simulation studies.
(Mark Croom, 41174)

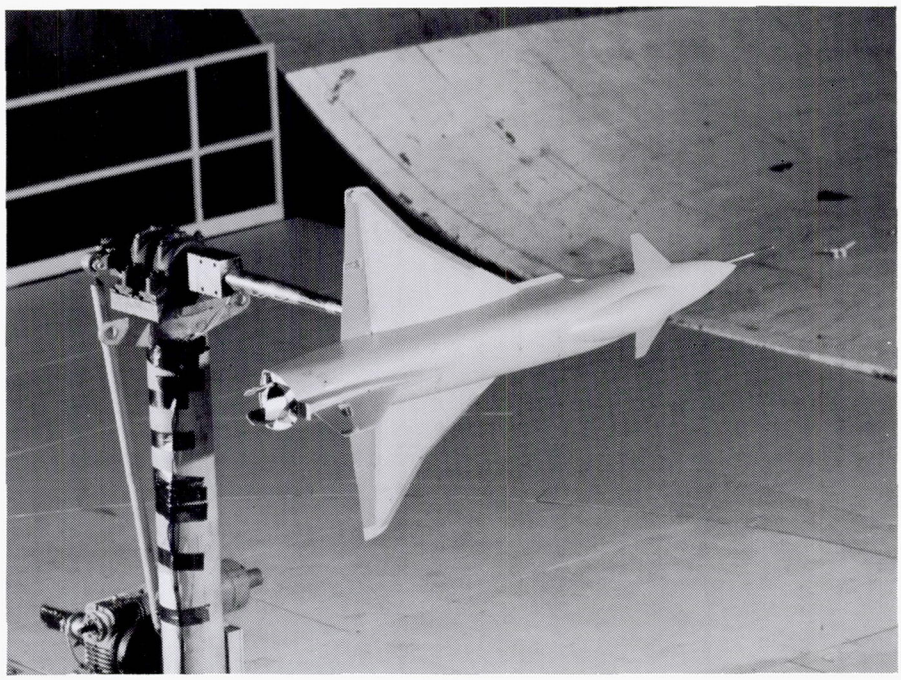

Dynamic force tests of X-31 model. L-89-3865

Advanced Turboprop

A joint NASA/industry cooperative program was developed to investigate the low-speed static and dynamic stability and control characteristics of advanced turboprop business/transport aircraft. A parametric investigation of both two-surface and three-surface configurations was conducted using a 17.5-percent scale model in the Langley 30- by 60-Foot Tunnel. Configuration parameters included wing sweep, canard size, and horizontal tail location. The results of the study showed that the baseline configuration exhibited unstable roll damping, large asymmetric rolling moments, and reduced aileron effectiveness at the onset of stall. Wing leading-edge droops were designed to alleviate these deficiencies, and the improvement was successfully demonstrated in tethered free-flight tests of the baseline model. In addition, the configuration study showed large potential improvements in cruise performance for three-surface configurations.

The continuing development of the advanced turboprop has led to the design of a new concept that has the propellers located above the horizontal stabilizer. This configuration is intended to reduce community noise due to a shielding effect of the horizontal stabilizer. In addition, the propellers are located aft of the rear fuselage bulkhead to minimize cabin noise.

At present, tests are being performed on the Over-the-Tail Advanced Turboprop model to investigate the effects of propeller and engine location on the stability and control characteristics of the design. This model is equipped with SR-7L advanced turboprop blades, which were designed to operate at high subsonic cruise speeds. Future plans include tests of an advanced turboprop transport design with the propellers located over the wing, which has been shown in previous wind tunnel tests to improve aerodynamic performance.

(P. L. Coe, G. S. Rhodes, and L. Glaab, 41150)

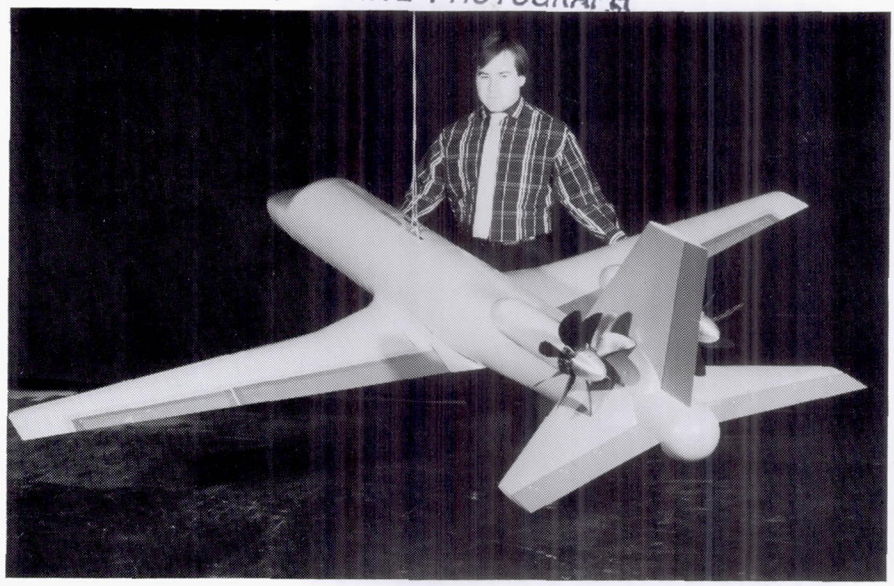

Over-the-Tail Advanced Turboprop concept. L-89-14718

Full-Scale F-18 HARV Forebody

New high-angle-of-attack technologies are being developed in the NASA High-Angle-of-Attack Technology Program in order to enhance the maneuverability and agility of future fighter aircraft. Research on forebody aerodynamics is an important part of the flight test program being conducted on the NASA F-18 High-Alpha Research Vehicle (HARV).

In order to provide large-scale model data in support of the HARV flight test program, an investigation has been conducted on a full-scale model of the HARV forebody. The figure shows the F-18 HARV forebody mounted in the tunnel during the tests. The investigation consisted of a variety of tests including force, moment, and surface pressure measurements over a large angle-of-attack and sideslip range. Tuft studies and oil-flow surveys provided a method of identifying regions of separated flow, including primary and secondary separation lines. A laser light vapor screen was used to study the vortices generated by the forebody separated flow at high angles of attack. Tests were conducted to optimize the effectiveness of actuated forebody strakes for providing aerodynamic yaw control for the configuration at high angles of attack by manipulating the position and strength of these forebody vortices.

Results on the basic model will be used for flight test correlation and for providing an experimental data base for use in the development and validation of high-angle-of-attack analytical prediction methods. The pressure

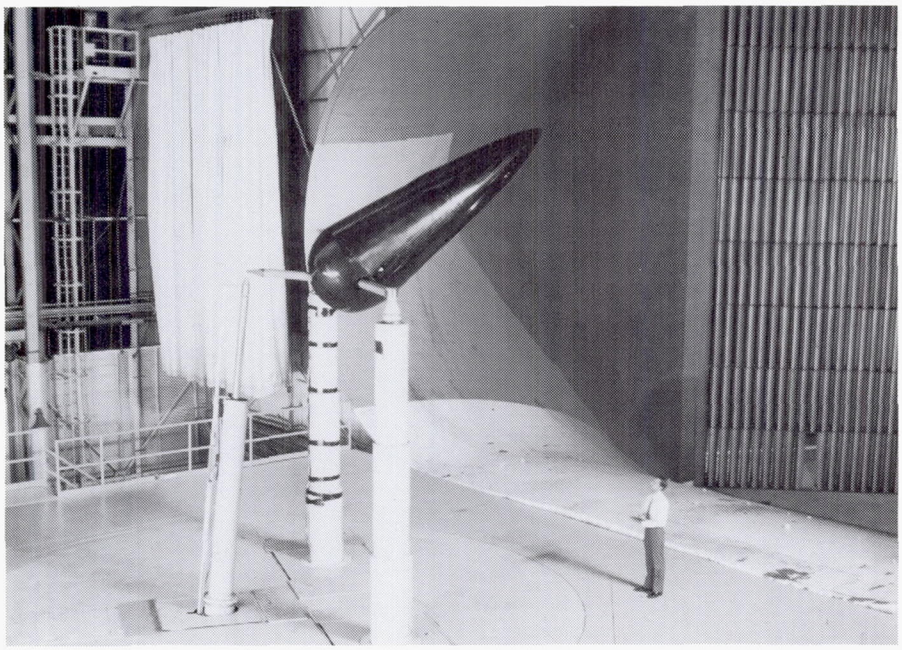

Full-scale F-18 HARV forebody model during tunnel tests. L-89-13208

data also will be used for calibration of a Flush Air Data System (FADS) on the F-18 HARV. Test results with forebody strakes will be used to guide the design of actuated strakes for flight test demonstration and for validation of subscale model data.
(F. L. Jordan, G. H. Shah, L. J. Glaab, D. G. Murri, and L. P. Yip, 41136)

Flow Visualization Using Liquid Crystals on Heated Substrate

Flow visualization has traditionally been an important diagnostic tool in determining the state of the aerodynamic boundary layer. The liquid-crystal technique has proved to be a reliable flow visualization tool for many test conditions; however, it has shown undesirable limitations in low-speed applications. An experiment was conducted to assess the usefulness of a heated substrate to enhance the response of the liquid-crystal coating at low speeds. The experiment was conducted in the Langley 12-Foot Low-Speed Tunnel on an unswept wing with a chord of 16 in. at speeds ranging from 29 ft/s to 58 ft/s. An Inconel foil and a conductive ink were used as the substrates. The figure shows the results from a test at 41 ft/s and an angle of attack of 0°. The test surface was heated approximately 3° above the ambient temperature. The Inconel foil is the substrate on the left in the figure; the conductive ink substrate is on the right. Transition is clearly visible as the pattern changes from the light region to the dark region at 65-percent chord. An intentional turbulent wedge emanates from the leading-edge region on the ink half. With the promising results of this experiment, it appears that a viable flow visualization technique can be developed for low-speed applications. The experiment showed that substrates having higher resistance may be needed in order to reduce the amount of electrical current used to heat the surface.
(Clifford J. Obara, 43941)

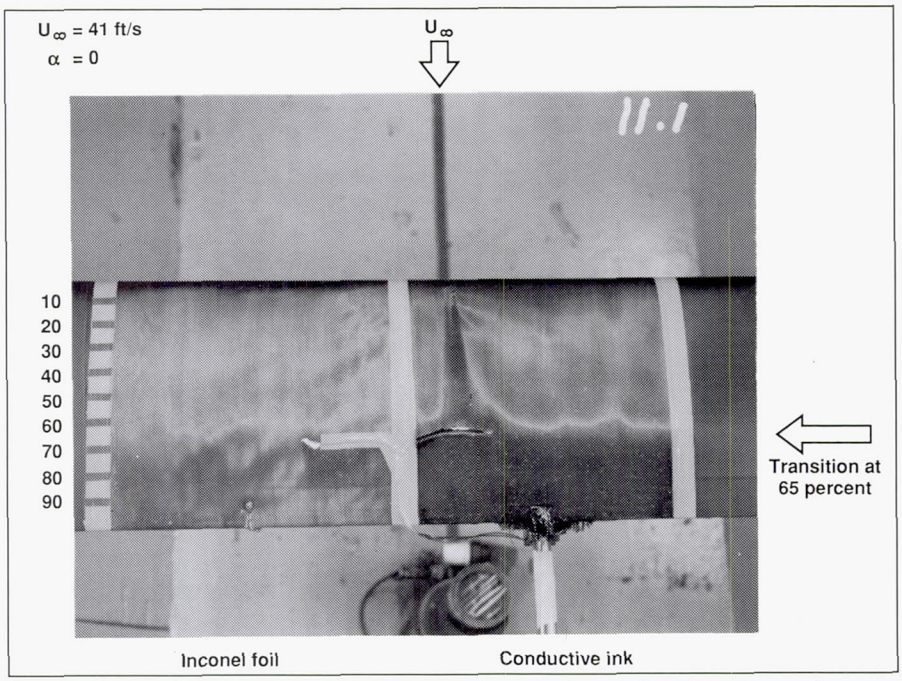

Boundary-layer transition as visualized using heated substrate and liquid crystals (V = 41 ft/s and α = 0°).

Low-Turbulence Pressure Tunnel

The Langley Low-Turbulence Pressure Tunnel (LTPT) is a single-return closed-circuit tunnel that can be operated at pressures from near vacuum to 10 atm. The test section is rectangular in shape (3 ft wide and 7.5 ft in height and length), and the contraction ratio is 17.6:1. The LTPT is capable of testing at Mach numbers from 0.05 to 0.50 and unit Reynolds numbers from 0.1×10^6/ft to 15×10^6/ft. The tunnel has provisions for removal of the sidewall boundary layer by means of a closed-loop suction system mounted inside the pressure chamber. This system utilizes slotted vertical sidewalls just ahead of the model test section, and the removed air is reinjected through an annular slot downstream of the test section. A flow control system allows the flow and pressure requirements to be varied as dictated by tunnel operation. This system can be used to provide boundary-layer control (BLC) for low-drag airfoil research.

A BLC system for high-lift airfoil testing is also available. This system utilizes compressed dry air and involves tangential blowing from slots located on the sidewall mounting end plates. Flowmeters can be used to monitor the amount of air blown into the tunnel. An automatically controlled vent valve is utilized to remove the air injected into the tunnel by this system. A high-lift model support and force balance system is provided to handle both single-element and multiple-element airfoils. The LTPT has been modified to add a passive suction BLC system for high-lift testing and a three-component laser Doppler velocimeter (LDV).

The measured turbulence level of the LTPT is very low due to the large contraction ratio and the many fine-mesh antiturbulence screens. The excellent flow quality of this facility makes it particularly suitable for testing low-drag airfoils. Recent flow quality measurements in the LTPT indicate that the velocity fluctuations in the test section range from 0.025 percent at Mach 0.05 to 0.30 percent at Mach 0.20 at the highest unit Reynolds number.

The drive system is a 2000-hp direct-current motor with power supplied from a motor-generator set. The tunnel stagnation temperature is controlled by a heat exchanger, which provides both heating and cooling via steam injectors and modulated valves that control the flow volume of water through a set of coils.

High-Lift Research

A cooperative test program in the LTPT between Douglas Aircraft Company and Langley Research Center is under way. The objectives of this research program are to gain an understanding of the effects of increasing the Reynolds number up to flight values on the maximum lift characteristics of advanced multielement high-lift airfoil geometries and to provide detailed flow measurements to guide further development of computational methods. Previous tests of NASA high-lift airfoils have indicated that some form of tunnel sidewall boundary-layer control (BLC) is absolutely required to ensure spanwise uniformity of the flow near maximum lift condi-

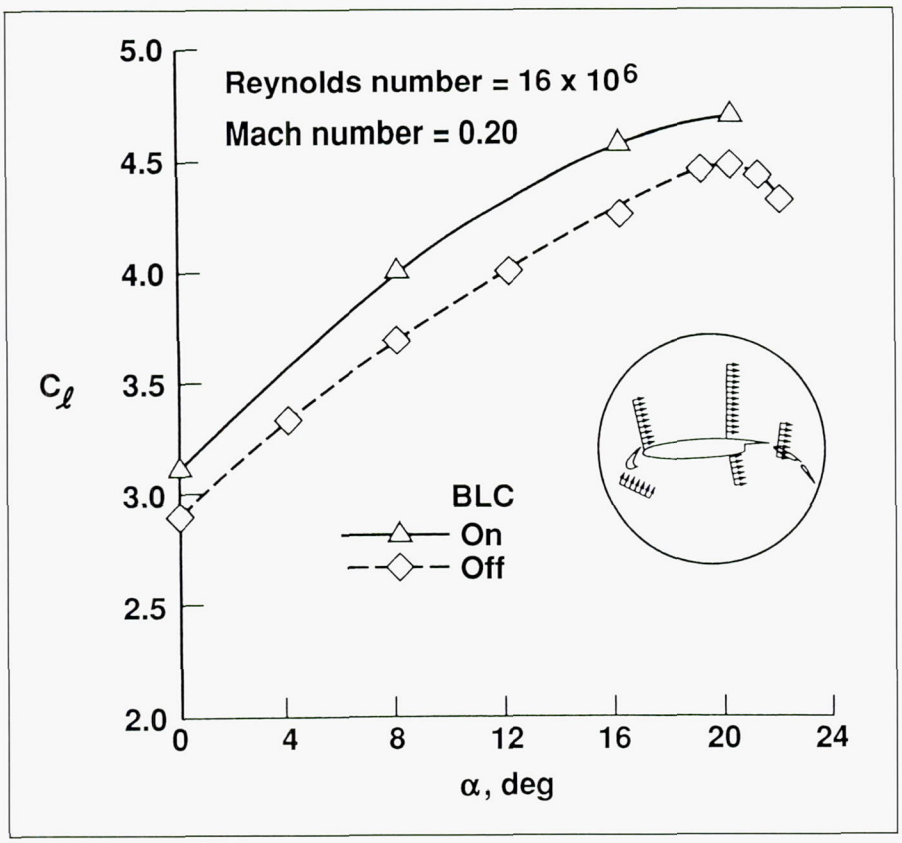

Effect of blowing (BLC) on lift curve.

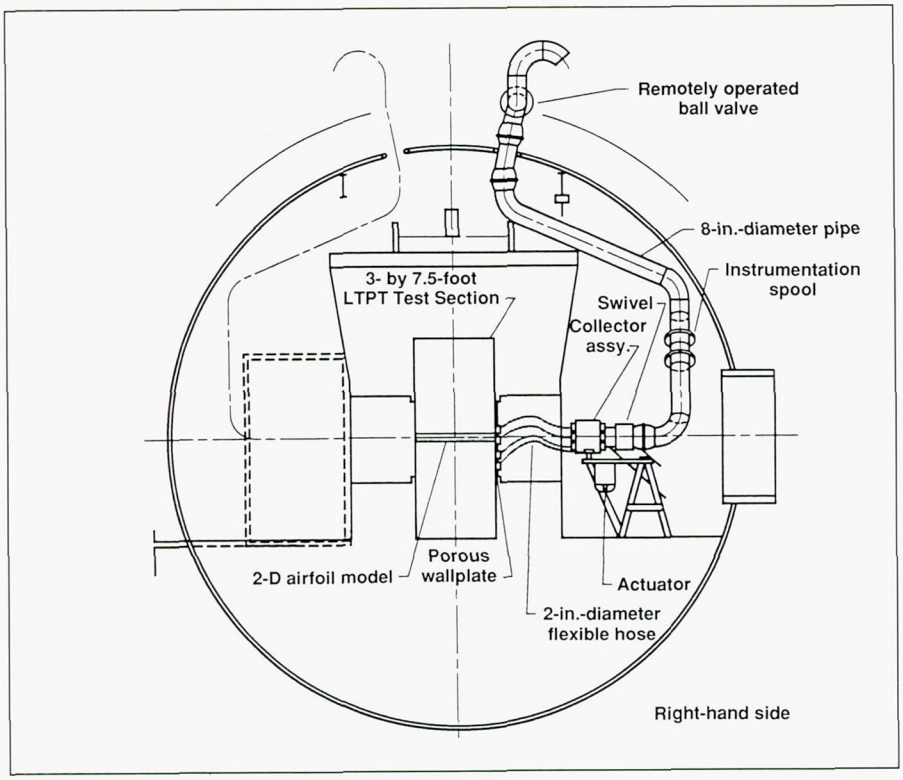

Boundary-layer venting system.

tions. Two sidewall BLC systems are being evaluated; these systems include discreet tangential blowing of air through slots located on the model end plates and distributed suction using porous end plates connected to a passive venting system.

The first figure shows the blowing configuration and its effect on the performance of the Douglas Aircraft Company's high-lift model. The loss of lift without BLC is a result of nonuniform spanwise flow due to tunnel sidewall boundary-layer separation. The second figure is a schematic showing the right-hand view of the passive venting system. This venting system was recently calibrated to account for changes in the tunnel flow parameters due to mass flow through the porous plates. The sidewall boundary-layer vents through the porous plates, passes through eight constant-diameter hoses, and flows into the collector. The collector efficiently integrates flow from the individual hoses. The spoolers are instrumented to measure accurately the mass flow through the venting system, which is a passive suction system that vents to the atmosphere. Due to this venting, the tunnel must be pressurized in order to provide BLC. Also, a new computerized wake-survey rake suitable for drag determination of high-lift airfoils and a fast-response electrically scanned pressure system has been installed in the LTPT for this research program.

(Keith B. Paschal, 41005)

20-Foot Vertical Spin Tunnel

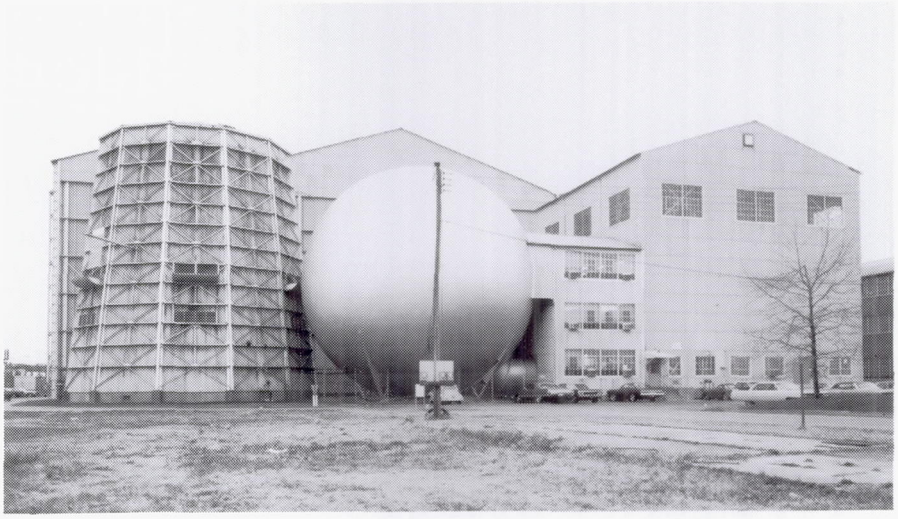

The Langley 20-Foot Vertical Spin Tunnel is the only operational spin tunnel in the United States and one of only two such tunnels in the free world. The tunnel, which is used to investigate spin characteristics of dynamically scaled aircraft models, is a vertical tunnel with a closed-circuit annular return passage. The vertical test section has 12 sides and is 20 ft wide and 25 ft high. The test medium is air. Tunnel speed can be varied from 0 ft/s to 90 ft/s with accelerations to 15 ft/s^2. This facility is powered by a 1300-hp main drive.

Spin recovery characteristics are studied by remote actuation of the aerodynamic controls of models to predetermined positions. Force and moment testing is performed with a gooseneck rotary-arm model support, which permits angles of attack from 0° to ±90° and sideslip angles from 0° to ±20°. Motion picture and video records are used to record the spinning and recovery characteristics in the spin tunnel tests. Force and moment data from the rotary balance tests are recorded in coefficient form and stored on magnetic tapes.

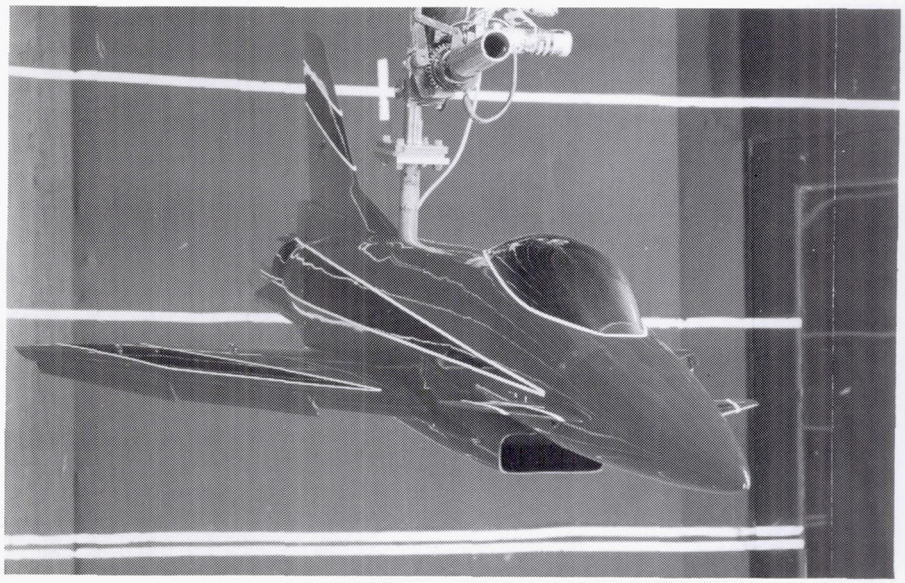

X-31 model on Rotary Balance Apparatus.

Spin Tunnel Investigation of YA-7F Airplane

At the request of the U.S. Department of Defense, a spin tunnel investigation has been conducted in the 20-Foot Vertical Spin Tunnel on a 1/28-scale model of the YA-7F airplane. The YA-7F is a derivative of the A-7 series that has been proposed for U.S. Air Force service. The objective of the spin investigation was to examine the spin and spin recovery characteristics of the YA-7F for comparison with the original A-7 and to establish the size requirements for an emergency spin recovery parachute for the flight test airplane. Model tests have shown that the spin results for the YA-7F are generally similar to those of the original A-7, but the YA-7F has some more clearly established spin modes, including a flat, relatively fast erect spin mode from which marginal recoveries were achieved. The existence of these spin modes necessitated the lengthening of the spin chute

1/28-scale model of the YA-7F airplane. L-89-8123

towline to keep the parachute clear of the wake of the spinning airplane.

Rotary balance tests of the YA-7F configuration were also conducted in the 20-Foot Vertical Spin Tunnel. These tests generated an aerodynamic data base for use in simulation and analysis of spinning conditions, and the results showed good correlation with the free-spinning results.
(D. Bruce Owens, Raymond D. Whipple, and Daniel M. Vairo, 41194)

7- by 10-Foot High-Speed Tunnel

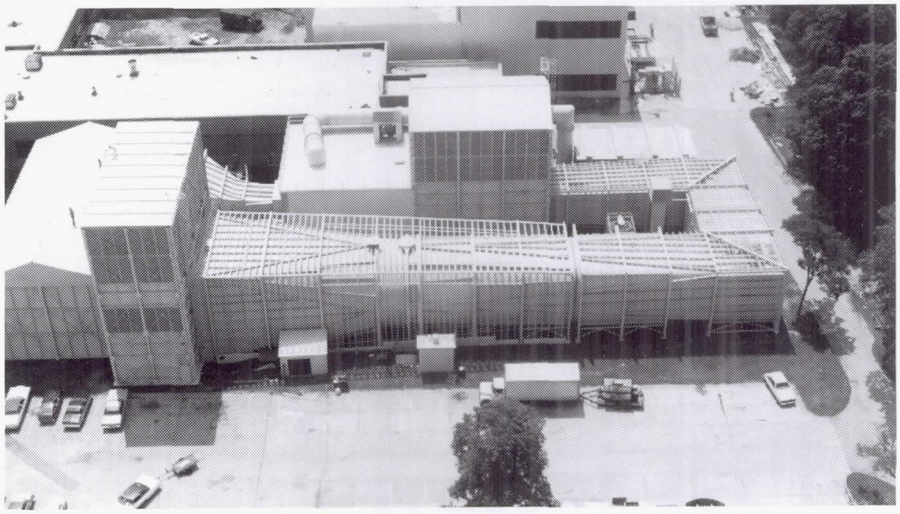

The Langley 7- by 10-Foot High-Speed Tunnel (HST) is a closed-circuit single-return continuous-flow atmospheric tunnel with a solid-wall test section 6.6 ft high, 9.6 ft wide, and 10 ft long. The tunnel is fan driven and is powered by a 14,000-hp electric motor. It operates over a Mach number range from 0.0 to 0.9 to produce a maximum Reynolds number of 4×10^6/ft. In addition to static testing of models to high angles of attack and large sideslip angles, the facility is equipped for both steady-state roll and oscillatory stability testing.

The facility has an important role in a wide range of basic and applied aerodynamic research, including advanced vortex lift concepts, drag reduction technology, highly maneuverable aircraft concepts, and the development of improved aerodynamic theories, such as the difficult separated-flow and jet interaction effects needed for computer-aided design and analysis.

The flow visualization capability of the facility has been upgraded through the installation of a permanent laser vapor screen system.

Drag Reduction by Spanwise Blowing From Wingtip

Results from small-scale model tests indicate that spanwise blowing from the tip of a low-aspect-ratio wing significantly increases the lift near the tip and can also diffuse the tip vortex and displace it outboard. The changes to the tip vortex suggest that blowing can reduce the downwash induced on the wing and consequently reduce the induced drag. A semispan wing with slots in the wingtip has been tested in the Langley 7- by 10-Foot High-Speed Tunnel (HST) to study the effect of blowing on drag (as shown in the figure).

The semispan wing had an aspect ratio of 5.8 and a leading-edge sweep of 33. Seven different wingtips, each with two blowing slots, were tested to study the effects of slot length, vertical location, chordwise location, in-plane exhaust direction, and out-

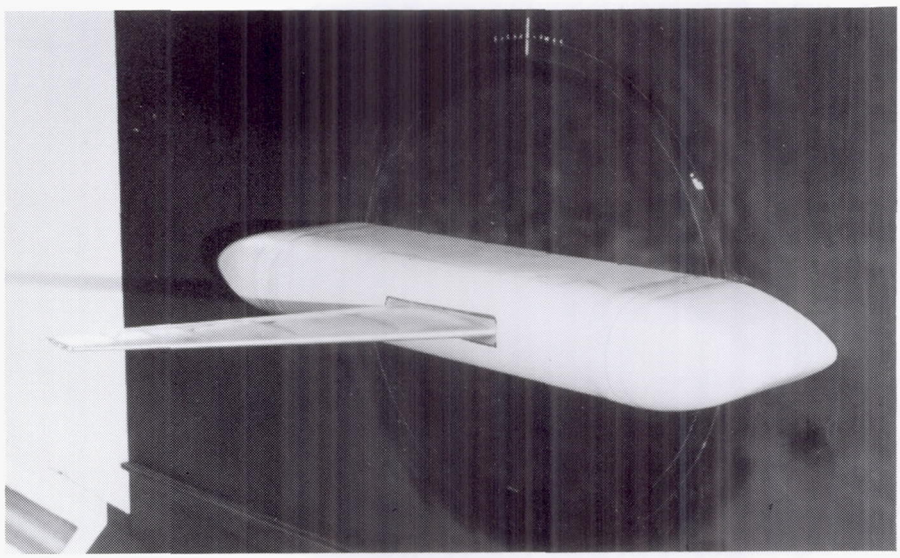

Semispan wing with spanwise blowing from wingtip. L-89-10608

of-plane exhaust direction. The wing forces and moments were measured by a five-component strain-gauge balance. The spanwise load distribution was determined from the chordwise integration of the static pressures at the 25-, 50-, 70-, 80-, and 90-percent semispan locations. Each wingtip was tested over an angle-of-attack range from $-2°$ to $11°$ without blowing, with blowing from one jet, and with blowing from both jets. Most of the tests were performed at a Mach number of 0.3.

Preliminary results indicate that the wing drag is reduced for long blowing slots (15 to 40 percent of the tip chord) at a moderate jet momentum coefficient of 0.008. An increase in the wing-root bending moment of approximately 1 percent with blowing exists. The ram drag associated with the jet formation is approximately the same as the reduction in the wing drag.
(Raymond E. Mineck, 42879)

Flow Vane Investigation

Angles of attack and sideslip are routinely measured on research aircraft through the use of small, pivoting vanes that align with the local airflow direction. One type of flow vane consists of a thin rectangular balsa flag mounted on a pivot shaft and statically balanced by a small counterweight. This vane assembly has lower inertias and, consequently, better response characteristics than other commonly used vanes that are fabricated of metal. However, because it is impossible to completely seal the balsa wood against moisture absorption, these vanes are prone to warp over time, with the shape on any given day being dependent on the moisture content of the balsa at that time. The resultant measurement errors may be significant and can change from day to day, making accurate calibration impractical.

In order to alleviate this problem, a vane assembly having similar geometric and inertial characteristics but fabricated with synthetic materials was developed for aerodynamic evaluation. The new vanes consisted of fiberglass skins laminated to a nylon honeycomb core. Two test articles were built, one having a constant vane thickness and the other having a tapered thickness distribution. The two test articles and a standard balsa vane were tested at Mach numbers up to 0.85 and dynamic pressures up to 660 lb/ft^2 in the 7- by 10-Foot HST.

Test results indicate that the balsa vane showed measurement errors that were fairly constant across the range of test parameters, but the composite vanes showed errors that were dependent on dynamic pressure. In addition, the tapered composite vane configuration developed a high-frequency aeroelastic oscillation at the highest dynamic pressure of the tests. Consequently, it was determined that additional development and evaluation are necessary before these vanes can be considered flightworthy.
(James B. Hallissy, Clifford J. Obara, David A. Kershner, and Homer F. Rush, 42865)

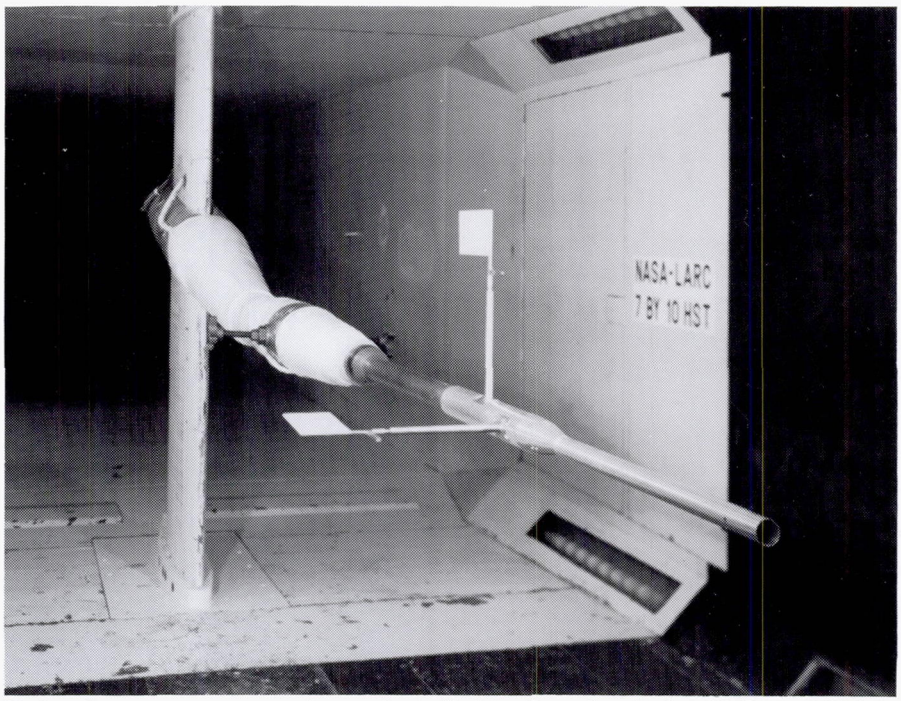

Balsa flow vanes on noseboom installed in Langley 7- by 10-Foot HST.
L-89-4223

14- by 22-Foot Subsonic Tunnel

The Langley 14- by 22-Foot Subsonic Tunnel (formerly the 4- by 7-Meter Tunnel) is used for low-speed testing of powered and unpowered models of various fixed- and rotary-wing civil and military aircraft. The tunnel is powered by an 8000-hp electrical drive system, which can provide precise tunnel speed control from 0 ft/s to 318 ft/s with the Reynolds number per foot ranging from 0 to 2.1 × 10^6. The test section is 14.5 ft high, 21.8 ft wide, and approximately 50 ft long. The tunnel can be operated as a closed tunnel with slotted walls or as one or more open configurations when the sidewalls and ceiling are removed to allow extra testing capabilities, such as flow visualization and acoustic tests. The tunnel is equipped with a two-component laser velocimeter system. Furthermore, boundary-layer suction on the floor at the entrance to the test section and a moving-belt ground board for operation at test section flow velocities to 111 ft/s can be installed for ground effect tests.

Langley Research Center has completed significant modifications to the 14- by 22-Foot Subsonic Tunnel to improve and expand its aerodynamic and acoustic test capability. One of the more significant aerodynamic improvements was achieved through the use of flow deflectors installed downstream of the first corner of the tunnel circuit to improve the performance of the tunnel fan. The deflectors resulted in a more uniform velocity distribution into the tunnel drive system and eliminated regions of large-scale flow separation in the return leg of the tunnel circuit.

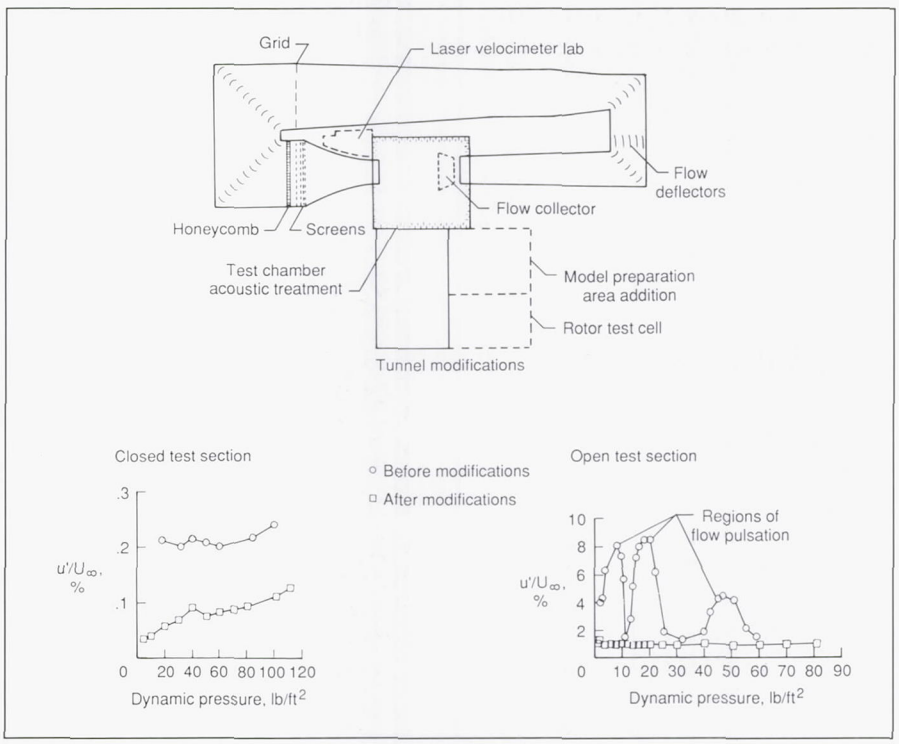

Effect of flow improvement modifications on longitudinal turbulence intensity (u'/U_∞).

A turbulence reduction system consisting of a grid, a honeycomb, and four fine-mesh screens dramatically reduced the level of

longitudinal turbulence intensity in the tunnel test section. This system provided a reduction in turbulence of 50 percent or more for the closed test section configuration. Periodic flow pulsations that occurred at several speeds in the unmodified configuration of the open test section were eliminated by the installation of a new flow collector.

Acoustic reverberations in the open test section were reduced through the use of sound-absorbing panels on the test chamber walls. A major operational improvement was achieved through the construction of a specially designed laser velocimeter laboratory for setup and maintenance of the two-component laser velocimetry system. Finally, an addition to the model preparation area, which includes a support system and rotor test cell, provides the capability to assemble and test rotor models in hovering conditions prior to actual entry into the tunnel.

Joint Army/Bell Helicopter Textron Flow Field Measurement Program

A joint program with the U.S. Army and Bell Helicopter Textron (BHT) has been conducted to investigate the high power consumption in the aft portion of the helicopter rotor disk. The objectives of the program conducted in the Langley 14- by 22-Foot Subsonic Tunnel were to define the inflow to the rotor disk and the resultant wake and to correlate the measurements with rotor blade loads and performance analyses. Flow visualization, the tunnel laser velocimetry system, and pressure-instrumented model rotor blades provided by BHT were used to acquire flow velocity and blade pressure data at selected operating conditions (generally at wind speeds of 156 knots). The data acquired in the program will be used to further the understanding of the rotor power consumption problem. The information will be shared with other helicopter manufacturers as agreed to by representatives of BHT.

The laser velocimetry system includes a high-powered laser that measures two velocity components of flow around and through the rotor disk, a remotely controlled flow seeding system that injects many 1.7 μm particles for a high data rate, and sophisticated computer systems that acquire and reduce data. The computers precisely control the flow measuring point that can span the width of the tunnel. The system has taken years to develop and now is quite productive. Bell Helicopter Textron provided the 10-ft-diameter, highly instrumented rotor and the power system to drive the rotor. In addition to flow measurements, flow visualization with smoke was video recorded. Video enhancement with digitization techniques available at Langley Research Center has been accomplished to provide a greater understanding of rotor inflow/wake at the high wind speed conditions tested. The successful acquisition of this information when digested will contribute to enhancement of rotor performance predictions and thus better helicopter design.

(Joe W. Elliott, Danny R. Hoad, Susan L. Althoff, and Richard H. Sailey, 45055)

Particle Sizing Tests

The Langley 14- by 22-Foot Subsonic Tunnel instrumentation includes a major laser Doppler

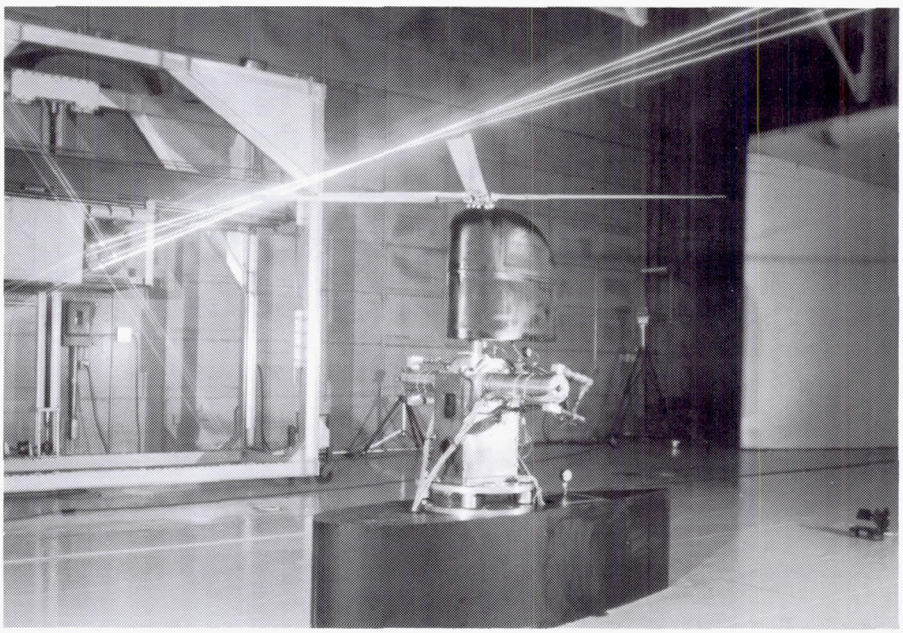

Installation of Bell Helicopter Textron rotor test apparatus and laser velocimeter in Langley 14- by 22-Foot Subsonic Tunnel. L-89-6555

velocimeter (LDV) system. The measurement accuracy is dependent on the dynamic response of the laser light scattering media. The scattering material used in this facility is composed of 1.7-μm-diameter polystyrene latex spheres. These particles are suspended in a 50-percent by volume water/alcohol solution. The mixture is injected in the airflow via an array of spray nozzles located in the facility settling chamber. The low vapor pressure of the water/alcohol mixture allows it to evaporate as it travels 85 ft to the test section.

The purpose of the particle sizing test was to verify that the process of injection and subsequent evaporation process of the liquid carrier do not result in agglomeration of a significant number of the particles. These tests were conducted with a commercial aerodynamic particle sizer. With the tunnel operating at a speed of 50 ft/s, samples of the seeded air in the tunnel test section were taken. These samples were obtained for particle/liquid concentrations ranging from 0.65 $\times$ 10^8 to 2.59 $\times$ 10^8 particles per milliliter. The typical results of the tests are shown in the figure depicting particle counts versus log diameter. Two particle count peaks occurred. The first peak is at approximately an 0.75-μm diameter and is the residual particulate background of the tunnel. This residual background is present with or without the tunnel wind on. Test comparisons of the residual background with and without the injection of the unseeded liquid carrier are essentially the same. This comparison suggests that the liquid carrier is not a significant contributor to the facility background. The second peak of the particle size distribution plot occurred at a 1.6-μm particle diameter. This peak was displaced to a one-particle-size channel below the expected peak value of 1.7 μm. The two-sigma deviation of each distribution is 0.2 μm.

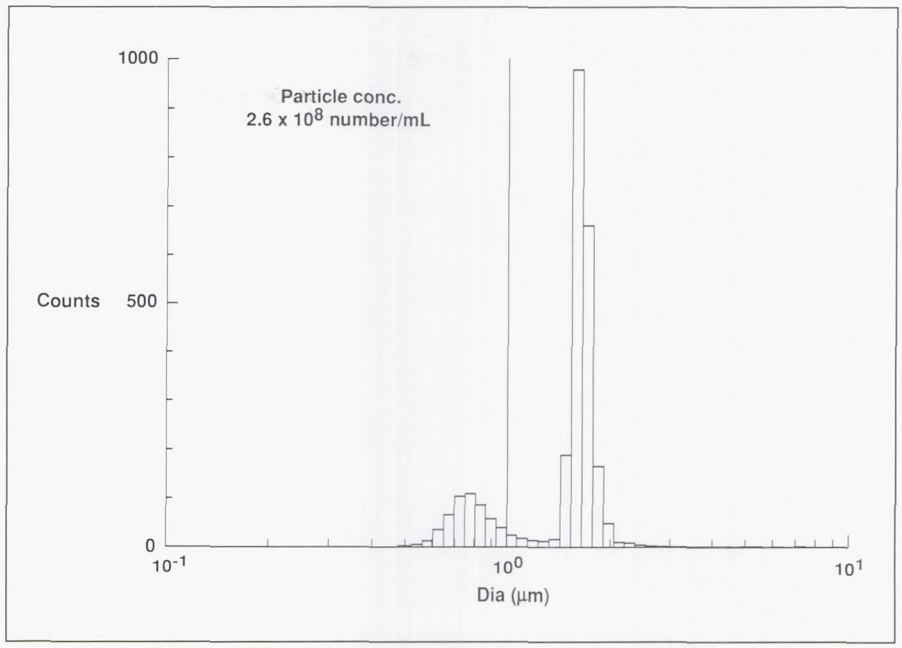

Number of particle counts versus log diameter for Langley 14- by 22-Foot Subsonic Tunnel seeder.

The selected nominal LDV seed particle diameter is 1.7 μm. The results of the particle sizing tests show that the maximum aerodynamic particle size is 1.6 μm $\pm$0.2 μm, and little or no agglomeration of the particles exists. A secondary residual background particle peak also occurs at 0.75 μm $\pm$0.2 μm. This secondary background will not decrease the measurement accuracy. If this secondary background should significantly contribute to the detected background noise, it could reduce the measurement precision. No indication of significant background noise has been observed.

(T. E. Hepner, W. W. Hunter, 44594, Cecil Nichols, and Joe Elliott)

Effect of Solidity on Propeller/Nacelle Forces

The forces generated by a propeller (when the inflow to the propeller disk is at an angle to the thrust line) are major contributors to pitch and yaw stability on propeller-driven aircraft. While it is well-known that these propeller forces are a function of the number of blades, no published data have existed for the high numbers of blades which are used in the new advanced designs. A test was conducted recently in the Langley 14- by 22-Foot Subsonic Tunnel using a sting-mounted counterrotation propeller and nacelle to determine the effect of blade solidity on propeller-generated forces by varying the number of blades used.

The configurations tested were combinations of 0, 4, and 8 blades per hub. Each configuration was tested over a nacelle angle-of-attack range from –4° to 90° at three blade angle set-

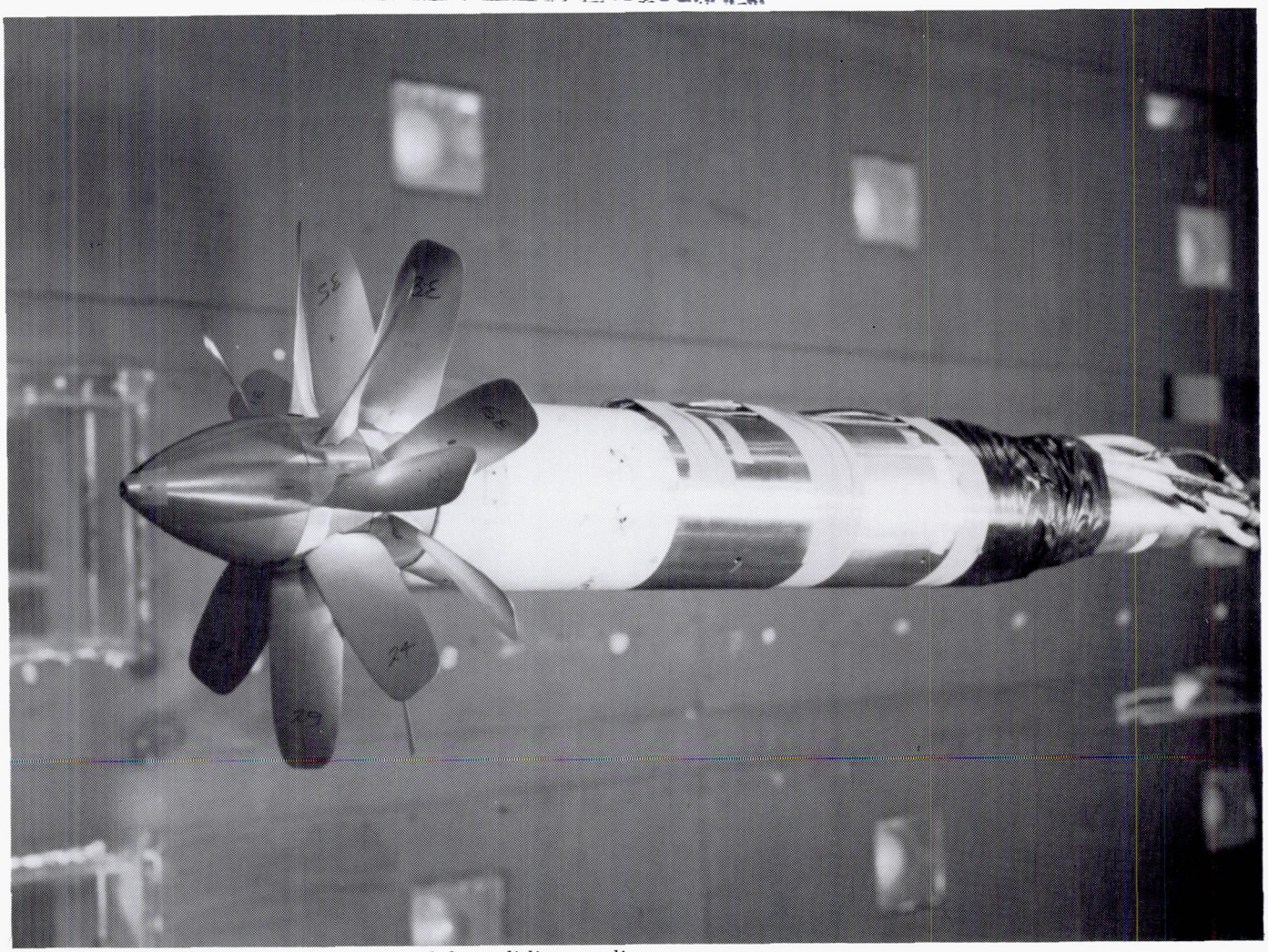

Counterrotation propeller system used for solidity studies.

tings and over a range of power settings typically used during takeoff and approach conditions. The results show a variation of propeller normal force with both solidity and nacelle angle of attack. These data provide a needed addition to the propulsion integration design data base for advanced turboprops.

(Dana J. Dunham, 45061)

Performance Tests of LASE External Heat Exchanger

Tests were performed in the Low-Velocity Aerodynamic Research Tunnel (LVART) to determine the performance of the uniquely designed external heat exchanger for the Lidar Atmospheric Sensing Experiment (LASE). The LVART is associated with the Langley 14- by 22-Foot Subsonic Tunnel. The heat exchanger is designed to cool an alexandrite laser system housed in the Equipment Bay (Q-Bay) of the ER-2 aircraft and is attached externally underneath the fuselage. Estimates of cooling the Q-Bay with a conventional staggered tube design indicated marginal results. Thus, a design was developed to increase the frontal tube area exposed to the air. This design consisted of 28 circular finned aluminum tubes (0.413 in. interior diameter) arranged in two parallel banks.

Previous wind tunnel tests were carried out in which the performance of a prototype design configuration was compared to the performance of a conventional staggered configuration. These tests indicated that the design configurations outperformed the conventional staggered configuration by approximately 6 percent at a flight coolant Reynolds

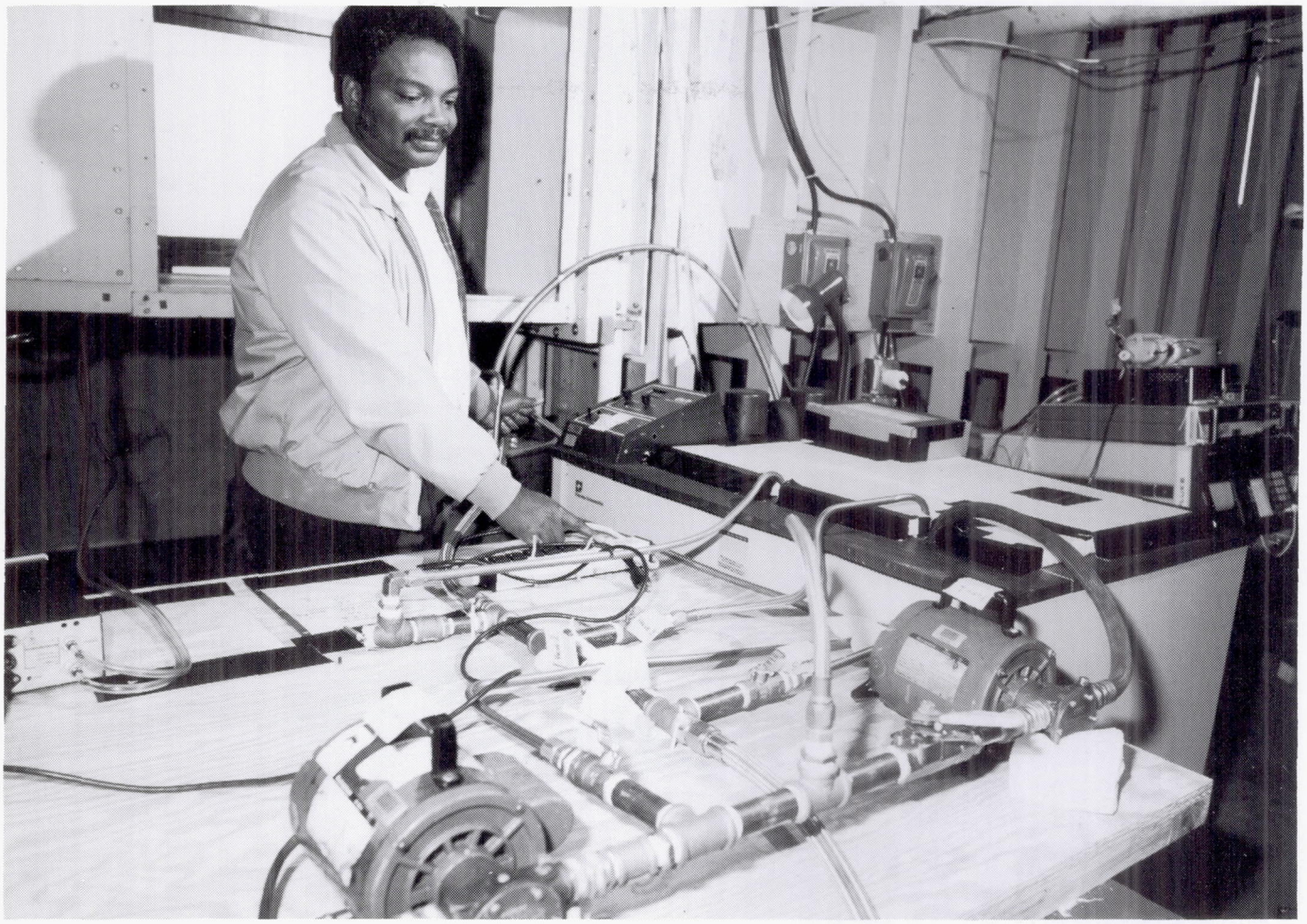

Facility test setup. L-89-14214

number of 3500. This comparison was reevaluated with the flight heat exchanger because several modifications were made to the prototype before the flight unit was completed. Additional tests were also performed to predict the performance of the flight heat exchanger over the LASE flight envelope and determine all margins of operation.

The flight heat exchanger was used as the wind tunnel test model. The figure shows the support plumbing, the isobath, and the heat exchanger located in the tunnel test section in the background. The tubes were housed in a rectangular enclosure 3.75 in. high, 22 in. wide, and 36 in. long. A damper door, located at the frontal opening, is used to control the amount of air passing through the heat exchanger. A solution of 60 percent ethylene glycol and 40 percent water was circulated through the tubes at flow rates equivalent to flight conditions. These flow rates resulted in coolant Reynolds numbers of 3013 to 4821. As shown in the figure, an isobath was used to provide a constant temperature fluid source, and several temperature and pressure probes were used to monitor the fluid and tunnel air properties.

Wind tunnel tests were carried out at an airflow Reynolds number simulating flight conditions of 2.8×10^5/ft to 8.3×10^5/ft. These Reynolds numbers resulted in tunnel velocities of approximately 42 ft/s to 140 ft/s. Results of the tests indicate that at flight coolant Reynolds numbers of 3013 and 4821, the flight design outperforms the conventional design by 1 percent and 4 percent, respectively. Air pressure drop and fluid and air temperature results were used in a heat exchanger analysis code to predict performance over the LASE flight envelope. These results showed adequate margins over the entire flight profile and stable control of the heat exchanger damper door for all possible door positions. **(Brian D. Killough, 47047)**

8-Foot Transonic Pressure Tunnel

The Langley 8-Foot Transonic Pressure Tunnel (TPT) is a variable-pressure slotted-throat wind tunnel with controls that permit independent variations of Mach number, stagnation pressure and temperature, and dew point. Air is circulated through the circuit by an axial compressor located downstream of the test section diffuser and driven by an electrical drive system. The test section is square with filleted corners and a cross-sectional area approximately equivalent to an 8-ft-diameter circle. The floor and the ceiling of the test section are axially slotted (approximately a 6.9-percent porosity in the calibrated test region) to permit continuous operation through the transonic speed range. The sidewalls are solid and fitted with windows for schlieren flow visualization. The contraction ratio of the test section is 20:1.

Tunnel stagnation pressure can be varied from a minimum of approximately 0.25 atmosphere at all test Mach numbers to approximately 1.0 atmosphere at a Mach number of 1.2, approximately 1.5 atmospheres at high subsonic Mach numbers, and approximately 2.0 atmospheres at Mach numbers of 0.4 or less. Temperature is controlled by water from an outside cooling tower circulating through cooling coils across the corner of the tunnel circuit upstream of the settling chamber. The tunnel air is dried until the dew point temperature is reduced enough to prevent condensation in the flow by use of dryers using silica gel desiccant.

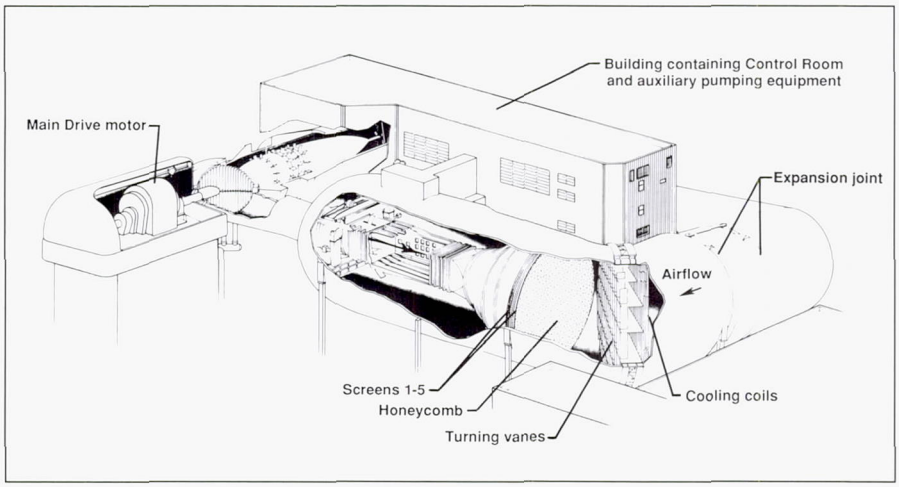

Schematic of Langley 8-Foot Transonic Pressure Tunnel. L-89-1339

Based upon both centerline probe and wall pressure measurements, generally uniform flow is achieved over a test section length of at least 50 in. at Mach numbers of 0.20 to 1.20. The higher the Mach number, the shorter the region of uniform flow becomes. The tunnel is capable of achieving Mach numbers to approximately 1.3, but most testing is limited to a maximum Mach number of 1.2, since the calibrated region of the test section for $M = 1.3$ is farther downstream than for lower Mach num-

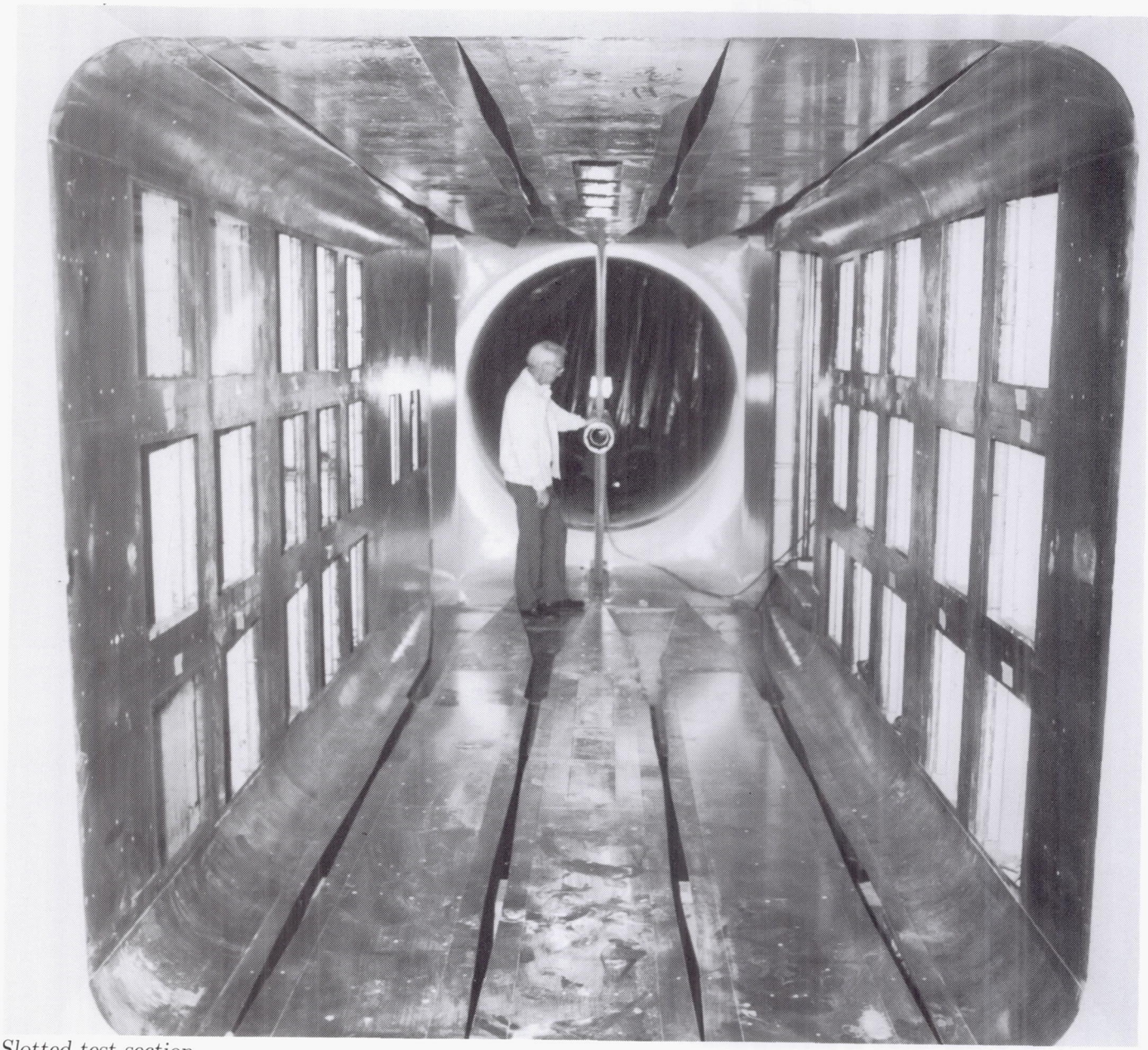

Slotted test section.

L-88-11585

bers and requires that a model be located further aft in the test section.

The 8-Foot TPT is a very versatile wind tunnel capable of supporting basic fluid dynamics research as well as a wide range of applied aerodynamic research. With the installation of screens and honeycomb in conjunction with the recently completed Laminar-Flow-Control Experiment, the quality of the flow in the test section is suitable for performing reliable code validation experiments. The test section already is instrumented with many ceiling, floor, and sidewall pressure orifices; more orifices could be added easily if desired. In addition, fixed chokes and test section slot covers are currently being designed which would permit data to be obtained on both open and closed tunnel configurations as well as improve the flow quality in the test section by blocking upstream propagation of diffuser noise.

Recalibration and Flow Quality Tests

Following the completion of the Laminar-Flow-Control Experiment, the test section of the

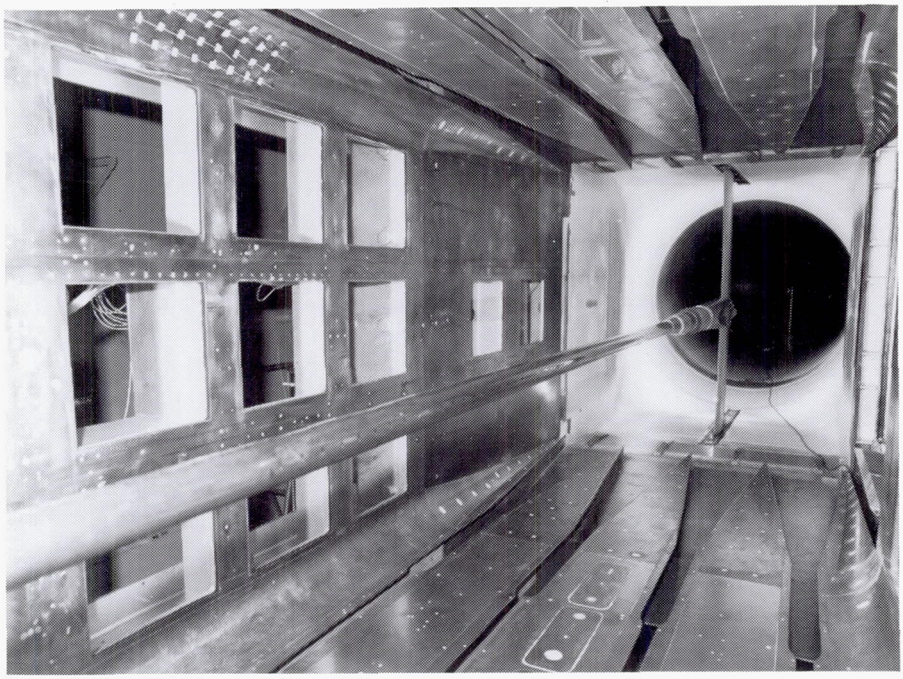

Centerline calibration tube in 8-Foot TPT. L-89-04367

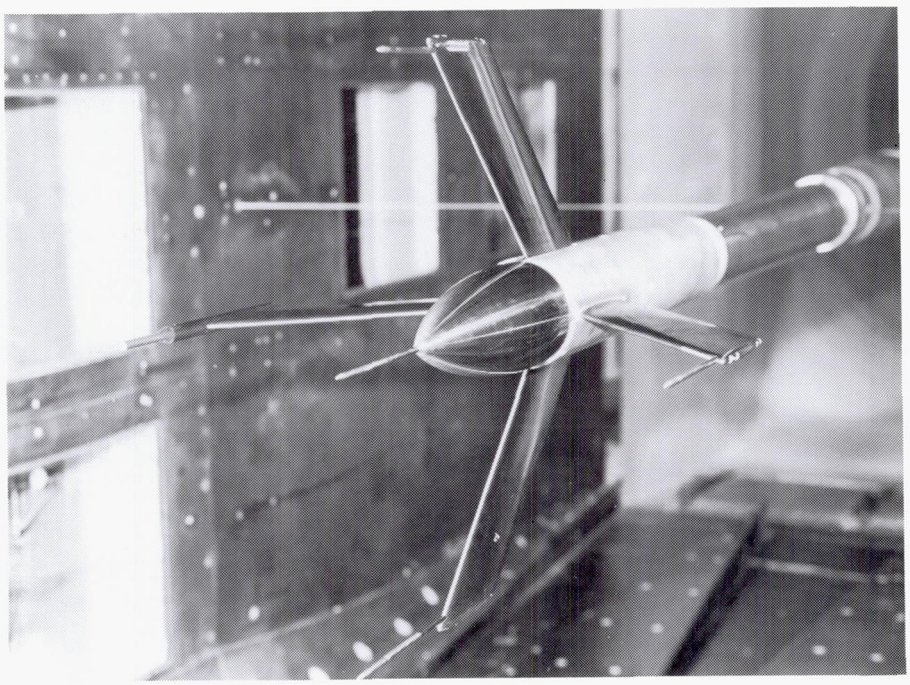

Four-finned probe in 8-Foot TPT. L-89-05879

8-Foot TPT was restored to its original slotted three-dimensional transonic test configuration. Except for the addition of screens and honeycomb in the settling chamber, the tunnel is in essentially the same configuration as when it was last calibrated in 1972. Tests were undertaken to calibrate the test section free-stream Mach number against the Mach number based on plenum pressure and to determine the effect of the honeycomb and screens on the test section flow quality.

For the Mach number calibration, the same centerline tube and wall orifices were used as had been utilized for the earlier 1972 calibration. Mach numbers were obtained from static pressures every 0.5 in. in the test section. Although the analysis is not yet complete, no reason exists to expect any significant deviation from the 1972 calibration.

The flow-quality tests were conducted using hot-wire anemometers and a Kulite mounted on a four-finned probe on the centerline of the test section. Several Kulites also were installed on the surface of the test section walls and on the tip of a sidewall-mounted strut. These data are still undergoing analysis. Comparison with earlier flow-quality data measured before the installation of the honeycomb and screens is difficult because of the advances in hot-wire anemometry techniques in the intervening years, but the turbulence levels are as low as any found in this type of facility.
(Charles D. Harris and Cuyler W. Brooks, Jr., 41054)

Transonic Dynamics Tunnel

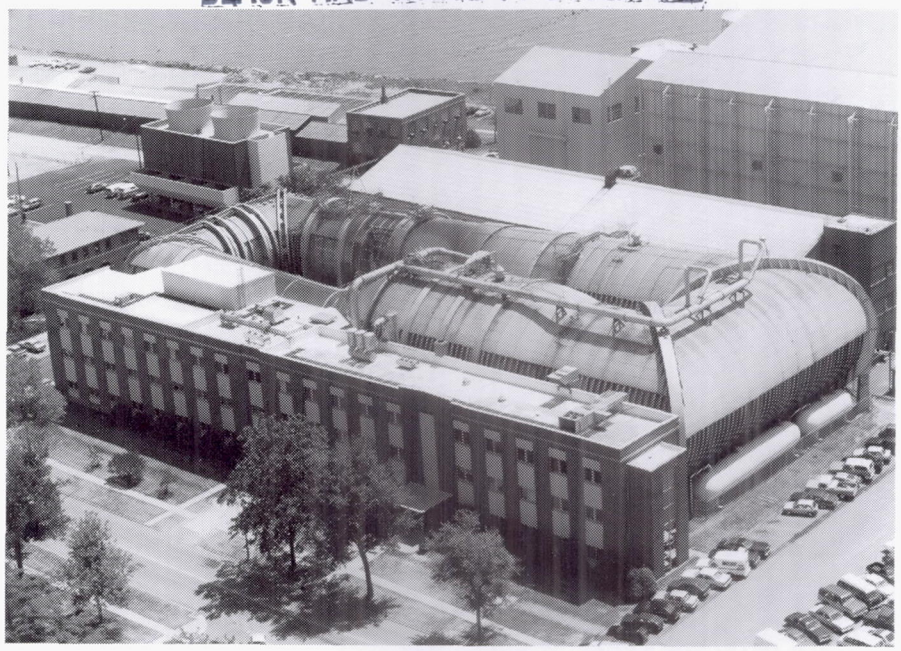

Conversion of the original Langley 19-Foot Pressure Tunnel into the Transonic Dynamics Tunnel (TDT) was begun in the late 1950's to satisfy the need for a large transonic wind tunnel dedicated specifically to work on the dynamics and aeroelastic problems associated with the development of high-speed aircraft. Since the facility became operational in 1960, it has been used almost exclusively to clear new designs for safety from flutter and buffet, to evaluate solutions to aeroelastic problems, and to research aeroelastic phenomena at transonic speeds.

The tunnel is a slotted-throat single-return closed-circuit wind tunnel with a 16-ft by 16-ft test section. The stagnation pressure can be varied from slightly above atmospheric to near vacuum, and the Mach number can be varied from 0 to 1.2. Test section Mach number and density are both continuously controllable. A 30,000-hp fan motor is used to drive the test medium at various velocities. The facility can use either air or a heavy gas (R12) as the test medium. The tunnel has a reclamation system so that the heavy gas can be purified and reused.

The facility is equipped with many features uniquely suited to dynamic and aeroelasticity testing. These features include a computerized data acquisition system especially designed to rapidly process large quantities of dynamic data, a system for rapidly reducing test section Mach number and dynamic pressure to protect models from damage when aeroelastic instabilities occur, a system of oscillating vanes to generate sinusoidal variations in tunnel flow angle for use in gust response studies, and special mount systems that enable simulation of airplane free-flight dynamic motions and of launch vehicle ground wind loads.

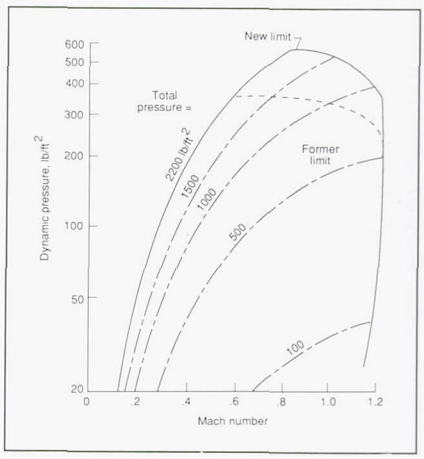

Former and present operational boundaries of TDT.

The heavy gas (R12) medium is usually used during aeroelastic testing in the TDT because it has several advantages over air for dynamically scaled models. The R12 is four times heavier than air, and this allows for the design of heavier (and consequently stronger) models that still meet the mass density scaling ratios for proper modeling of full-size aircraft. Furthermore, the speed of sound in R12 is one-half that of air; this allows for lower dynamic frequency scaling ratios that benefit data acquisition and model safety and for lower tunnel power requirements during operation. Currently the heavy gas reclamation system is being upgraded through a fiscal year 1989 Major Construction of Facilities (CoF) project, which is due to be completed in late 1991.

Planform Curvature Effects on Flutter of Swept Wing

One configuration being studied for High-Speed Civil Transport (HSCT) applications involves curving the leading and trailing edges of the outboard portion of the wing to improve aerodynamic performance. Because little is known of the effects of leading-edge curvature on wing flutter, the present study was undertaken to determine experimentally the effects of planform curvature on transonic flutter of a series of moderately swept wing models and to compare the experimental results with analytical results.

Three generic flutter models were designed and fabricated to represent the outboard portion of a HSCT wing. The radii of curvature of the leading edges of the three models were infinity (no curvature), 200 in. and 80 in., respectively. The planform area for all models was the same, 900 in^2, as were the length and location of the root and tip chords. The leading-edge sweep angle of the uncurved wing was 53°. A photograph of the moderately curved model is shown in the first figure.

The flutter boundaries that were obtained over the Mach number range of 0.6 to 1.0 are presented in the second figure as the variation of the Flutter Speed Index (FSI) with Mach number. The FSI, a nondimensional velocity parameter that is frequently used to correlate flutter results obtained for different models, depends on flow conditions, structural stiffness, and planform geometry. The analytical boundaries were calculated using FAST (Flutter Analysis Software System), which is a flutter prediction program using subsonic kernel function unsteady aerodynamics. The experimental data show that the FSI increases as the planform curvature is increased. This trend also is seen in the analytical results that agree well with the experimental data. Furthermore, the flutter results for the curved leading-edge configurations do not exhibit any unusual characteristics that would preclude, from a flutter point of view, the use of such designs on advanced configurations.

(Donald F. Keller and Maynard C. Sandford, 41259)

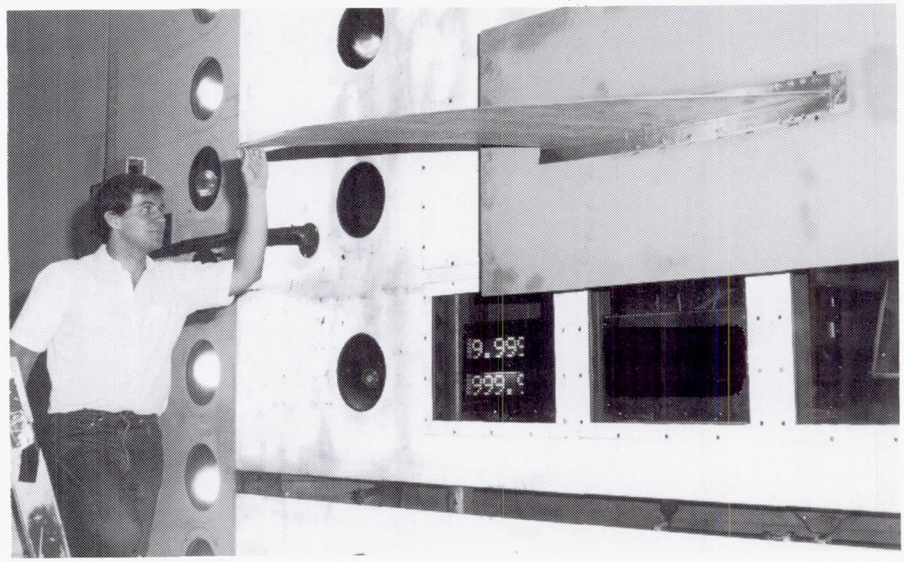

HSCT model mounted on sidewall. L-89-5086

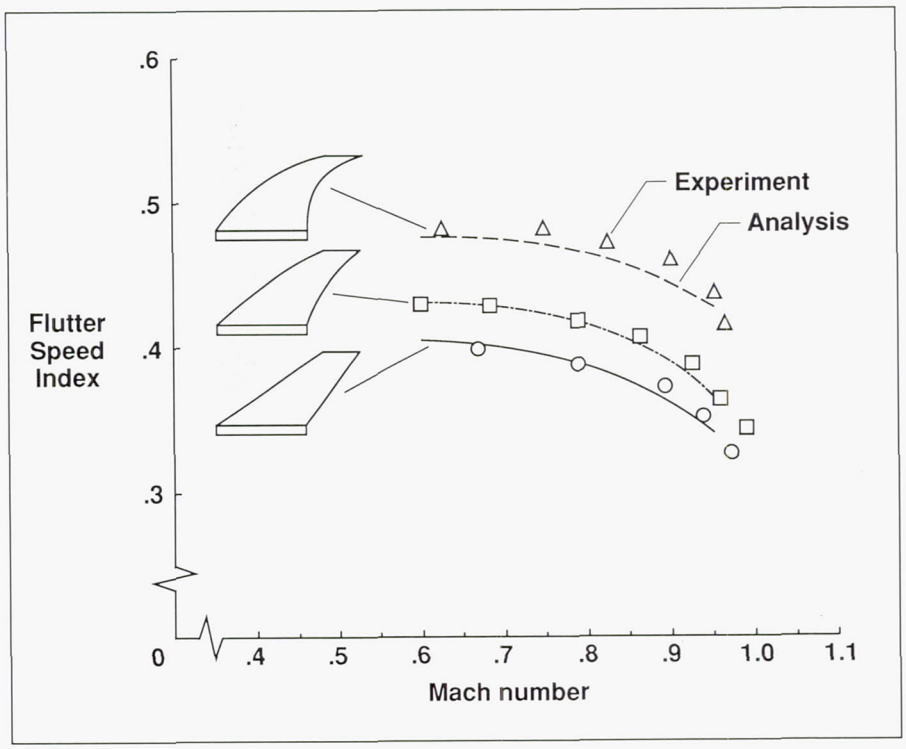

Flutter speed results for three HSCT planforms.

Aileron-Buzz Characteristics for Generic NASP Model

Aileron buzz is a high-frequency trailing-edge control surface oscillation that can occur at transonic speeds. Although buzz is often a low-amplitude vibration, it sometimes results in catastrophic dynamic instabilities that can lead to a loss of aircraft control. Because the National Aero-Space Plane (NASP) vehicle may have a full-span trailing-edge control surface, a research study has been undertaken to determine the buzz characteristics for this type of control surface mounted on a highly swept delta wing (as might be used on a NASP configuration).

The model tested consisted of a 60°-swept delta wing with a full-span control surface attached to the trailing edge. The photograph in the first figure shows the model configuration. The control surface was attached to the main wing by using two flexures. The rotational frequency of the aileron could be changed by using flexures of different stiffness, and three different levels of flexure stiffness were used. Some of the aileron-buzz results are shown in the second figure as the variation of dynamic pressure with Mach number. The shaded symbols indicate where sinusoidal, undamped (constant amplitude) aileron oscillations occurred. The square symbols mark the least stiff flexure case, and the circle symbols indicate the middle stiff flexure case. The diamond symbols mark the stiffest flexure case. The crosshatched area and solid symbols indicate where the oscillations became divergent. In the subsonic range, aileron oscillations were not observed for dynamic pressures up to 200 lb/ft^2 (tunnel limit). In the transonic range, each of the three configurations tested exhibited aileron buzz. Aileron oscillations in this region ranged from a low-amplitude, steady-state condition to an explosive, or divergent, condition. Because aileron oscillations did not occur in the subsonic range, it is probable that all oscillations observed throughout this test were shock induced. Two other results were learned from these tests. First, the Mach number at which steady-state oscillations occur increased with aileron frequency (stiffer flexure), and second, the amplitude of the undamped oscillations (for a given aileron spring-rate) appeared to be proportional to dynamic pressure.

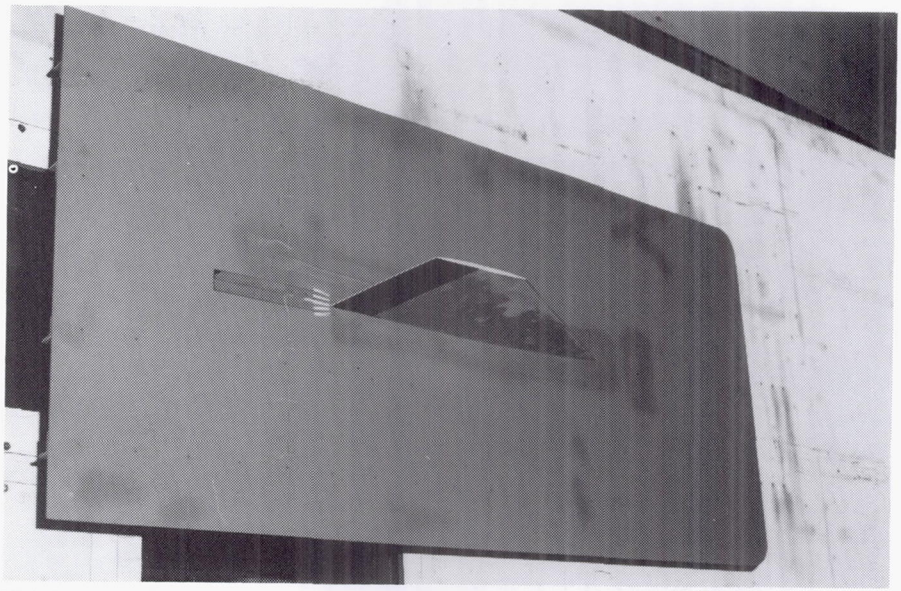

NASP aileron-buzz model. L-89-2456

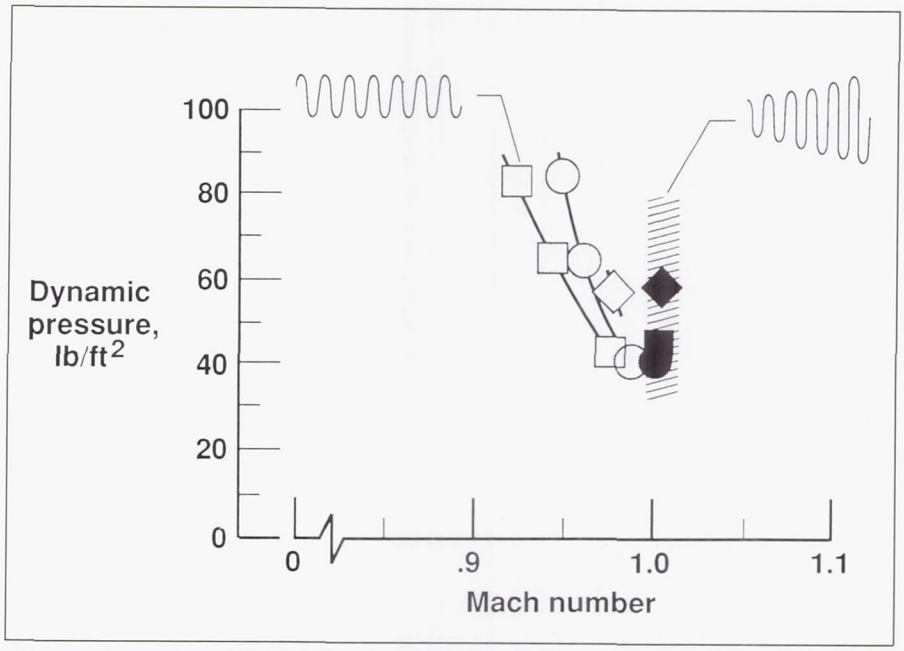

Aileron-buzz instabilities for three flexure stiffnesses.

The experimental results also revealed that aileron oscillations became divergent at Mach 1 for all configurations tested.
(Ellen C. Parker and Charles V. Spain, 41258)

Multi-Input/Multioutput Active Flutter Suppression System

The Active Flexible Wing (AFW) Program is a joint Langley Research Center/Rockwell International Corporation program with the overall goal of demonstrating the effectiveness of multi-input/multioutput (MIMO), multifunction digital control systems to favorably change aeroelastic response. Specific research objectives of the program are to validate the analysis, synthesis, simulation, and test methodologies necessary to perform such a demonstration. The cornerstone of this research is a series of wind tunnel tests of a sophisticated aeroelastic model.

A photograph of the AFW wind tunnel model mounted in the wind tunnel test section is shown in the figure. The model is equipped with leading-edge and trailing-edge aerodynamic control surfaces for implementing a variety of active control functions. During this series of tests, one of several tests planned to study a variety of active control concepts, single-function, digital MIMO active flutter suppression systems were implemented and their performance evaluated. Model flutter boundaries were determined for the active flutter suppression systems that were not operating (open loop). Subcritical response data were obtained for three active flutter suppression systems that were operating (closed loop), with each designed using different concepts. During these tests the wind tunnel model hardware, digital computer hardware and supporting software, and controller performance evaluation software worked extremely well. The test results showed that the active systems were very effective in favorably changing the flutter characteristics of the AFW model. It was clearly demonstrated that the flutter dynamic pressure of the model could be increased by more than 20 percent by using active flutter suppression.

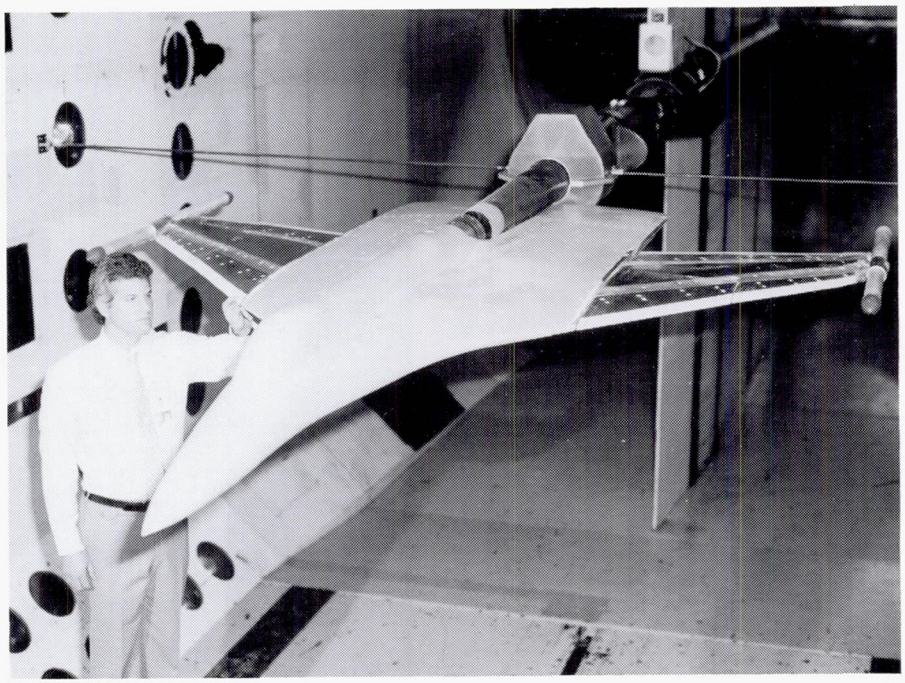

AFW model mounted on sting. L-89-12442

This wind tunnel test afforded the opportunity to validate the analysis, synthesis, simulation, and test methodologies. The knowledge and insight gained from this test, especially where experimental results and analytical predictions differ, are extremely valuable and provide a firm foundation upon which to build future research studies focusing on active flutter suppression and other active control applications.
(Boyd Perry III and Stanley R. Cole, 42840)

Reduction of Rotorcraft Vibrations by Use of Blade Nonstructural Mass

Historically, rotorcraft have experienced substantial vibration problems. One means of reducing these vibrations is through the addition of nonstructural mass to the rotor blades. These masses are intended to tune the blades so that the vibrations are reduced to an acceptable level. Generally, these problems have been addressed in the postdesign phase by modifying the rotor systems on prototype or production aircraft. However, recent rotor blade design techniques have attempted to provide low-vibration characteristics without later re-

quiring design modifications. This design method requires the use of highly accurate analytical prediction techniques. Many of the early attempts to design low-vibration rotors have been unsuccessful due to the inadequacy of these prediction methods. The objectives of this research program are to systematically investigate helicopter vibration reduction through the use of nonstructural blade masses and to obtain an experimental data base for correlation, validation, and development of analytical prediction methods.

Aeroelastically scaled model rotor blade hardware was fabricated for testing on the Aeroelastic Rotor Experimental System (ARES). A photograph of the ARES mounted in the wind tunnel is presented in the first figure. The model rotor blades were constructed to facilitate the insertion of tungsten or steel masses at 13 preselected stations along the span of each blade. Tests were conducted to provide parametric data of the effects of mass radial placement, both size and location, on rotorcraft vibrations throughout a representative forward-flight speed range. Data were obtained for three different thrust conditions at representative propulsion forces throughout the forward-flight speed range. Rotor trim condition was also a test variable. A sample of the test results is shown in the second figure. This plot shows four-per-revolution vertical fixed-system loads for a single tungsten mass located at several different radial locations. Reductions in load of up to 30 percent were achieved by the appropriate selection and placement of a nonstructural mass, clearly showing that the addition of nonstructural mass has the potential for substantially reducing vibration levels.

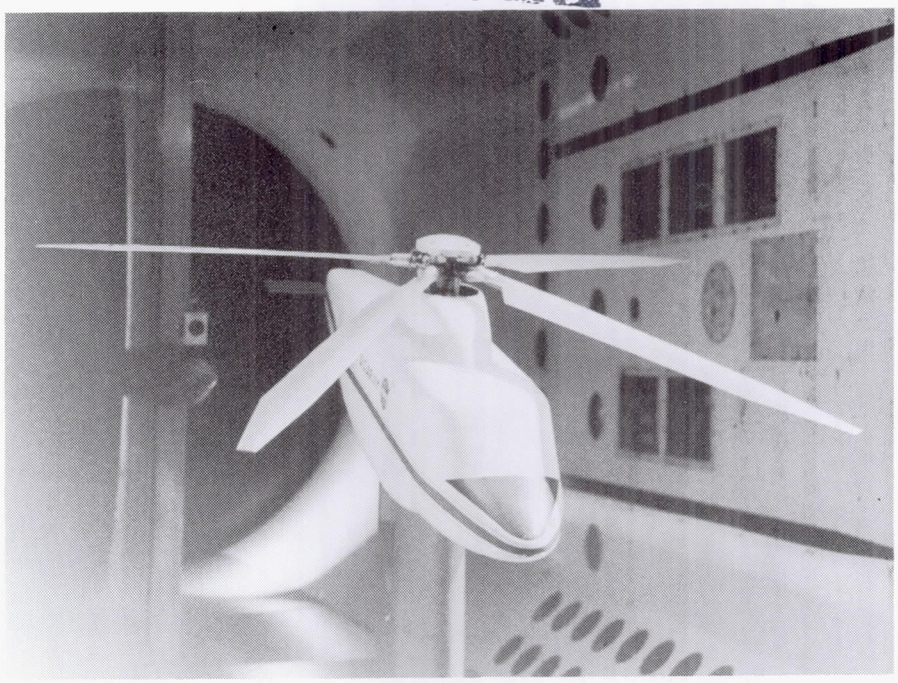

ARES model with research blades installed. L-90-324

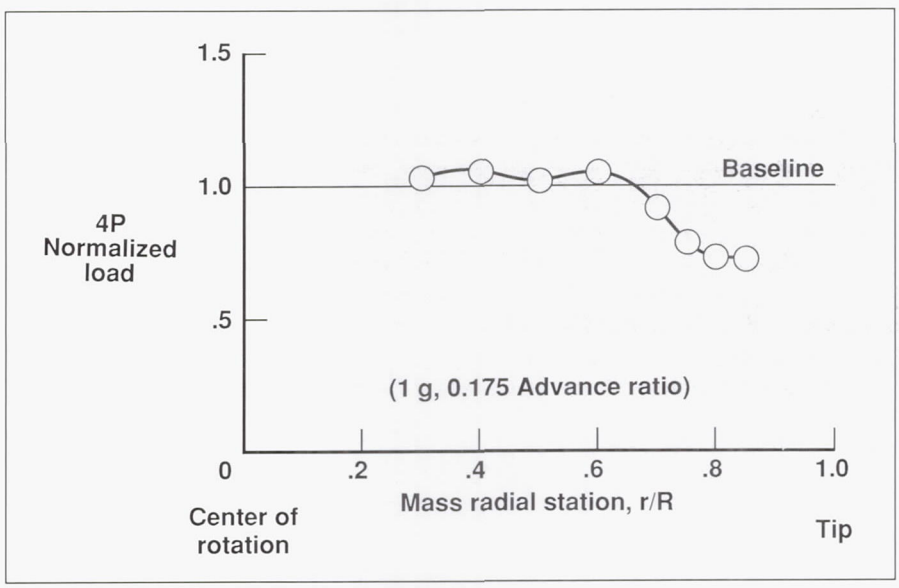

Effect of mass radial location on dynamic loads.

(Matthew L. Wilbur, William T. Yeager, Jr., Paul H. Mirick, Jeffrey D. Singleton, and W. Keats Wilkie, 41268)

Reduction of Rotor Impulsive Noise Using Higher-Harmonic Pitch Control

One of the most objectionable types of helicopter noise is due to blade-vortex interaction (BVI). This impulsive noise

source is due to aerodynamic interaction of the rotor blades with previously shed blade tip vortices. Analytical studies have indicated that decreases in blade lift and/or vortex strengths should reduce the intensity of the interactions and thus noise. Based on this concept, the use of higher harmonic control (HHC) of blade pitch angle, historically studied as a means to reduce helicopter vibration, would offer potential for noise reduction.

A study was conducted using the ARES with a four-bladed 9-ft-diameter rotor in the TDT. In the photograph (first figure), microphones are shown positioned upstream and downstream of the model. A unique sound power measurement technique was developed for the test because of the TDT reverberance and Freon environment. Using a specially developed open-loop HHC system, prescribed higher harmonic pitch motion was superimposed on the normal blade pitch for a broad range of rotor operating conditions. It was found that the pitch control could significantly increase or decrease the noise depending on the control amplitudes and phases. An HHC input of particular interest was a four-per-revolution collective blade pitch motion giving a $-1°$ amplitude at $60°$ blade azimuth. This pitch corresponds to the pitch being minimized near predicted BVI locations.

The second figure shows a contour plot of the noise reductions found when this pitch control was used. The dB level reductions shown are the differences of spatially averaged noise levels between the control and no-control cases in which the flight conditions are matched. The flight range shown is for descending flight conditions typical of landing approach. The noise reductions (up to 4.7 dB) are greater for the lower speeds where, without HHC, impulsive BVI noise is most severe. The results show the noise reduction

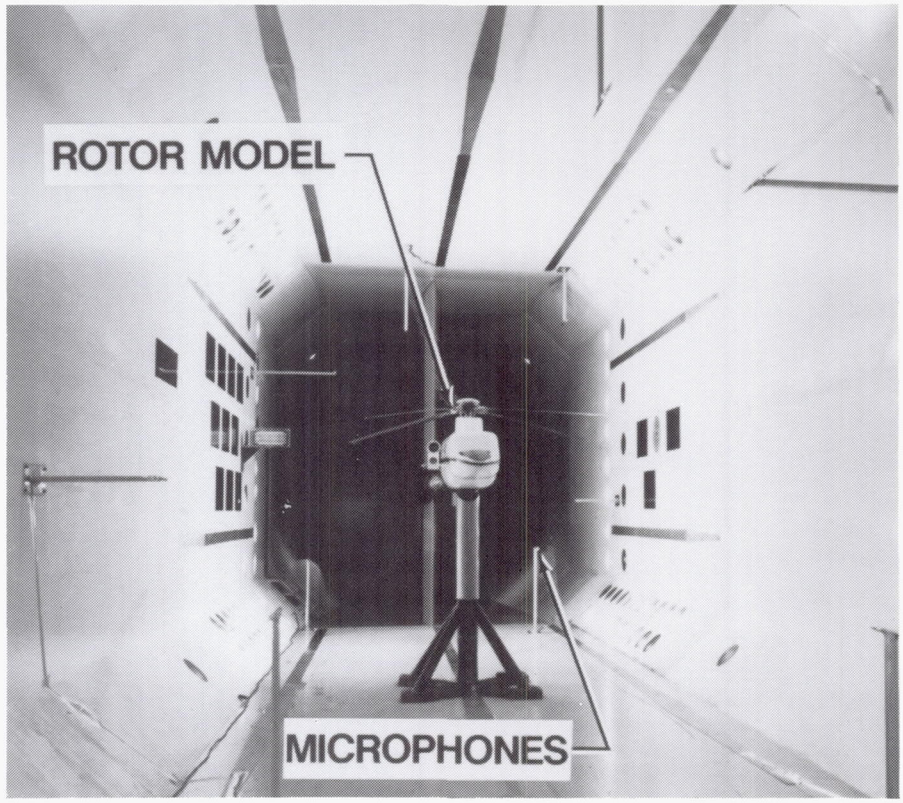

ARES noise test in TDT. L-89-3859

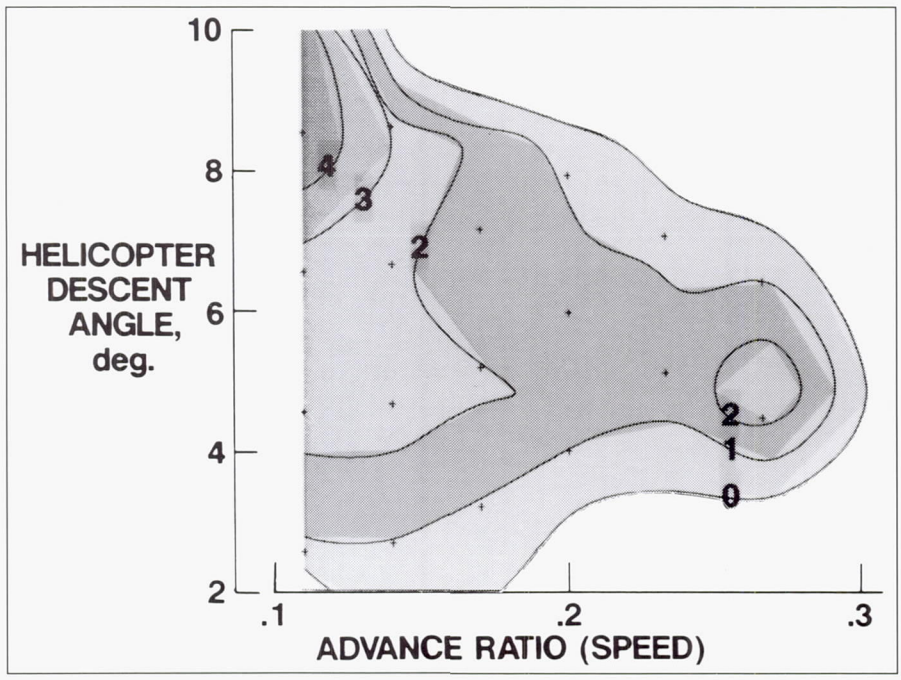

Reduction in BVI noise level (dB).

concept to be viable. The effects of higher harmonic pitch controls on vibration and noise directivity remain to be addressed.
(Thomas F. Brooks, Earl R. Booth, Jr., and William T. Yeager, Jr., 43634)

Ground Wind Loads for Atlas II

The *Atlas II* expendable booster is being developed by the General Dynamics Corporation to launch both military and commercial payloads into orbit. It is longer than previous Atlas configurations and will be able to launch larger and heavier payloads. As with all launch vehicles, there is concern about ground wind loads while the vehicle is on the launch pad being prepared for launch. The *Atlas II* is required to withstand loads produced by winds up to 30 knots. Ground wind loads include both steady drag loads and dynamic loads resulting from oscillatory flow around the vehicle. To determine the characteristics of the ground wind loads of the *Atlas II*, a 1/12-size dynamically scaled model was tested. A photograph of the test apparatus is shown in the first figure. The model booster and umbilical tower were bolted to a large turntable that could be rotated 360° to simulate ground winds from any compass bearing. The payload fairing shown in the figure simulated a 14-ft-diameter full-scale fairing that will be used for large payloads. A simulated 11-ft-diameter fairing was also tested. The damper that extends out from the gantry to the booster was also simulated in the wind tunnel tests.

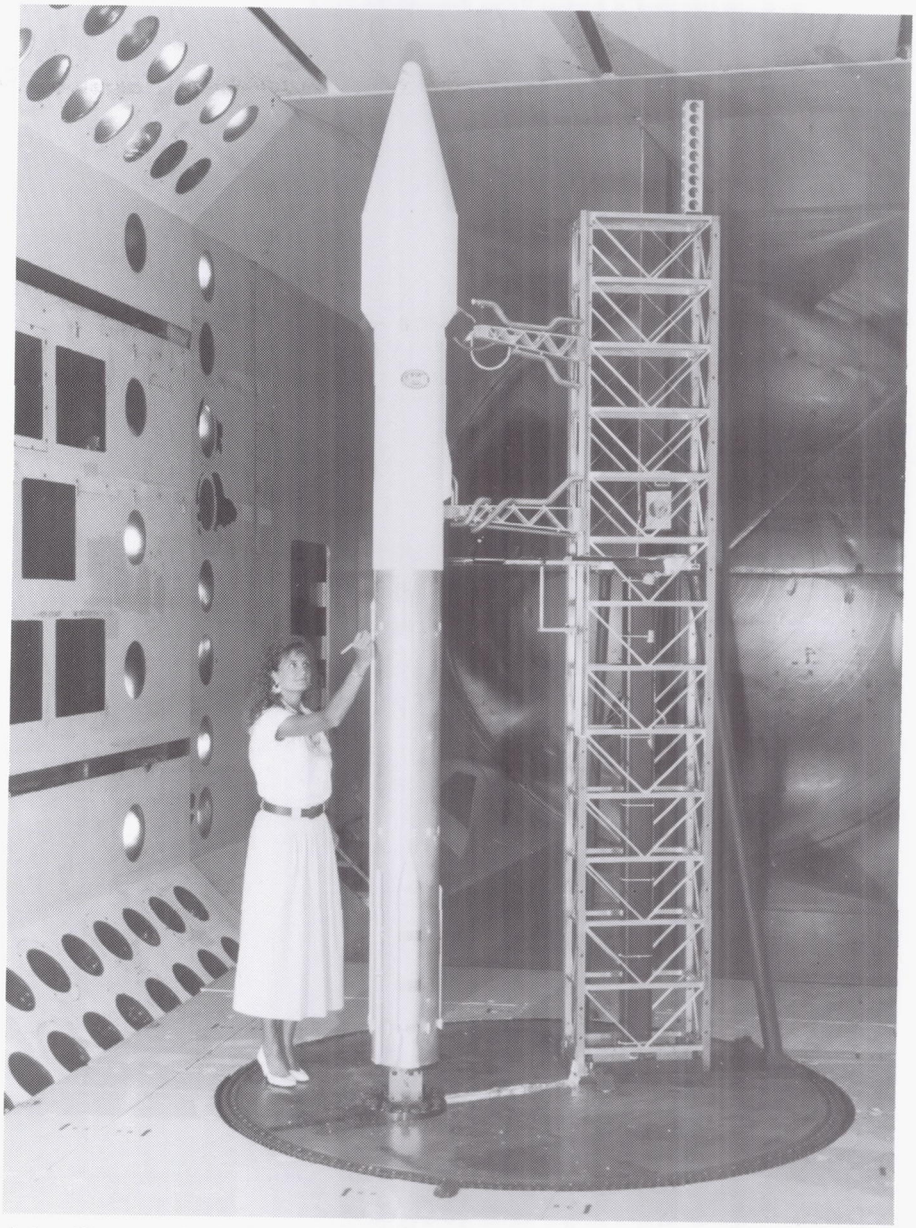

Atlas II ground wind loads model mounted on turntable. L-89-7023

The variation of the resultant bending moment (a vector addition of steady and dynamic moments) near the base of the model booster for one fuel condition and at a typical wind compass bearing with wind velocity is shown in the second figure. The model data have been scaled to the full-scale values. The critical limit bending moment for the full-scale booster is also shown. Data obtained without the damper show that the critical limit is exceeded at approximately 23 knots. With the damper installed, however, the bending moment at 30 knots is less than the critical limit.

These tests have shown that, if final launch procedures are begun only when the weather forecast is good, launches will rarely, if ever,

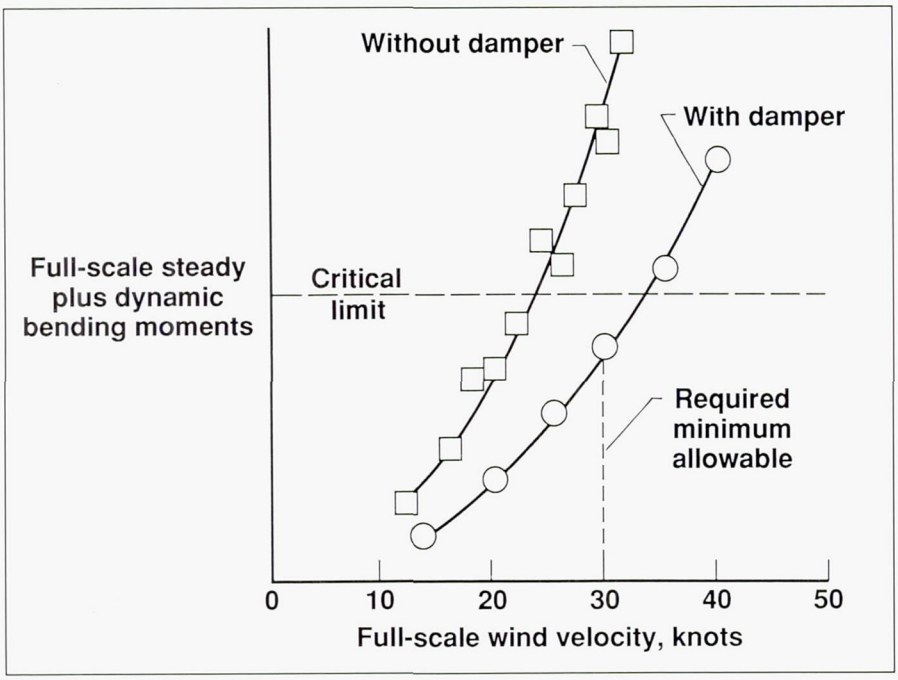

Atlas II ground wind loads with and without damper.

have to be scrubbed because of excessive winds after the fueling process has begun.

(Moses G. Farmer, Ellen C. Parker, and Bryan E. Dansberry, 41263)

16-Foot Transonic Tunnel

The Langley 16-Foot Transonic Tunnel is a closed-circuit single-return continuous-flow atmospheric tunnel. Speeds up to Mach 1.05 are obtained with the tunnel main-drive fans, and speeds from Mach 1.05 up to Mach 1.30 are obtained with a combination of main-drive and test section plenum suction. The slotted octagonal test section measures 15.5 ft across the flats. The tunnel is equipped with an air exchanger with adjustable intake and exit vanes to provide some temperature control. This facility has a main-drive power of 60,000 hp, and a 36,000-hp compressor provides test section plenum suction.

The tunnel is used for force, moment, pressure, flow visualization, and propulsion-airframe integration studies. Model mounting consists of sting, sting-strut, and fixed-strut arrangements; propulsion simulation studies are made with dry, cold, high-pressure air.

The 16-Foot Transonic Tunnel has undergone several major modifications. These include a floor-mount system to facilitate semispan model testing and a model preparation area for model buildup and calibration.

Off-Design Performance of Supersonic-Cruise Expendable Nozzles

Nozzles utilized for one-way missions (e.g., missiles) must be designed for light weight and low cost. These requirements dictate a simple, fixed-geometry nozzle design. Nozzles designed for supersonic cruise generally require variable-geometry features for high performance at both subsonic and supersonic speeds. Thus, nozzles designed for expendable, supersonic-cruise vehicles require innovative features that take advantage of internal exhaust flow separation patterns or allow variable geometry with little increase in nozzle weight.

A cooperative experimental investigation with Allison Gas Turbine has been conducted to assess the off-design performance of innovative nozzle designs intended for use on expendable, supersonic-cruise vehicles. A typical nozzle configuration installed in the 16-Foot Transonic Tunnel test section is shown in the figure. The nozzle shown represents a simple variable-geometry scheme that utilizes explosive bolts for operation. At subsonic speeds, four simple flaps would lock with explosive bolts into a closed position forming a small circular-shaped exit. As vehicle speed increases, two of the explosive bolts would be activated to release two of the flaps and form a larger exit area (and nozzle expansion ratio) as shown in the figure. At supersonic cruise, the remaining two flaps would be released to form a cruciform-shaped exit and an even larger exit area. Tests were conducted at an angle of attack of 0° over a Mach number range from 0 to 1.27. High-pressure air was used to simulate jet exhaust at nozzle pressure ratios from 1.0 (jet off) to approximately 10.0. A six-component balance was used to measure forces and moments on the nozzle.

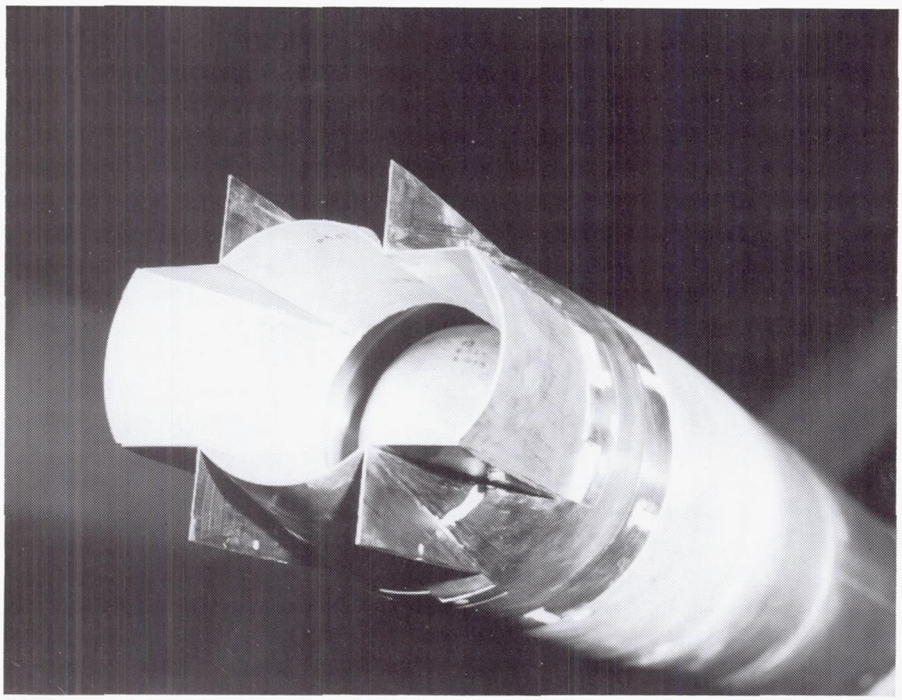

Simple variable-geometry nozzle configuration. L-89-06481

Preliminary results indicate that fixed geometry nozzles designed to take advantage of internal flow separation patterns at low nozzle pressure ratios (typical of subsonic operation) did not operate efficiently at subsonic speeds. In addition, the base shape of the aft turbine fairing (internal centerbody visible in the figure) had little effect on nozzle performance. Internal static pressure measurements on the nozzle divergent flaps indicate that massive exhaust flow separation occurred inside all nozzle configurations tested at subsonic speeds. These results indicate that a simple variable geometry scheme may be required for efficient vehicle performance at both subsonic and supersonic speeds.

(R. J. Re, 43005, B. L. Berrier, and J. G. Taylor)

Superfan Nacelle Drag on Low-Wing Transport Model

Advances in structural materials, machining methods, and computer-aided design techniques have allowed the use of more efficient, high-aspect-ratio wings in commercial transport aircraft. Improvements in turbofan efficiency realized by increasing the ratio of fan flow to core flow (that is, bypass ratio or BPR) have produced larger nacelle sizes for the same thrust. Therefore, the size of the nacelles relative to the wing chord has grown dramatically. This raises the potential for much higher installed nacelle interference drag (due to detrimental effects of the pylon/nacelle on the wing flow field, or the wing on the pylon/nacelle flow field).

An experimental program has been conducted on unpowered flow-through, pylon-mounted nacelles simulating turbofans (superfans) with a BPR of approximately 20 installed on a twin-engine low-wing transport model. For comparison purposes, current technology nacelles simulating turbofans with a BPR of approximately 6 were also tested. The model used for

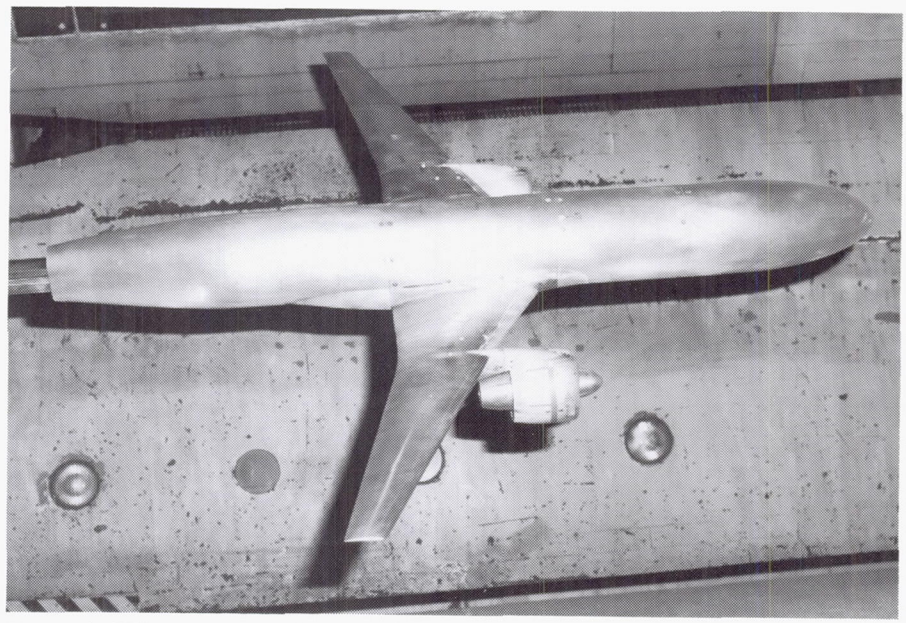

Pratt & Whitney superfan nacelles on low-wing transport model.

L-89-03317

these tests is a generic twin-engine, low-wing transport model having a 60-in. wing span and a supercritical airfoil with 21° sweep at the ¼ chord line. Douglas Aircraft Company in Long Beach, California, designed the wing and baseline nacelles in the early 1980's for a cruise Mach number of 0.77 to obtain better fuel economy in response to the fuel crisis of 1977. One pair of superfan nacelles was designed more recently by Douglas Aircraft Company, and the other pair, shown in the figure, was designed by Pratt & Whitney of East Hartford, Connecticut. Tests were conducted in the 16-Foot Transonic Tunnel at Mach numbers from 0.50 to 0.80 and at angles of attack from –4° to 6°. Nacelle incidence and toe-in angles, relative to the model centerline, were varied to determine the best orientation for minimum drag with the pylon/nacelles mounted at the 0.4 semispan location on the wing.

Results of this investigation indicate that superfan nacelles can be installed with little or no interference drag penalties. Even though their larger sizes do produce higher nacelle skin friction drag levels, compared to the baseline nacelles, the higher nacelle drag is more than offset by the predicted, improved specific fuel consumption, resulting in substantially lower aircraft direct operating costs.

(O. C. Pendergraft, Jr., 43008, R. J. Re, A. M. Ingraldi, and T. T. Kariya)

Transonic Characteristics of Advanced Vectoring Nozzles

An experimental investigation has been conducted to determine the uninstalled performance characteristics of two advanced vectoring exhaust nozzles. Transonic wind tunnel tests were made with an axisymmetric nozzle in which vectoring was accomplished through actuation of the divergent section of the nozzle. This concept permits divergent flap vectoring through the use of synchronizing rings and actuators and by universal joint attachments of the divergent flaps at the nozzle throat. The other nozzle tested was a spherical convergent flap type that maintains the circular duct shape to the nozzle throat resulting in a spherical-shaped convergent-flap section. Then, the divergent flaps and sidewalls form a rectangular flowpath from the nozzle throat to the exit. Thrust vectoring with this concept is achieved by rotation (in any direction) of the rectangular divergent section about the spherical-shaped convergent-flap section (similar to the motion of a ball and socket joint).

High-pressure air was used to simulate the jet exhaust. Forces and moments on the afterbody/nozzle (downstream of the metric break) were measured with a six-component strain-gauge balance. External static pressure orifices were located on the nozzles. Model variables included nozzle divergent flap length and yaw vector angle. Tests were conducted at Mach numbers from 0 to 1.28 and a nozzle pressure ratio from 1.0 (jet off) to approximately 8.

Preliminary results indicate that the spherical convergent flap nozzle generally had lower nozzle drag than the axisymmetric vectoring nozzle over the range of Mach numbers tested. Both nozzles, however, had nearly the same yawing moment characteristics at a yaw vector angle of 20°.

(F. J. Capone, 43004, and G. T. Carson, Jr.)

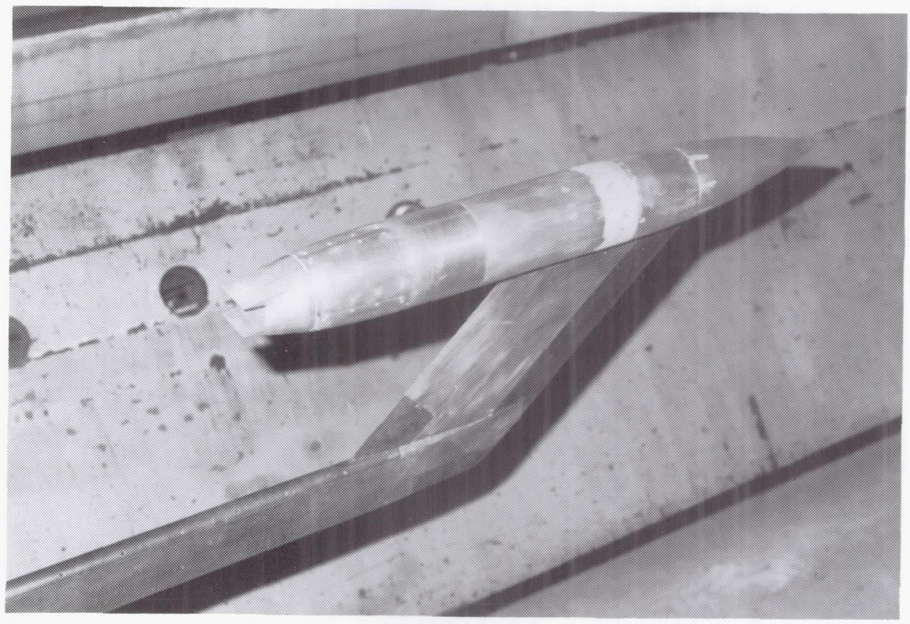

Model with spherical convergent flap nozzle. L-89-05743

National Transonic Facility

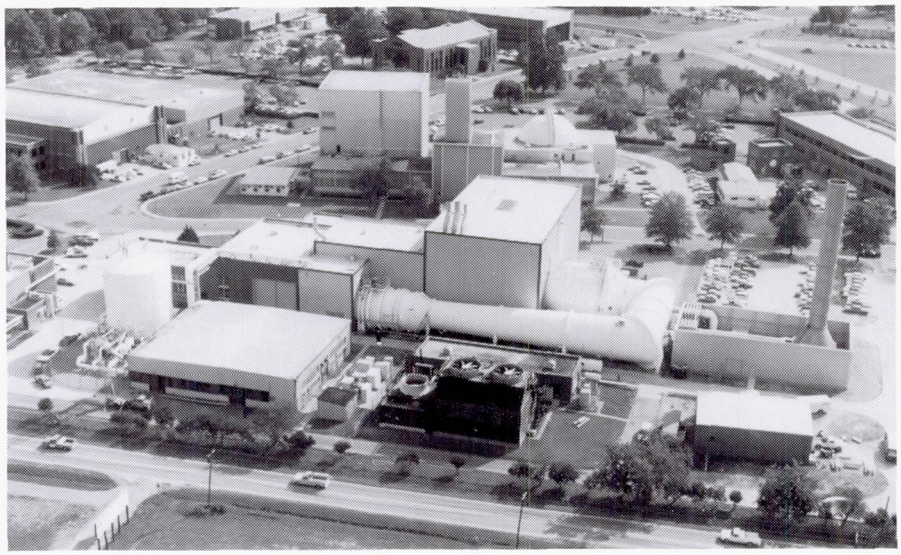

The National Transonic Facility (NTF) is a cryogenic fan-driven transonic wind tunnel designed to provide full-scale Reynolds number simulation in the critical flight regions of most current and planned aircraft. The NTF can operate at Mach numbers from 0.2 to 1.2, stagnation pressures from 1 atm to 9 atm, and stagnation temperatures from 340 K to 80 K. The maximum Reynolds number capability is 120 × 10^6 at a Mach number of 1.0, based on a reference length of 0.25 m.

Construction of the NTF was completed in September 1982. The tunnel was declared operational in August 1984, and aerodynamic calibration and research and development testing were begun in that year.

On January 18, 1989, the tunnel hardware immediately upstream of the fan came loose and went through the fan, resulting in the fan blades being damaged beyond repair. The recovery from the fan blade mishap is now complete. Operational checkout of the NTF in the air mode of operation has been completed. However, problems with the liquid-nitrogen pumps, not associated with the mishap, have resulted in the operational checkout of the facility over its full operational envelope being delayed until 1990.

Model Deformation Measurements With Improved Video Photogrammetry System

Charge Coupled Device (CCD) cameras and computer-controlled video frame digitization boards have been incorporated into a system to photogrammetrically measure wing deflection and twist at the NTF. This system is an improved version of an earlier system that included high-

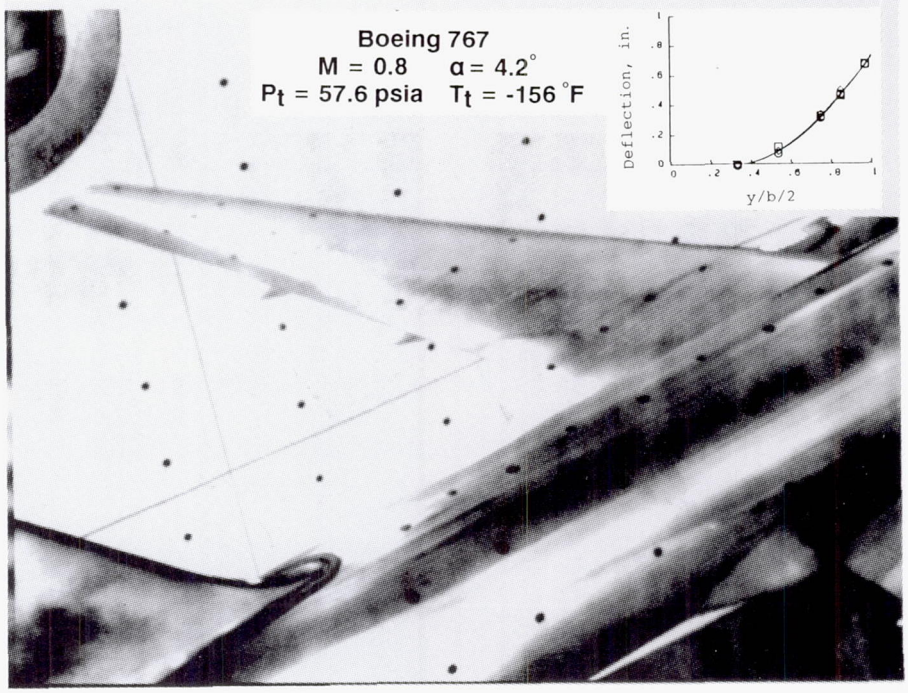

Video image of Boeing 767 model recorded at NTF.

resolution tube-type cameras. The new system eliminates both the vibration-induced distortion associated with tube cameras and the manual processing of video hardcopy images necessary in the earlier system.

The new system was used to acquire data on a targeted Boeing 767 model at the NTF. In the figure, the Mach number M was 0.8, the angle of attack α was 4.2°, the total pressure P_t was 57.6 psia, and the total temperature T_t was −156°F. The maximum wingtip deflection for this condition was found to be 0.71 in. The maximum wing twist was less than 1°. The wall targets that surround the wing on the figure were used to check for image jitter, which could affect the accuracy of the measurement, by comparing the repeatability of the image coordinates for this condition to the repeatability without flow at ambient conditions. The image jitter was found to be small enough not to appreciably affect the accuracy. In addition, image motion of the fuselage and wing targets was found to be consistent with rigid-body lateral motion.

(A. W. Burner, 44635, W. L. Snow, and S. G. Flechner)

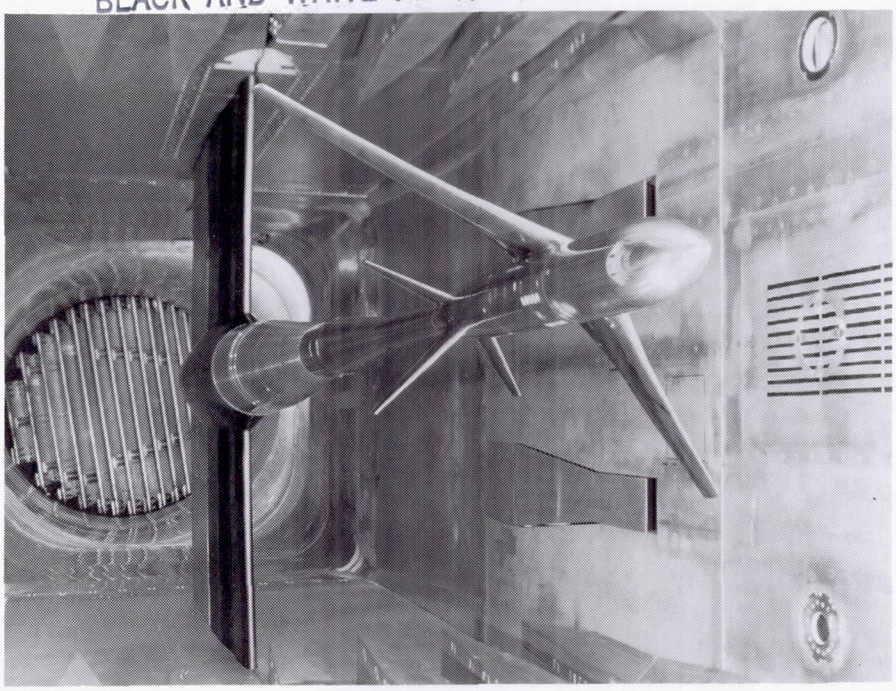

Pathfinder I in NTF. L-86-10666

Reynolds Number Effects on Subsonic Energy-Efficient Transport Model

An investigation has been conducted in the NTF to determine Reynolds number, aeroelasticity, boundary-layer transition, and nonadiabatic wall temperature effects for a subsonic, energy-efficient transport model *(Pathfinder I)*. The model was tested over a Mach number range from 0.50 to 0.86 and a Reynolds number range from 1.9×10^6 to approximately 23.0×10^6 (based on mean geometric chord). The majority of the data were taken using cryogenic nitrogen; data at a Reynolds number of 1.9×10^6 were taken in air. Longitudinal force and moment, wing pressure, and wing thermocouple data were taken.

The data indicate that increasing the Reynolds number resulted in greater effective camber of the supercritical wing and horizontal tail, thus resulting in greater lift and pitching-moment coefficients at nearly all angles of attack for a Mach number M of 0.82. As Reynolds number was increased, the untrimmed lift/drag ratio L/D increased, the angle of attack for maximum L/D decreased, drag creep was reduced significantly, and drag-divergence Mach number increased slightly. Data repeatability for both modes of operation of the NTF (air and cryogenic nitrogen) was generally very good, and nonadiabatic wall effects were estimated to be small. Transition-free and transition-fixed configurations had significantly different force and moment data at $M = 0.82$ for low Reynolds numbers, and very small differences were noted at high Reynolds numbers.

(Peter F. Jacobs and Blair B. Gloss, 42855)

0.3-Meter Transonic Cryogenic Tunnel

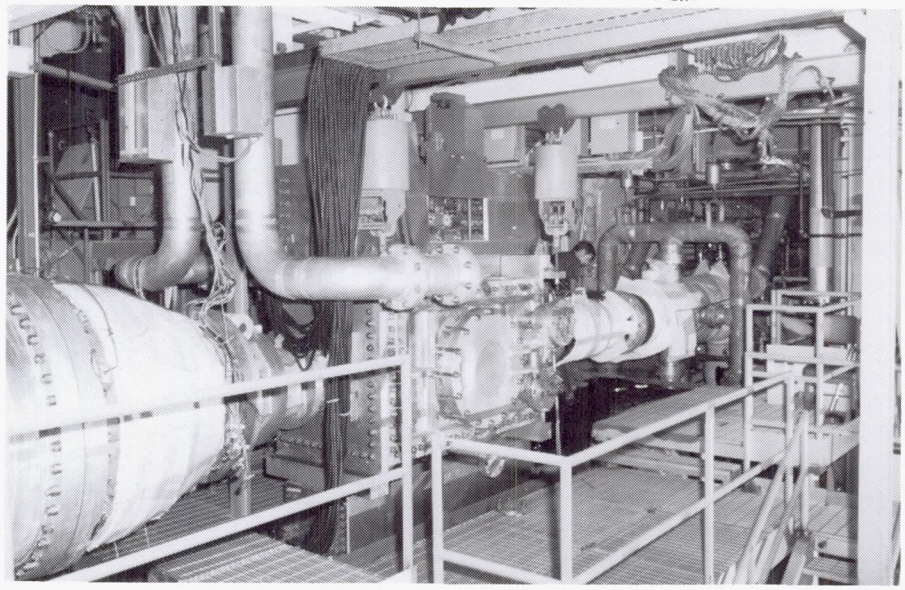

The Langley 0.3-Meter Transonic Cryogenic Tunnel (TCT) is a closed-circuit cryogenic pressure tunnel. The test section Mach number is variable between 0.2 and approximately 1.3, with suitable adjusted test section shapes. The stagnation pressure can vary from slightly over 1 bar up to 6 bars and the stagnation temperature from 340 K down to approximately 77 K (–196° C). The test gas is nitrogen. The wide ranges of pressure and temperature allow the study of approximately a 30-to-1 range in Reynolds number effects. A maximum Reynolds number of more than 100 × 10^6/ft is possible. The 0.3-Meter TCT has automatic control of Mach number, pressure, and temperature.

The tunnel was placed in operation in 1973 as a three-dimensional pilot tunnel to demonstrate the cryogenic wind tunnel concept at transonic speeds. The successful demonstration of the cryogenic concept in the 0.3-Meter TCT played a major role in the decision to build the U.S. National Transonic Facility (NTF). Subsequently, the 0.3-Meter TCT has played a major part in the Advanced Technology Airfoil program because the tunnel allows Reynolds number effects to be studied in two-dimensional testing. The 0.3-Meter TCT currently is involved in the evaluation of testing techniques for improving data quality (by minimizing boundary interferences) in both two- and three-dimensional testing. The combination of flight Reynolds number

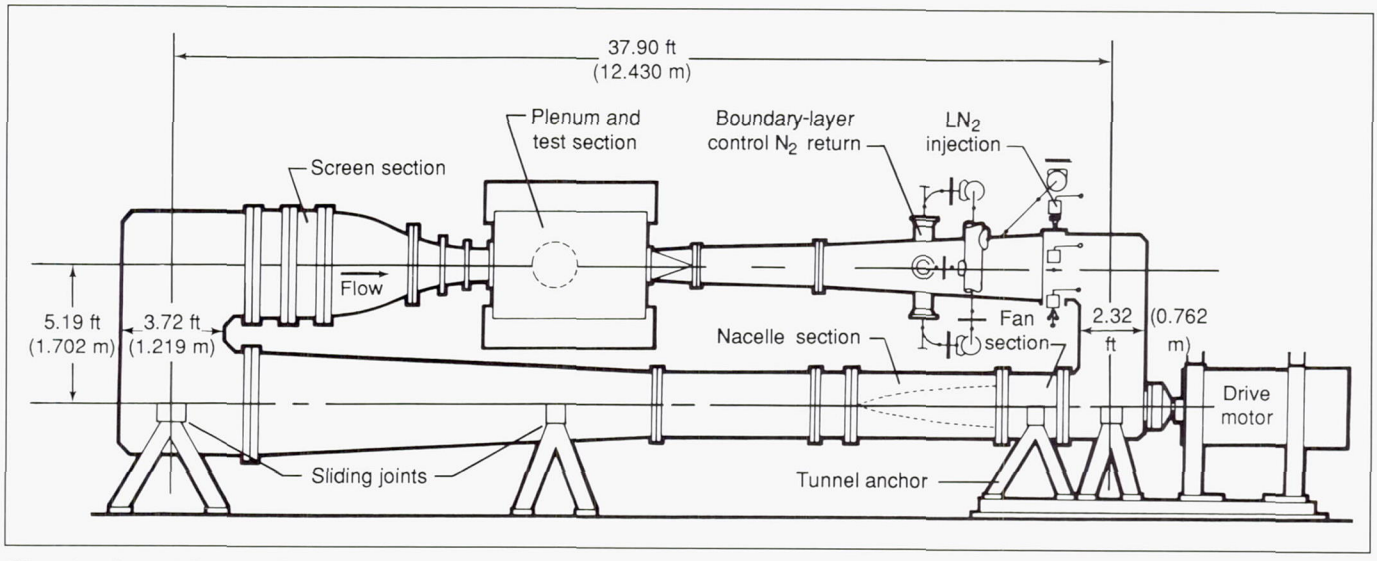

Sketch of 0.3-Meter TCT with 13-in. by 13-in. two-dimensional Adaptive Wall Test Section installed.

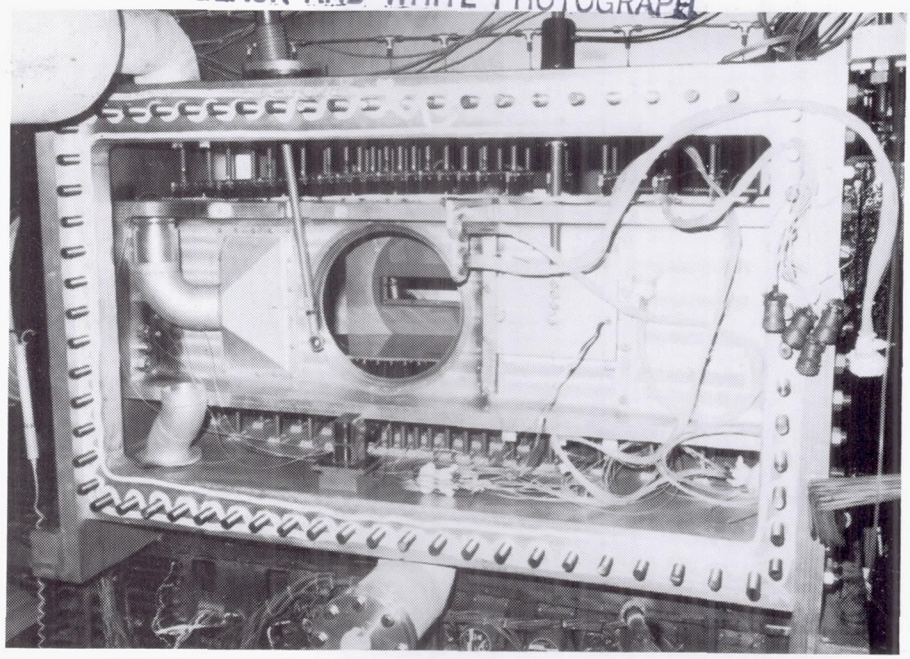

View of 0.3-Meter TCT AWTS with left side of surrounding pressure shell removed.

capability and minimal boundary interferences makes the 0.3-Meter TCT a powerful tool for aeronautical research at transonic speeds.

During more than 15 years of operation, the 0.3-Meter TCT has run with three different test sections. The original test section was octagonal with a sting-type model support system. In 1975, an 8-in. by 24-in. two-dimensional test section was installed with slotted top and bottom walls. In 1985, a new Adaptive Wall Test Section was installed.

The Adaptive Wall Test Section (AWTS) is nominally square with 13 in. sides and has an effective length of 55.8 in. This unusual transonic test section has four solid walls with a flexible floor and ceiling. The complete test section is enclosed in a pressure shell that forms a 73.2-in.-long insert into the 0.3-Meter TCT tunnel circuit.

A system of 21 computer-controlled jacks supports each flexible wall. These flexible walls are made of 308 stainless steel. The AWTS has motorized model support turntables and a traversing wake survey probe, both of which are computer controlled.

For each data point, the flexible walls are adapted to shapes that drastically minimize wall interferences that would otherwise exist. In two-dimensional testing, the walls follow streamline shapes that would exist around the model if it were in free air. The floor and ceiling of the test section in effect become invisible to the model. With wall interferences minimized, the model size and therefore the Reynolds number capability of the tunnel can be increased. In addition, the removal of noisy slots in the test section gives the added benefit of much improved data quality.

For two-dimensional testing, the AWTS has provisions for both active and passive sidewall boundary-layer control (BLC). Porous plates can be fitted into the rigid sidewalls just upstream of the model location. This BLC system allows the investigation of another source of boundary interference.

Tests have been conducted in the AWTS with two-dimensional airfoils ranging in chord from 6 in. to 13 in. Chord Reynolds numbers of more than 100×10^6 have been achieved. The walls have been adapted successfully with lift coefficients up to 1.5 and Mach numbers up to 0.95. Sidewall-mounted wings and three-dimensional wing bodies have been tested recently to evaluate the wall adaptation techniques for minimizing three-dimensional wall interference.

Sidewall Boundary-Layer Removal and Wall Streamlining in Airfoil Tests

Airfoil tests in two-dimensional wind tunnels have two primary sources of interference which include the top and bottom wall interference, which is uniform across the model span, and the airfoil-sidewall junction flow, which varies along the span. To keep the wall interference effects small on model measurements, the Langley 0.3-Meter Transonic Cryogenic Tunnel (0.3-Meter TCT) employs two special test section wall features. First, the top and bottom walls are flexible. The walls are moved to free-air streamline shapes; this relieves the constraining effect. Second, the test section sidewalls have perforated panels mounted ahead of the model station. Removal of flow through the perforated

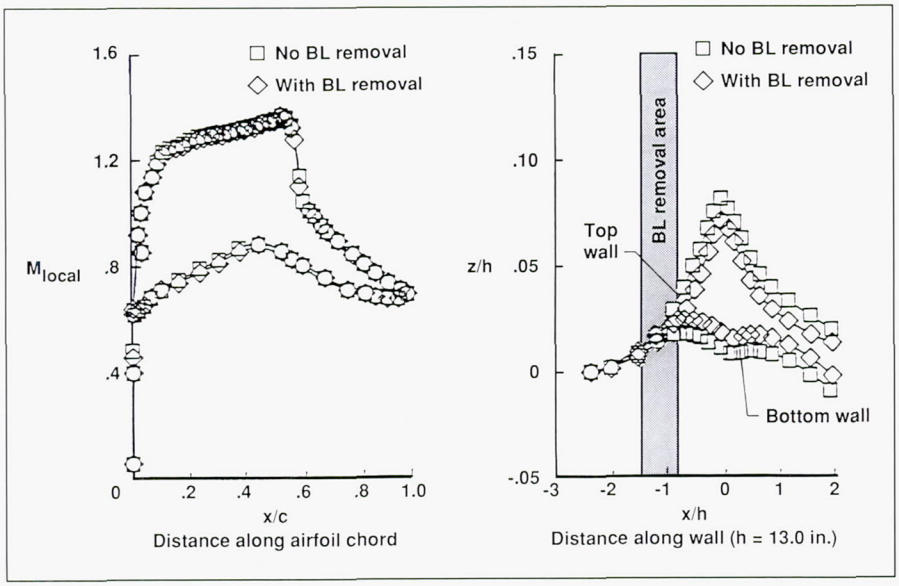

Effect of sidewall boundary-layer removal on wall streamlining (M = 0.765 and $R_c = 20 \times 10^6$).

panels thins the boundary layer (BL) at the model station. With reduced boundary-layer thickness, the extent of three-dimensional flow at the airfoil-sidewall junction is smaller.

The objectives of this study were to validate the combined wall movement and sidewall boundary-layer removal operation and evaluate the extent of sidewall influence in the 0.3-Meter TCT airfoil test data. The study employed a 9-in.-chord c supercritical airfoil model, which was designed and fabricated at the National Aeronautical Establishment (NAE) of Canada. The test section height h (13 in.) to model chord ratio and the width to chord ratio are both equal to 1.4. The relatively large model size for the test section represented a severe test case for wall movements and sidewall flow removal under cryogenic conditions.

The flow removal from the sidewalls, while reducing the boundary-layer thickness, also introduces a change in the test Mach number. The adaptive capability of the top and bottom walls allows the walls to be moved in order to adjust for these changes. This capability allows evaluations of sidewall removal while maintaining a constant Mach number.

The airfoil tests were made with and without sidewall removal for the same M (0.765) and Reynolds number R_c (20×10^6). The walls were moved iteratively to free-air streamline shapes. The boundary-layer removal operation did not introduce any difficulty in the wall streamlining process. The study showed that the removal influence on airfoil pressure measurements at mid-span was small. This suggests that the sidewall influence in the 0.3-Meter TCT is probably small due to relatively thin boundary layers that are less than 1 percent of the test section width. However, the boundary-layer removal influenced the wall shapes significantly. The walls had to be moved closer to the model to maintain the same test Mach number in spite of the reduced mass flow in the model region.

(A. V. Murthy and E. J. Ray, 46359)

Transition Detection by Infrared Imaging in Cryogenic Environment

Cryogenic wind tunnel testing was developed as a means of matching the Reynolds numbers on models to those on airplanes in flight. This matching is required for proper reproduction of the viscous interaction between the body and the airflow. In particular, knowledge of the location of the boundary-layer transition from a laminar to a turbulent state is crucial.

Infrared imaging is the method of choice among flow visualization techniques for transition detection in conventional wind tunnels. For the cryogenic environment, this method has, in principle, the right attributes because it is nonintrusive and conducive to high-productivity testing. This method also provides an easily interpretable global picture of the wing boundary-layer regimes. However, two main difficulties arise when implementing this technique at low temperatures. The first problem is due to the sharp drop in the radiated energy with decreasing temperatures according to the T^4 energy radiation law. The second difficulty is due to the continuous shifting to longer wavelengths of the peak energy radiation as the

target temperature goes down (Wienn's displacement law). To evaluate this technique at low temperatures, a commercially available camera, sensitive to infrared radiation in the 8 μm to 12 μm range, was selected. The camera was mounted outside the 0.3-Meter TCT. The optical path for the airfoil radiation passed through a system of two windows (test section and plenum walls) and two front-surface mirrors inside the plenum to direct the radiation; the windows were zinc selenide and germanium, respectively.

The target airfoil was a modified 12-percent supercritical airfoil with a 9-in. chord and 13-in. span. The airfoil structural spar was Vascomax C-200 covered with a thin composite skin to reduce the surface reflections and minimize the heat conduction into the substrate.

According to the Reynolds analogy, the heat transfer coefficient and the skin friction coefficient behave similarly under fully developed boundary-layer flows. Therefore, the boundary-layer characteristics can be inferred from its thermal signature on the airfoil surface. To enhance the thermal signature of the transition, a positive temperature perturbation (smaller than 1 percent of the free-stream temperature) was imposed on the flow. The subsequent temperature response of the surface showed the effects of the difference between the heat transfer coefficients under the laminar and the turbulent boundary-layer regime; the part of the airfoil under the turbulent boundary-layer heated faster than the part under the laminar regime. The figure shows the result of a pixel-by-pixel subtraction of two thermograms taken before and after the temperature perturbation; the lighter area is under the turbulent flow. The focus is on the temperature difference between the laminar and turbulent areas of the airfoil rather than on the absolute temperature of its surface. This technique also filters out apparent temperature differences on the airfoil surface due to local variations in the emittance. Using this method, natural and forced transition were detected at free-stream and surface temperatures down to 170 K.

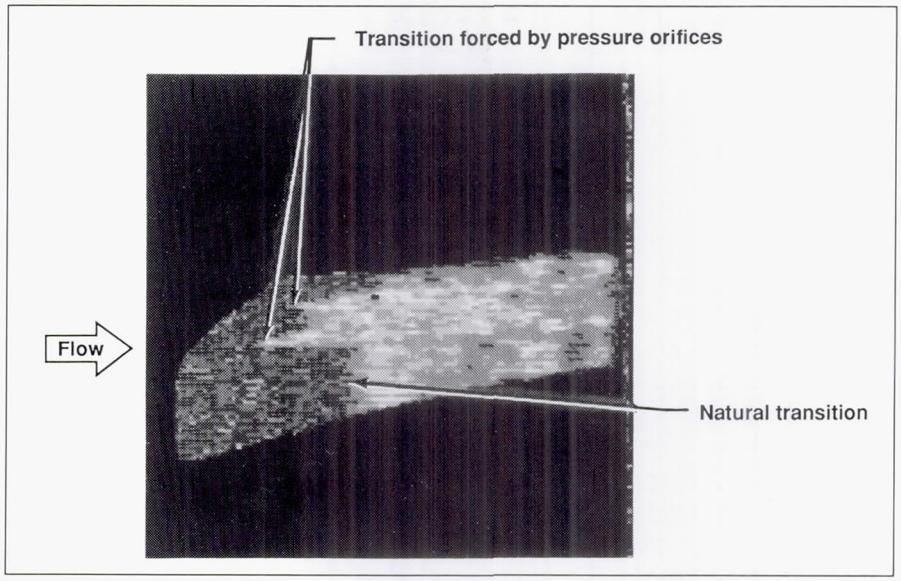

Transition detection by IR imagery in the 0.3-Meter TCT ($T_\infty = 220$ K, $M_\infty = 0.56$, and $Re_c = 4.65 \times 10^6$).

One interesting finding was that the pressure orifices on the airfoil surface caused enough of a disturbance to trip the boundary layer. Another finding was that the compression region behind a shock wave could be detected by its thermal signature on the airfoil. Some of the results obtained in this study were confirmed with micro-thin hot films deposited directly on the airfoil surface.

(Ehud Gartenberg and William G. Johnson, Jr., 45133)

Unitary Plan Wind Tunnel

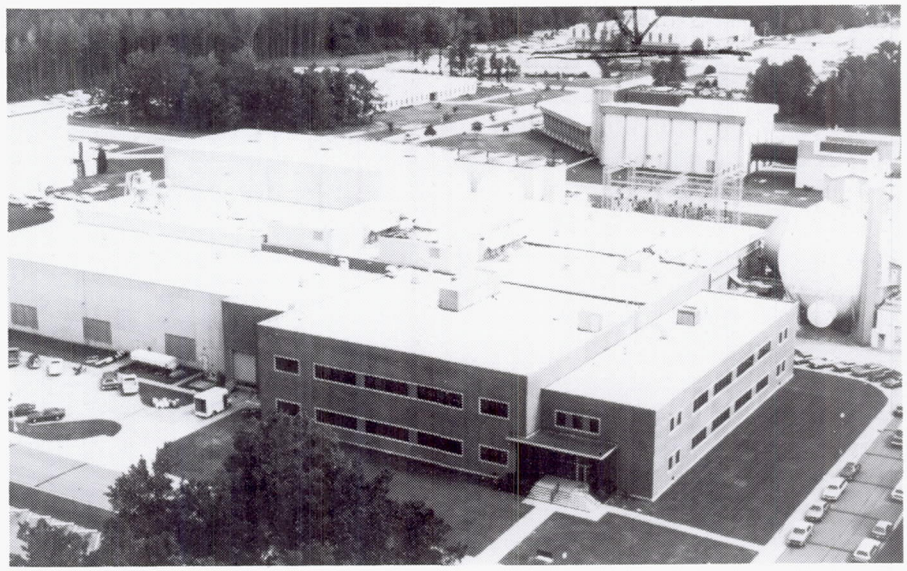

Immediately following World War II, the need for wind tunnel equipment to develop advanced airplanes and missiles was recognized. The military and the National Advisory Committee for Aeronautics (NACA) developed a plan for a series of facilities which was approved by the United States Congress in the Unitary Wind Tunnel Plan Act of 1949. This plan included five wind tunnel facilities, three at NACA laboratories and two at the Arnold Engineering Development Center. The Langley Unitary Plan Wind Tunnel (UPWT) was among the three built by NACA. The UPWT is a closed-circuit continuous-flow variable-density tunnel with two 4-ft by 4-ft by 7-ft test sections. The low-range test section has a design Mach number range of 1.5 to 2.9, and the high-range section Mach number varies from 2.3 to 4.6. The tunnel has sliding-block-type nozzles that allow continuous variation in Mach number while on-line. The maximum Reynolds number per foot varies from 6×10^6 to 11×10^6 depending on Mach number. The tunnel is used for force and moment, pressure distribution, jet effects, dynamic stability, and heat transfer studies. Flow visualization data, which are available in both test sections, include schlieren, oil flow, and vapor screen.

Supersonic Aerodynamic Characteristics of Proposed Personnel Launch System Lifting-Body Configuration

NASA is considering a Personnel Launch System (PLS) to supplement the Space Shuttle in transporting crew to and from Space Station *Freedom*. The system is launched by an expendable booster and consists of a personnel carrier vehicle for 8 to 10 crew and passengers. Several candidate configurations are being studied for the carrier vehicle. One of the proposed shapes is a lifting-body configuration approximately 25 ft in length. This configuration has a low aspect ratio with a flat undersurface and a blunt base. Three fins for aerodynamic control are mounted on the upper aft body. The centerline fin is relatively small, and the larger outboard fins are rolled outward 40° from the vertical. The fins have thick flat plate cross sections with cylindrical leading edges and blunt trailing edges. Control surfaces, referred to as elevons, make up the trailing edges of the outboard fins. The entire center fin is pivoted about the midpoint of its root chord to act as a yaw control device. In addition, the vehicle has four body flap control surfaces (two on the upper body and two on the lower). These surfaces are flush with the body contour and are only deflected outward.

A series of wind tunnel investigations has been undertaken to define the aerodynamic characteristics of this lifting-body configuration across the speed range from low-subsonic to hypersonic conditions. The current test was conducted in the UPWT using an 0.07-scale model. The tests were made at Mach numbers from 1.6 to 4.5 at a constant Reynolds number of 2.0×10^6/ft (3.4×10^6 based on body length). The model was sting mounted through its base, and forces and

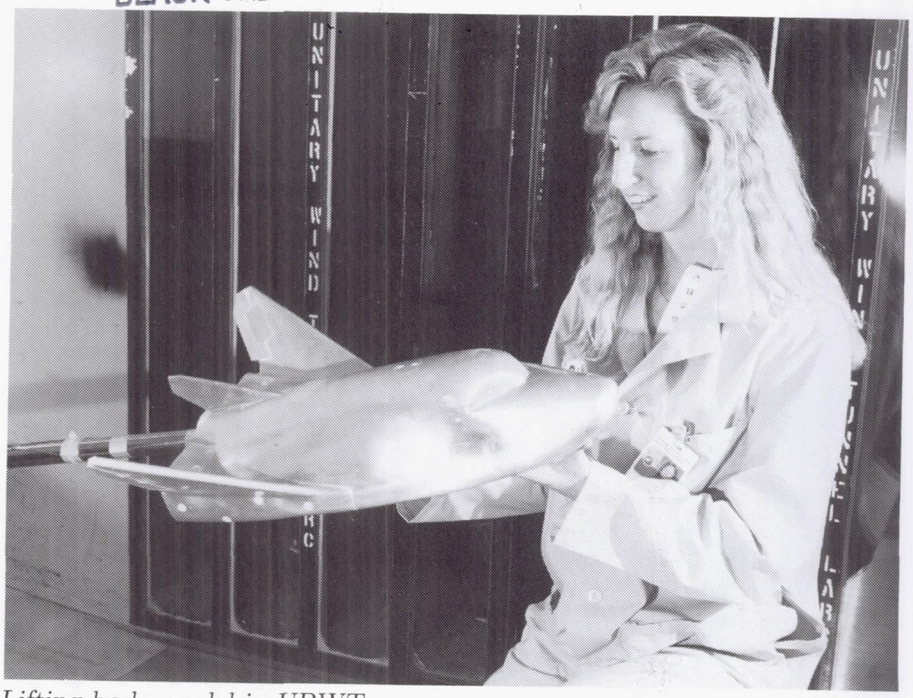

Lifting-body model in UPWT. L-88-03903

moments were measured with an internally mounted strain-gauge balance.

Results of the investigation indicated that the lifting-body configuration has supersonic aerodynamic characteristics that appear promising for a PLS. The model was longitudinally and laterally stable at supersonic Mach numbers about its design center-of-gravity position of 0.54 body length. At a Mach number of 4.5, it trimmed with controls neutral near the maximum lift/drag ratio, a value of 1.3. Longitudinal control deflections in excess of $-10°$ or combined elevon and body flap deflections are needed to trim and control the vehicle at positive lift values through the Mach range of 3.5 to 2.

(George M. Ware, 45246)

Aerodynamics of Tactical Missile With Opposing Wraparound Tail Fins

Tube-launched tactical missiles often employ wraparound fins that can be folded against the missile body for compact storage within the launch tube. These fins are normally curved in the same direction to match the body surface, with each fin covering approximately one-fourth of the body circumference when folded. When these curved fins are used as tail surfaces, mechanical deployment can be a problem due to the limited space available in the aft region of a missile. Another method of deploying this type of fin is to use the energy of the rocket exhaust to blast the fins into their deployed position. This method would require four side-mounted exhaust ports to deploy the four conventional wraparound fins.

A study has been conducted on an alternate design whereby the fins are mounted on the body in opposing pairs, with one folded beneath the other prior to deployment. In this manner, only two nozzles would be required to deploy all four fins. This configuration has vertical symmetry, and thus it will not possess the inherent rolling motion of the conventional wraparound design. To permit this configuration to be controlled with simple planar canards, a rolling moment must

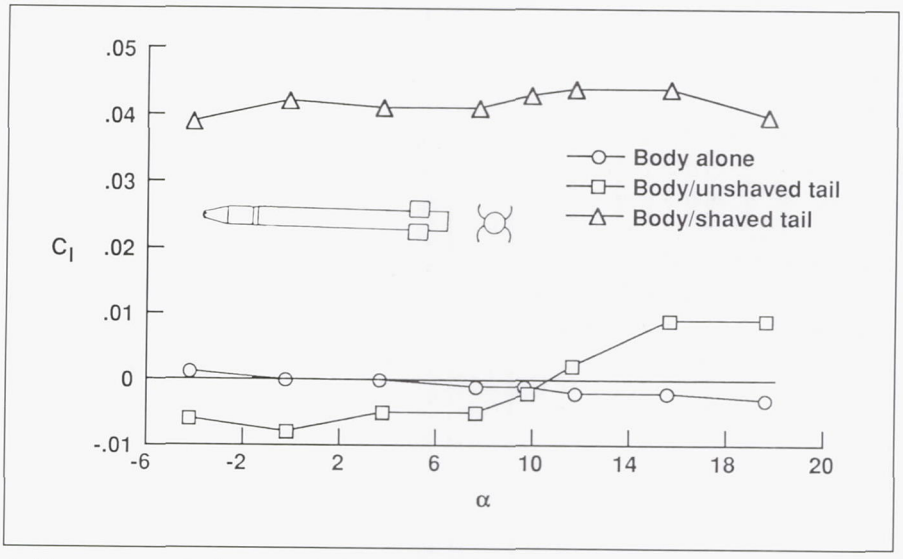

Rolling-moment characteristics of opposing wraparound tail missile (Mach = 1.6, ϕ = 0, and no canards).

be produced on the configuration. One unconventional method of achieving this moment is to shave very shallow bevels on each tail fin.

Tail fins with and without beveling were tested at low supersonic Mach numbers, over a range of angles of attack α, roll angles ϕ, and canard deflection angles. Typical rolling-moment characteristics for this configuration are shown in the figure. The unbeveled tails and the body alone produce little rolling moment C_l. The beveled tails, however, introduce a significant rolling moment to the configuration. Moreover, this moment is virtually constant with angle of attack. Thus shallow beveling of the opposing wraparound tail fins appears to be an effective method of producing the desired rolling motion for this configuration.
(Jerry M. Allen, 45592)

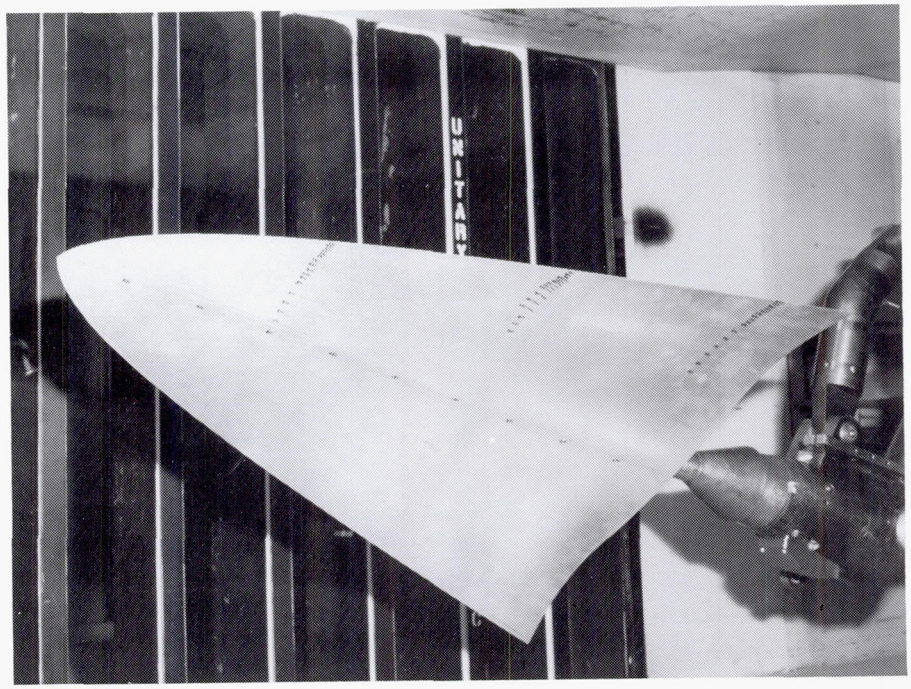

Mach 4 waverider model. L-88-11595

Experimental Evaluation of Mach 4 Waverider Model

A waverider configuration that was optimized for Mach 4 flight was designed using a hypersonic cone-derived waverider optimization code that was developed by the University of Maryland under a NASA grant. Tests were conducted on a model of this configuration in the UPWT. Force and moment, pressure, and flow-visualization (i.e., vapor-screen, oil-flow, fluorescent minitufts, shadowgraph, and schlieren photographs) data were obtained to determine the aerodynamic characteristics of this family of shapes. The test Mach numbers ranged from 1.5 to 4.5 for Reynolds numbers varying from 1×10^6/ft to 4×10^6/ft. Angles of attack varied from –16° to 14°, and the sideslip angles varied from –5° to 5°. The model geometry was generated for a configuration that would produce an optimized maximum lift-to-drag ratio $(L/D)_{max}$ for wind tunnel test conditions. A baseline model was also fabricated which maintained the same area distribution as the optimized configuration but with the upper surface flattened to remove the effect of camber and dihedral.

The experimental data showed good agreement with results from the optimization code (at the design conditions) and with theoretical results from an Euler solver. Shadowgraph and schlieren photographs verified that the bow shock was very nearly attached to the leading edge of the model at the design conditions. The minituft and oil-flow photographs showed that the flow at the design Mach number remained attached on the upper surface throughout the angle-of-attack range and that the flow remained attached for angles of attack above –4° on the lower surface.
(Steven X. S. Bauer, 45946)

Aerodynamic Forces, Moments, and Pressure Distributions on Generic Store Separating From Cavity at Supersonic Speeds

Results from several investigations defining the aerodynamic characteristics of stores separating from cavities at supersonic speeds have been reported in the literature. These investigations have been generally for specific missile configurations, and, in most cases, only force and moment measurements are presented. An experimental inves-

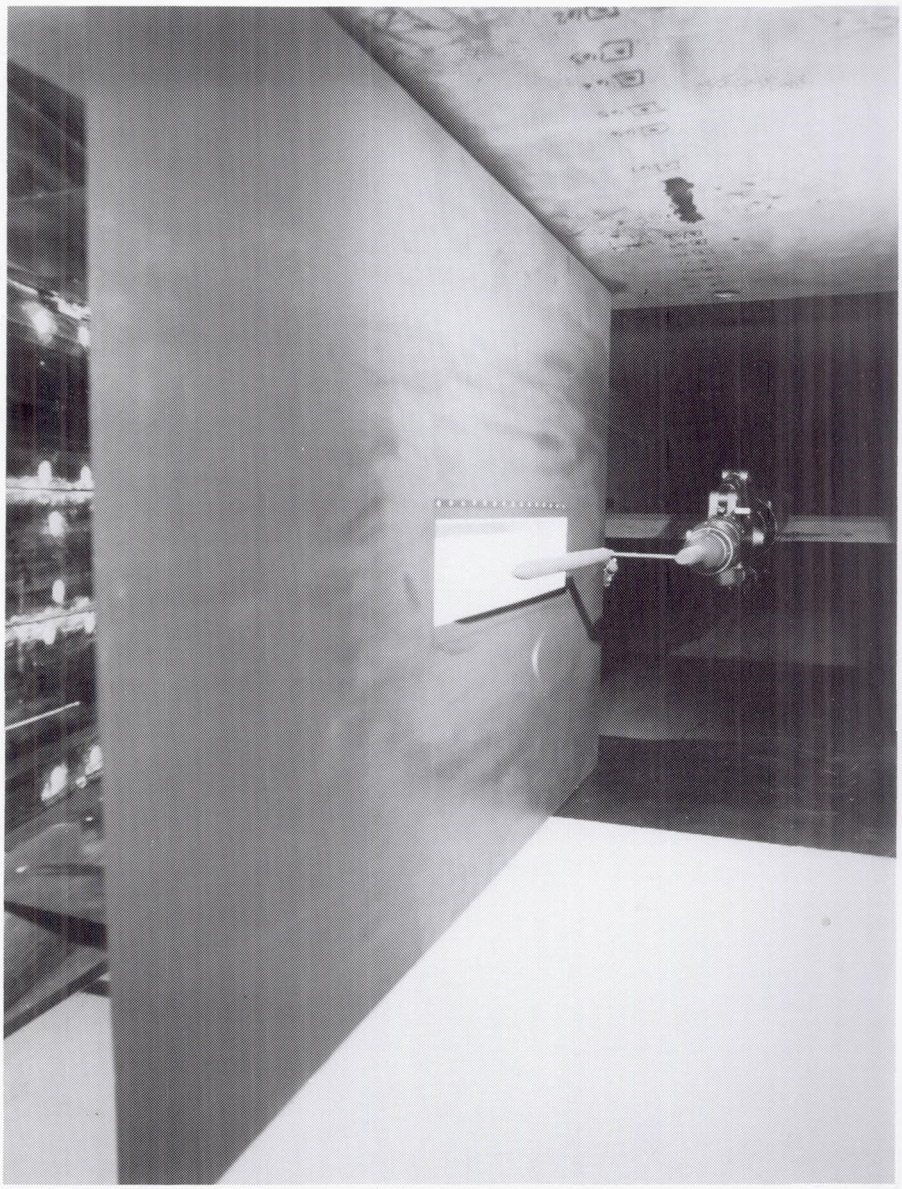

Installation of separation model in UPWT. L-89-06995

tigation was recently completed in the UPWT to provide force, moment, and surface-pressure data on a generic store separating from a generic box cavity. The cavity was installed in a vertical splitter plate that simulated the parent body.

A generic store shape was selected in order to simplify the store flow field and to make the test article more amenable to simulation by computational fluid dynamics (CFD) techniques. Separate store models were used to obtain the pressure measurements and the force and moment measurements. The store pressure model was instrumented with 100 pressure orifices, and the force and moment model was instrumented with a six-component strain-gauge balance. These store models were ogive-nose cylinders that had a length-to-diameter ratio of 20.00.

Measurements were obtained for the store separating from a box cavity whose depth was varied to give cavity length-to-depth ratios L/h of 16.78, 12.07, and 6.73. The tests were conducted on free-stream Mach numbers of 1.69, 2.00, and 2.65. Preliminary results for the store separating from the two shallow cavity configurations (L/h = 16.78 and 12.07) showed very large longitudinal and circumferential pressure gradients occurring on the store when it was located inside or near the cavity; these pressure distributions resulted in large positive pitching moments on the store. When the store separated from the deep cavity (L/h = 6.73), pressure gradients on the store were small, and the pitching-moment coefficients were approximately zero.

(Robert L. Stallings, Jr., Floyd J. Wilcox, Jr., and Dana K. Forrest, 42877)

Supersonic Aerodynamic Characteristics of Mach 3 High-Speed Civil Transport Configuration

In support of the Langley Research Center High-Speed Airframe Integration Research (HiSAIR) program, wind tunnel tests were conducted to determine the supersonic aerodynamic characteristics of a High-Speed Civil Transport (HSCT) configuration. The tests were conducted in both test sections of the UPWT at Mach numbers from 1.6 to 3.6 for a Reynolds number of 2×10^6/ft. Angles of attack ranged from –2° to 10°, and sideslip angles ranged from –4° to 4°.

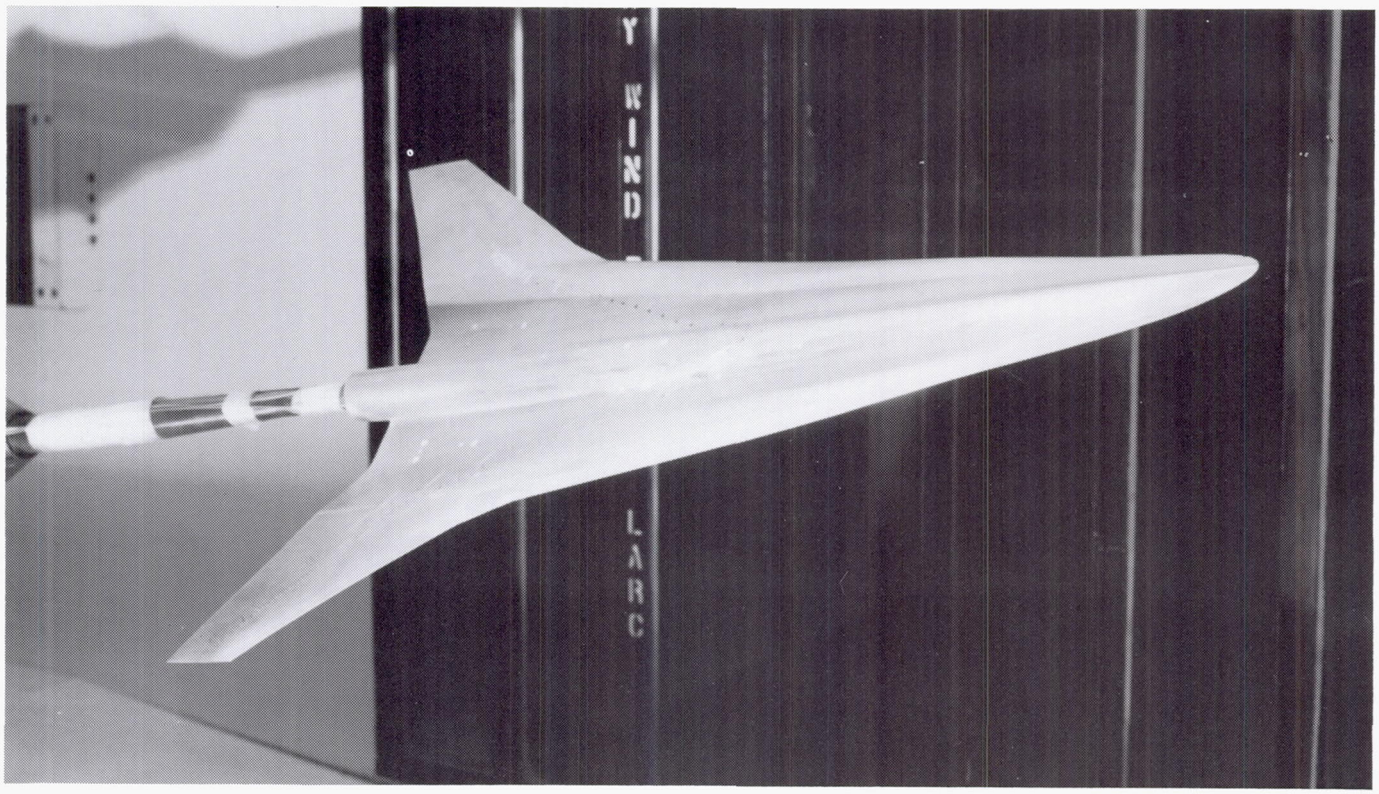

Wind tunnel model of HSCT concept. L-89-12987

The blended wing-body configuration has a blunt nose planform, a highly swept inboard wing panel, a moderately swept outboard wing panel, and a wingtip that is either straight or curved. Force and moment and flow-visualization data have been acquired on the configuration with a straight wingtip with and without nacelles. Data on the curved wingtip configuration will be acquired at a future date.

Preliminary analysis of the test results indicates that the cruise performance is slightly below the initial estimates. The pitching-moment characteristics exhibited an unstable trend at low angle of attack which increased at higher angles due to tip stall. The results from these tests will be used to refine the overall performance estimates for this HSCT configuration and will provide a baseline from which configuration improvements can be analyzed in the HiSAIR program.

(Gloria Hernandez, Jeffrey D. Flamm, and Peter F. Covell, 45572)

Supersonic Performance Characteristics of NASP Parametric Inlet Model

In support of the National Aero-Space Plane (NASP) Program, tests were conducted on a parametric inlet configuration in the high Mach number test section of the UPWT at Mach numbers from 2.3 to 4.6.

The purpose of this investigation was to determine performance on sidewall compression inlets and the effects inlet starting mechanism components have on inlet performance. The performance characteristics were determined by measuring sidewall pressure distributions, pressure recovery, mass capture, spilled mass, and spillage drag. Several inlet geometric parameters (including variations in aspect ratio, contraction ratio, and sidewall compression angle) were investigated. These data will be extremely valuable for future computational fluid dynamics code validation studies.

Preliminary analyses of the test results show the merit of variable geometry inlets for optimum performance throughout the supersonic speed range.

(William A. Corlett, 45911)

Hypersonic Facilities Complex

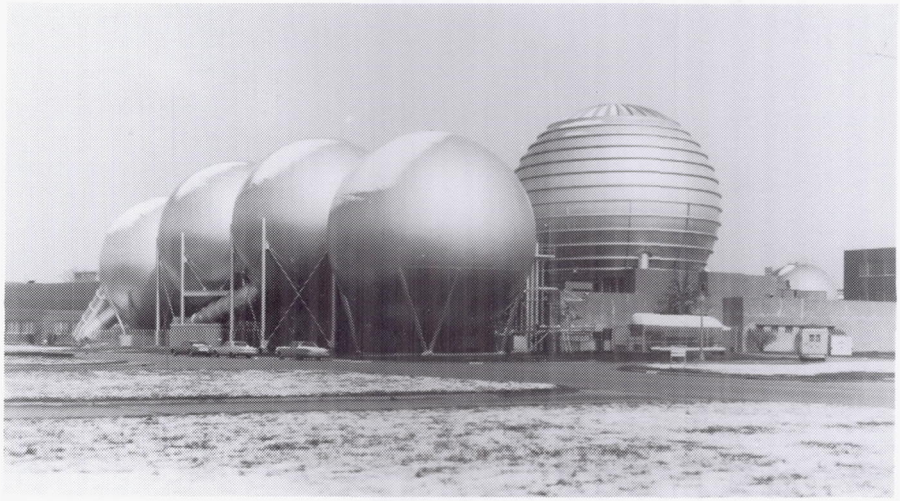

The Hypersonic Facilities Complex consists of several hypersonic wind tunnels located at four Langley Research Center sites. They are considered as a complex because together these facilities represent a major unique national resource for wind tunnel testing. The complex currently includes the Hypersonic CF_4 (tetrafluoromethane) Tunnel ($M = 6$), the Mach 6 High Reynolds Number Tunnel, the 20-Inch Mach 6 Tunnel, the Mach 8 Variable-Density Tunnel, the 31-Inch Mach 10 Tunnel, the Hypersonic Nitrogen Tunnel ($M = 17$), and the Hypersonic Helium Tunnel ($M = 20$). These facilities are used to study the aerodynamic and aerothermodynamic phenomena associated with advanced space transportation systems, including future space transfer and Personnel Launch System vehicles; to support the development of the National Aero-Space Plane technology, lunar and Mars entry vehicles, and hypersonic missiles and transports; and to perform basic fluid mechanics studies, to establish data bases for calibration of computational fluid dynamics (CFD) codes, and to develop measurement and testing techniques. A significant amount of the current testing in these facilities is classified, thus restricting the amount and content of test results that can be reported in the open literature.

This complex of facilities provides an unparalleled capability

CF_4 TUNNEL

$M_\infty = 6$ CF_4 $R_\infty = 0.25\text{-}0.55 \times 10^6$

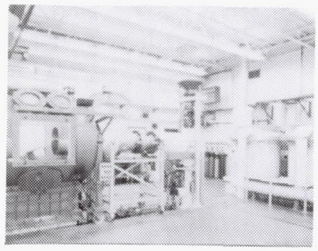

HIGH R_∞ M-6 TUNNEL

$M_\infty = 6$ AIR $R_\infty = 0.8\text{-}42.0 \times 10^6$

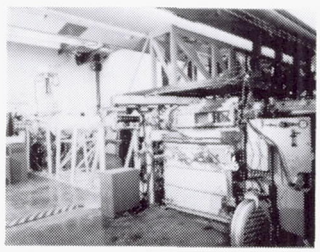

20-INCH M-6 TUNNEL

$M_\infty = 6$ AIR $R_\infty = 0.7\text{-}9.0 \times 10^6$

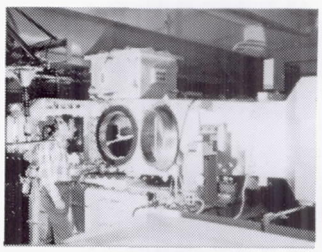

M-8 VAR.-DENS. TUNNEL

$M_\infty = 8$ AIR $R_\infty = 0.1\text{-}10.7 \times 10^6$

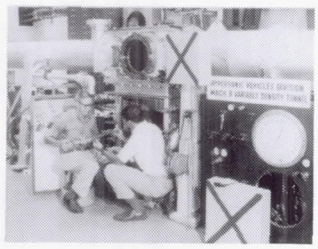

31-INCH M-10 TUNNEL

$M_\infty = 10$ AIR $R_\infty = 0.4\text{-}2.4 \times 10^6$

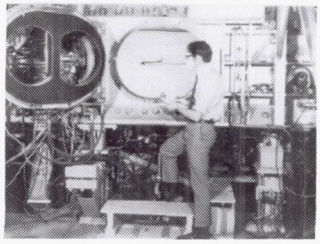

NITROGEN TUNNEL

$M_\infty = 17$ N_2 $R_\infty = 0.35 \times 10^6$

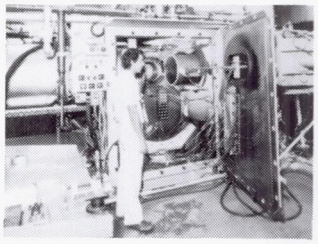

HELIUM TUNNEL

$M_\infty = 19\text{-}21.6$ He $R_\infty = 3.5\text{-}12.5 \times 10^6$

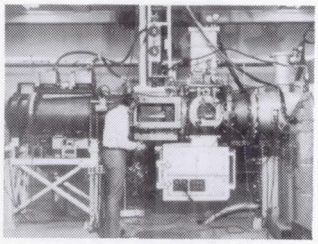

at a single installation to study the effects of Mach number, Reynolds number, test gas, and viscous interactions on the hypersonic characteristics of aerospace vehicles. Several modifications are being made to the facilities to improve their reliability, flow quality, and capability.

Rayleigh-Raman Scattering Measurements

An instrument to measure local gas density has been installed and tested in the 20-Inch Mach 6 Tunnel as part of current work to provide nonintrusive measurements for the National Aero-Space Plane CFD validation effort at Langley Research Center. This instrument was designed to provide single-point density measurements using the Raman scattering approach as well as one-dimensional local density profiles that combine Rayleigh scattering with a Charge Coupled Device (CCD) camera for imaging. The initial tests were designed to define the potential of the technique and the improvements required to reach that potential. Measurements were made in the free-stream flow over the entire operating envelope of the facility.

The results of the Raman point measurements of density plotted against expected density (based on stagnation conditions) are shown, and the agreement is good. The data acquisition rate needs to be improved; this can be accomplished by using a higher frequency and/or energy laser source. It should be noted that the Raman measurement is sensitive only to the nitrogen content of the gas flow; this differs from the Rayleigh measurement, which is sensitive to all flow constituents. This difference was very significant for these measurements because, unlike the Raman data, the Rayleigh measurements do not correlate with free-stream density. To clarify, the dependence of the Rayleigh signal on stagnation pressure and temperature was established experimentally over a wide range of run conditions. The Rayleigh data indicate that the Rayleigh signal is probably due to a free-stream nucleation process. Significantly, these data also indicate that this measurement interference may disappear in a model flow field; therefore, one-dimensional density measurements may be possible in this region.

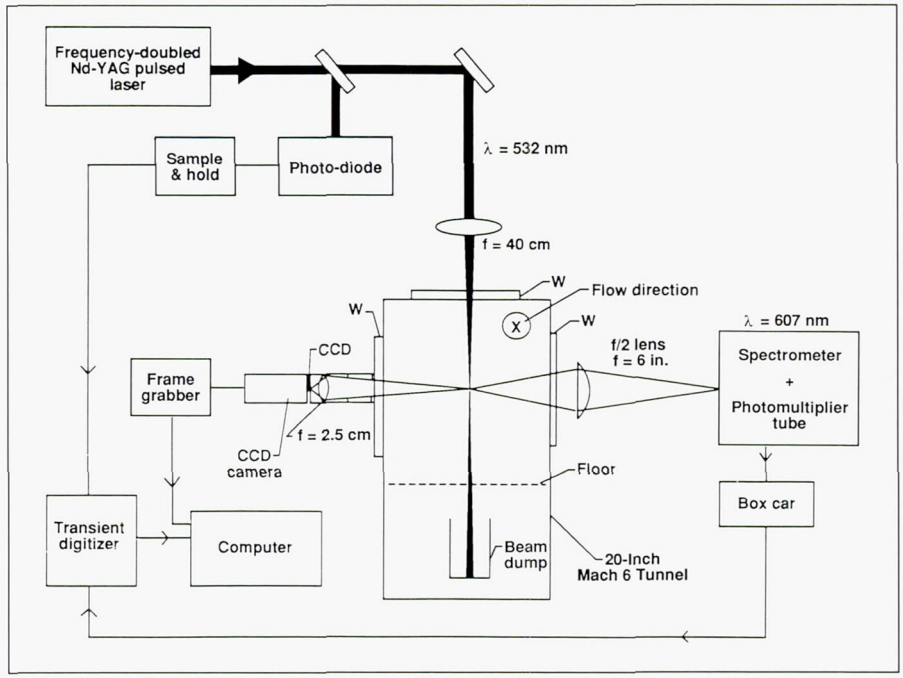

Experiment schematic.

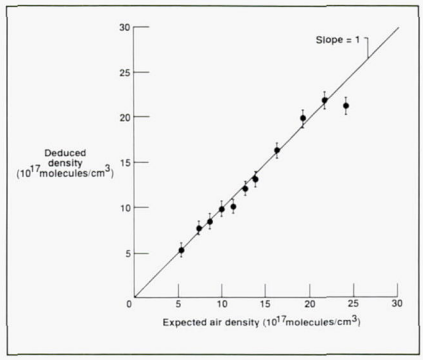

Raman measurements.

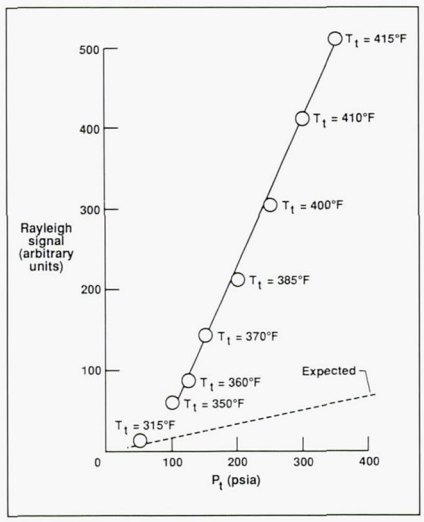

Rayleigh measurements.

(B. Shirinzadeh, 44604, M. E. Hillard, and R. J. Exton)

NASA/ONERA Cooperative Study: Aerodynamic and Aerothermodynamic Tests at Mach 6 and Mach 10 in Air

The National Aeronautics and Space Administration has entered into an agreement with the French aerospace research organization ONERA (Office National d'Etudes et de Recherches Aérospatiales) to perform aerodynamic and aerothermodynamic tests of the same model in Langley Research Center and ONERA hypersonic wind tunnels. The purpose is to compare the results, test techniques, and facilities used by both organizations. The configuration chosen was a generic, winged reentry vehicle consisting of an ogive nose section faired into a flat-sided fuselage, wings of similar airfoil section to those of the U.S. Space Shuttle orbiter, and wedge-shaped tip fins. The agreement included tests at Mach numbers of 6 and 10 in air and Reynolds numbers Re from 0.5×10^6/ft to 7.6×10^6/ft.

Force and moment tests were conducted in the 20-Inch Mach 6 Tunnel and 31-Inch Mach 10 Tunnel for an angle-of-attack α range from $-2°$ to $45°$ at Reynolds numbers of 0.5×10^6/ft, 2.0×10^6/ft, and 7.6×10^6/ft at Mach 6 and 0.5×10^6/ft and 2.2×10^6/ft at Mach 10 so that the effects of Mach and Reynolds numbers can be separated. Preliminary results show a slight rotation of the pitching-moment C_m curve due to Mach number (nose up for higher Mach number) for $\alpha > 8°$. The maximum lift-to-drag L/D ratio decreased with the higher Mach number.

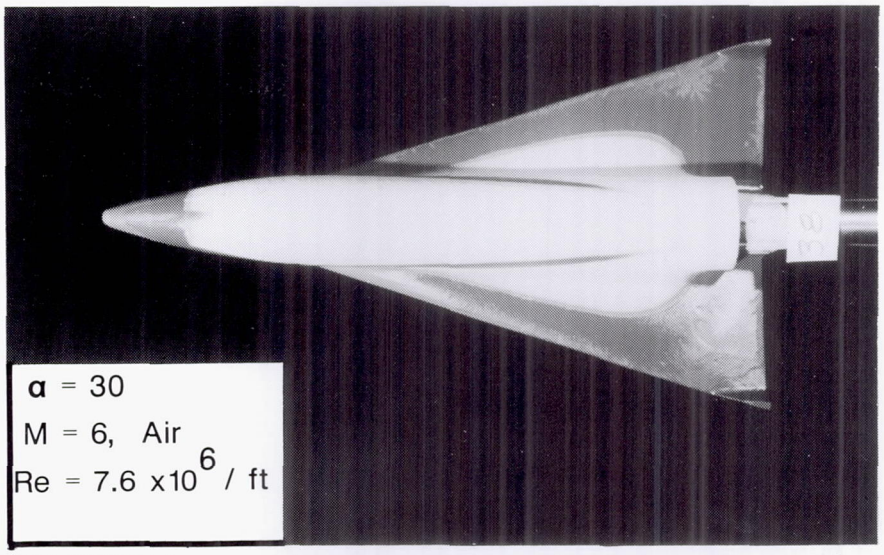

NASA/ONERA cooperative agreement thermal mapping with $\alpha = 30°$, $M = 6$ in air, and $Re = 7.6 \times 10^6$/ft. L-90-2931

Thermal mapping tests have been made for several conditions in the 20-Inch Mach 6 Tunnel. The phase-change paint technique was employed using Stycast models. Angles of attack of 0°, 15°, and 30° were tested for both windward and leeside heating. The leeside pattern shown indicates low heating except in the nose and wing leading-edge regions. Heating due to vortex scrubbing on the sides of the fuselage can also be seen.
(G. J. Brauckmann, 45234)

Surface Pressure and Shock-Layer Pitot-Pressure Profiles for 6°/12° Cone/Flare at Mach 6 in Air

Surface pressure and shock-layer pitot-pressure profiles were obtained on a 6°/12° cone/flare model as part of a National Aero-Space Plane computational fluid dynamics code validation study. Tests were conducted in the 20-Inch Mach 6 Tunnel at Reynolds numbers Re of 2.0×10^6/ft, 5.9×10^6/ft, and 7.6×10^6/ft at an angle of attack of 0°.

The model was approximately 9.5 in. long with a flare starting at 6 in. from the nose. Pressure orifices were located in a single line at 22 longitudinal stations (0.25-in. spacing) and at 90° circumferential increments for four longitudinal stations. The nose radius was sharp for most of the tests. Several runs were made with an 0.060-in. nose radius.

The pitot-pressure survey was performed with a miniature probe having a diameter of 0.013 in. The probe entrance was flattened into an oval shape with a height of approximately 0.007 in. The pressure transducer was water cooled and located approximately 2.5 in. from the probe tip. Surveys were made by traversing from a given orifice on the model surface through the shock layer.

Preliminary data obtained at a Mach number M of 6, Re of 7.6×10^6/ft, and nose radius of 0.060 in. are shown. The

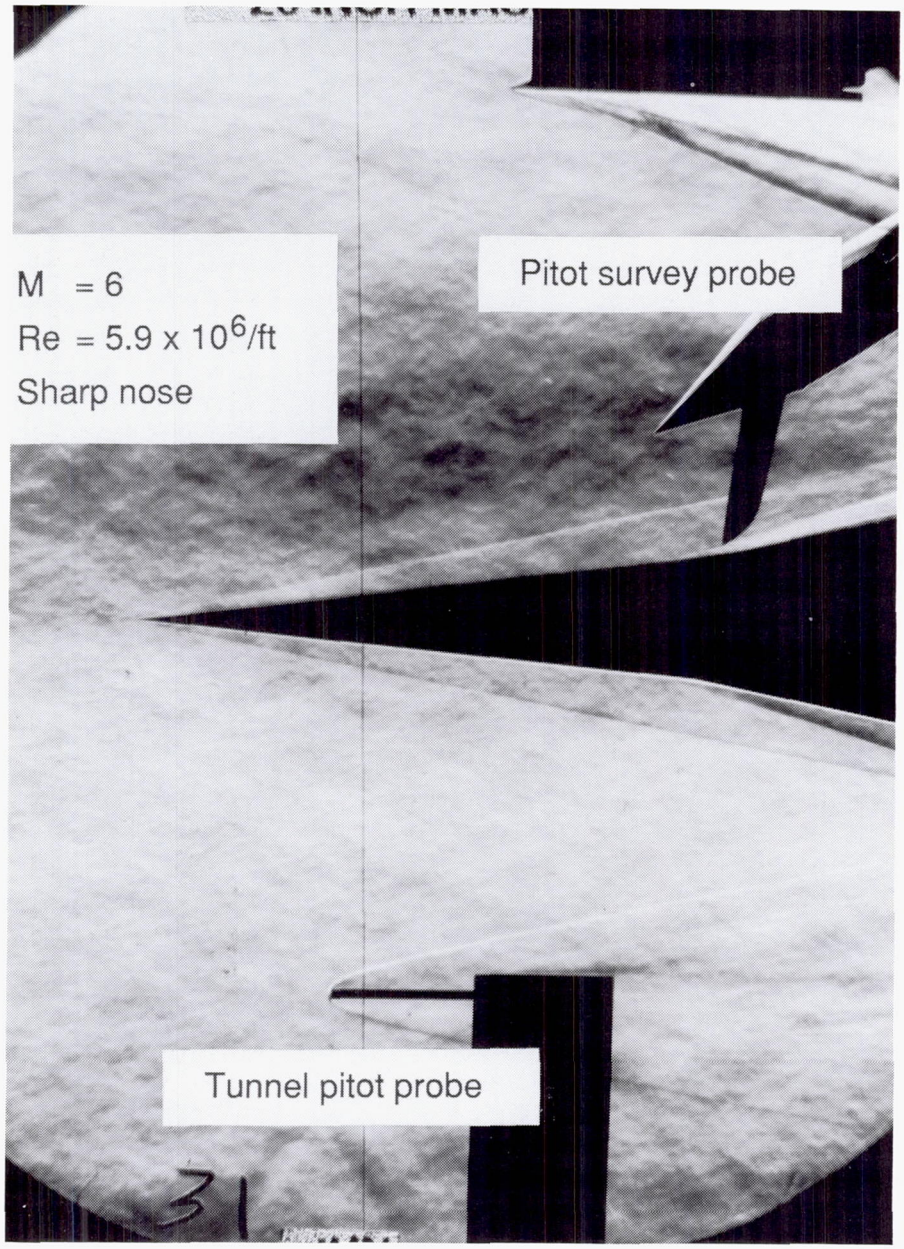

Schlieren photograph of cone/flare model and pitot survey probe in 20-Inch Mach 6 Tunnel.

surface pressure plot indicates a pressure rise before the flare is reached, possibly due to a small separated region in front of the flare moving the shock forward, or due to pressure feeding upstream through the boundary layer. The pitot profile has three plateau regions that include the boundary layer, the interior shock from the flare, and the bow shock. Schlieren photographs were also obtained to aid in interpretation of the data.

(G. J. Brauckmann, 45234)

Applications of Optical Fluorescence Thermography Imaging System

An optical fluorescence thermal imaging system has been developed for hypersonic aerothermodynamic studies using a two-color phosphor thermography technique. Thermal images provide temperature data with time for surface heat-transfer calculations. Temperature-sensitive ceramic coatings, or phosphors, are used. When excited by ultraviolet radiation, these coatings fluoresce visually. Test measurements are based on relative wavelength fluorescence.

Aerothermodynamic tests were performed using the thermal imaging system in various hypersonic facilities at Langley Research Center. Tests were conducted in the Hypersonic Helium Tunnel at Mach 20 to map heating distributions on epoxy plastic models of a Personnel Launch System (PLS) lifting body (as shown in the figure) and a winged transatmospheric vehicle. Tests showed detailed leeward and windward surface heating patterns. Measurements also were made for quantitative heat-transfer analysis on a glass/ceramic model of an aeroassisted orbital transfer vehicle (AOTV). These measurements were made alongside thin-film instrumentation. Tests were conducted in the Hypersonic CF_4 Tunnel at Mach 6 to simulate aspects of real-gas effects on payload heating. Tests have revealed complex heat flow through the model due to the number of gauges at the surface and conduction through gauge wiring. In a separate study in the 20-Inch Mach 6 Tunnel, thermal mapping

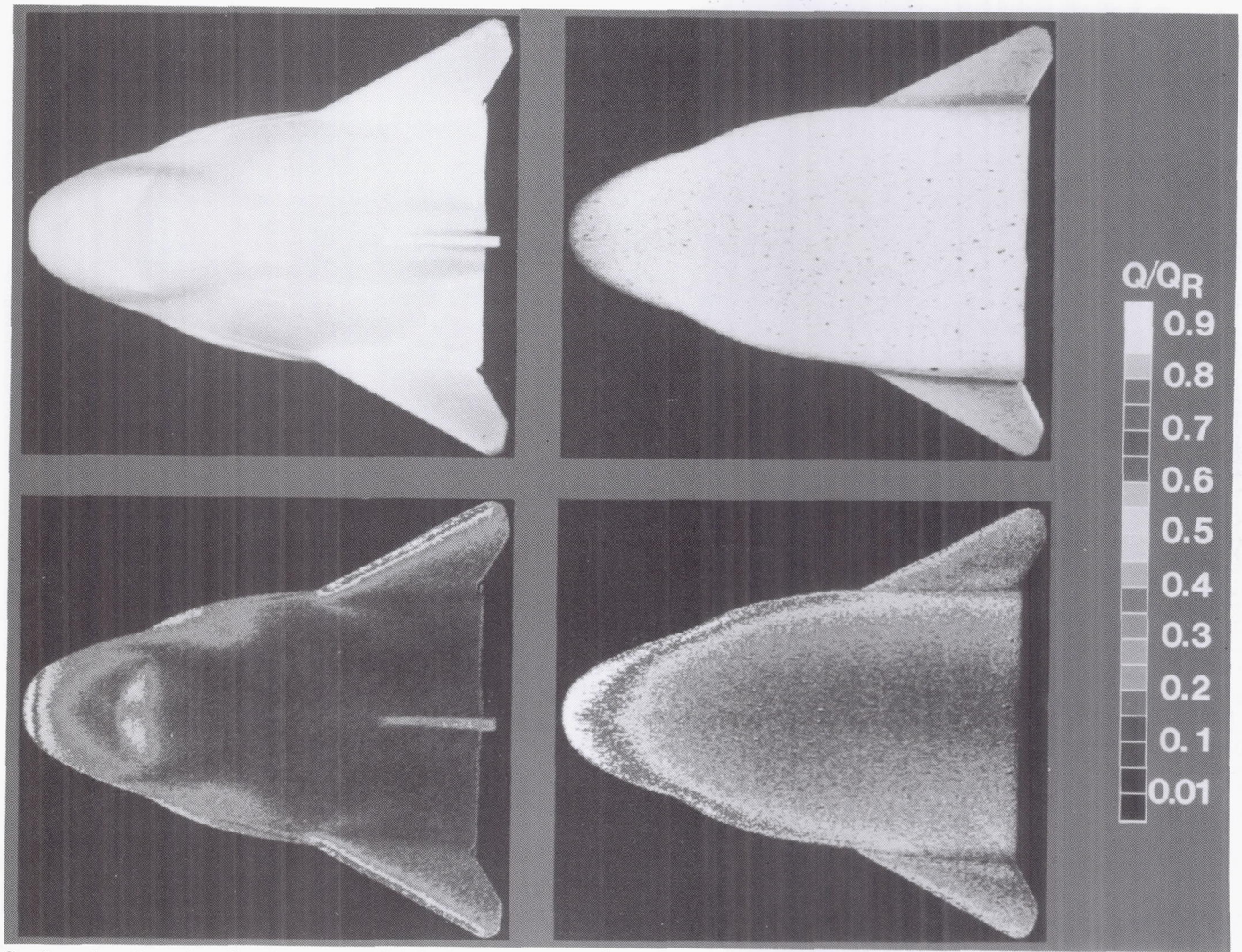

Surface heating distribution on PLS lifting body at Mach 20 in helium (angle of attack = 16°, Reynolds number based on model length = 6×10^6, and wall temperature/total temperature = 0.45). L-89-13161

data were taken to support analysis of pressure measurements.

Most recently, in the 31-Inch Mach 10 Tunnel, tests were conducted for computational fluid dynamics code calibration using cast ceramic quartz models of a Space Shuttle orbiter and a National Aero-Space Plane forebody. Ceramic quartz fidelity models are being developed simultaneously with optical fluorescence thermography techniques to provide inexpensive and accurate aerothermodynamic test models.

(Gregory M. Buck, 45240)

Experimental Investigation of Aerobrake Near Wakes

Flow in the near wake of an aeroassisted space transfer vehicle aerobrake configuration is of interest because of its potential influence on any payload located in this region. The chief concern is that the payload may experience high localized heating resulting from the impingement of a high-temperature free-shear layer. This free-shear layer is formed by the boundary layer separating off the shoulder around the entire periphery of the aerobrake and tending to converge in the near-wake region.

In one series of tests in the 20-Inch Mach 6 Tunnel, the magnitude and distribution of this impingement heating were measured on a simulated payload (a cylinder) behind an 0.22-scale model of the Aeroassist Flight Experiment vehicle forebody. The oil-flow technique was used in a second series of tests to visualize surface streamline directions. More recently, the magnitude and distribution of surface pressures on the payload were also measured

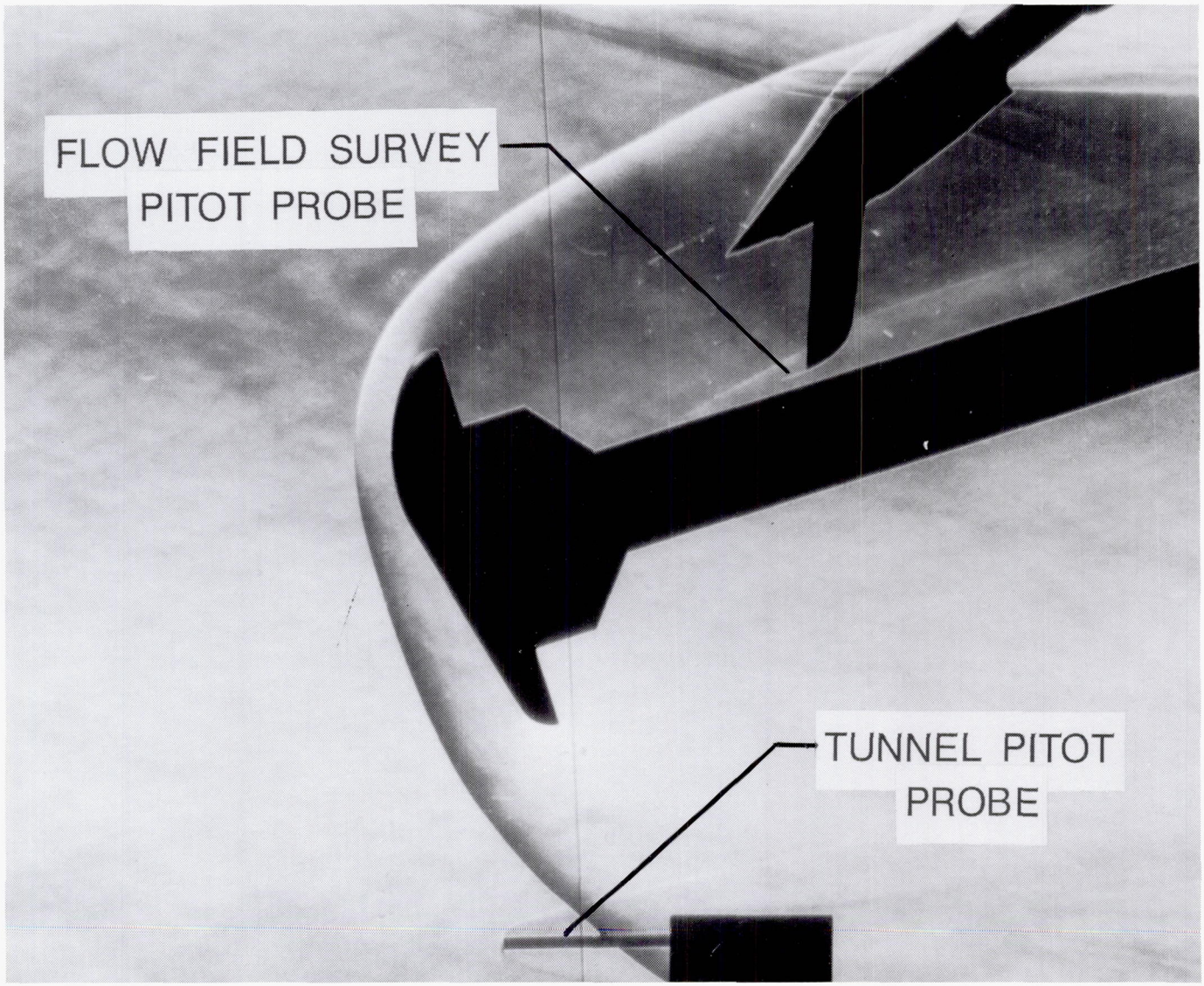

Schlieren photograph showing 0.22-scale model of Aeroassist Flight Experiment vehicle forebody with a simulated payload in 20-Inch Mach 6 Tunnel at $\alpha = 0°$.

in the 20-Inch Mach 6 Tunnel. Heating and pressure tests were carried out with the same model configuration and at the same run conditions. The tests were conducted with the model at angles of attack α from $-10°$ to $+10°$ and at nominal free-stream unit Reynolds numbers of 0.5×10^6/ft and 2.0×10^6/ft. In conjunction with the surface pressure measurements, an 0.013-in.-diameter traversing pitot-pressure probe was used to perform flow surveys in the near-wake region between the payload surface and the bow shock with the model at an angle of attack of $0°$.

Preliminary results indicate that the trends in the heating and pressure distributions are very similar. Values of heating and pressure are very low near the aerobrake base, but in the free-shear layer impingement region, the heating and pressure are approximately 40 and 13 percent, respectively, of the aerobrake stagnation point values. The free-shear layer impingement region is well defined by peaks in both heating and pressure levels and by surface oil-flow streamlines. Locations of the free-shear layer and the reattachment shock downstream of the impingement region were detected in the wake flow field by the traversing pitot-pressure probe.

(M. DiFulvio, W. L. Wells, and G. C. Ashby, Jr., 45229)

Scramjet Inlet Testing at Mach 6

Careful design of primary engine components such as the inlet is necessary to exploit effectively the potential of propulsion-airframe integration for hypersonic cruise vehicles such as the National Aero-Space Plane (X-30). In order to identify geometric parameters pertinent to improved inlet performance, two existing three-dimensional sidewall compression inlet wind tunnel models with leading-edge sweeps of 30° and 70° have been tested in the Hypersonic CF_4 Tunnel at Mach 6. The models represented moderate to highly swept configurations and were tested over a range of contraction ratios, cowl locations, and Reynolds numbers. The models were instrumented with 42 static pressure orifices distributed on the sidewalls, baseplate, and cowl. Schlieren movies were made of each test for flow visualization of the entrance plane and cowl region.

In order to obtain an approximate characterization of the flow field, a modification to the two-dimensional inviscid oblique shock theory was derived to accommodate the three-dimensional effects of leading-edge sweep. This theory qualitatively predicted the reflected shock structure/sidewall impingement locations and the observed increase in spillage with increasing leading-edge sweep. The primary effect of moving the cowl forward was to capture the flow that would have otherwise spilled out ahead of the cowl. Increasing the contraction ratio (moving the sidewalls closer together) increased the number of internal shock reflections and hence incrementally increased the sidewall pressure distribution. Significant Reynolds number effects were noted over a small range of Reynolds numbers.

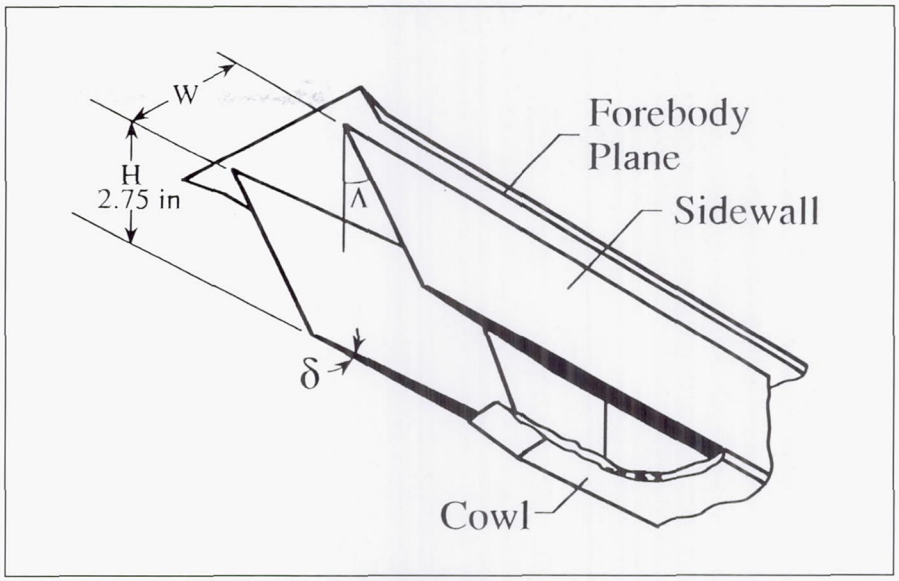

Inlet model shown in flight orientation.

The present work represented the largest model tested in the Hypersonic CF_4 Tunnel to date. In these tests, the tunnel remained started following model injection. Based on measured static pressures on the tunnel nozzle wall, no significant blockage effects were noted. In addition to evaluating the effects of various geometric parameters on the performance of the inlet, this research provides an enhanced computational fluid dynamics code calibration data base because data for a virial gas environment were obtained.
(Scott D. Holland, 45248)

Aerothermodynamic Measurements on Proposed Assured Crew Return Vehicle

Langley Research Center is studying a lifting-body concept as a candidate for the Assured Crew Return Vehicle (ACRV) which would serve as a safeguard for Space Station *Freedom* personnel. This configuration, which also is being studied as a candidate for the Personnel Launch System (PLS), is similar to the NASA HL-10 and M2-F2 and the U.S. Air Force X-24A lifting-body concepts studied in the 1960's. An 0.02-scale representation of the proposed configuration was tested in the 31-Inch Mach 10 and 20-Inch Mach 6 Tunnels (in air) as well as the Hypersonic CF_4 Tunnel and the Hypersonic Helium Tunnels at Mach 6 and Mach 20, respectively, to develop an experimental aerothermodynamic data base. Thermal mapping patterns, heat-transfer distributions, and surface streamline patterns were obtained at angles of attack of 0° to 40° and unit Reynolds numbers of 0.25×10^6/ft to 8×10^6/ft.

As expected, areas that experienced the highest heating were the nose and the tip-fin leading edges. Windward centerline heating distributions were compared

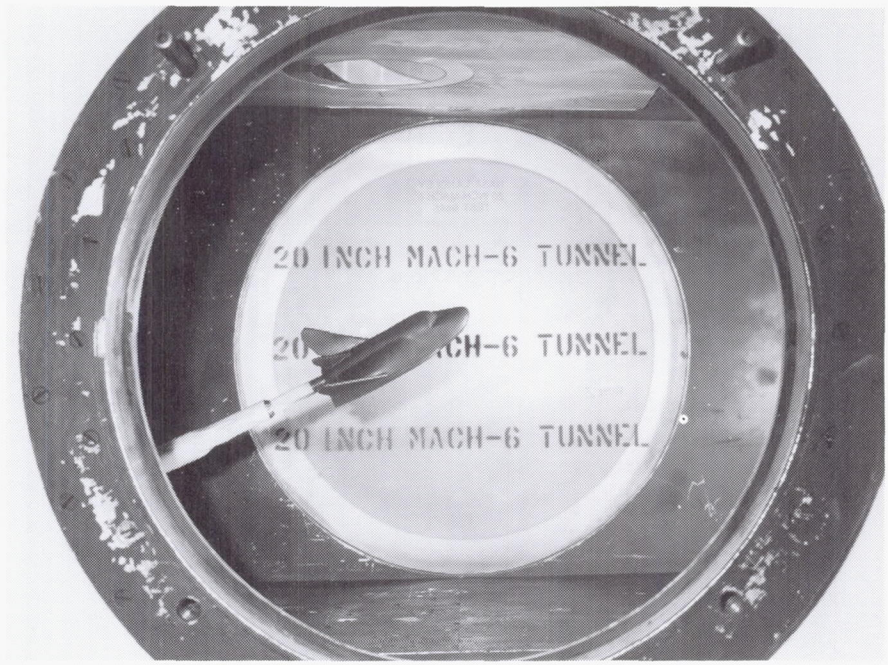

Thermal mapping model in 20-Inch Mach 6 tunnel. L-89-05736

with those obtained on the HL-10 lifting-body configuration, and the agreement was excellent. The effect of Reynolds number on windward centerline heating coefficients was negligible, whereas an increase in angle of attack, as expected, produced increased heating. Planform shaping was responsible for the appearance of streamwise-oriented embedded boundary-layer vortices that resulted in localized striation heating patterns on the windward surface. Shear-layer reattachment on the canopy face was observed at all test conditions and resulted in high heating rates. Leeward cross flow separation and centerline vortex reattachment were evident across the Reynolds number and angle-of-attack ranges, indicative of a complex flow field. Leeward reattachment near the base of the model, where control surfaces would be located, was observed in both the heating and oil-flow patterns.

(Thomas J. Horvath, 45236)

Assessment of Two Heat-Transfer Measurement Techniques

Because of the increased importance of heat-transfer measurements for computational fluid dynamics code validation and the subsequent increased demand for aerothermodynamic models, the Langley Research Center instrumentation capability is being severely taxed in the fabrication and installation of thin-film heat-transfer gauges. To increase the model completion rate, alternative sensor construction techniques are being explored.

A study is under way in the 31-Inch Mach 10 Tunnel to assess fabrication and installation refinements and requirements for thin-film and coaxial thermocouple heat-transfer sensors. This facility was chosen because of its excellent flow quality and uniformity. The study was designed to compare, for the same test model and free-stream conditions, the sensitivity, repeatability, durability, and accuracy of the two types of sensors and their refinements. Also included in the study was an evaluation of the relative ease of their fabrication and use. The selected models were flat-faced cylinders, instrumented on the front face and aligned normal to the flow. Heat-transfer data were obtained at conditions covering the current operating range of the facility.

Preliminary results indicate that the performance of the gauges that are painted on the model is comparable to that of the gauges that are sputtered.

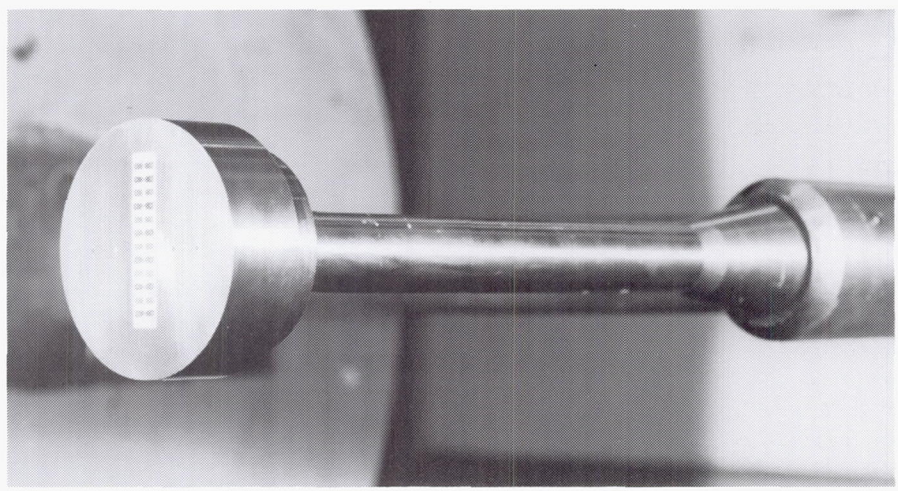

Heat-transfer model installed in 31-Inch Mach 10 Tunnel. L-89-13521

Hand-painted thin-film sensors significantly reduce the time required to instrument a model compared with the current mechanical process of sputtering. In order to translate the response of the thin-film resistance sensor into heating rates, the thermophysical properties of the sensor backing or substrate material must be known. A substrate calibration unit has been constructed at Langley Research Center to evaluate substrate properties. This unit is currently being utilized to study substrate properties associated with hand-painted thin-film sensors.

In addition, fast-response coaxial surface thermocouples are being evaluated for possible use in the Hypersonic Facilities Complex. Coaxial thermocouples are attractive from an economical viewpoint because they can be reused many times and are simple to install. The data from the coaxial thermocouples are presently being analyzed to determine their usefulness as heat flux sensors in the hypersonic wind tunnels.

(Thomas J. Horvath, 45236)

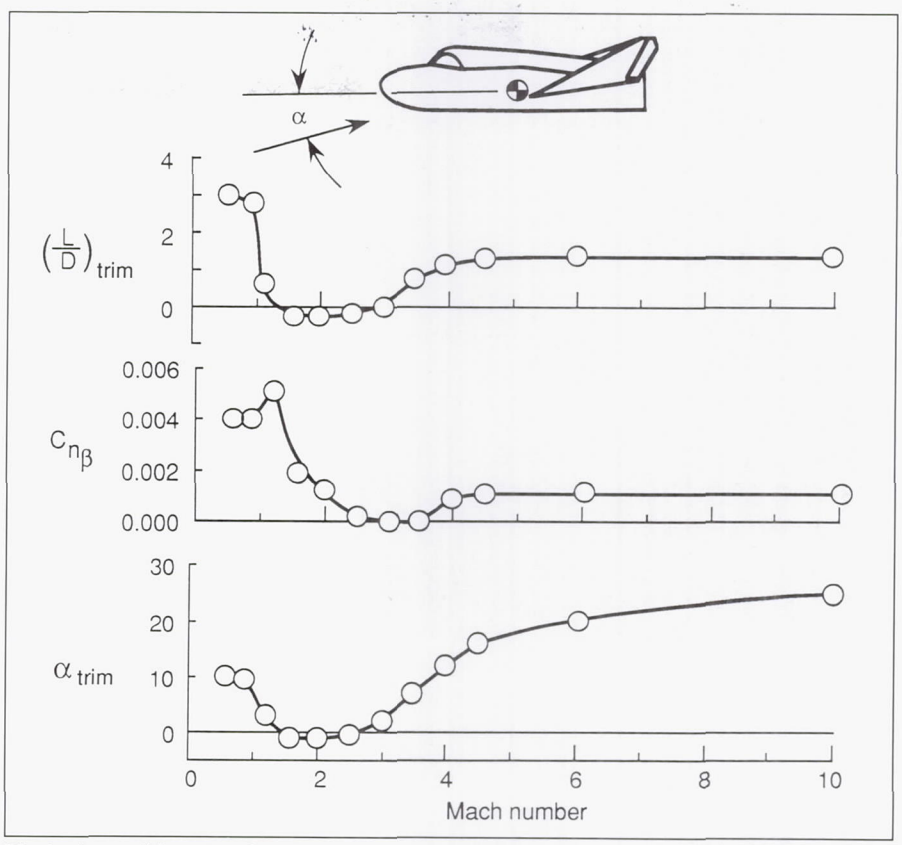

Variation of longitudinal trim characteristics for proposed ACRV configuration with Mach number. (No controls deflected; C_{n_β} is directional stability parameter.)

Experimental Aerodynamic Characteristics of Proposed Assured Crew Return Vehicle Lifting-Body Configuration

An extensive hypersonic aerodynamic/aerothermodynamic data base for the Langley Research Center proposed Assured Crew Return Vehicle (ACRV) lifting-body concept is being developed at Langley. The experimental data base, when completed, will include forces and moments, pressures, and heat transfer rates measured over the windward and leeward surfaces of the ACRV. These data will be used to calibrate computational fluid dynamics (CFD) codes over a wide range of hypersonic continuum-flow conditions.

Recently, tests were performed in the Hypersonic Facilities Complex to examine the effects of angle of attack, Reynolds number, and normal shock density ratio on measured aerodynamic coefficients for the ACRV. The high normal shock density-ratio aspect of a real gas in thermochemical equilibrium was investigated at Mach 6 by testing in ideal air (a density ratio equal to 5.25) and in CF_4 (a density ratio equal to 12.0). The Reynolds number was varied from 0.60×10^6/ft to 7.5×10^6/ft in air and from 0.25×10^6/ft to 0.58×10^6/ft in CF_4. Comparison of these preliminary hypersonic results to aerodynamic measurements recently obtained in the high-subsonic, transonic, and supersonic speed regimes indicated that the vehicle has significant cross range capability due to its high lift-to-drag ratio at hypersonic speeds. One of the favorable attributes of this lifting-body configuration at subsonic and transonic speeds is its self-trimming capability (i.e., controls undeflected). As supersonic speed is attained, the vehicle loses this capability to produce a desirable trim condition and thus requires the aid of negative control deflections to produce a positive lift, a positive lift-to-drag ratio at trimmed conditions $(L/D)_{trim}$, and a trimmed angle

of attack $\alpha_{trim} > 0°$. At free-stream Mach numbers ≥ 4.0, trim characteristics are once again favorable with trim occurring at positive lift and near $(L/D)_{max}$.
(John R. Micol, 45250, and George Ware)

Investigation of Test Core in Hypersonic CF_4 Tunnel at Low Pressure

The Hypersonic CF_4 Tunnel uses tetrafluoromethane (CF_4) as a test gas, which allows a partial simulation of real-gas effects for hypersonic entry vehicle aerodynamic and aerothermodynamic research. The facility is usually operated with a reservoir pressure of approximately 1500 psia. Tests on vehicle configurations that fly at high altitudes require a much lower operating pressure. Tests were reported last year which demonstrated that the tunnel could be operated at a pressure as low as 110 psia and still produce a usable test stream of Mach 6. Recently, an abbreviated calibration was performed with a pressure rake having 41 pitot probes to determine the test-core size and uniformity at different axial distances from the nozzle exit for low-pressure operation.

Test-core size and uniformity for a total pressure of approximately 135 psia were found to be not significantly different from those at 1500 psia. At either pressure, the core size tended to diminish with distance from the nozzle exit. At the lower pressure, the uniform core size also decreased with run time (as shown in the figure). Analysis of the data indicates the need for additional vacuum pumping capability to reduce the pressure outside the core in the open-jet test section, thereby avoiding the reduction in core diameter. However, sufficient test time is available with the present facility components for heat transfer measurements or pressure measurements on blunt bodies. A diffuser has been designed and built to enhance significantly the flow recovery process and provide additional run time; this diffuser will be installed in 1990.
(R. E. Midden, W. L. Wells, and H. H. Senter, 45230)

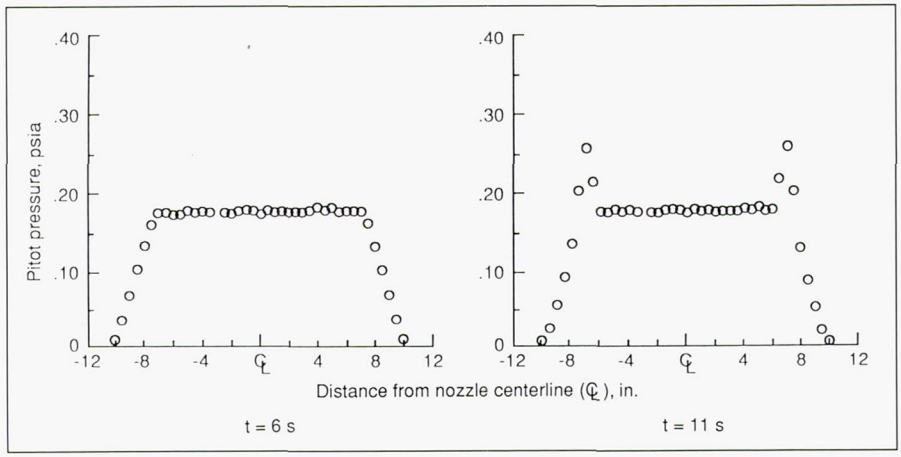

Pitot pressure distribution across test stream for two elapsed test times at 6 in. downstream of nozzle exit; total pressure is 134 psig.

Experimental Aerodynamics of General-Purpose Heat Source Modules

The hypersonic aerodynamic characteristics for general-purpose heat source (GPHS) modules were determined during a recent study in the 31-Inch Mach 10 Tunnel. The GPHS modules, which are rectangular brick-like shapes containing plutonium oxide pellets, are utilized in the radioisotope thermoelectric generator of the Galileo spacecraft. The objective of this study was to obtain representative hypersonic aerodynamics for the carbon-carbon modules experiencing radical ablation deformations at various angles of attack, sideslip angles, and roll angles. These data were requested by the Department of Energy in order to determine ablative heating and flight trajectories of GPHS modules in the event of reentry of the individual modules following an unanticipated breakup of the Galileo spacecraft.

Several full-scale modules were tested (as shown in the figure) which represented successive ablation of the module having one large surface that is oriented normal to the free-stream direction. The ablated GPHS module geometries had been determined from arc jet tests of actual modules at the Ames Research Center. The module on the left side in the figure is the unablated GPHS module; the module on the right side is an aluminum casting of the most extremely ablated module resulting from

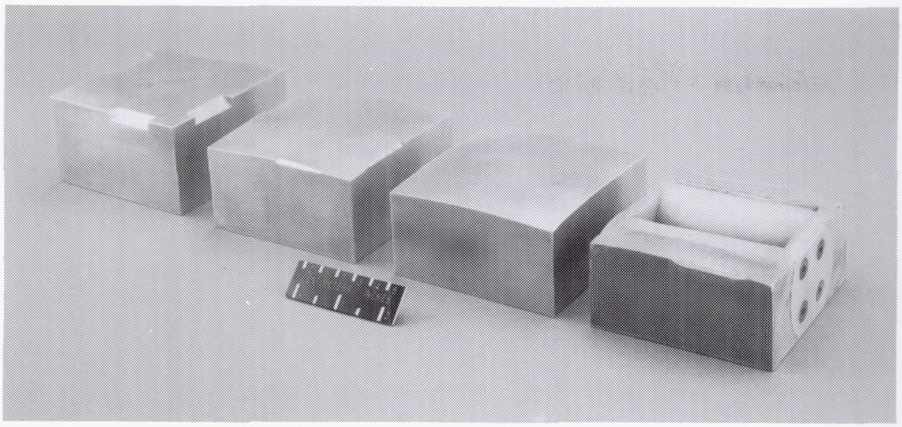

General-purpose heat source models. L-88-13176

the arc jet tests. The two middle bricks in the figure represent intermediately ablated modules. Also tested for comparison with the data from the completely ablated module casting was a simple geometric representation of the completely ablated configuration. Investigation results indicated that the effects of ablation on pitching and yawing moments are much more significant and hence play a larger part in influencing the module trajectories than do variations in axial, normal, and side forces for fixed module orientations.

(W. Pelham Phillips, 45239)

Experimental Investigation of Transatmospheric Vehicle Concept With Minimum-Drag Forebody

Experimental aerodynamic investigations of a transatmospheric vehicle (TAV) concept incorporating a minimum-wave-drag forebody shape have been performed at Mach numbers of 6 and 10. This study is part of an ongoing general research effort to determine the effects of Mach number, Reynolds number, density, and wall temperature ratio over a wide range of flow conditions on the hypersonic aerodynamic and aerothermodynamic characteristics of generic TAV configurations. The present force and moment studies were made in the 20-Inch Mach 6 Tunnel and 31-Inch Mach 10 Tunnel at angles of attack from $-4°$ to $20°$ at sideslip angles of $0°$ and $-2°$. Test Reynolds numbers (based on fuselage length) were 1.8×10^6 and 2.4×10^6 at Mach 6 and Mach 10, respectively. The model was designed to facilitate component buildup tests and utilized variable wing incidence for longitudinal trim. Flow-through and blocked-off engine modules were also tested. The model was mounted in the tunnels using a dorsal blade sting arrangement to minimize the effects of support interference on configuration aerodynamics.

Significant reductions in configuration drag at low angles of attack were realized for the minimum-wave-drag forebody when it replaced a modified 1/4-power-series forebody. The center-of-pressure location for the baseline TAV configuration (minimum-drag forebody) occurred at approximately the 57-percent model length station at a Mach number of 10. Configuration buildup test results indicate that incremental drag increases are attributed to the additions of the engine compression ramp, the flow-through engine, and the blocked-off engine. The experimental results of these studies were in agreement with predictions obtained using the Langley Research Center Aerodynamic Preliminary Analysis System (APAS).

(W. Pelham Phillips, 45239)

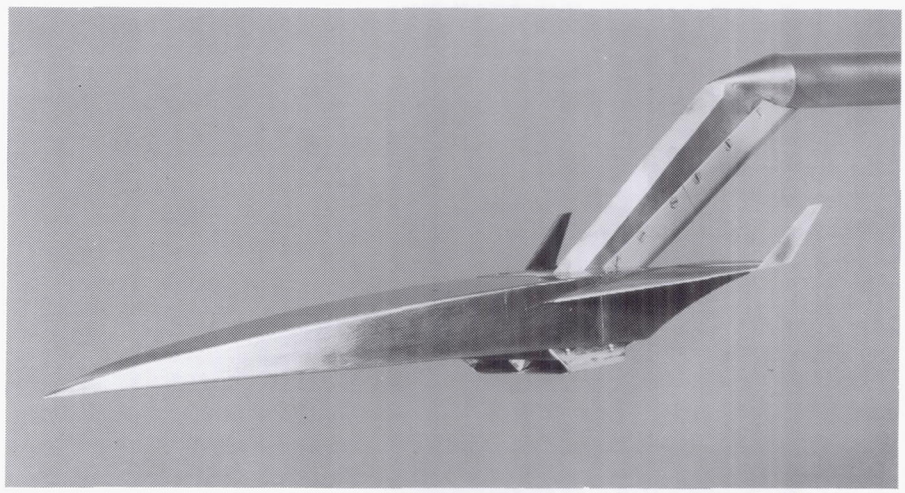

Transatmospheric vehicle model with minimum-drag forebody. L-89-4825

Hypersonic Data Base Development for Test Technique Demonstrator Supporting NASP Technology Maturation

A National Aero-Space Plane (NASP)-like configuration, designated the Langley test technique demonstrator (TTD), is being studied in the Hypersonic Facilities Complex (HFC) to develop test techniques for advancing particular NASP technology areas (for example, engine/airframe integration) and to develop an aerodynamic/aerothermodynamic data base. This data base is being developed by researchers in the Space Systems Division and the Applied Aeronautics Division of Langley Research Center. The HFC has the capability to produce data over a wide range of Mach numbers M, Reynolds numbers Re, and isentropic exponents γ; because of the excellent flows provided by these facilities, this data base is particularly well-suited for the calibration of advanced computational fluid dynamics (CFD) codes. Existing and newly developed test techniques are being and will continue to be used to develop the data base. The configuration and its test results are classified and therefore are not presented.

A comprehensive series of tests was planned for this configuration; these tests included force and moment measurements, pressure distributions, heat transfer and thermal mapping, and oil-flow and other flow visualization in the 20-Inch Mach 6, Hypersonic CF_4, 31-Inch Mach 10, and Hypersonic Helium Tunnels. The table in the figure shows the overall test matrix including tests that have been completed, as well as those that remain to be accomplished. Completed this past year as indicated in the table were a majority of the oil-flow, thermal-mapping, and other flow visualization tests; a significant portion of the force and moment tests; and some precursor pressure distribution tests that were performed on inexpensive models with limited instrumentation (primarily examining tunnel starting/blockage phenomena). The thermal-mapping tests included the phase-change coating technique and the two-color thermographic phosphor technique at Mach numbers of 6 and 10 in air and at Mach 20 in helium. Limited comparisons of the CFL3D CFD code were made with the helium tunnel pressure distributions with encouraging results.

(William C. Woods, 45238)

KEY: X TESTS COMPLETED
X/ PRELIMINARY TESTING

FACILITY M, γ Re/ft X 10^6	TEST TECHNIQUE					
	OIL FLOW	THERMAL MAPPING	SCHLIEREN, ELEC BEAM	HEAT TRANSFER	PRESSURE DIST.	FORCE & MOMENT
20-IN. M 6 TUNNEL 6, 1.4 .5 – 8	X	X	X			X
HYPERSONIC CF_4 TUNNEL 6, 1.2 .2 – .5						
31-IN. M 10 TUNNEL 10, 1.4 .25 – 2	X	X	NOT APPLICABLE		X/	
HYPERSONIC He TUNNEL 20, 1.667 1 – 18	X	X	X		X/	X

TTD test matrix.

Inlet Boundary-Layer Simulation at Hypersonic Speeds

The National Aero-Space Plane study has produced airplane concepts that feature an airbreathing propulsion system that is integrated with the fuselage forebody. The fuselage forebody produces a sizable boundary layer that is ingested into the propulsion system inlet. Meaningful inlet performance experiments require that the entire forebody be modeled or that an alternate method be utilized to produce an artificially simulated boundary layer. Because it is impractical to represent the entire forebody in inlet tests conducted in small hypersonic wind tunnels, a method that had shown promise for simulating the incoming boundary layer at supersonic speeds was investigated at hypersonic speed in the 20-Inch Mach 6 Tunnel.

A photograph of the test model, which consisted of a rectangular inlet model with parallel sidewalls, is shown in the figure. A honeycomb device was placed in the channel upstream of the cowl. The honeycomb had variations in cell size, length, and vertical distribution of length in order to selectively remove momentum from the flow to reproduce a naturally occurring boundary-layer momentum defect. Data included surface temperature

Boundary-layer simulation model.

and pressure measurements, inlet pitot-pressure surveys, and oil-flow photographs.

Preliminary analysis of the data indicates that the contoured honeycomb produces a simulated boundary-layer profile but that shock losses make the technique less promising at hypersonic speeds relative to supersonic applications.

(A. B. Blair, Jr., A. R. Porro, and W. R. Hingst, 45735)

IR Thermography for Hypersonic Flow

Infrared (IR) thermography is being investigated for providing nonintrusive qualitative and quantitative surface temperature

and heat transfer measurements on models in hypersonic facilities. This research activity has been conducted in the 20-Inch Mach 6 Tunnel and the 31-Inch Mach 10 Tunnel. The IR imager used is a single-detector 8-μm to 12-μm imager with substantial improvement in spatial resolution compared to the older generation imagers.

A series of tests were conducted on a proposed Personnel Launch System (PLS) lifting body in the 20-Inch Mach 6 Tunnel. The test conditions for the figure were a Mach number of 6, an angle of attack of 25°, and a Reynolds number of 7×10^6/ft. The IR image provides surface temperature distributions of the model 3 s after the model has been injected into the tunnel. The data were compared to streamline patterns obtained from oil-flow experiments for qualitative purposes. The thermal manifestations of some aerodynamic phenomena (such as separation and stagnation region and vortex impingement) are observed on the infrared image.

(Kamran Daryabeigi, 44745, Thomas J. Horvath, and Gregory M. Buck)

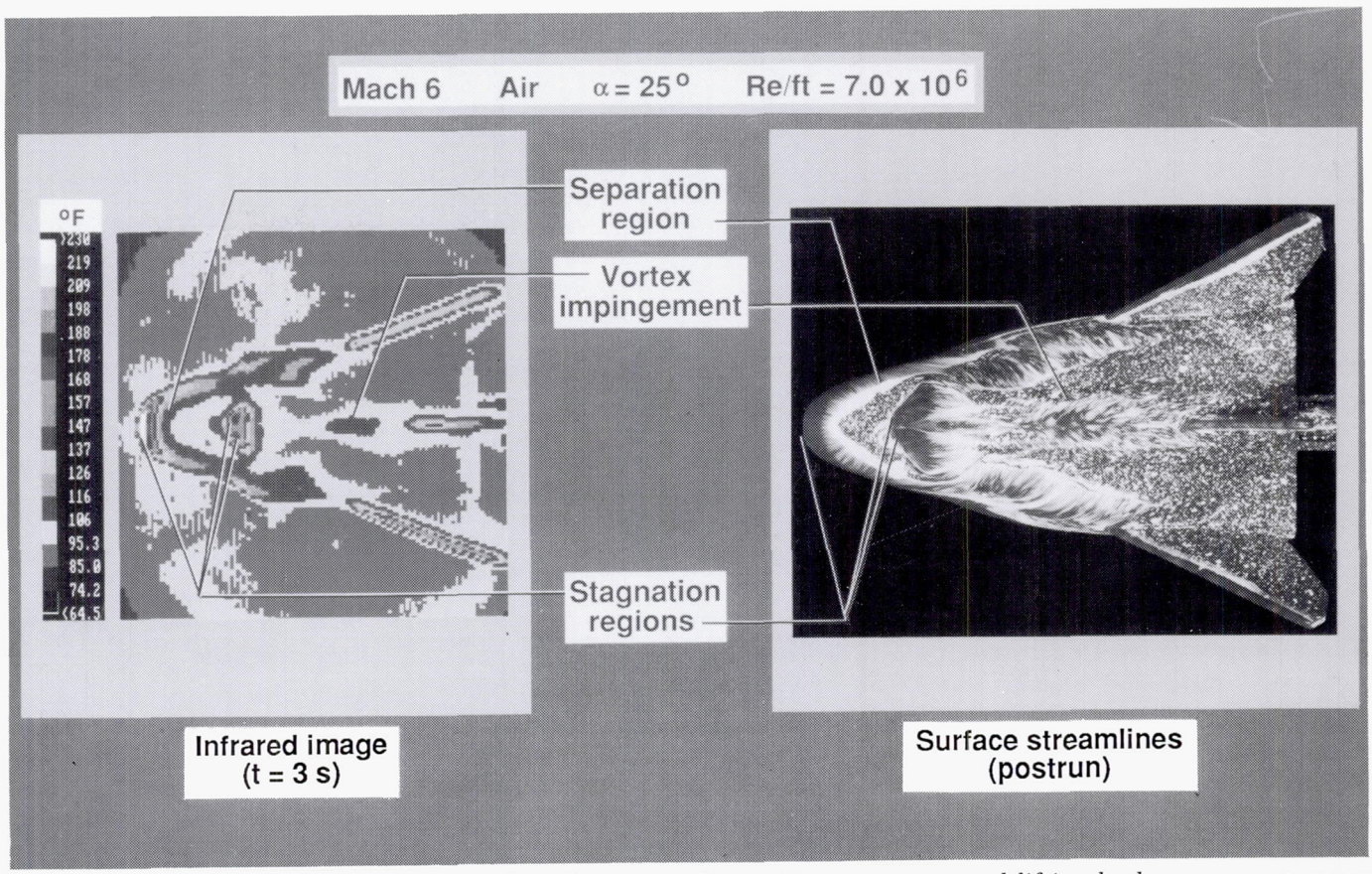

Comparison of infrared thermal image and surface streamline patterns on proposed lifting body. L-89-6327

Scramjet Test Complex

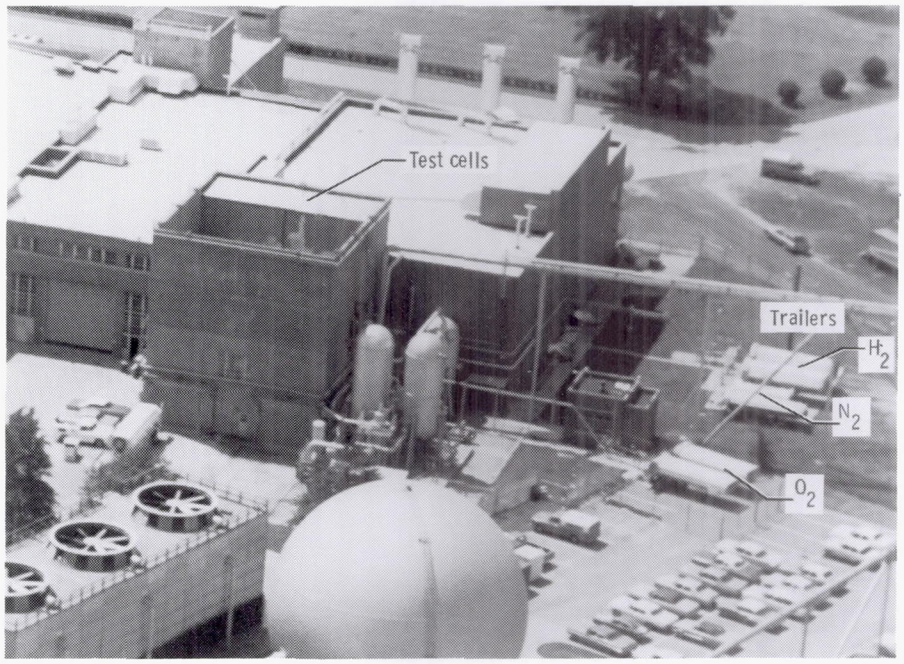

After an almost 15-year lull in interest for hypersonic flight, there is again a strong emphasis on the potential for a number of applications. These applications include an Aero-Space Plane or transatmospheric vehicle, which would be able to take off from a conventional runway and fly to orbit, as well as a variety of hypersonic airplane concepts for military reconnaissance, strike, or semiglobal transports. Langley Research Center has maintained a research team that has been working on basic hypersonics continuously throughout the last several decades. Facilities that played a key role at Langley in developing the present Space Shuttle configuration have been applied to a wide variety of other aerospace vehicles. Langley, the lead Center in defining Shuttle II, has been the only research organization in the Nation to continuously maintain a viable effort in hydrogen-fueled supersonic combustion ramjet propulsion since the 1960's. Ground tests of subscale engines conducted in the Scramjet Test Complex have demonstrated levels of net thrust sufficient to accelerate at Mach 4 and to cruise an airplane at speeds up to Mach 8 and beyond. These results are entirely consistent with the projection of attractive performance up to much higher speeds, even approaching orbital velocity.

A research program to develop technology for a hydrogen-burning airframe-integrated supersonic combustion ramjet (scramjet) propulsion system has been under way for several years at Langley. The experimental portion of this research consists of tests of engine components (inlets, combustors, and nozzles) and complete, component integration engine models.

Small-scale inlet tests for "screening" potential inlet designs are performed in a 9-in. by 9-in. Mach 4 blowdown tunnel. Larger scale inlet tests are performed in various other Langley aerodynamic wind tunnels. Small-scale direct-connect combustor tests that simulate a portion of the engine combustor are conducted in Test Cell #2 to provide basic research data on supersonic mixing, ignition, and combustion processes. The hot test gas is supplied to the combustor models by a hydrogen-air-oxygen combustion heater, which maintains 21-percent free oxygen by volume to simulate air with enthalpy levels ranging up to Mach 8 flight speeds. Various facility nozzles produce the desired combustor entrance flow conditions.

Designs from the individual component tests are assembled to form component integration engines so that tests can be conducted to understand any interactions between the various engine components and to determine the overall engine performance. These component integration tests are conducted in engine test facilities. The feature that separates these propulsion facilities from aerodynamic wind tunnels is their capability to produce true-velocity, true-temperature, and true-pressure flow for flight simulation.

The Combustion-Heated Scramjet Test Facility (CHSTF, Test Cell #1) uses a hydrogen-air-oxygen combustion heater to

Small-Scale Inlet Tests

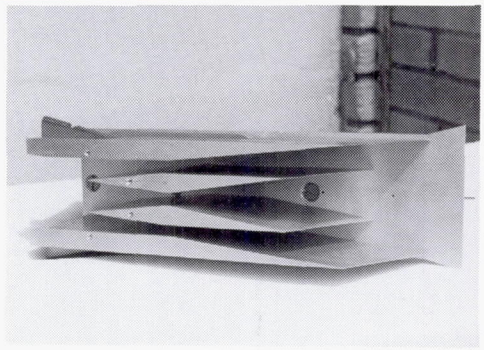

Inlet Model

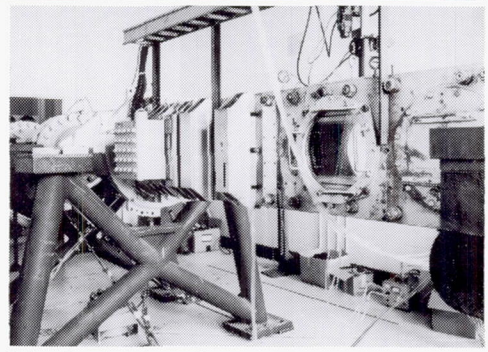

Mach 4 Blowdown Tunnel

Small-Scale Combustor Tests

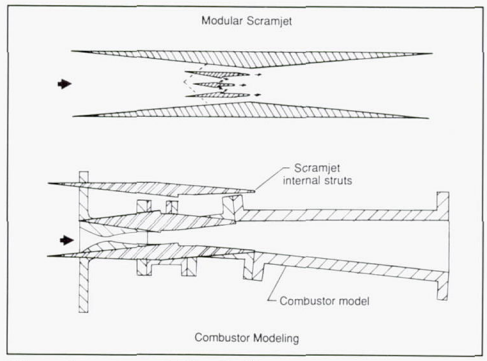

Combustor Modeling

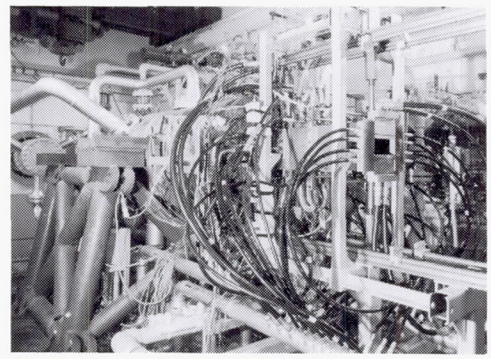

Test Cell # 2

Engine Model Tests

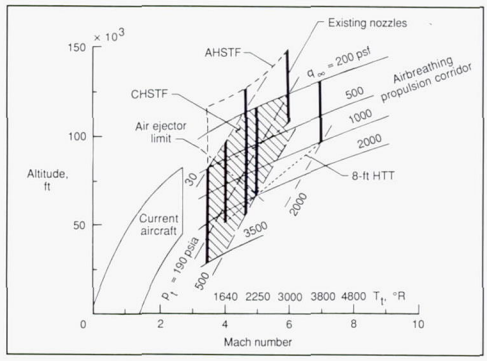

Potential Test Capability

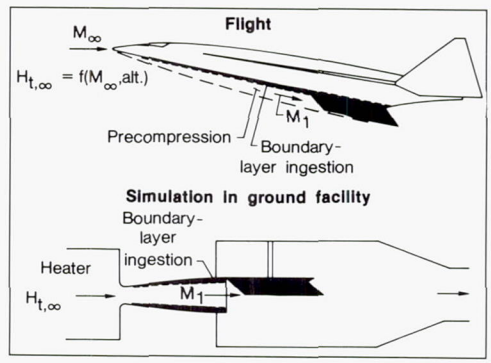

Flight Condition Simulation

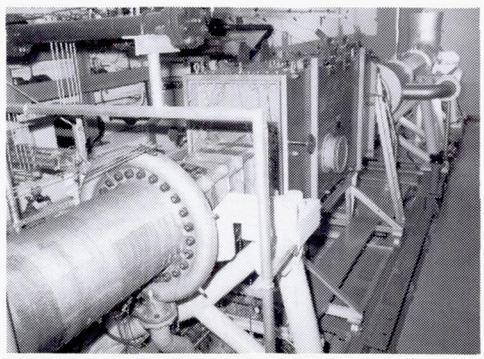

CHSTF; Test Cell # 1

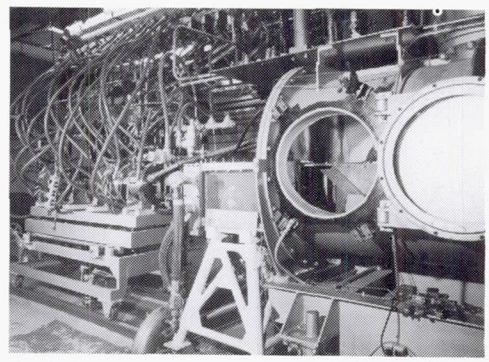

AHSTF

duplicate Mach 4 flight enthalpy. The test gas is exhausted to the atmosphere with the aid of an air ejector. A Mach 3.5 contoured nozzle with a 13-in.-square exit is presently attached to the heater to yield a free-jet tunnel flow (simulating Mach 4 flight conditions) for subscale engine tests. The Arc-Heated Scramjet Test Facility (AHSTF) uses an electric-arc heater to produce enthalpy levels corresponding to flight speeds up to Mach 8. The tunnel exhausts into a 100-ft-diameter vacuum sphere. Eleven-in.-square exit nozzles (Mach 4.7 and 6) are used to deliver a free-jet tunnel flow for scramjet engine tests. The same size models (frontal view approximately 6 in. by 8 in.) are tested in both these facilities.

An oxygen replenishment system and new facility nozzles are being added to the 8-Foot High-Temperature Tunnel (8-Foot HTT), which is presently part of the Aerothermal Loads Complex. This tunnel will then be capable of testing large-scale engines (approximately 20 in. by 28 in.), multiple engines, or engines that have full nozzle expansion surfaces at Mach numbers of 4, 5, and 7. In addition, the operational capability of the Combustion-Heated Scramjet Test Facility is being enhanced by a new test gas heater, a new Mach 4.7 nozzle, and a new vacuum sphere/steam ejector system. Upon completion of these modifications, the 8-Foot HTT, together with the smaller scale facilities described, will comprise a Scramjet Test Complex at Langley unequaled in the Western World. The potential operational envelope of this complex would extend over a flight Mach number range from 3.5 up to 7. Some of the current testing in these facilities is classified, thus restricting the amount and content of test results that can be reported in the open literature.

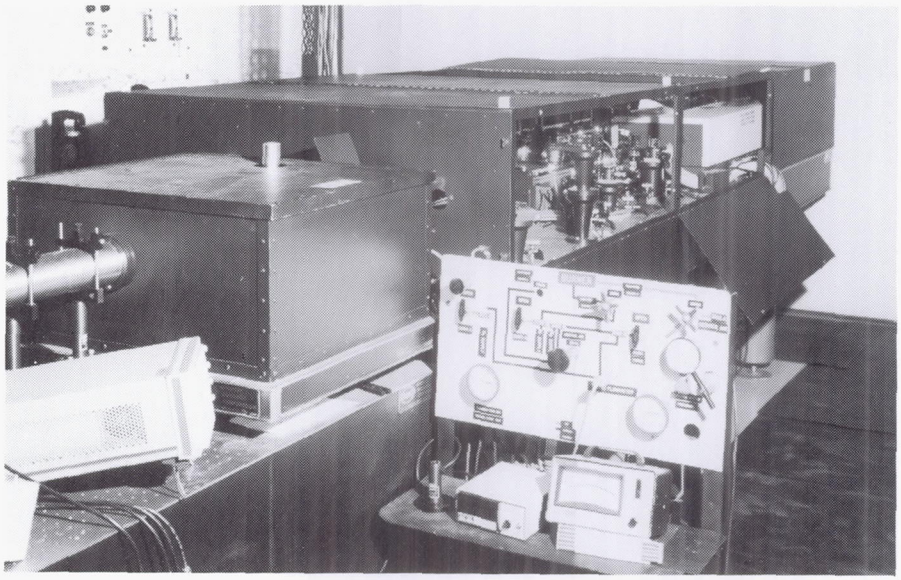

CARS optical system in NDL facility. L-85-5639

Considered part of the Scramjet Test Complex is a Nonintrusive Diagnostics Laboratory (NDL), which contains the Coherent Antistokes Raman Spectroscopy (CARS) optical system and laboratory scale combustion devices used for fundamental combustion studies. Four devices that include an electronically heated furnace and three hydrogen-air combustion devices (a subsonic diffusion burner, a supersonic diffusion burner, and a premixed flat flame burner) provide an air temperature range from 300 K to 2200 K and a velocity range from air at rest to Mach 2 for study. Nonintrusive simultaneous measurements of temperature, nitrogen, and oxygen density have been made with the CARS system. The laboratory facility, shown in the figure, provides space for the various development versions of the CARS optical system and facilities for handling air, hydrogen, and oxygen at high pressure as well as an exhaust duct for the burner products. Computer facilities are adjacent to the laboratory for burner control and data collection and processing. A new CARS system, configured to endure the harsh environment (>150 acoustic dB), is being assembled for use in Test Cell #2.

Investigation of Mixing Augmentation for Parallel Supersonic Fuel Injection

The objective of this research is to explore techniques to enhance mixing in scramjet (supersonic combustion ramjet) combustors. For high-speed propulsion applications, the fuel is used as a coolant. Injecting heated fuel from downstream-facing nozzles produces thrust. The disadvantage of downstream injection is that it results in long mixing lengths. The technique discussed here used wall-mounted ramp fuel injectors to improve mixing of fuel injected nearly parallel into a Mach 2 scramjet combustor flow.

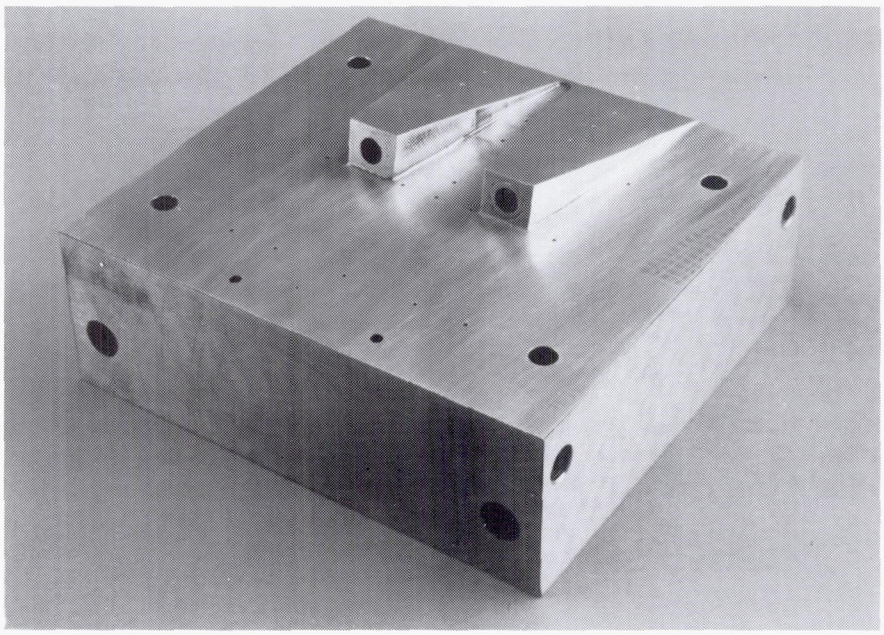

Parallel injector. L-88-8392

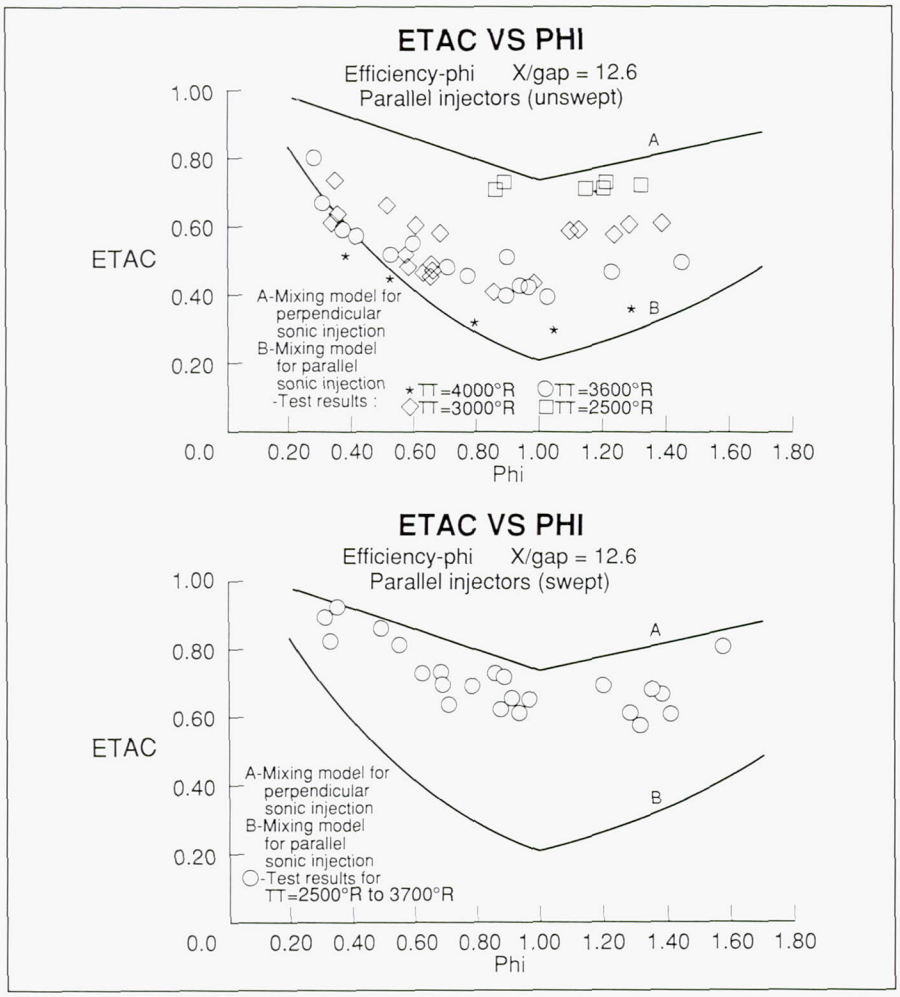

Variation of combustion efficiency with fuel equivalence ratio.

The first figure is a photograph of the fuel injector block with swept wall ramp injectors. The swept ramps were used to induce additional vortical motion into the oncoming air and enhance the mixing. Another block with ramps with unswept sidewalls was also tested. The results are shown in the second figure. The plots show the computed efficiency (ETAC) as a function of the amount of fuel added/stoichiometric fuel (phi) for the configurations at a distance 12.6 duct heights from the injectors. Tests were conducted for total temperatures from 2500°R to 4000°R. The swept data indicated little temperature dependence, and the fuel mixed nearly as well as the mixing model predicted for perpendicular injection. The unswept design exhibited total temperature dependence and mixed more like the parallel injection prediction at high temperatures. Tests were conducted in the AHSTF.

(G. Burton Northam, Diego C. Capriotti, Carl S. Byington, and Issac Greenburg, 46248)

Subscale Scramjet Engine Tests

Hydrogen-burning combustion tests have been conducted of three different subscale supersonic combustion ramjet (scramjet) engine models. The tests were conducted in cooperation with Johns Hopkins University Applied Physics Laboratories (JHU APL), Pratt and Whitney (P&W), and Rocketdyne (RD). Performance results obtained during these tests have increased the scramjet data base in support

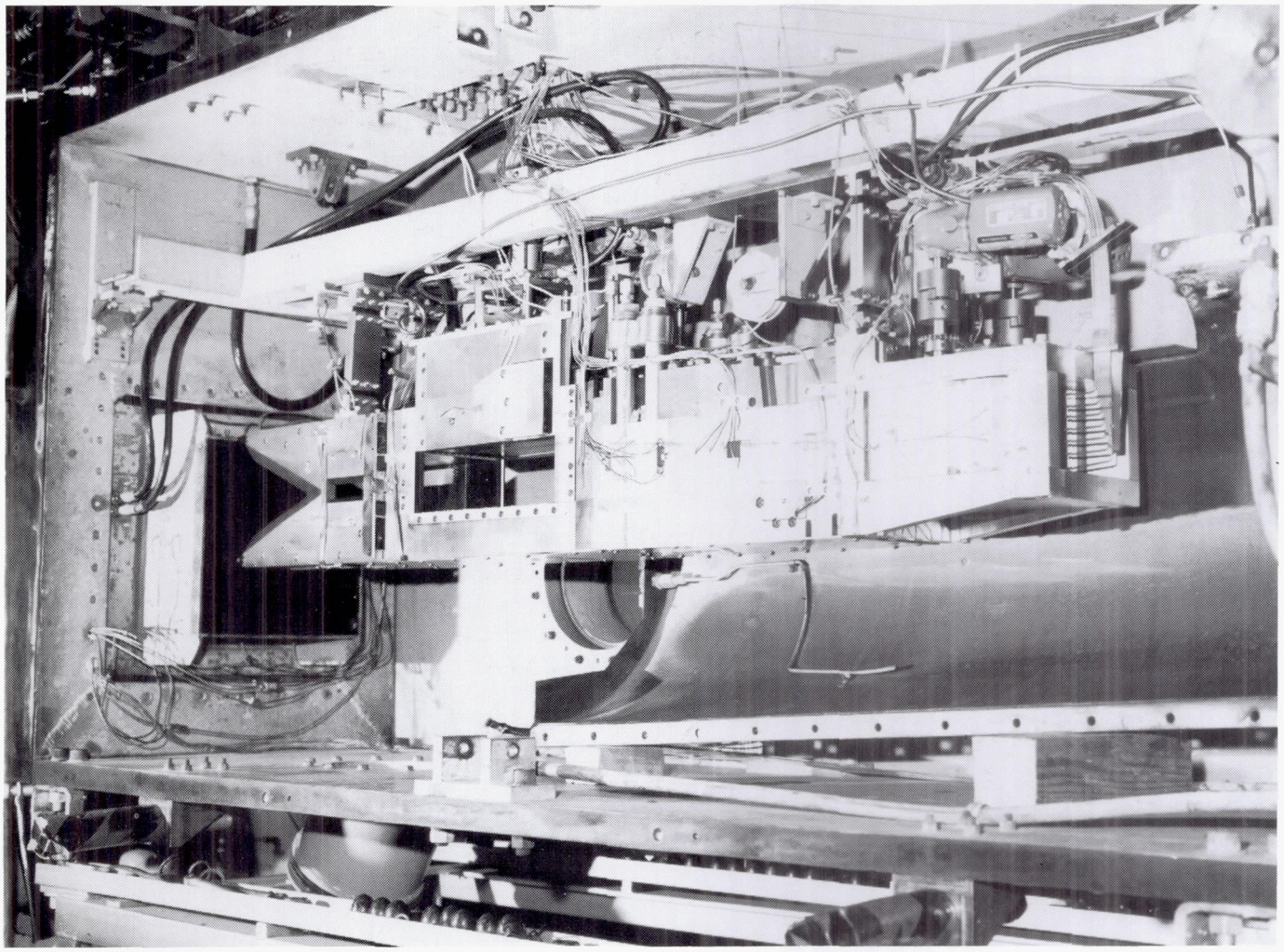

JHU APL NASP B-1 engine model installed in Combustion-Heated Scramjet Test Facility. L-88-09836

of the National Aero-Space Plane (NASP) Technology Maturation Program.

The engines were tested in the Arc-Heated Scramjet Test Facility (AHSTF) at simulated conditions for flight Mach numbers of 4.7, 5.5, 7.0, and 8.0 and in the Combustion-Heated Scramjet Test Facility (CHSTF) at simulated flight conditions for Mach 4 and 5.5. During the calendar year 1989, a total of approximately 600 tests were conducted, of which a majority were combustion tests. A representative model of the JHU APL engine installed in the CHSTF is shown in the figure. Measured quantities are wall static pressure distributions, hydrogen fuel flows, longitudinal force, heat fluxes, pitot pressures, gas samples, and high-frequency pressure measurements. Ambient temperature hydrogen fuel was injected from many different injector configurations to investigate the effectiveness of perpendicular and tangential injection and hole size, spacing, and patterns. Flameholding was demonstrated during most tests with hydrogen fuel injected from upstream and downstream stations. Combustion-induced inlet interaction limits were explored. The effectiveness of many other different parameters also was investigated as shown.

(Earl H. Andrews, Jr., R. Wayne Guy, James M. Eggers, Scott R. Thomas, and Randall T. Voland, 46240)

Fluctuating Pressure Loads in Scramjet Engine Model

Unsteady pressure loads in the boundary layers of scramjet engines are of interest from

the standpoints of combustion instability onset and structural design of engine components. These fluctuating loads are generated by combustion processes, boundary-layer turbulence, and shock/boundary-layer interactions. A scramjet engine model designed by the Johns Hopkins University Applied Physics Laboratories was installed in the Combustion-Heated Scramjet Test Facility at Langley Research Center. Pressure transducers were installed at eight locations on the top wall of the scramjet model, including the inlet and combustor sections as shown in the first figure. During a 25-s test run, step changes in heat release rate were induced by a fast-acting valve in the hydrogen fuel supply line, as shown by the fuel flow increase in the upper curve (second figure).

In the second figure, time histories for sensor locations #4 and #5, upstream of the combustor, show a dramatic effect of these changes in the heat release rate on the fluctuating pressures in the boundary layer. Peak-to-peak pressures range from approximately 7 psi (sensor #4) to 10 psi (sensor #5) at the high heat release rate as compared to less than 2 psi peak to peak for the low heat release rate. Assuming a Gaussian-type probability density distribution for these pressures, the corresponding sound pressure levels at the high heat release rates would be 172 dB and 175 dB, respectively. These levels are at least 11 dB to 14 dB above corresponding levels at the low heat release rates.

These data suggest that combustion processes can generate large fluctuating pressures that propagate upstream through the sublayer portion of a supersonic boundary layer. This phenomenon has important implications for scramjet engine design.

(Tony L. Parrott, 45273)

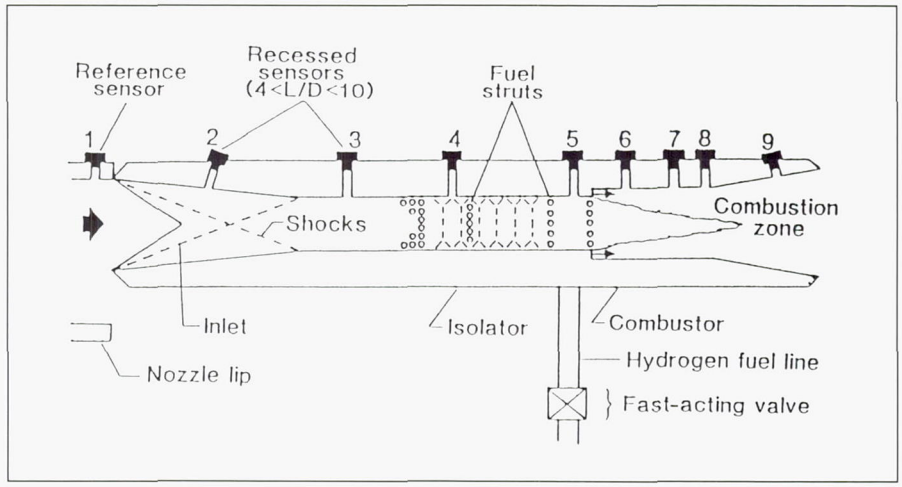

Sketch of scramjet engine model with pressure sensor locations indicated.

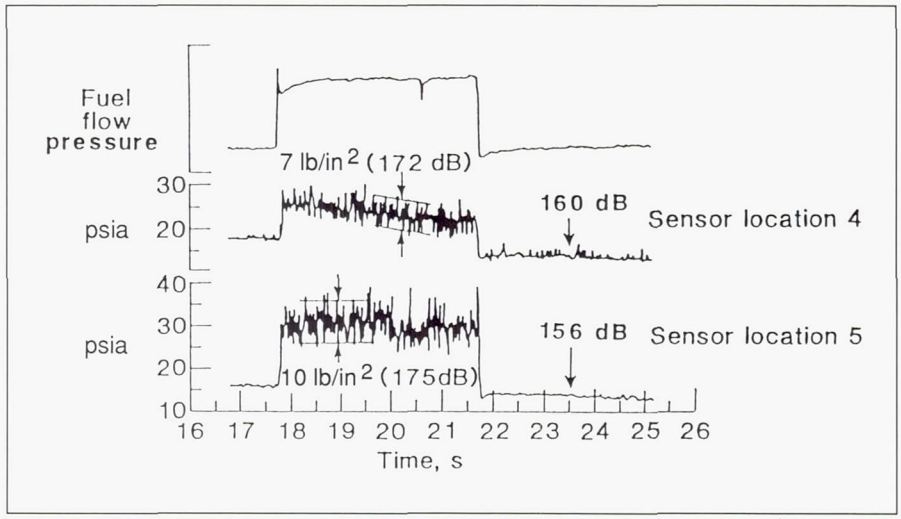

Pressure time histories associated with step increase in fuel flow.

Aerothermal Loads Complex

The Aerothermal Loads Complex consists of four facilities that are used to carry out research in aerothermal loads and high-temperature structures and thermal protection systems. The 8-Foot High-Temperature Tunnel (8-Foot HTT) is a Mach 7 blowdown-type facility in which methane is burned in air under pressure and the resulting combustion products are used as the test medium with a maximum stagnation temperature of approximately 3800°R in order to reach the required energy level for flight simulation. The nozzle is an axisymmetrical conical contoured design with an exit diameter of 8 ft. Model mounting is semispan or sting with insertion after the tunnel is started. A single-stage air ejector is used as a downstream pump to permit low-pressure (high-altitude) simulation. The Reynolds number ranges from 0.3 to 2.2 × 10^6/ft with a nominal Mach number of 7, and the run time ranges from 20 s to 180 s. The tunnel is used for studying detailed thermal-loads flow phenomena as well as for evaluating the performance of high-speed and entry vehicle structural components. A major effort is under way to provide alternate Mach number capability as well as O_2 enrichment for the test medium. This is being done primarily to allow models that have hypersonic airbreathing propulsion applications to be tested.

The 7-Inch High-Temperature Tunnel (7-Inch HTT) is a 1/12-scale version of the 8-Foot HTT with basically the same capabilities as the larger tunnel. It is used primarily as an aid in the design of larger models for the 8-Foot HTT and for aerothermal loads tests on subscale models. The 7-Inch HTT is currently being used to evaluate various new systems for the planned modifications of the 8-Foot HTT.

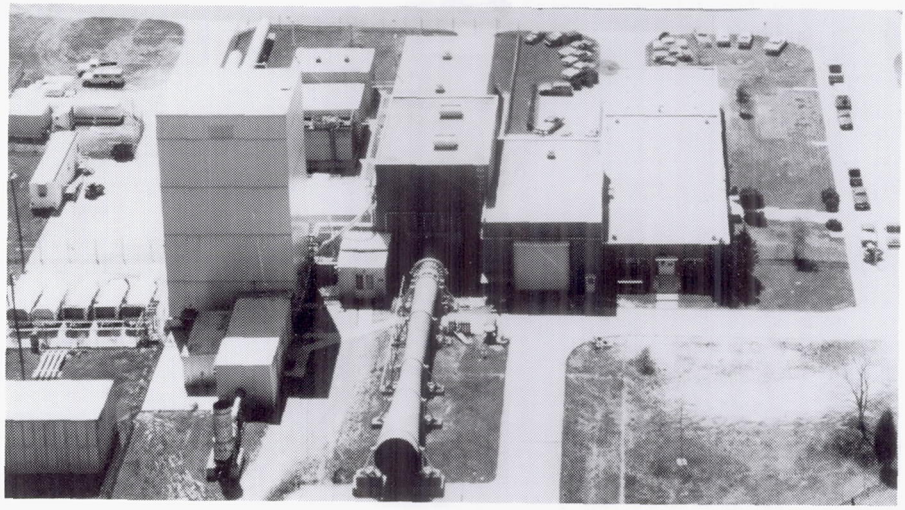

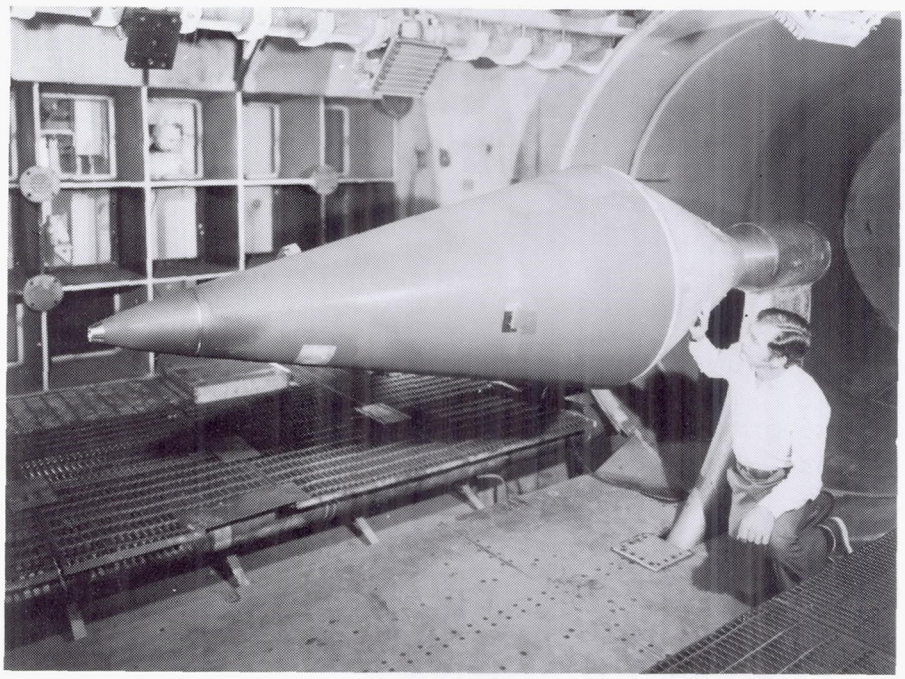

8-Foot High-Temperature Tunnel, $M = 7$, $R_n = 0.3 - 2.2 \times 10^6$, and $H = 700 - 1000$ Btu/lb.

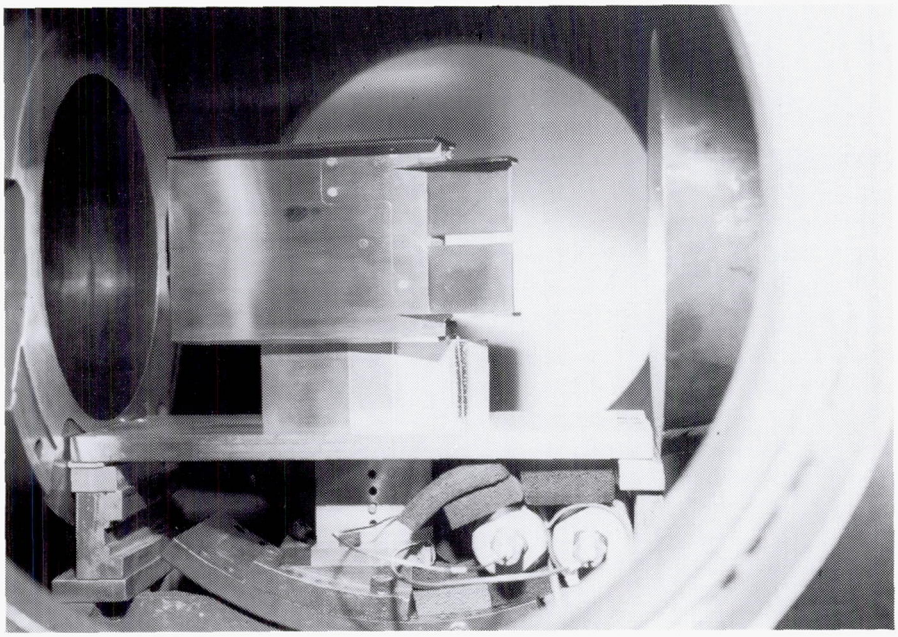

7-Inch High-Temperature Tunnel, $M = 7$, $R_n = 0.3 - 2.2 \times 10^6$, and $H = 700 - 1000$ Btu/lb.

The 20-MW and 5-MW Aerothermal Arc Tunnels are used to test models in an environment that simulates the flight reentry envelope for high-speed vehicles such as the Space Shuttle. The amount of energy available to the test medium in these facilities is 9 MW and 2 MW, respectively. The 20-MW tunnel has a dc arc heater, and the 5-MW tunnel has a three-phase ac arc heater. Test conditions (such as temperature, flow rate, and enthalpy) vary greatly because a variety of nozzles and throats are available. Model sizes can range from 3 in. in diameter to 1-ft by 2-ft panels. These facilities are currently on standby status.

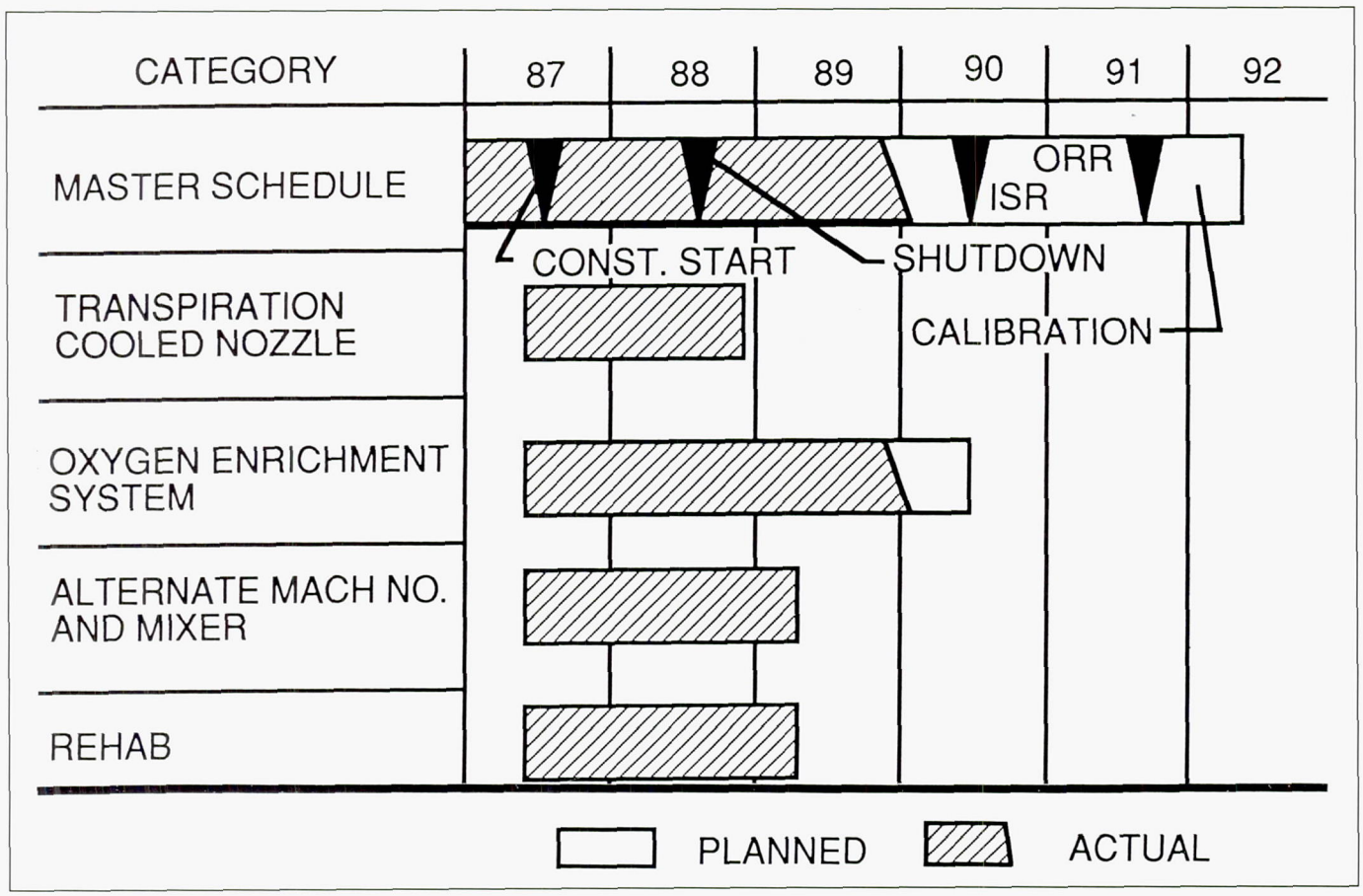

8-Foot HTT modification project schedule; ISR is integrated systems review; ORR is operational readiness review.

Acoustics Research Laboratory

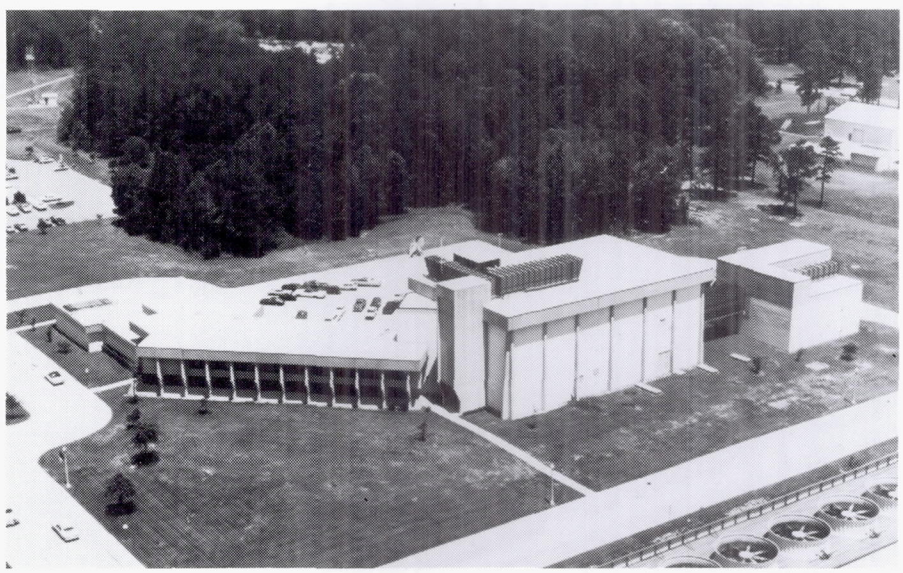

The Langley Acoustics Research Laboratory (ARL) provides the principal focus for acoustics research at Langley Research Center. The ARL consists of the anechoic quiet-flow facility, the reverberation chamber, the transmission loss apparatus, and the human-response-to-noise laboratories. The anechoic quiet-flow facility has a test chamber treated with sound-absorbing wedges and is equipped with a low-turbulence, low-noise test flow to allow aeroacoustic studies of aircraft components and models. The test flow, which is provided by either horizontal high-pressure or vertical low-pressure air systems, varies in Mach number up to 0.5. The reverberation chamber, which is used to diffuse the sound generated by a noise source, provides a means to measure the total acoustic power spectrum of the source. The transmission loss apparatus has a source and a receiving room, which are joined by a connecting wall. A test specimen such as an aircraft fuselage panel is mounted in the connecting wall for sound transmission loss studies. The human-response laboratories consist of the exterior effects room, the anechoic listening room, and the Freedom space station/aircraft acoustic simulator.

Three laboratory companions of the ARL are the Anechoic Noise Facility, the Jet Noise Laboratory, and the Thermal Acoustic Fatigue Apparatus (TAFA). The Anechoic Noise Facility is equipped with a very-high-pressure air supply used primarily for simulating nozzle exhaust flow. The Jet Noise Laboratory has two coannular supersonic jets for studying turbulence evolution in the two interacting shear flows that are typical of high-speed aircraft engines. Hot supersonic jets with temperatures corresponding to those associated with afterburners can also be simulated in the Jet Noise Laboratory. The TAFA provides the capability to subject flat structural panels to high-level acoustic pressures and high-temperature radiant heating to 1200° F.

Sonic Boom Simulator

A sonic boom simulator has been constructed in the ARL for use in tests to examine human response to sonic booms. This effort is part of a larger program to study the feasibility of acceptable overland supersonic flight. The acoustic energy contained in sonic booms is predominantly at low frequencies and cannot be reproduced using conventional loudspeaker arrangements. A solution is to have loudspeakers radiate into an enclosed volume containing the test subject. Effective simulation requires that the enclosure must have rigid walls and be airtight. The figure illustrates the array of loudspeakers mounted in the door of the concrete enclosure, which is lined with sound-absorbing foam. The sonic boom pressure signatures are computer generated in order to attain precise control of the amplitude and phase of the signal and to overcome some of the inadequacies of the sound reproduction system. The sonic boom simulator is now operational and is being calibrated for Langley Research Center man-rating requirements. The first tests will examine the benefits of sonic boom shaping

Interior view of the sonic boom simulator. L-89-14359

and will be compared with predictions from a sonic boom loudness model.

(Kevin P. Shepherd, 43583)

Polarization-Preserving Optical Fiber Link for Laser Velocimeter System

A series of tests were conducted with a laser velocimeter (LV) system in the Jet Noise Laboratory with a convergent-divergent (C-D) type supersonic nozzle (as shown in the first figure) using propane burner combustion.

Previous experience with the LV in the vicinity of the nozzle region was a degradation of the laser performance due to the test cell temperature (>120°F) and high acoustic level (>140 dB). To overcome this problem, a 20-m Polarization-Preserving Single-Mode Optical Fiber (PPSMOF) of the Panda type was used as a transmission link between an Ar^+ laser and the measurement optics. The transmission link permitted the relocation of the laser to a protected region of the test area.

The PPSMOF provided a power transmission efficiency of approximately 50 percent for an input laser power level of 500 mW at a 514.5-nm wavelength. The delivered power level was satisfactory, and once the optics alignment was set, no further readjustment was required. Data were taken for the velocity component along the nozzle axis. Typical LV measurements of the nozzle velocity profile are shown in the second figure. The test re-

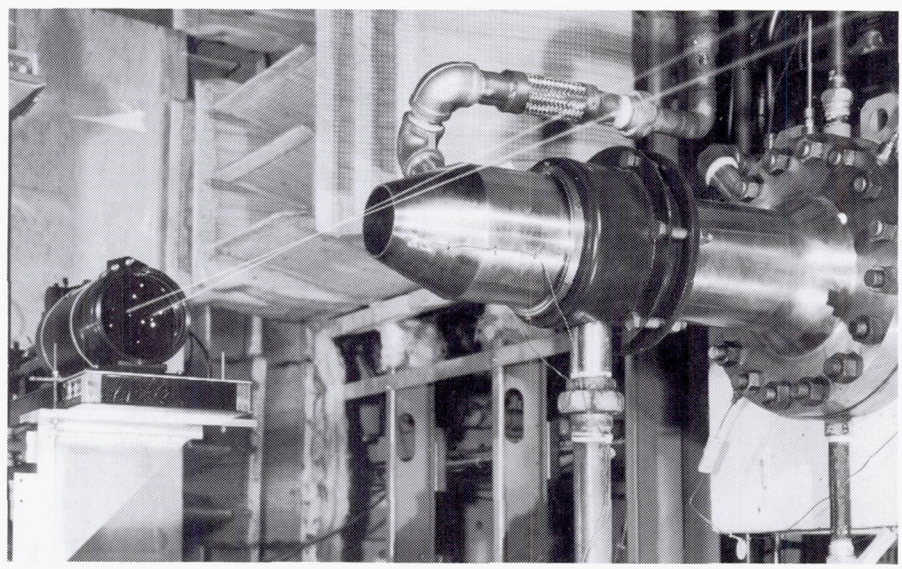

C-D jet nozzle with measurement scanning optics that are remotely linked to Ar^+ laser by 20-m PPSMOF. L-89-8604

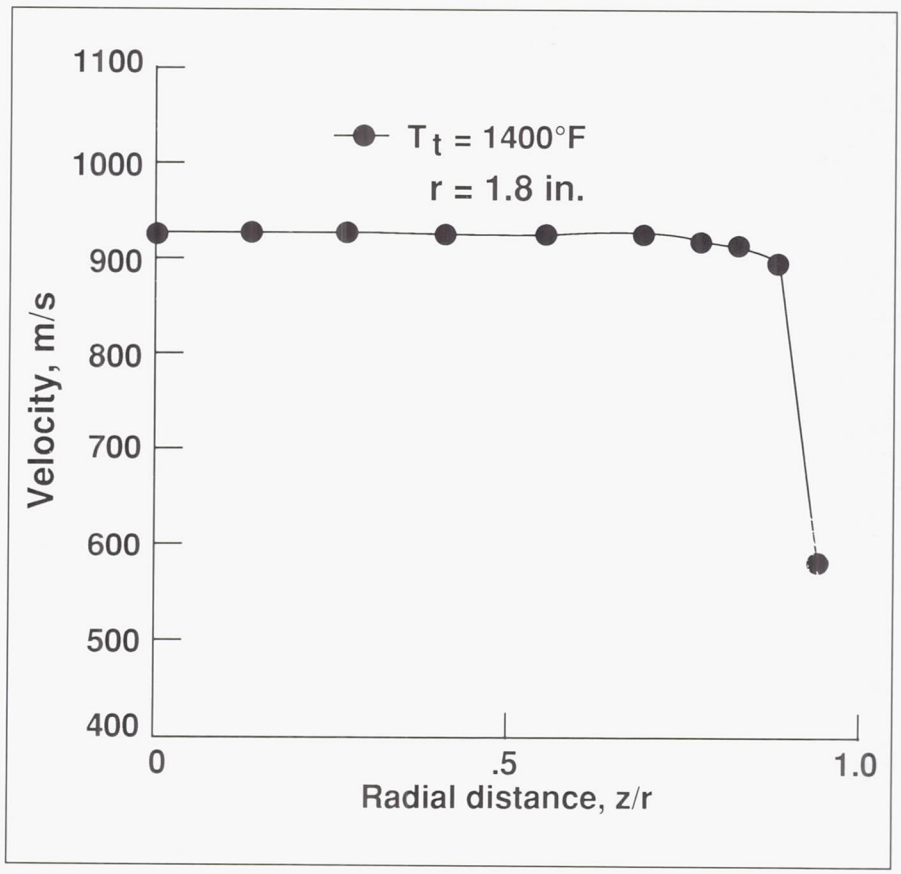

LV measurements of Mach 2 C-D nozzle velocity profile, displaced 0.25 in. beyond exit plane.

sults showed that the PPSMQF is an effective way to isolate a high-power laser source from a hostile medium.
(K. K. Tedjojuwono, 44595, and B. J. Jansen, Jr.)

En Route Noise Test

A flight experiment, referred to as the En Route Noise Test, was conducted in cooperation with Lewis Research Center (LeRC) and the Federal Aviation Administration (FAA) to investigate the propagation of advanced turboprop noise. The experiment, conducted in May 1989 at White Sands Missile Range, consisted of flying the LeRC Propfan Test Assessment (PTA) airplane over a microphone array. Ninety flyovers of the PTA airplane were measured at altitudes of 15,000 ft

PTA airplane.

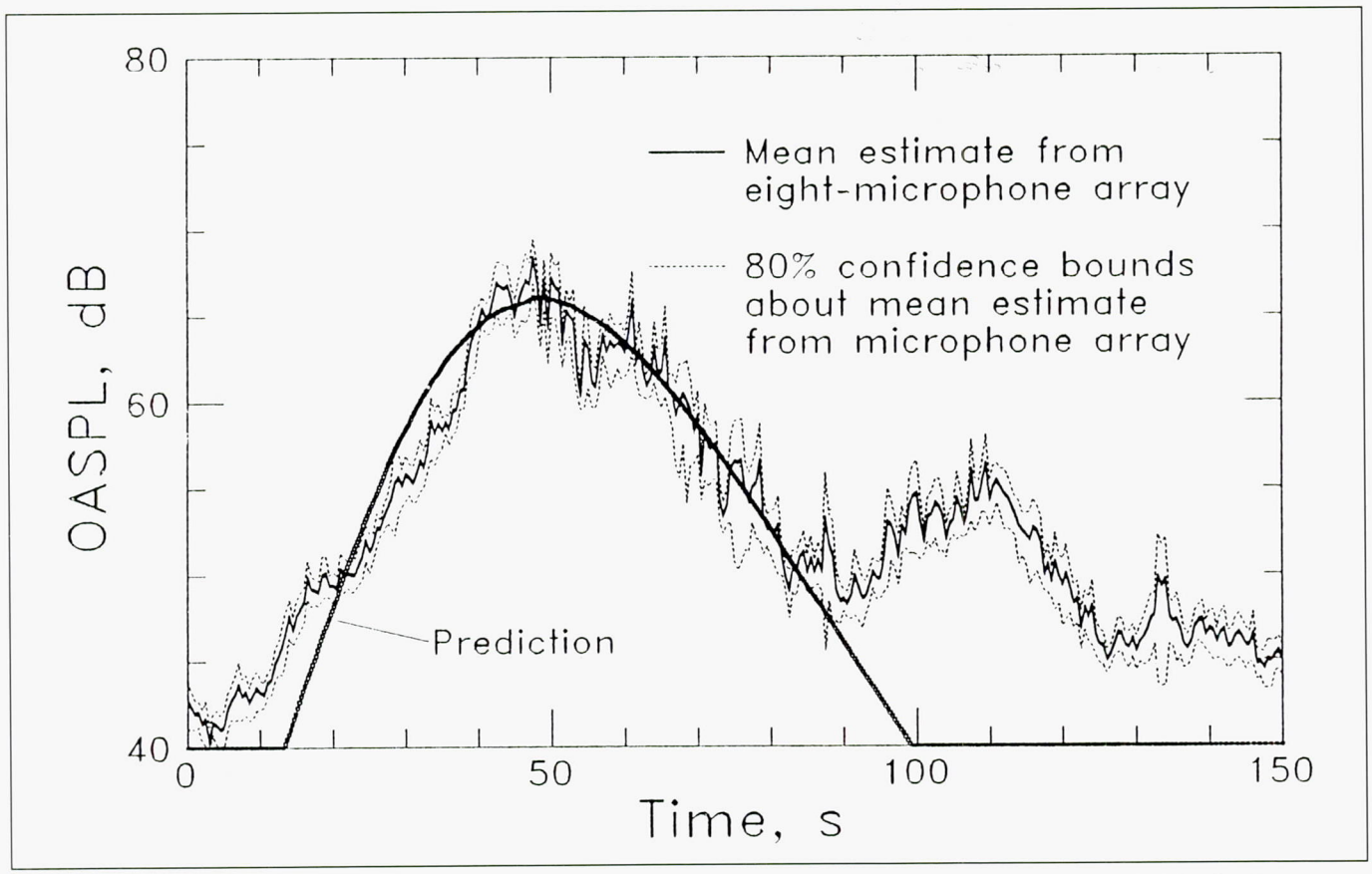

Comparison between measured and predicted ground-level noise for overflight of 30,000 ft and M of 0.7.

to 30,000 ft and at Mach numbers ranging from 0.540 M to 0.77 M.

Shown in the first figure is a photograph of the PTA airplane. The plot in the second figure is a comparison between predicted and measured ground-level overall sound pressure level (OASPL) versus time for a run of 30,000 ft and M of 0.7. The measured results are an ensemble average from eight ground-level microphones. The 80-percent confidence bounds are typically within 1 dB of the average, which is indicative of a high-quality measurement. The predicted results in the plot were made with a two-dimensional ray-tracing propagation model.

The agreement between predicted and measured advanced turboprop flyover noise is good. The second hump at approximately 110 s in the data is due to jet noise and was not predicted. Because of propagation-induced variability, past comparisons between predicted and single microphone measurements showed less agreement. The application of ensemble-averaging techniques to the en route noise issue has demonstrated that ray-tracing propagation models are adequate to predict average noise levels on the ground from advanced turboprops operating at cruise conditions.

(William L. Willshire, Jr., 45270)

Noise Control in Composite Model Fuselage

With the advent of composites as the primary fuselage structural material, a great deal of effort has gone into defining their static and dynamic load-carrying abilities. However, due primarily to the lighter weight of these composites, the noise transmission characteristics have been shown to suffer. Without a thorough understanding of the noise transmission mechanisms for realistic built-up composite structures, effective advantage may not be taken of innovative solutions such as passive and active damping and active noise and vibration control. A comprehensive test on a realistic composite structure under carefully controlled

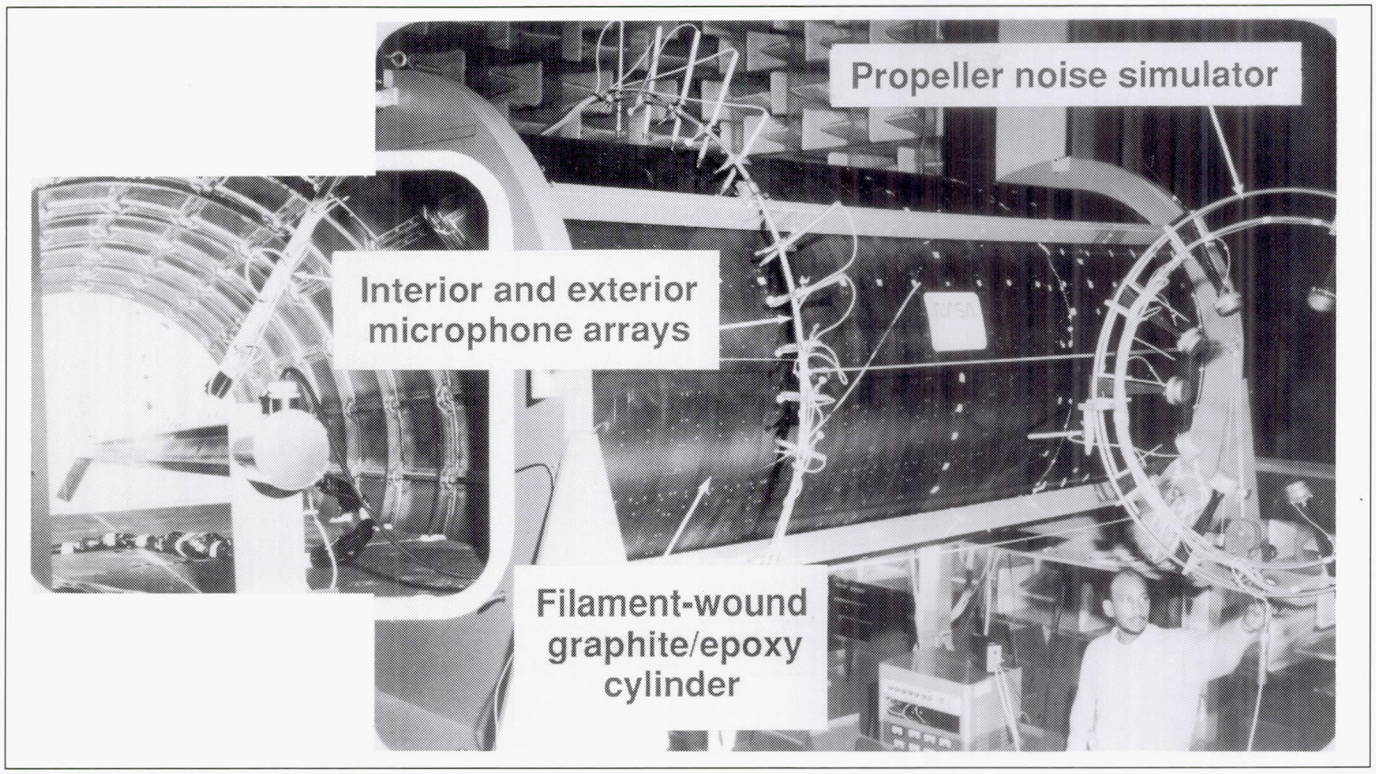

Composite fuselage interior and exterior in Acoustic Test Chamber. L-90-304

conditions has been performed to address these issues as well as the effect of source structure on noise transmission.

The cylinder structure shown in an anechoic chamber of the Acoustics Research Laboratory consists of a continuously wound graphite-filament cylinder of nine plies laid at five different angles, giving a thickness of 0.067 in. Continuously bonded rings spaced every 15 in. and 22 equally spaced stringers make the 12-ft-long and 5.5-ft-diameter structure representative of an aircraft fuselage. A floor has been installed, and tests have been completed both with and without acoustic foam damping installed on the interior walls.

A data base has been generated consisting of measurements of the exterior pressure distribution over the cylinder surface, 22 accelerometer measurements on a circumference in a fixed-source plane, and an extensive mapping of the interior three-dimensional pressure field. Exterior sound fields over a range of frequencies from 20 Hz to 900 Hz were provided by a single acoustic point source, by two point sources on opposite sides of the cylinder (operated both in-phase and out of phase), and finally by a phased array of point sources which provides the trace velocity of a propeller. In addition, source spacing effects were investigated.

This experiment represents the first attempt to experimentally define the structural-acoustic coupling mechanisms in a large-scale fuselage model. Analysis of the data has revealed that the interior sound field is strongly affected by exterior noise source phasing; this is expected due to the low damping inherent in untreated composite structures. Noise transmission loss in the source plane is 15 dB to 20 dB for the untreated interior and 20 dB to 25 dB for the foam-treated interior for frequencies above approximately 160 Hz. Comparisons with analytical models that predict the scattered exterior pressure field and the interior sound pressure level are in progress.

(Todd B. Beyer, 43580)

Noise Control in Fuselage Structures Using Piezoceramic Actuators

Active control techniques have attracted a great deal of attention stemming from their potential for low-frequency noise control in aerospace vehicles. This potential has been demonstrated in ground as well as flight tests. Most evaluations have focused on the use of acoustic control sources located within the cabin cavity. An alternative technique with additional potential is the use of force actuators inputting control directly to the fuselage structure. This technique has the significant advantage that the source distribution of the control source is identical to the offending noise source. Global noise control has been demonstrated in the laboratory with fewer control sources. However, concern arises from the local stress concentrations as well as the wide range of modes generated by the use of point forces on structures.

One alternative to the use of conventional shaker inputs is the use of piezoceramic patches bonded or embedded on the structure. These actuators work by expanding and contracting their planar surface when a voltage is applied to conducting upper and lower surfaces. One such actuator is shown bonded to the surface of a cylinder in the inset of the figure. The dimensions of this actuator are 0.5 in. by 2. in. This actuator is a two-layer assembly that will input a bending moment directly to the structure. Single-layer actuator configurations strain the surface to which they are bonded, and due to the actuator being displaced from the neutral axis, they input both extensional forces and bending moments. These actuators have been found to exercise surprising authority in inputting energy into structural systems, especially in frequency ranges where interior noise is of concern.

A preliminary evaluation of this test concept was implemented on the structural cylinder shown in the figure. The aluminum cylinder is 20 in. in diameter, 48 in. long, and 0.062 in. thick, with interior rings and an attached floor. Interior noise fields were generated by an acoustic noise source adjacent to

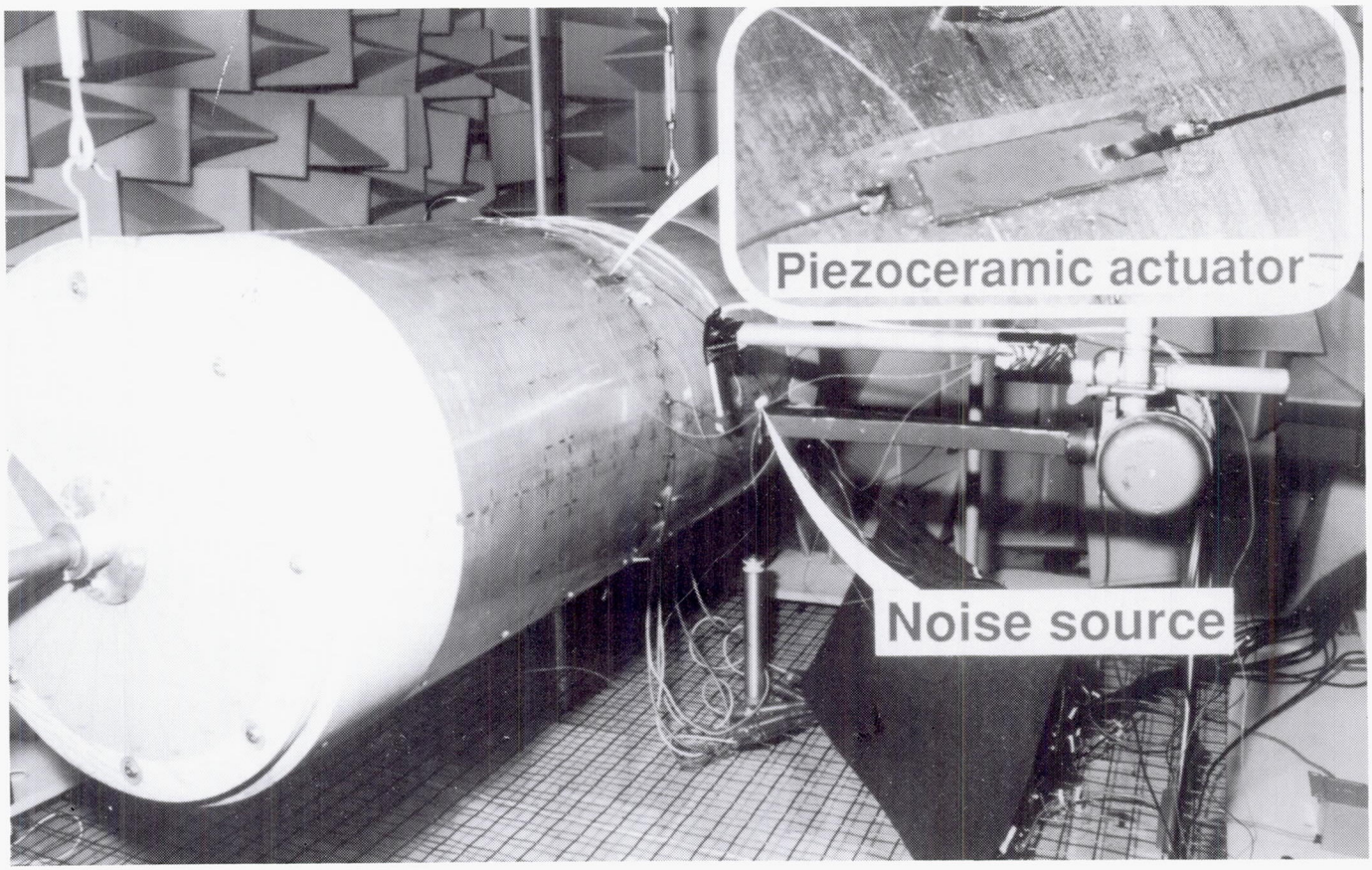

Fuselage model in test chamber showing piezoceramic actuator. L-90-301

the cylinder. Control over this structurally transmitted noise was exercised with either one or two piezoceramic actuators, one of which is shown in detail. Interior sound pressure levels up to 85 dB were controlled with overall reductions of 8 dB to 15 dB for frequencies from 240 Hz to 700 Hz.

(Richard J. Silcox, 43590)

Prediction and Directivity of Low-Frequency Rotor Noise

The low-frequency noise due to unsteady loading on the rotor disk can be a significant contributor to the total noise from a helicopter. This noise, which dominates the first few harmonics of the main rotor blade passage frequency, can be important both for community annoyance and military detection reasons.

Noise data from a recent rotor noise experiment in the German/Dutch acoustic wind tunnel, the DNW (Duits-Nederlandse Windtunnel), were employed to define the directivity of low-frequency rotor noise and to validate a noise prediction method. The experiment was performed and funded by the German Aerospace Research Establishment, the Deutsche Forschungsanstalt für Luft- und Raumfahrt (DLR). Langley Research Center participated as part of an ongoing Letter of Agreement on rotor acoustics research. Although not performed in a Langley facility, this work is included because of its importance to rotor noise research.

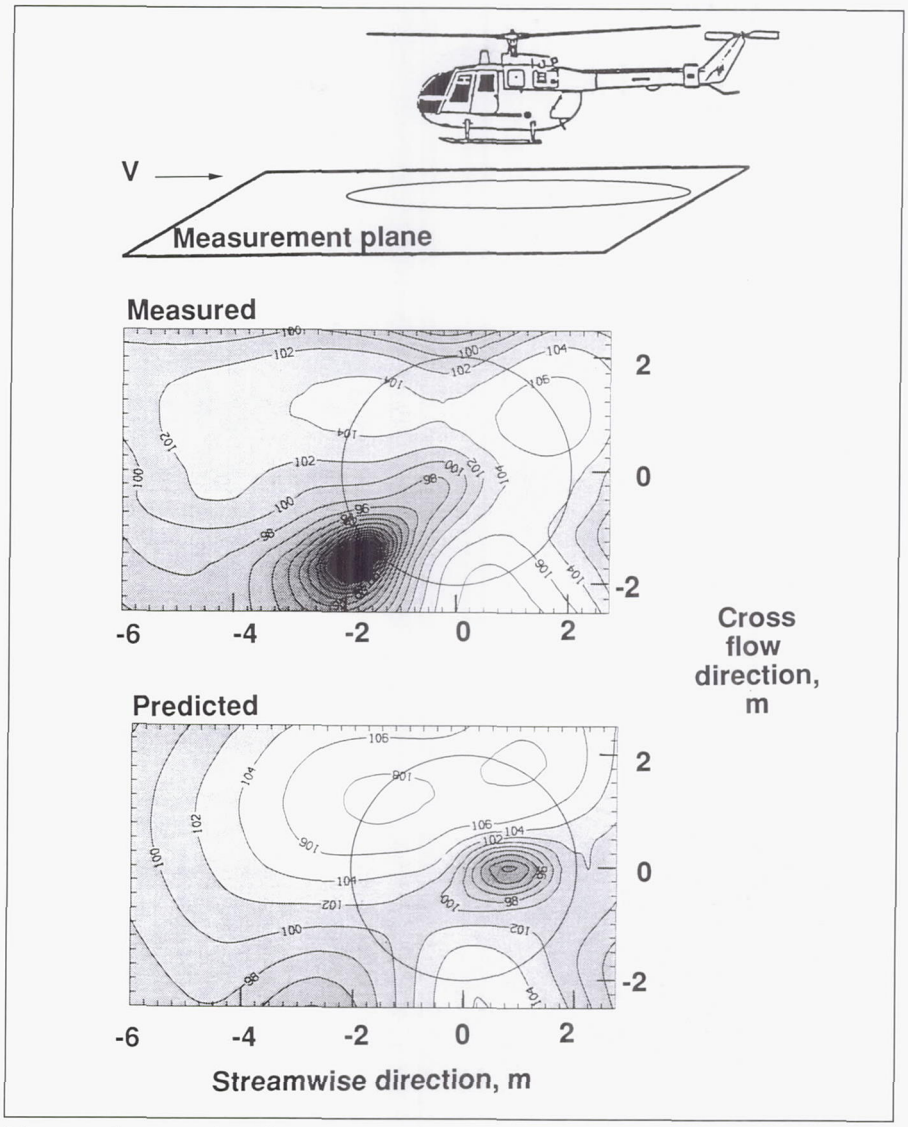

Measured versus low-frequency rotor noise.

Directivity patterns of the low-frequency loading noise were made from both measured data and predictions. The measured data were acquired on a horizontal plane under the model rotor. Predictions were then computed for the same measurement locations. The prediction method uses the newest version of the Comprehensive Analytical Model of Rotorcraft Aerodynamics and Dynamics, called CAMRAD/JA, to predict the dynamics, aerodynamics, and performance. Farassat's acoustic formulation 1A, which is coded in WOPWOP, is used to predict the noise. The lift distribution from CAMRAD/JA is converted to a pressure distribution using a model based on thin wing theory, which is then used by WOPWOP to predict the noise at a given observer location. A comparison of measured versus predicted loading noise for a 25-m/s condition is shown in the figure, which indicates good agreement in many regions, although there are some notable differences. It is anticipated that coupling CAMRAD/JA output with a full-potential code for in-

put to WOPWOP (planned for 1990) will improve some of the discrepancies.
(Michael A. Marcolini, Casey L. Burley, and Ruth M. Martin, 43629)

High-Subsonic Acoustic Wind Tunnel

The High-Subsonic Acoustic Wind Tunnel (HSAWT) is a proposed new wind tunnel designed specifically for acoustic testing. Capable of using either heavy gas or air as a working medium, the HSAWT will perform acoustic tests from Mach numbers of 0.05 to 0.80 at large Reynolds numbers. Although intended primarily as an aeroacoustic facility, the tunnel will also be used for aerodynamic and aeroelastic investigations. Three interchangeable test section configurations, namely, an 18-ft by 22-ft closed throat, an 18-ft by 22-ft open jet surrounded by an anechoic chamber, and a 16-ft by 16-ft slotted throat, will offer the flexibility required to meet testing requirements. The HSAWT is designed to meet not only current aeroacoustic testing needs but also the testing requirements for the aeroacoustic tests of tomorrow.

Currently, a study of the aerodynamics of the wind tunnel circuit is being conducted using a 1/60-scale model HSAWT to validate experimentally the wind tunnel circuit. As shown in the figure, the model is fabricated of plexiglass and aluminum and is presently configured as an open-circuit indraft tunnel designed to operate in air at low speeds. An external suction fan powers the model, providing repeatable flow conditions in the tunnel circuit. Tunnel velocity surveys have been conducted using small pitot probes that were traversed across a given section. Velocity surveys in various sections of the tunnel were used to evaluate tunnel performance. Analysis of data taken to date indicates that the wind tunnel circuit is operating within expected bounds.
(Earl R. Booth, Jr., 43627)

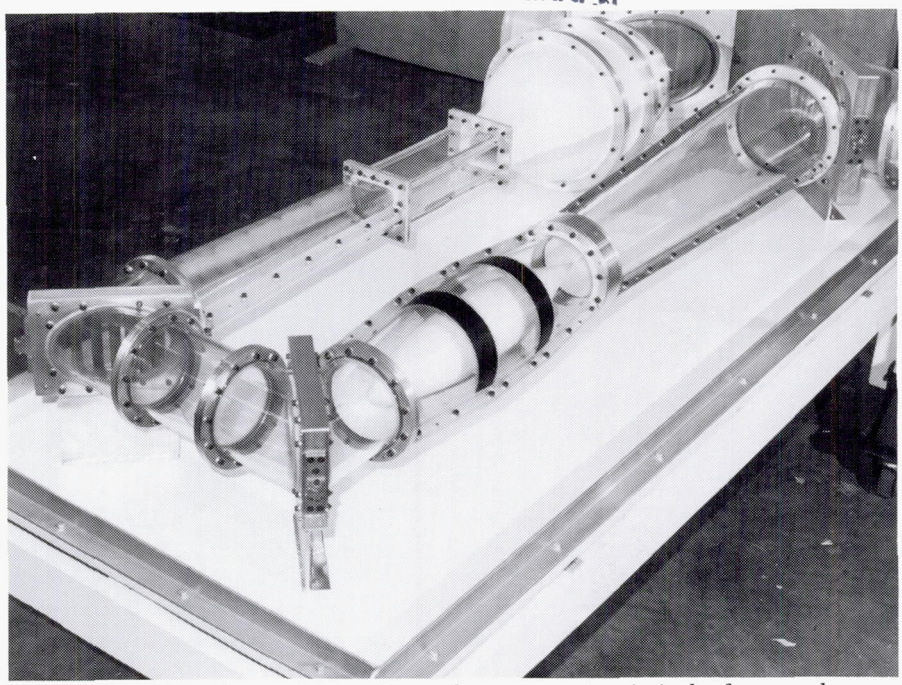

HSAWT 1/60-scale model configured as open-circuit indraft tunnel.

L-89-11208

Avionics Integration Research Laboratory—AIRLAB

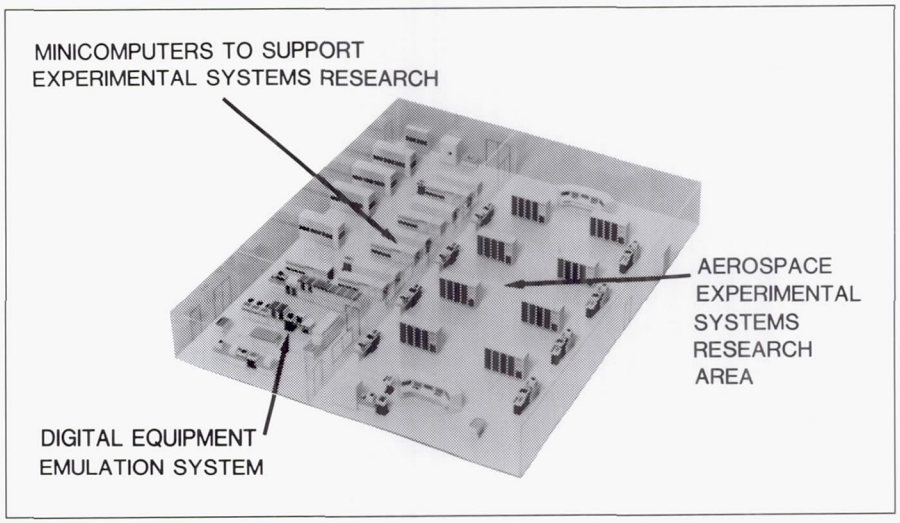

The United States leads the world in the development, design, and production of commercial and military aerospace vehicles. To maintain this leadership role throughout the 1990's and beyond will require the incorporation of the latest advances of digital systems theory and electronics technology into fully integrated aerospace electronic systems. Such efforts will entail the discovery, design, and assessment of systems that can dramatically improve performance, lower production and maintenance costs, and at the same time provide a high, measurable level of safety for passengers and flight crews.

AIRLAB has been established at the Langley Research Center to address these issues and to serve as a focal point for U.S. Government, industry, and university research personnel to identify and develop methods for systematically validating and evaluating highly reliable, fully integrated digital control and guidance systems for aerospace vehicles.

The increasing complexity of electronic systems entails multiple processors and dynamic configurations. These developments allow for greater operational flexibility for both normal and faulty conditions, thus impacting and compounding the validation process. Whereas a typical reliability requirement for current electronics systems is a probability of failure of less than 10^{-6} at 60 min, the requirement for flight-critical electronic controls is for a probability of failure of less than 10^{-9} at 10 hr. Obviously, a new validation process is essential if this significant increase in reliability (four orders of magnitude) is to be achieved and believed.

Validation research in AIRLAB encompasses analytical methods, simulations, and emulations. Analytical studies are conducted to improve the utility and accuracy of advanced reliability models and to evaluate new modeling concepts. Simulation and emulation methods are used to determine latent fault contributions to electronic system reliability and hence aircraft safety. Experimental testing of physical systems is conducted to uncover the latent interface problems of new technologies and to verify analytical methods.

AIRLAB is a 7600-ft^2 environmentally controlled structure located in the high-bay area of Building 1220. AIRLAB houses a number of microcomputer and minicomputer resources and several special fault-tolerant research hardware test specimens dedicated to the support of validation research. The minicomputer resources consist of eight Digital Equipment Corporation VAX 11/750 computers, one VAX 11/780 computer, five MicroVAX II computers, two VAXstation 3200's, eight Sun workstations, eight IBM-PC compatibles, and seven MacIntosh PC's. These resources are used to control experiments (such as fault insertions and performance monitoring); retrieve, reduce, and display engineering data; develop and validate simulations; and develop and validate analytical reliability and performance estimation tools. Also included in AIRLAB are a Lightning Upset test bed and three advanced fault-tolerant computer systems; the Fault-Tolerant Multiprocessor (FTMP); the Fault-Tolerant Processor (FTP); and the Verifiable Integrated Processor for Enhanced Reliability (VIPER). These systems are designed to explore fault-tolerant techniques for future flight-critical aerospace applications and to serve as research test beds for validation studies in AIRLAB.

Electromagnetic Effects Testing of Fault-Tolerant Control Systems

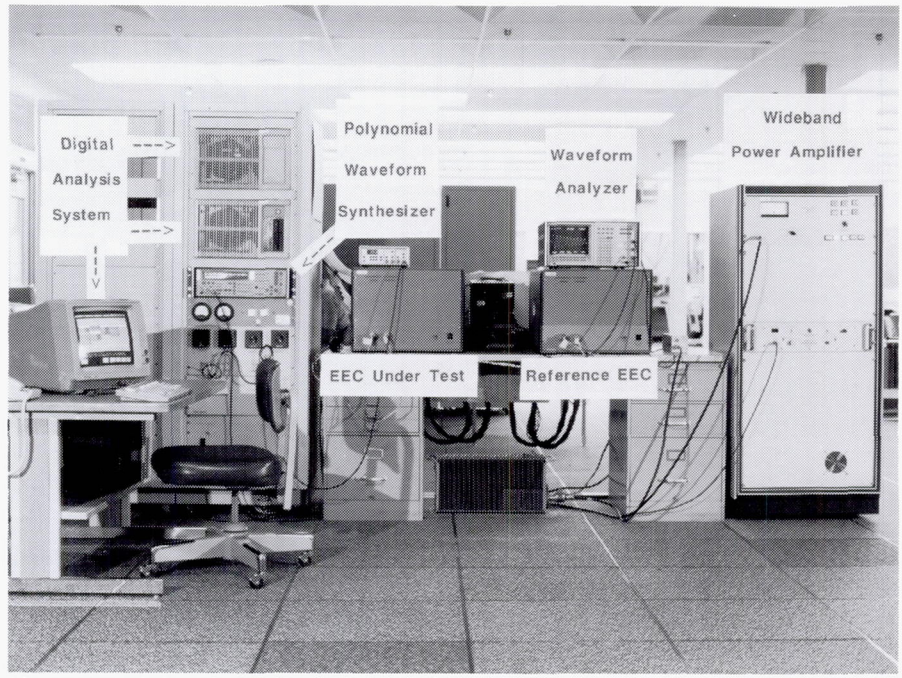

Upset test laboratory in AIRLAB facility. L-89-05807

Control systems for advanced aircraft will have very high reliability specifications that must be met in adverse as well as nominal operating conditions. Severe operating conditions can result from electromagnetic disturbances caused by lightning, high-energy radio frequency (HERF) transmitters, and nuclear electromagnetic pulses (NEMP). Perturbations to computer-based control systems that can be caused by electromagnetic disturbances are functional error modes that involve no component damage. These error modes are collectively known as upset modes, can occur simultaneously in all of the channels of a redundant control system, and are software dependent. To date, there are no comprehensive guidelines or criteria for detecting upset modes, designing upset recovery mechanisms, or performing upset tests or analyses on digital control systems.

An upset test methodology has been developed for fault-tolerant control systems. The laboratory test configuration involves the unit under test and an unperturbed reference unit. The controller under test is perturbed by transient signals that are representative of induced electromagnetic disturbances. Each controller will be interfaced to a simulation of the plant so that the closed-loop dynamics of the system are represented. The operation of the plants is compared during tests so that cases in which acceptable control is not maintained by the faulted controller can be flagged in real time. The upset test methodology is being demonstrated using an electronic engine control (EEC) unit as an experimental test bed. The EEC is a control unit manufactured by the Hamilton Standard Division of United Technologies, which provides electronic controls for Pratt & Whitney aircraft engines. It is a full-authority controller and a dual-channel system that operates with a primary/secondary channel redundancy strategy. The transient signal is generated by a polynomial waveform synthesizer and amplified in a wideband power amplifier with a maximum output power of 1000 W and a frequency range of 10 kHz to 220 MHz. This analog signal is inductively coupled into the EEC, and the induced waveform is recorded by a waveform analyzer on which the fast Fourier transform (FFT) and energy/power spectrum can be performed. Digital data from the EEC are recorded on a digital analysis system having 240 input lines that simultaneously can capture data from four microprocessors with time correlation. Analog and digital data from the waveform analyzer and the digital analysis system are transferred via an IEEE 488 bus to a personal computer, which is used for display of data and transmission to a VAX 11/750 for analysis.

(Celeste M. Belcastro, 46182, and Klaus P. Zaephel)

Testing Generalized Gate-Level Logic System Simulator (GGLOSS)

A common approach in the reliability analysis of complex digital computer systems is to solve models that account for fault and error handling mechanisms. These models include parameters that require the analysis of gate-level behavior of faults in digital systems. Toward this end, Langley Research Center contracted with the Research Triangle Insti-

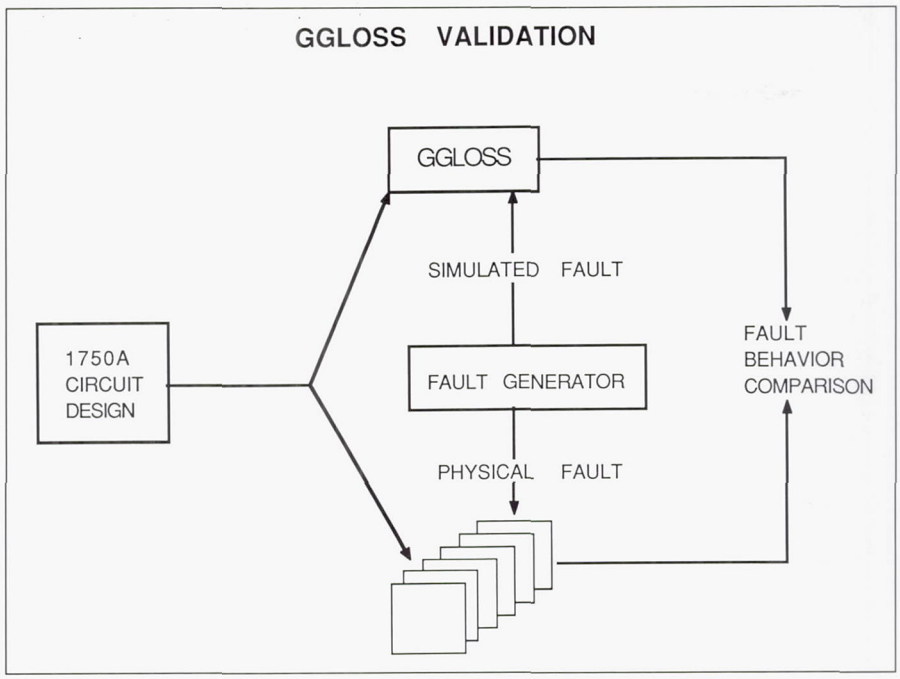

1750A with gate level test ports.

tute (RTI) to develop the Generalized Gate-Level Logic System Simulator (GGLOSS). The GGLOSS was designed specifically to be a high-speed gate-level fault simulator capable of simulating processors executing application programs.

To test the GGLOSS, a circuit of realistic complexity was required. Furthermore, a means to verify the implementation of the fault model was needed. The circuit simulated in this analysis was a laboratory prototype design of a microprocessor based on the MIL-STD-1750A instruction set architecture. One of the interesting features of the laboratory prototype is that it was built using specialized chips that allowed for the injection of stuck-at faults in the combinational logic of the Arithmetic Logic Unit. This feature allowed comparison of the effect of the simulated faults with equivalent faults injected in the actual hardware. The comparison was performed while executing the built-in self-test of the microprocessor. In each case, it was determined that the faulted behavior was simulated correctly. This comparison to faults in actual hardware was invaluable in assessing the correctness of the implementation of the GGLOSS fault model. Additionally, analysis of the GGLOSS simulation results uncovered a design flaw in the implementation of the microprocessor self-test routine.

Because the GGLOSS was designed to be able to simulate complete processors executing application programs at the gate level, a key development issue was simulator speed. By using two-valued logic, each wire in the simulated circuit requires only a single bit of storage in the host computer. Because the memory on a VAX is 32 bits wide, the GGLOSS is able to simulate 32 copies of the circuit in the same amount of time required to simulate a single copy. The GGLOSS maintains one unfaulted copy of the circuit for easy comparison, while allowing the user to inject faults independently in each of the other 31 copies. In addition, the GGLOSS compiles the circuit in such a way that components are evaluated in an invariant, predetermined order. Finally, the GGLOSS uses a combination of zero-delay and unit-delay simulation techniques in order to model combinatorial and sequential circuit elements, respectively. This combination of features gives the GGLOSS the ability to simulate approximately 10^6 gate evaluations per MicroVAX II CPU second while allowing the user the ability to monitor the effects of simulated faults.

(Paul S. Miner, 46201)

Fault Recovery Characteristics of Fault-Tolerant Multiprocessor

A new fault injection experiment design methodology was used to uncover and characterize problems with the Fault-Tolerant Multiprocessor (FTMP) error detection and faulty-unit isolation functions. The new methodology is based on two principles: faults should be injected mainly in signals with high fan-outs (e.g., control and enable signals) thus maximizing the amount of damage (the number of errors introduced) to the system, and the information/data necessary to determine the system state should be observable at all times in real time.

The figure shows the architecture of the FTMP test bed at AIRLAB. There are nine line replaceable units (LRU's), which

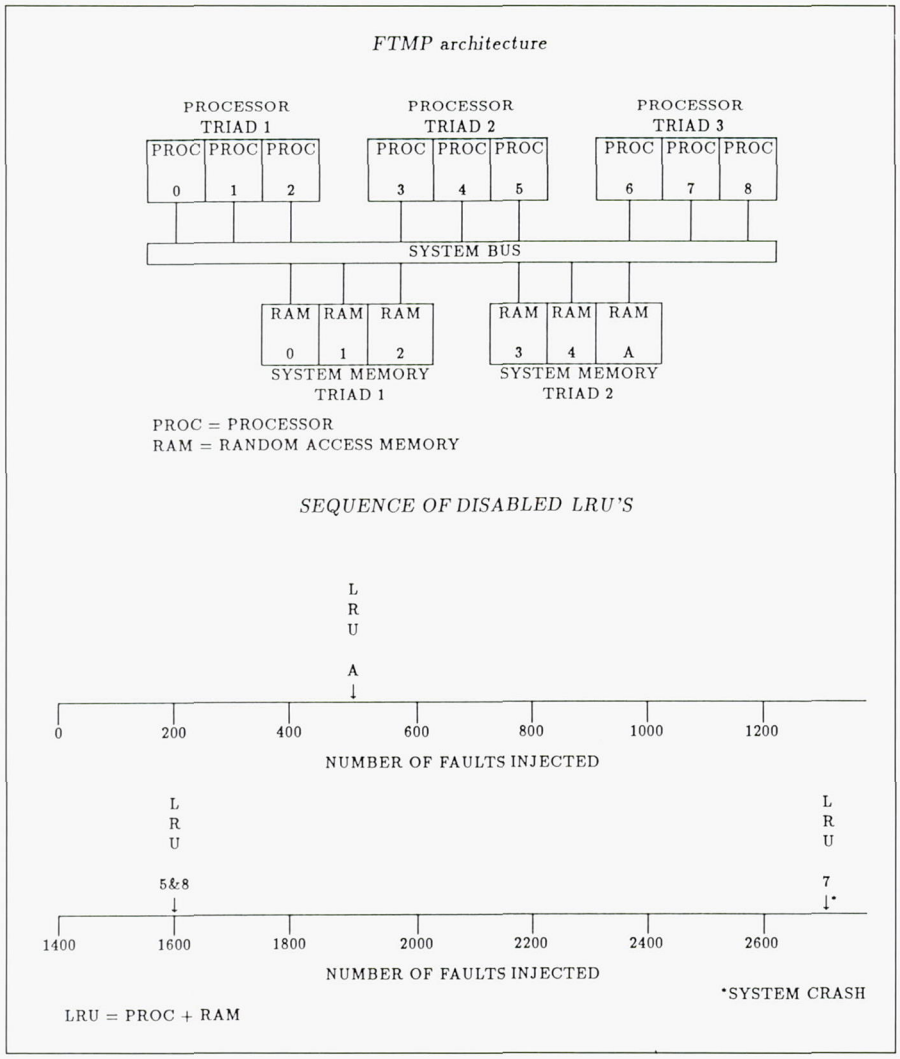

FTMP architecture and experimental data.

are interconnected by a redundant system bus. Each LRU contains a processor with cache, a system bus interface, and a system memory unit. At system restart, the processors and the memories are organized in triads to provide the redundancy required to tolerate a single fault anywhere in the system. The triads are tightly synchronized, i.e., all the processor (memory) components of a processor (memory) triad execute the same instruction (operation) on the same clock cycle. Thus synchronized, three copies of all input/output data from a triad are presented to the triple redundant system bus. The copies then are voted bit by bit to mask any errors that might occur due to a fault on any of the triad components.

The observed anomalies were discovered during hardware fault injection experiments performed on the FTMP test bed. During these experiments, the FTMP occasionally disabled the wrong units; this behavior continued until the system crashed after several thousand faults had been injected. The figure shows the average sequence of LRU's disabled during the experiments (faults injected in processor 3).

Weaknesses in the system design increase the probability that any active fault can exercise a part of the fault management software which handles "byzantine or lying" faults. Byzantine faults behave such that the faulted unit points to a working unit as the source of errors. The design weaknesses involve the interface between the simplex error detection hardware and the error processing software, the functional capabilities of the FTMP system bus, and the communication requirements of a multiprocessor architecture. The effect of these design weaknesses is to allow errors to occur concurrently with the reading of the simplex error detection data by the system. When the errors occur in certain time intervals during the detection data acquisition, the FTMP fault identification procedure incorrectly decides that only one LRU detected the error. This event triggers a software component, designed to handle "byzantine faults," which keeps track of the identity of the lone-accuser and disables it after a second event. In summary, the combined effects of the system's design weaknesses result in a significant probability that a fault-handling error occurs such that one fault causes two LRU's (a good unit in addition to the faulty unit) to be disabled.

(Peter A. Padilla, 46187)

Aerospace Controls Research Laboratory

The purpose of the Aerospace Controls Research Laboratory (ACRL) is to conduct research and testing of spacecraft control systems. The ACRL is equipped with modern microcomputer facilities for simulations, data acquisition, and real-time control system testing. Both control law testing using structural test articles and advanced control system component development are supported by the laboratory. The ACRL provides the controls community with facilities on which the performance of competing control laws may be compared.

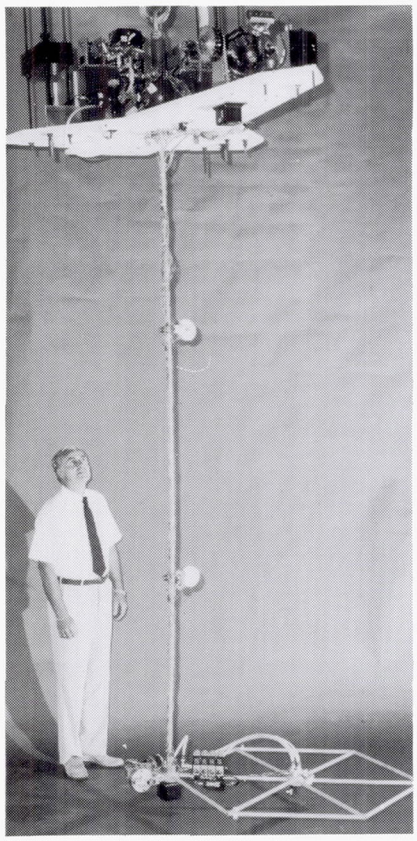

Spacecraft Control Laboratory Experiment (SCOLE). L-87-7321

Two structural test articles are currently available. One, the Spacecraft Control Laboratory Experiment or SCOLE, allows testing of control laws for a complete spacecraft. The test article mimics the Space Shuttle with a large flexible offset-feed antenna attached to the payload bay.

Reaction jets, control moment gyros, and torque wheels, along with accelerometers and rate sensors, permit real-time control law implementation on SCOLE (see the first figure). The other test article is the Grid experiment. This facility is designed to support research in the control

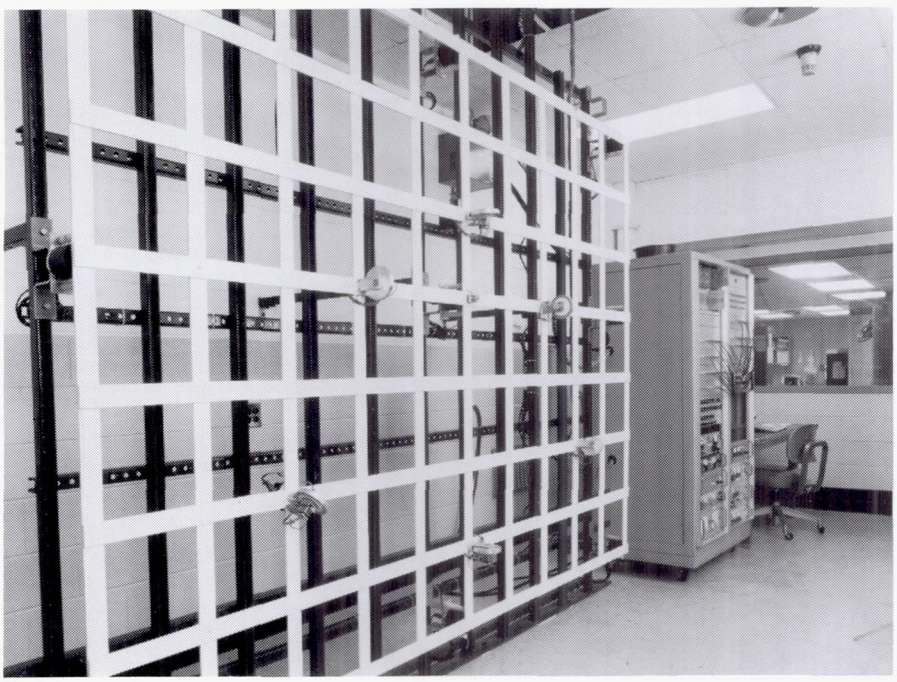

Grid experiment. L-84-10319

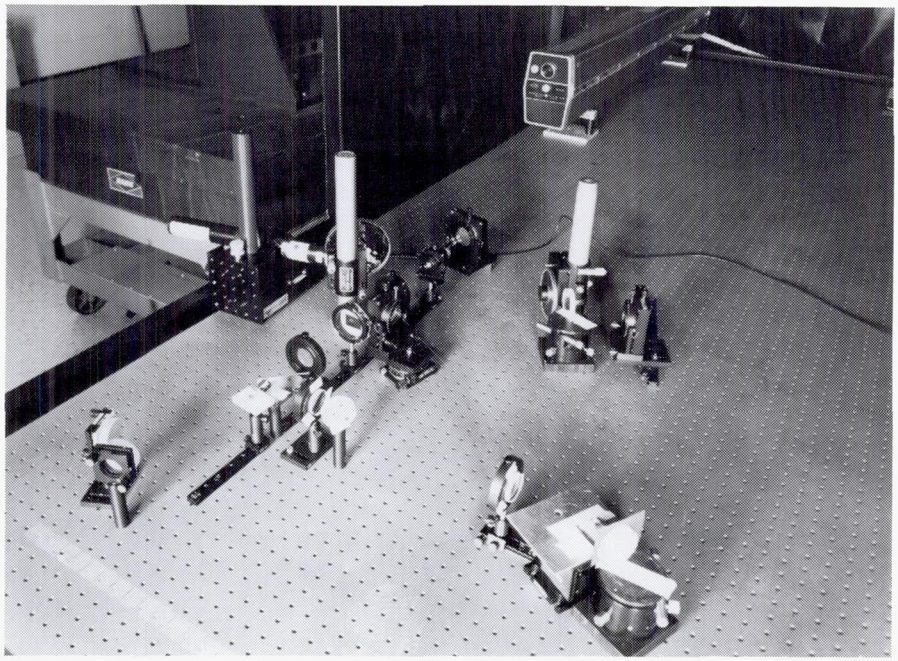

Advanced sensor and actuator facility. L-89-325

of flexible area structures. The grid, which is made of 2-in. by 1/8-in. cross-section aluminum bars bonded at 12-in. intervals to form a 7-ft by 10-ft lattice, is suspended vertically by two 2-ft-long cables and has appreciable low-frequency structural dynamics, inertial sensors and torque wheels, and microprocessor-based distributed computing components (see the second figure).

The advanced sensor and actuator facility supports research in control system components for space systems. Component development currently focuses on optical sensing and computing devices. Two different photogrammetric position tracking systems and an optical holographic image storage device are being developed. The facility (shown in the third figure) includes equipment for performing experiments in optics, two stable tables, optical mounts, lenses, mirrors, polarizers, beam splitters, photomultiplier tubes, a 5-mW HeNe laser and a 35-mW HeNe laser, a precision rotary stage, and laser beam steering systems.

Evaluation of Optical Sensor

A performance evaluation of a prototype of a new Charge Coupled Device (CCD) sensor has been performed. This sensor has been developed in the advanced sensors and actuators facility and is to be used to track the motion of large flexible space structures. The sensor consists of a linear CCD focal plane, cylindrical lens, driver board (shown in figure), and a digital signal processor for controlling sensor parameters and interfacing to an external computer system. Tests have been performed on the driver board and output signals as well as the circuit for automatic adjustment of sensor parameters such as integration time, gain, and background subtract. Specifications for the sensor include a 20-MHz data rate, high gain, low noise, and automatic adjustment of system parameters to achieve the best signal. Results of tests performed on the prototype sensor

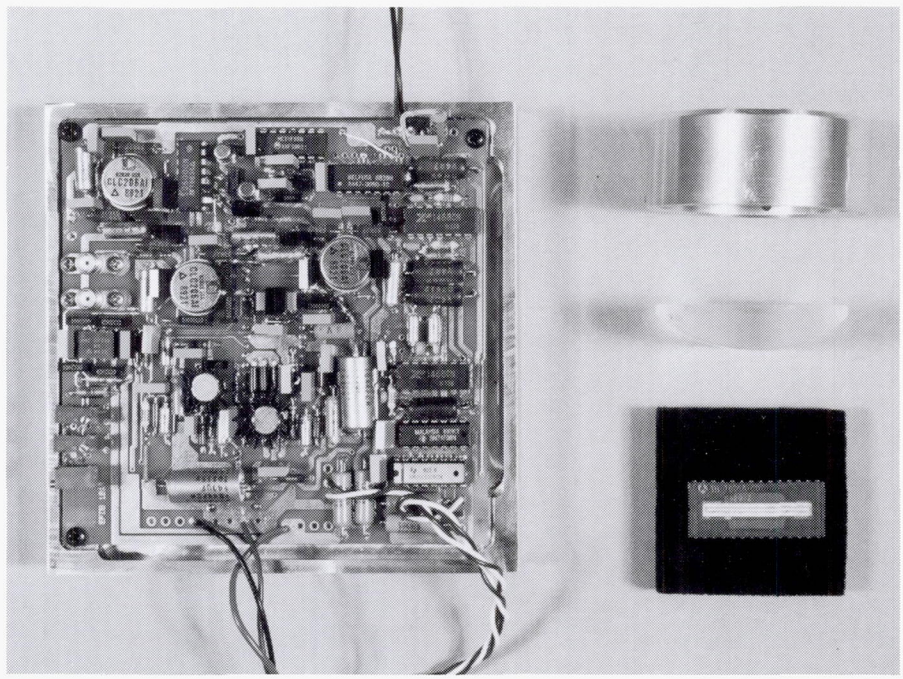

Charge Coupled Device optical sensors.

indicate that the performance of the sensor is within design specifications.
(Sharon S. Welch, 46611)

Holographic Optical Storage

Holographic optical storage is being investigated for use in distributed optical sensors and processors for control of flexible structures. A patent has been granted on a new holographic image storage device using two photorefractive crystals. The figure is a photograph of the laboratory setup of the two-crystal storage device. The laboratory setup uses two $BaTiO_3$ crystals to store a hologram of the Air Force Resolution Chart. A hologram of the resolution chart is stored in the first crystal by interfering the object beam with a reference beam. When this hologram is read out, a phase conjugate of the reconstructed object beam is generated. This phase conjugate beam becomes the object beam for the second crystal, and a hologram of this beam is stored by interfering it with a second reference beam. This hologram is then read out, and the original object beam is reconstructed. The reconstructed beam from the second crystal is directed back into the first crystal to be stored as the original beam was stored. The image information is stored by oscillating between the two crystals.

The output of the memory device also is shown in the figure. Tests have been conducted to determine the length of time the image can be stored and the parameters affecting storage time. Storage times in excess of a minute have been successfully demonstrated. Further tests are planned to determine how to extend the storage time and improve the resolution of the device.
(Sharon S. Welch, 46611)

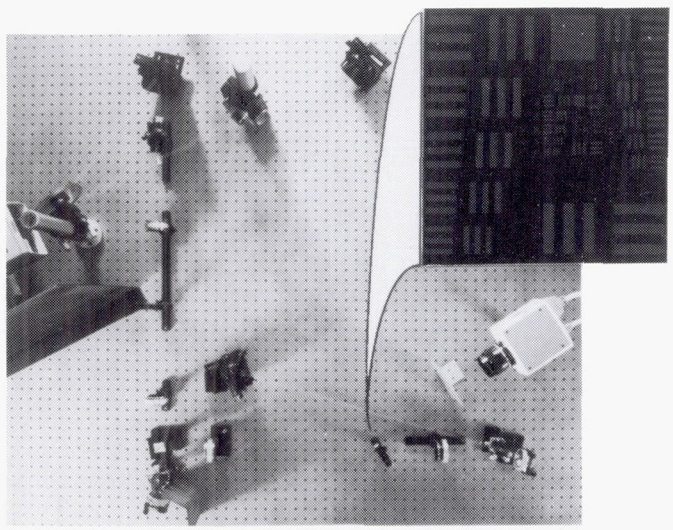

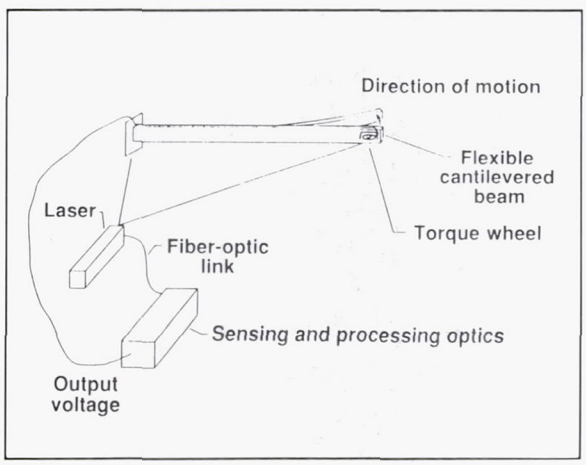

- **Patent Application Filed for Optical Memory**
- **Sensor Based on Optical Memory Device Under Development**
- **Flexible Beam Experiment Defined With OSP Control**

Integrated optical sensor/processor (OSP).

Transport Systems Research Vehicle (TSRV) and TSRV Simulator

The Transport Systems Research Vehicle (TSRV) and TSRV Simulator are primary research tools used by the Advanced Transport Operating Systems (ATOPS) Program. The goal of the ATOPS Program is to increase the operational capability of modern aircraft and foster their integration into the evolving National Airspace System.

The TSRV has two flight decks: a conventional Boeing 737 flight deck provides operational support and safety backup, and the fully operational research flight deck, positioned in the aircraft cabin, provides the capability to explore innovations in display formats, contents, and in-aircraft operations.

The "all-glass" research flight deck presents information to the crew via eight 8-in.-square electronic displays representative of the technology to become available in commercial transports

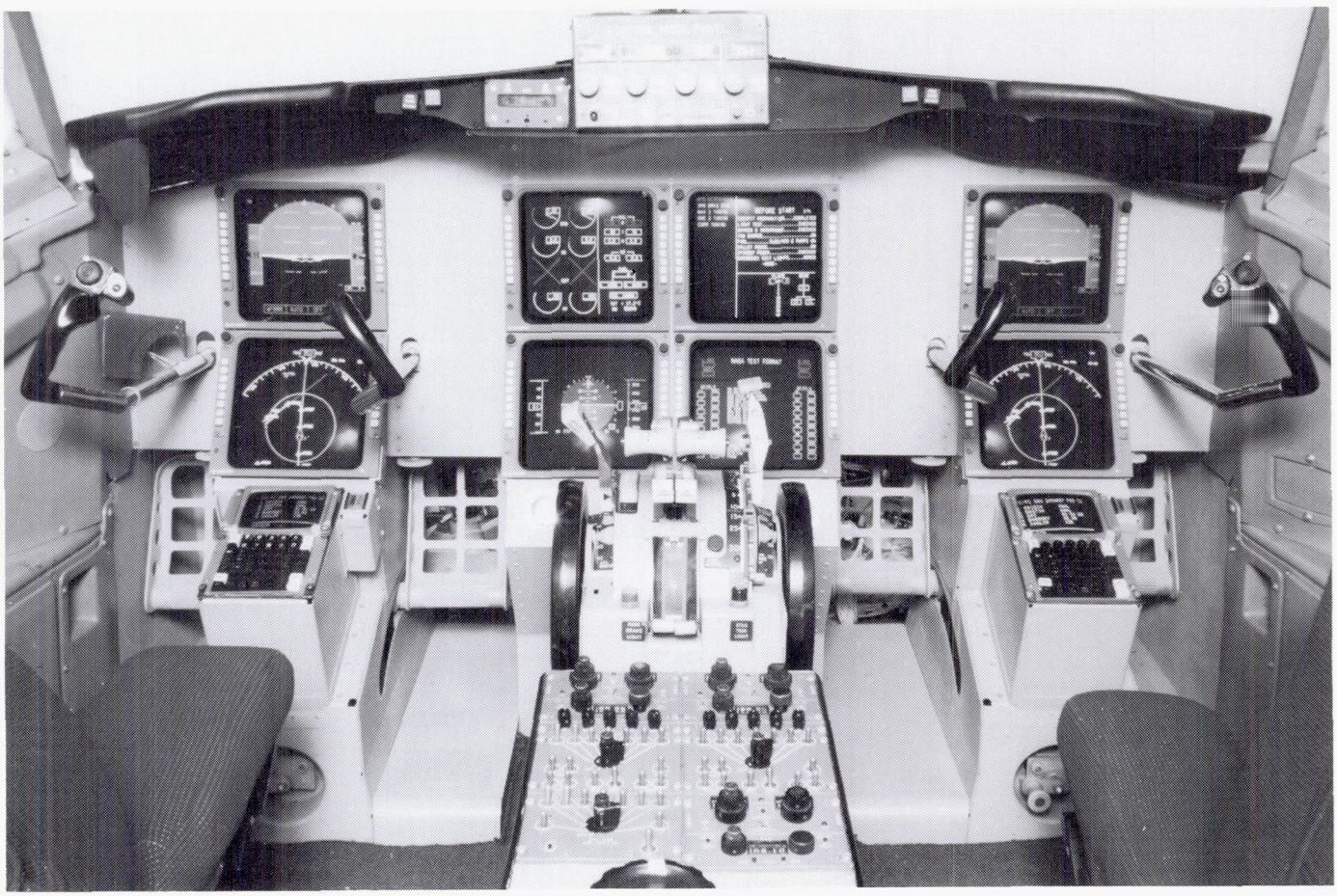

New TSRV aft cockpit configuration. L-87-3645

in the 1990's. The state-of-the-art color displays are driven by new, onboard computers and, most importantly, specially developed computer software. These new technologies make it possible to more clearly display information presented only partially or in scattered locations on existing electromechanical and first-generation electronic displays in today's aircraft.

In addition to video concepts for primary flight and navigation displays in front of both pilot and copilot, center panel displays provide the capability to monitor engine and system status and to manage aircraft systems operation. The center panel displays will permit research on how additional information can be displayed and used to improve situational awareness, air traffic control communications, flight management options, and traffic awareness.

The TSRV Simulator provides the means for ground-based simulation in support of the ATOPS Program. The Simulator, which is being modified to duplicate the upgraded aft flight deck located in the TSRV, allows proposed concepts in such areas as guidance and control algorithms, new display techniques, operational procedures, and man/machine interfaces to be thoroughly evaluated. The recent addition of four out-the-window display systems (driven by an Evans and Sutherland CT-6 Computer-Generated Imagery system) allows realistic out-the-window scenes to be presented to the crew. This system is capable of presenting daytime, nighttime, and all ranges of weather effects. Promising simulation research results become the subjects of actual flight test research.

Helmet-Mounted Display Synthetic Visibility System

The objective of this program was to define, develop, and evaluate a synthetic visibility system for performing safe, accurate, and consistent manual approaches and landings under visual meteorological conditions using video cameras and helmet-mounted displays (HMD's) in lieu of a normal cockpit windscreen.

This study was conducted as a joint Langley Research Center/McDonnell Douglas Corporation (MDC) program. The MDC provided a proprietary state-of-the-art HMD system that was augmented by Langley-determined supplementary symbology. Langley interfaced the system with the ATOPS Boeing 737 aircraft and conducted flight tests to evaluate the effectiveness of the concept. The system provided forward-looking television cameras that covered a field of regard 80° wide and 30° high. Helmet-mounted eyepieces displayed a 40° by 30° field of view depending on the direction in which the pilot looked as sensed by a magnetic (Polhemus) sensor on the helmet. An advantage of using the HMD is that the scene can be displayed in actual size (magnification factor of 1), not reduced size, to fit a head-down television monitor. Superimposed on the television scene was a set of supplementary symbology felt to be necessary to conduct a visual approach and landing. The symbology included airspeed, altitude and heading (all alphanumerics), flight path angle, longitudinal acceleration, airspeed error, flare cue, flight path reference line, waterline, and a pitch ladder.

Flight test evaluation of the system was completed in June 1989 using two NASA and two MDC evaluation pilots. Development and data gathering flight tests involved over 200 landings in a 32-hr flight test program.

Dispersion statistics

	Visual	HMD
X, mean	97 ft	97 ft
σ	202 ft	212 ft
Y, mean	2 ft	3 ft
σ	6 ft	10 ft
Sample	58	67

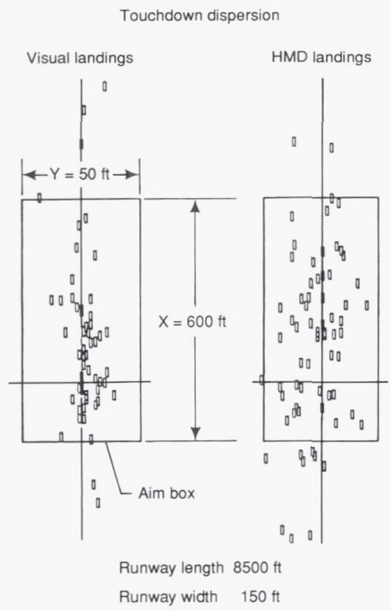

Helmet-mounted display. L-89-10889

Results indicated the feasibility of HMD's for landing high-performance aircraft. Touchdown dispersions using the HMD were comparable to visual landings. Thus, a synthetic visibility system for use in hypersonic vehicles may provide a suitable alternative to a traditional cockpit windscreen for the pilot during approach and landing. A synthetic visibility system would provide huge savings in weight and complexity over a Concorde-type droop snoot.

(James R. Hall, 43851, Kenneth R. Yenni, Lee H. Person, and J. W. Kelly)

Superiority of New Engine-Monitoring and Control System (E-MACS) Display Concept

The primary objective of this study was to provide an advanced aircraft engine display system designed to exploit the capabilities of electronic display media for increased pilot understanding of system performance while simultaneously reducing pilot mental work load and error. The underlying concept of this study was that a reduction in the mental work load associated with the utilization of displayed information may require that information be provided in a form more directly oriented to the user's task. The area of interest for this study was secondary flight display formats, with engine instruments as the specific application. This application area was chosen because it provided both a control task, engine power with throttle, and a systems monitoring task. A part-task evaluation in the TSRV Simulator was used to compare the E-MACS display with a modern, current-generation engine display format.

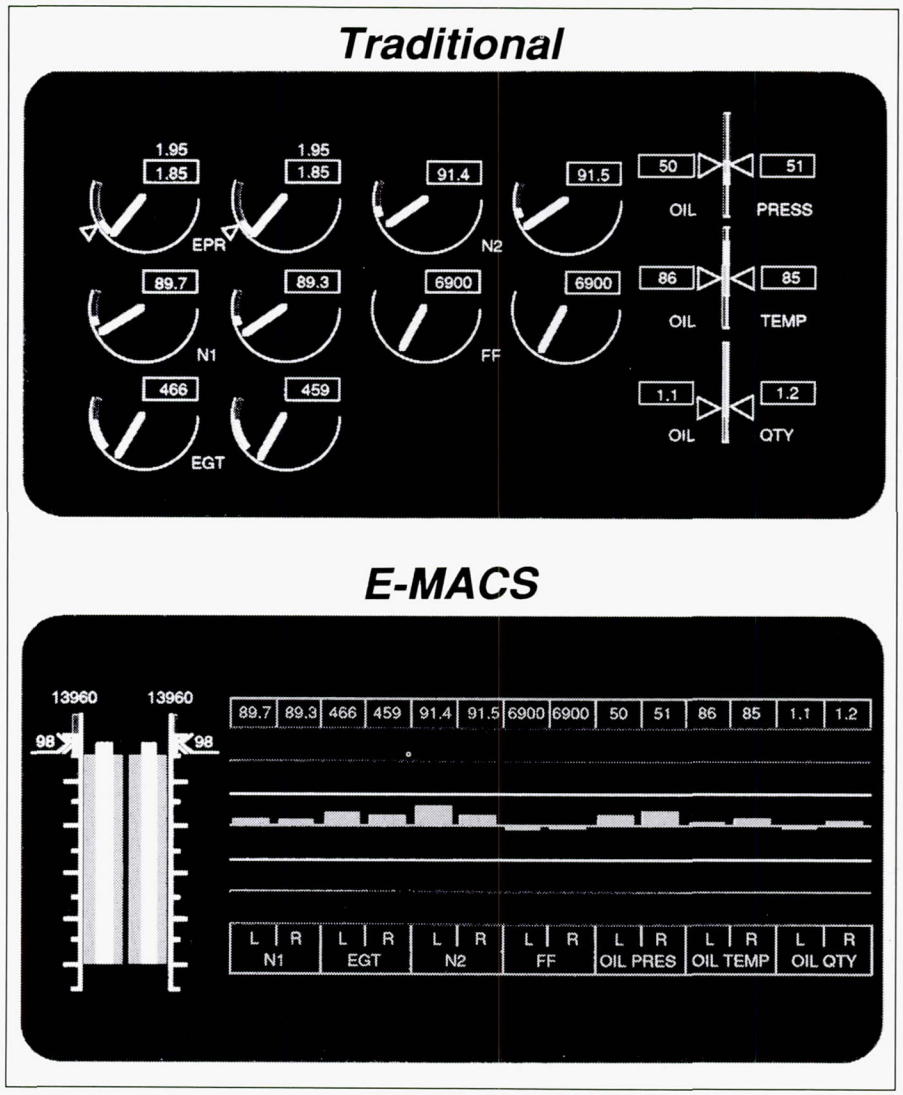

Comparison of traditional engine display with E-MACS concept.

The E-MACS display provides an innovative interface to the engine system for reduced pilot work load and increased situational understanding. The E-MACS display format provides unique display elements tailored to the pilot's task. For the control task, a display element based on a model of engine performance characteristics was used. This display element provided a direct indication of engine thrust relative to a computed maximum thrust available value. For the monitoring task, the emphasis was placed on presenting quantitative information in a form that may be processed cognitively in a qualitative manner. Column-deviation indicators were used as the display elements for monitoring, where the deviation was between the actual and a computed ideal value.

Sixteen pilots participated in a simulator evaluation of E-MACS. The test included takeoff and in-flight conditions with both normal and fault (degraded and out-of-tolerance) conditions.

As part of the evaluation, each pilot was presented with four different scenarios for each of the two display formats. Half of the scenarios involved fault situations. The subjective results of this test showed an overall preference for the E-MACS display relative to the traditional display. Additionally, the monitoring display elements seem to allow holistic viewing of the system information. The most significant result is that the use of the E-MACS display resulted in a 100-percent detection rate for all system faults relative to a 56-percent rate for the traditional display (at the 95-percent confidence level).

(Terence S. Abbott, 42009)

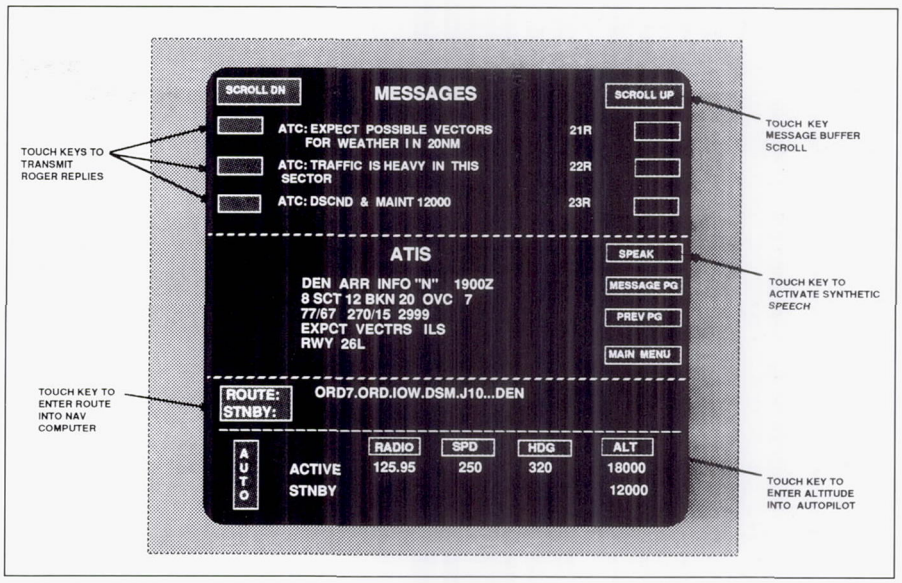

Three-window touch-sensitive data link interface.

Aircraft-ATC Information Transfer Simulation Study

Digital data link is a rapidly maturing technology for aircraft Air Traffic Control (ATC). Increased flight deck utilization of data link will result in increased National Airspace System safety and efficiency by reducing communication errors, relieving congested ATC radio frequencies, and enabling more information transfer between aircraft and ground facilities. A previous Langley Research Center study concluded that key flight deck issues in data link ATC communication are pilot communication work load, situational awareness, and pilot (instrument and out-the-window) vigilance. The primary objective of this effort was to examine methods of using data link ATC information transfer in combination with conventional voice radio to reduce pilot work load while maintaining situational awareness and minimizing adverse pilot vigilance effects resulting from the switch to a primarily visual ATC communication interface.

The study was conducted in the TSRV Simulator using a 6-in. by 6-in. touch-sensitive center panel, color CRT (cathode-ray tube) as the pilot data-link input/output interface. To reduce pilot work load, uplinked information (including routes, airspeeds, altitudes, headings, and radio frequencies) could be entered into the aircraft subsystems with a touch input on the data link interface. To assist the pilots in maintaining situational awareness, weather and traffic information were included in the uplinked ATC messages. To minimize the effects on pilot vigilance, a synthetic voice output capability allowed the pilots to receive messages without having to view the display.

The commercial airline flight crew subjects reported reduced work load attributed to the data link ATC communication process and to the pilot-initiated automatic input of data into the aircraft subsystems. Synthetic speech reduced the adverse effects on pilot vigilance because the pilots did not have to look at the display to receive messages; however, an increase in the time needed to acknowledge ATC instructions resulted. Pilot situational awareness was significantly improved because of the weather and traffic information added to the data-linked messages. It was demonstrated that, through application of data link technology in ATC information transfer, reductions in pilot work load can be achieved while minimizing losses in pilot situational awareness.

(Marvin C. Waller, 42025)

Airborne 4-D Flight Management in Time-Based ATC Environment

Advanced Air Traffic Control (ATC) systems are being developed which contain time-based (4-D) trajectory predictions of aircraft. Airborne flight management systems (FMS) exist or are being developed with similar 4-D trajectory generation capabilities. Differences between the ATC-generated profiles and those generated by the airborne 4-D FMS may introduce system problems. Significant design challenges must be addressed to ensure the compatibility of future airborne and ground-based systems.

A simulation experiment was conducted to explore integration of a 4-D-equipped aircraft into a 4-D ATC system. The TSRV Simulator was linked in real time to an Ames Research Center ATC simulation for this effort. Candidate procedures for handling 4-D-equipped aircraft were devised, and traffic scenarios were established which required time delays absorbed through speed control alone or in combination with path stretching. A unique vertical situation display, shown in the figure, provided the pilots in the TSRV cockpit with guidance for flying the 4-D trajectories.

The 4-D procedures and FMS operation were well received by the airline pilots, who achieved an arrival accuracy at the metering fix of 2.9 s standard deviation time error. Dissimilarities between airborne and ATC-generated speed strategies were found to be a problem under moderate traffic conditions when most of the traffic remained on established routes. The different cruise speeds of the TSRV (flying FMS-generated speeds) and the other traffic (flying ATC-generated speeds) produced potential in-trail conflicts that required controller intervention. The TSRV was found to be more efficient in flying trajectories with speeds that conformed to the ATC strategy when traffic conditions required speed control by ATC.

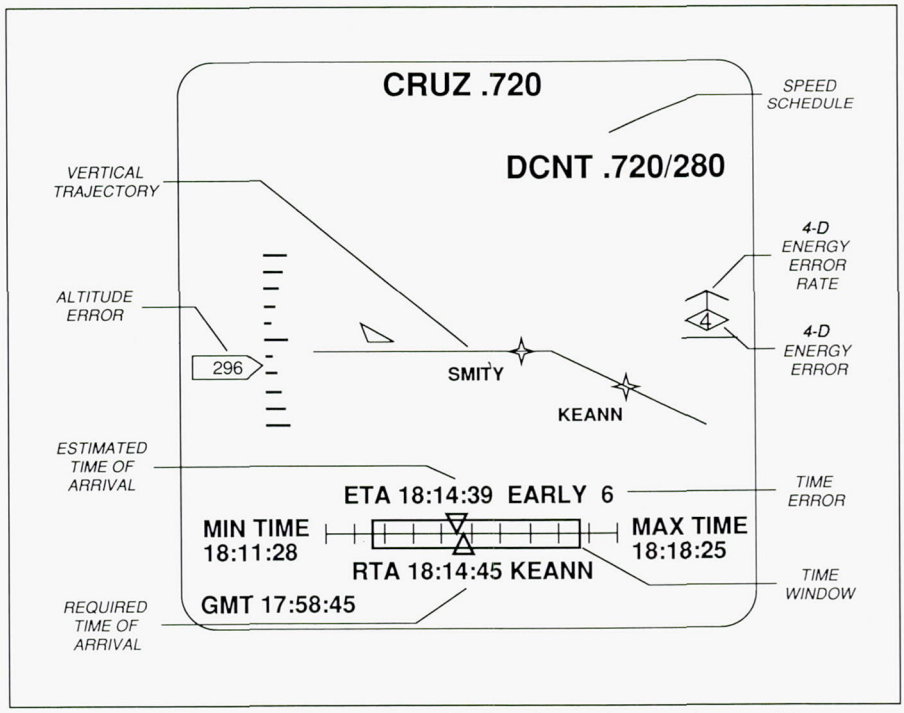

TSRV Simulator vertical situation display for airborne time guidance.

Heavy traffic conditions, where time delays forced off-route path stretching, were found to produce the greatest operational benefit of the airborne 4-D FMS. The pilots were able to consistently fly controller vectors to absorb time delays using their FMS vertical situation display to decide when to turn back on course. This procedure showed the potential to relieve controller work load while improving efficiency.

(David H. Williams, 42023)

Crew Station Systems Research Laboratory

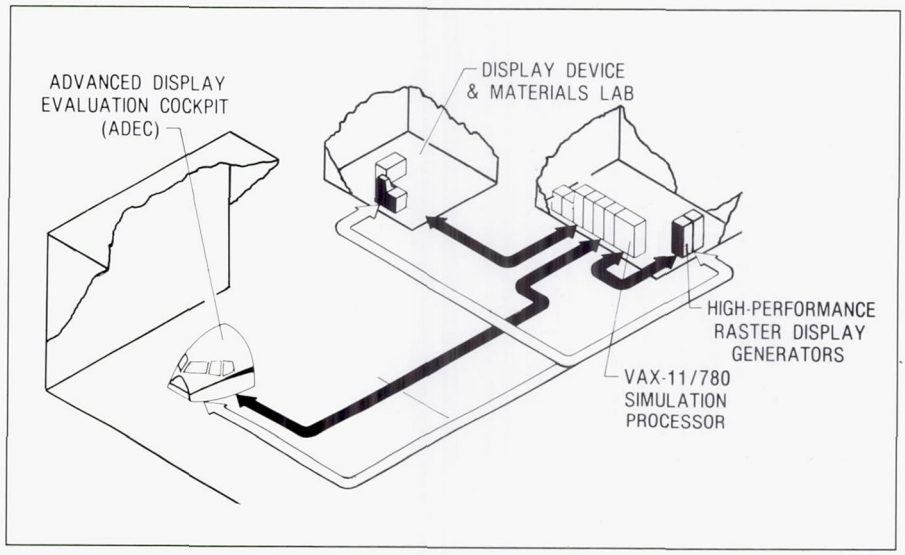

The trend in modern cockpits has been to replace electromechanical instruments with electronic control and display devices. The NASA Crew Station Electronics Technology research program is at the forefront of this trend with research and development activities in the areas of advanced display media, display generation, and cockpit controls/displays/flight subsystems integration. Specific areas of current interest are high-performance stereo pictorial primary flight display graphics; information management techniques; large-screen full-color display media; wide-screen, panoramic display concepts; virtual, panoramic, real-world displays; and image sensor fusion techniques.

The Crew Station Systems Research Laboratory (CSSRL) serves as a primary testing facility for the concepts and devices emerging from this research program. The laboratory provides a unique civil capability to conduct iterative development and pilot/vehicle experimental evaluation research for advanced cockpit technologies in a highly realistic flight simulation environment. The CSSRL also provides a lighting research facility that represents the full range of ambient and solar lighting conditions to be encountered by an aircraft cockpit and allows for the determination of not only the lighting characterizations of cockpit displays but also the determination of pilot/vehicle performance effects under realistic lighting conditions.

Major elements of the CSSRL are the Advanced Display Evaluation Cockpit (ADEC), which is a reconfigurable research cab; the Aircraft Cockpit Ambient Lighting and Solar Simulator (ACALSS), which provides real-world ambient and solar lighting conditions to the ADEC cockpit; and two separate general-purpose digital processors, one of which handles system input/output and vehicle math model simulation, while the other acts as host processor and preprocessor for two graphics generators. Other major elements include three high-performance raster graphics display generators (one of which has its own host co-processor), which provide sophisticated graphics formats to the display devices (cathode-ray tubes, flat panels, and helmet-mounted displays); a fiber optic link to the central computing facility, which can provide high-fidelity simulation math models for research requiring more complex vehicles; and a Display Device and Materials Laboratory, which provides facilities for flat-panel materials/device technology developments and photometric bench evaluations.

Achievement of Improved Tracking and Monitoring Performance Through Use of Stereopsis and Color Cueing

The use of monochrome helmet-mounted display (HMD) systems is becoming prevalent in today's complex flight mission environment. These HMD systems can provide stereopsis cueing as an almost natural byproduct for binocular helmet systems. The application of stereopsis (true depth) cueing to heads-down flight display concepts has demonstrated gains in pilot situational awareness and improved task performance. The use of color in information displays is somewhat similar to

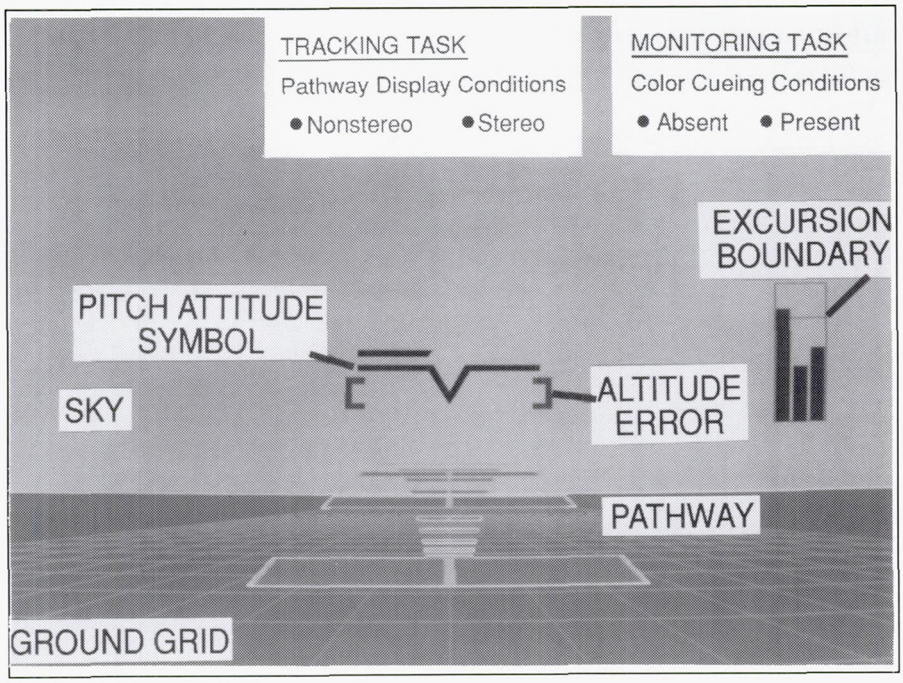

Display format and associated tasks. L-89-13515

the use of stereopsis cueing; in both cases, the advantages seem obvious and intuitive, but the disadvantage (i.e., additional cost) has caused their use to be debated. Unlike stereopsis, the technology for color is not yet available with today's HMD flight systems. The goal of this research was to assess the use of color cueing in peripheral monitoring displays and of stereopsis cueing in the foveal display of tracking information as may be encountered in future HMD systems.

A single-axis vertical tracking task for a rotorcraft, using a pathway-in-the-sky format (as shown in the first figure), was chosen as the primary task for the pilot-in-the-loop experiment. A monitoring

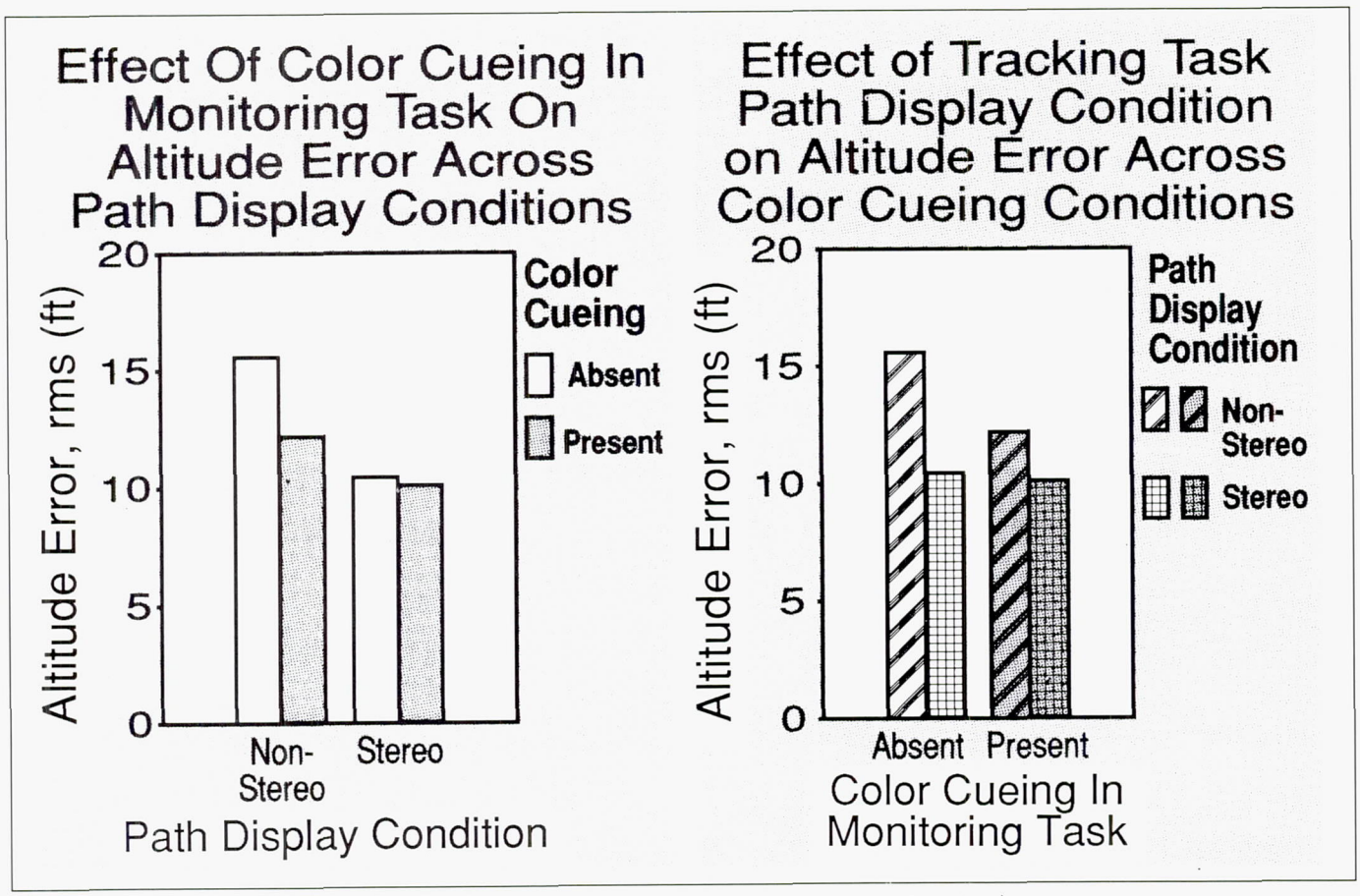

Tracking task performance effects (performance of five U.S. Army rotorcraft pilots).

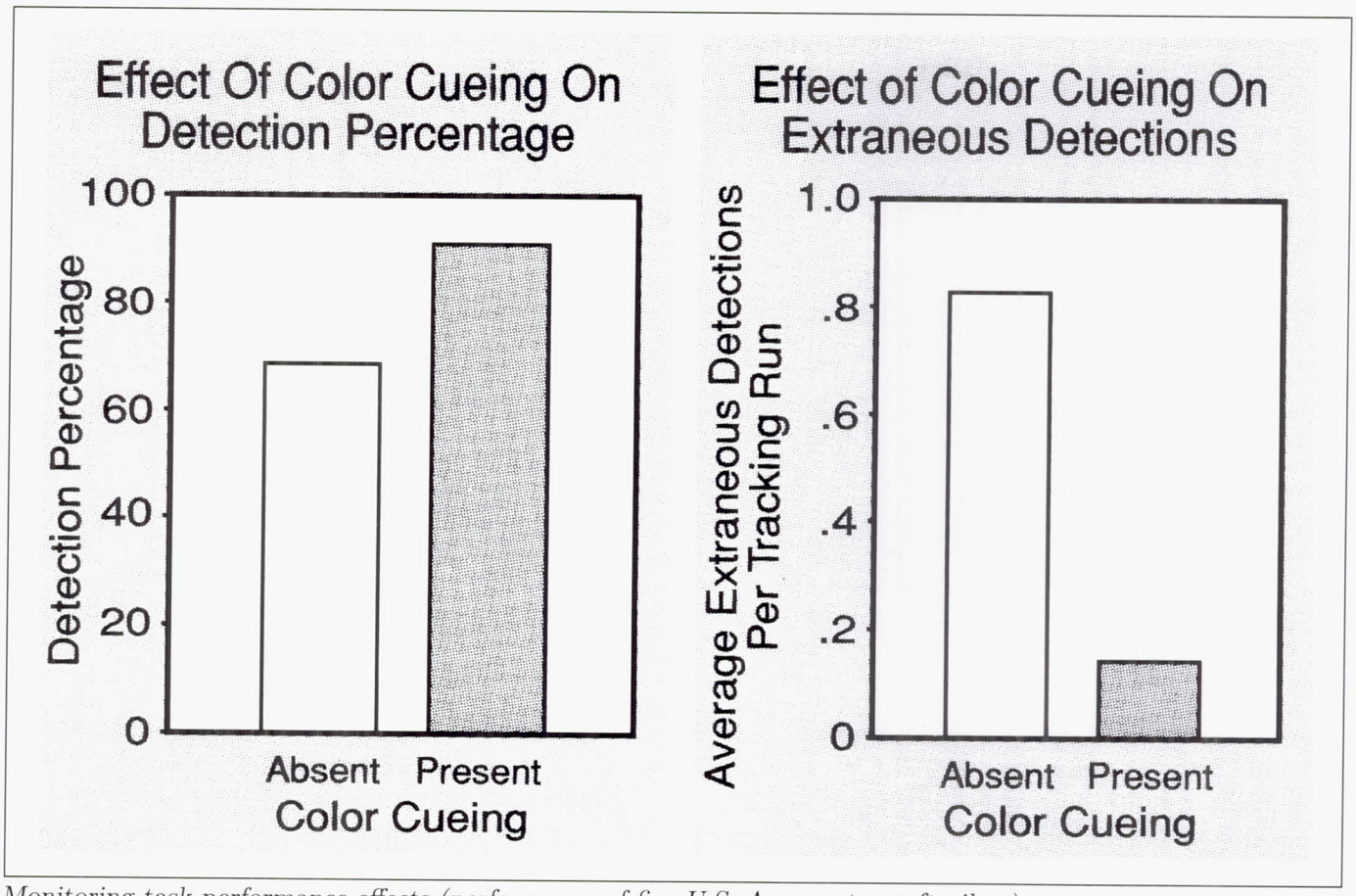

Monitoring task performance effects (performance of five U.S. Army rotorcraft pilots).

task (detection of boundary excursions) was presented in the periphery of the display (first figure). Because current HMD's cannot provide the capabilities of nonstereo and stereo cueing with color capability, a heads-up color CRT (cathode-ray tube) stereo monitor configuration was used to emulate an HMD. The total field of view of 40° was partitioned into a foveal area of 20° and left- and right-peripheral areas of 10°. The primary tracking task was presented as a nonstereo/stereo pathway in the foveal area, while the monitoring task was presented in the peripheral area, with the presence/absence of color cueing.

The addition of color cueing to the monitoring task resulted in improvements in the primary tracking task, but only when using a nonstereo pathway (as shown in the left-hand side of the second figure). The addition of stereopsis cueing to the pathway display resulted in improvements in the primary tracking task, with or without color in the monitoring task display (as shown in the right-hand side of the second figure). The addition of color cueing in the monitoring task display resulted in an increase in the number of correct boundary excursions detected by the pilots and in a decrease in the number of extraneous (false) detections (as shown in the third figure). In future HMD systems, the inclusion of both stereopsis cueing in the foveal area (to provide enhanced situational awareness in precision tasks) and color cueing in peripheral monitoring tasks (to enhance alerting functions) is desirable. **(Russell V. Parrish and Steven P. Williams, 46649)**

Dramatic Improvement in Stereo Depth-of-Field Display

Recent research in the application of stereopsis to real-world, three-dimensional (3-D), pictorial flight displays has demonstrated gains in pilot situational awareness and improved task performance and has documented pilot preference for stereo versions of these displays. These encouraging results have occurred despite

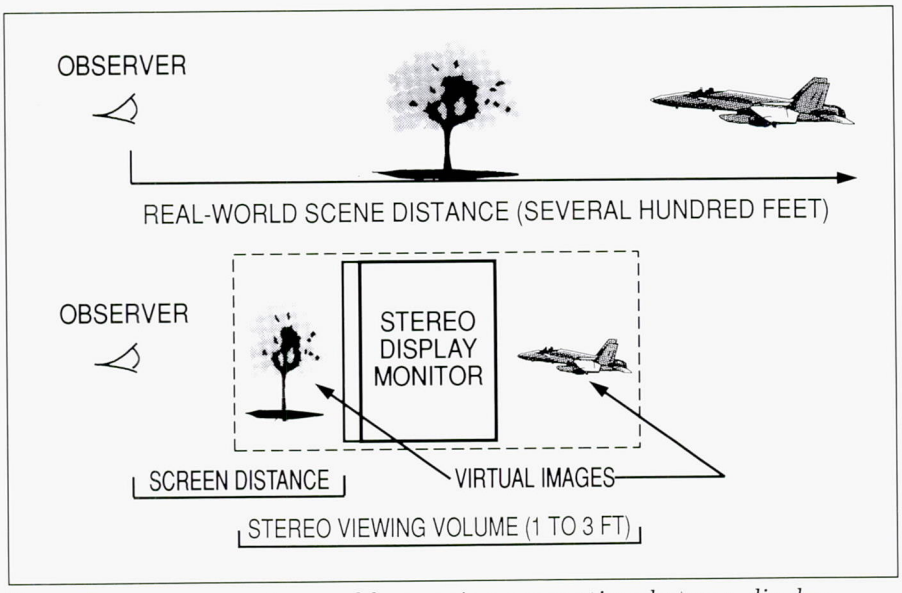

Scene-to-screen mapping problems using conventional stereo display technology.

Screen distance	Depth of viewing volume	Field of view (degrees)
19 in.	16.2 in.	40.0
38 in.	32.3 in.	20.6
57 in.	48.4 in.	13.8
Infinity (collimation)	Very large depth postulated	40.0

Stereo display viewing volumes.

the use of conventional directly viewed (noncollimated) stereo display technology that severely limits the stereo depth-viewing volume. It is well-known from psychophysical research that the effective range of human stereo vision is several hundred feet. Constraints are imposed by the limited depth-viewing volumes of conventional directly viewed stereo 3-D display hardware, in which the real-world depth cues of hundreds of feet are mapped into a virtual volume with only several feet of depth (as shown in the first figure). The objective of this proof-of-concept effort was to investigate whether or not a dramatic increase in depth-volume for stereo 3-D displays would be provided by the application of collimated optics to the stereo display source.

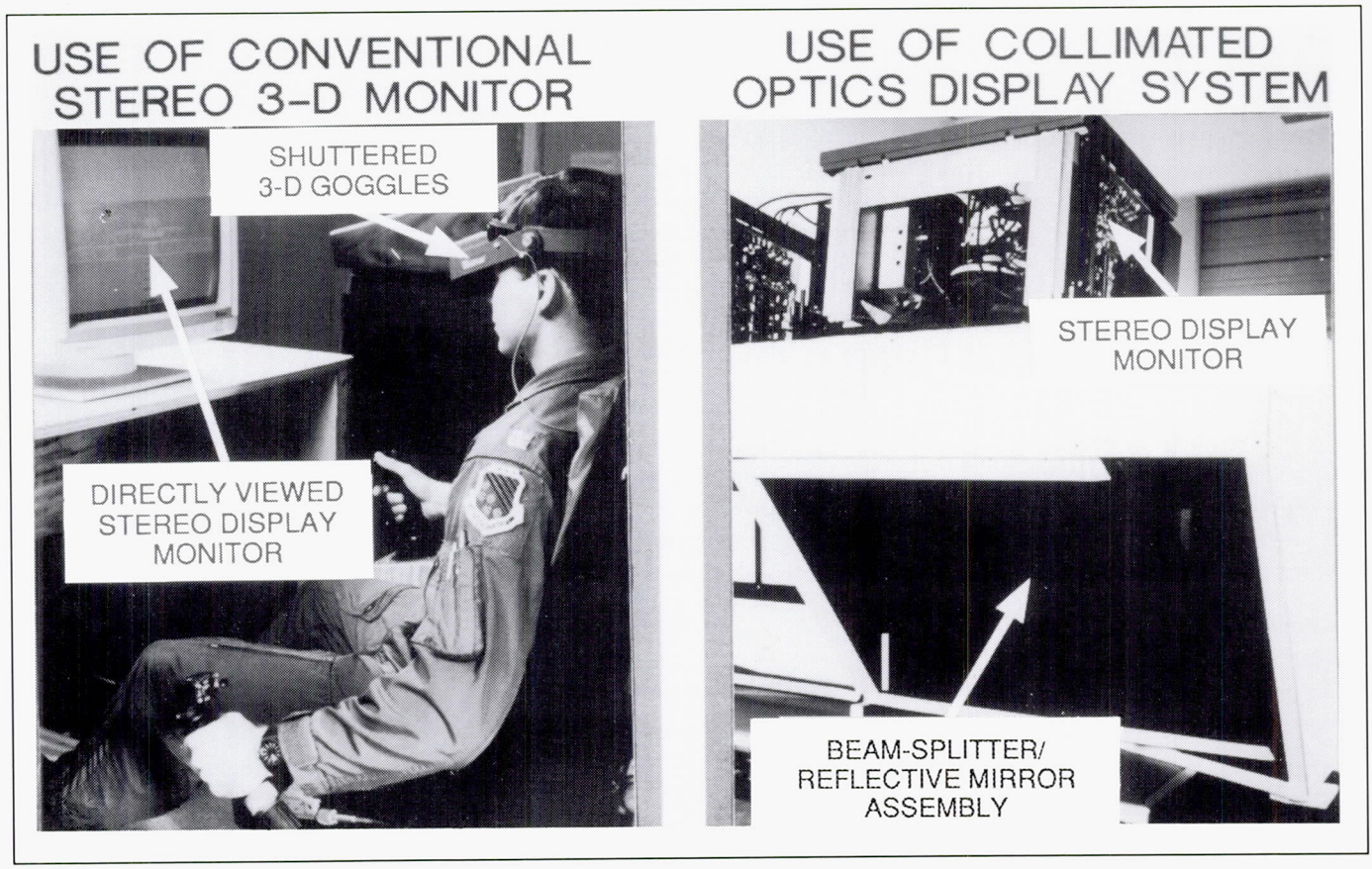

Stereo flight display test hardware.

Recent experiments at Langley Research Center discovered that the effective region of stereopsis cueing (i.e., the depth-viewing volume) increased with increasing viewer-screen distance (as shown in the second figure). However, this increase was accompanied by a decrease in the field of view of the system. Collimation of the display source would move the effective accommodation distance to near-infinity while maintaining the field of view at required levels. A dramatic increase in the depth-viewing volume was postulated due to relaxed accommodation/convergence restrictions. The conventional stereo 3-D monitor was mounted on a collimation system, and subjective determinations of the viewing-volume were made. These determinations revealed a one-hundredfold increase in depth compared to the conventional system (as shown in the third figure). Thus, a depth-viewing volume more commensurate with that of natural human vision was achieved. This dramatic increase in depth-viewing volume is a breakthrough in heads-down stereo display technology, and it will contribute to the full exploitation of stereopsis cueing in advanced display concepts, particularly in advanced applications such as a High-Speed Civil Transport (HSCT), which may require virtual windows and/or a see-through-the-nose pictorial display capability.

(Russell V. Parrish, Anthony M. Busquets, and Steven P. Williams, 46649)

Multicolor TFEL Display Fabrication Method Using Single-Phosphor Layer and Ion Implantation

Thin-film electroluminescent (TFEL) display technology is a candidate flat-panel display technology for future use in aircraft and spacecraft cockpits. Recently, full-color capability was achieved in TFEL displays through contractual research sponsored by NASA and the U.S. Army. However, the present method for fabricating full-color TFEL displays is highly complex in that it requires three separate phosphor deposition steps and three separate etching steps. The chemical etching is difficult to control and leads to low yields. The objective of this research was to develop and evaluate a new method of TFEL color display fabrication which would eliminate all the etching and two of the deposition steps, thereby resulting in a simpler fabrication method with higher yields.

A new method for the fabrication of multicolor TFEL displays was conceived and documented in the form of a U.S. patent application (NASA Case No. LAR 13616-1). To establish the feasibility of the fabrication method, which uses a single-phosphor layer in conjunction with ion implantation, a simplified test cell approach was utilized. The TFEL test cell was a single-phosphor-layer display having a 1-in. by 1-in. active area with 16 columns (as defined by addressing column electrodes). The single-phosphor layer used was ZnS:TbF_3 (zinc sulfide with 1 percent terbium fluoride), which is a green-emitting TFEL phosphor. Alternate columns of the test cell display were masked, and Mn (manganese) ions were implanted into the unmasked columns (as shown in the first figure). The regions receiving the ion implant become ZnS:TbF_3+Mn, which is a red-emitting phosphor. Following the implantation, the test cell was made into a functional TFEL display for testing through the addition of 16 row electrodes and an insulating (dielectric) layer.

Testing revealed that a two-color (red + green) TFEL display was successfully produced using a single deposition layer of host phosphor material and ion implantation in alternate columns. The ZnS:TbF_3 host phosphor, as deposited, emitted green light. The areas receiving the Mn ion

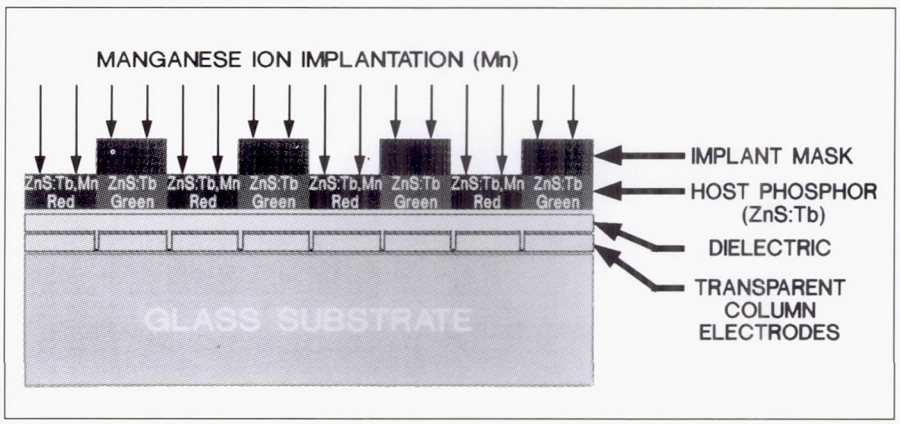

Multicolor TFEL flat-panel display fabrication by ion implantation.

L-89-10438

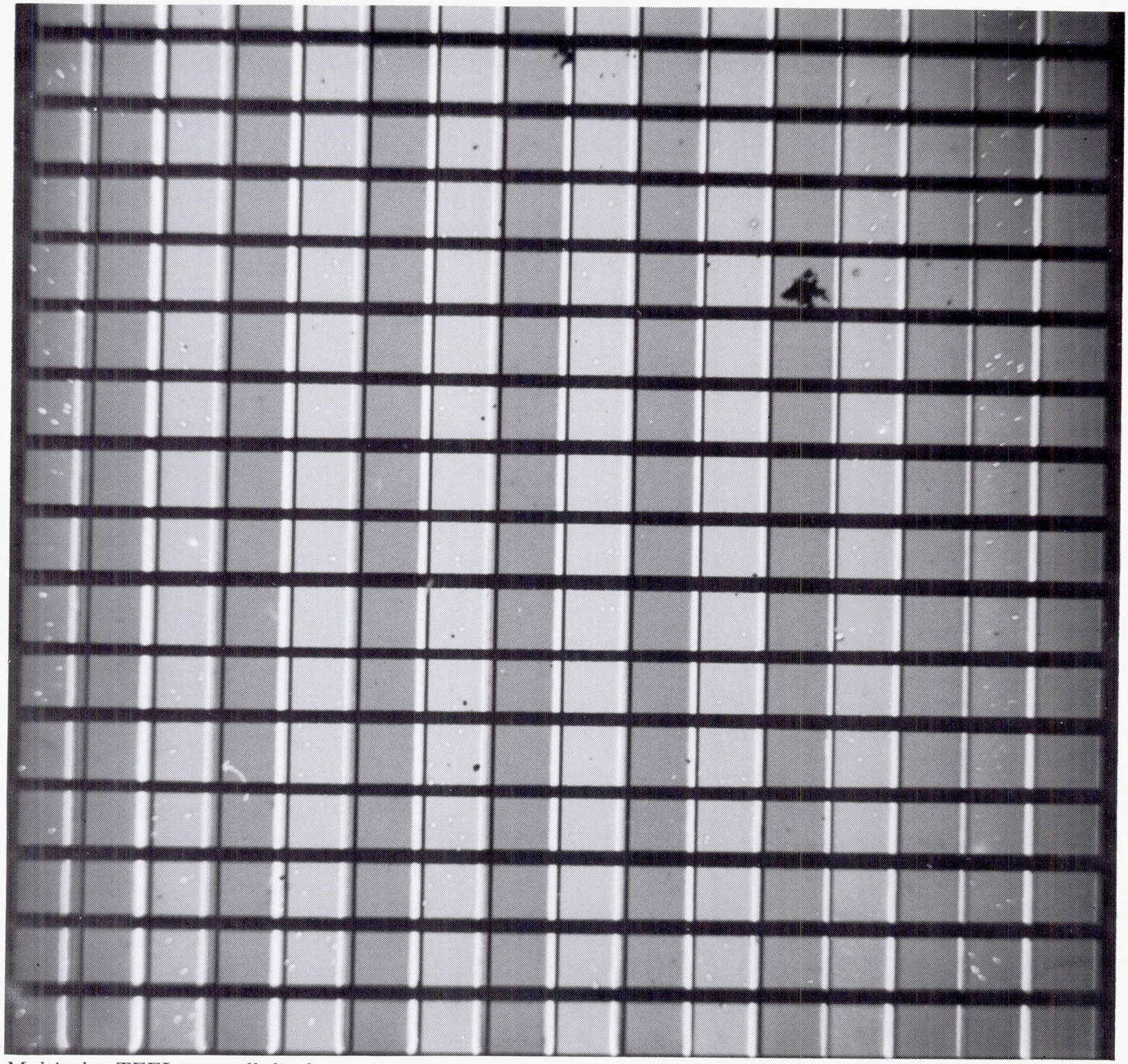

Multicolor TFEL test-cell display.

L-89-7775

implant emitted red-orange light. The resulting display device (as shown in the second figure) had eight green and eight red-orange stripes. The results of this experiment are proof of the concept of using ion implantation to produce multicolor TFEL displays having a single-deposition phosphor layer. This concept offers the possibility of a simpler fabrication process with higher yields than the currently used process by elimination of the difficult-to-control etching steps.

(James B. Robertson, 46654)

C-2

Human Engineering Methods Laboratory

The Human Engineering Methods (HEM) Laboratory has been established to develop measurement technology to assess the effects of advanced crew station concepts on the crew's ability to function without mental overload, excessive stress, or fatigue. The laboratory provides the capability for measurement of behavioral and psychophysiological response of the flight deck crew.

The facility comprises state-of-the-art bioinstrumentation as well as computer-based physiological data acquisition, analysis and display, and experiment control capability. Software has been developed which enables the demonstration of work load effects on the steady-state evoked brain response and transient evoked response signals as well as the monitoring of electrocardiographic (EKG), electromyographic (EMG), skin temperature, respiration, and electrodermal activity.

The Langley Research Center-developed oculometer capability has been integrated with the other physiological measurement techniques. Subjective rating and secondary task methods for assessing mental work load also have been implemented. A computer-based criterion task battery is available for preliminary testing (with human subjects) of work load techniques that are being validated prior to evaluation and application in the simulators. Satellite physiological signal conditioning and behavioral response capture stations are located at the simulator sites to provide human response measurement support for flight management and operations research.

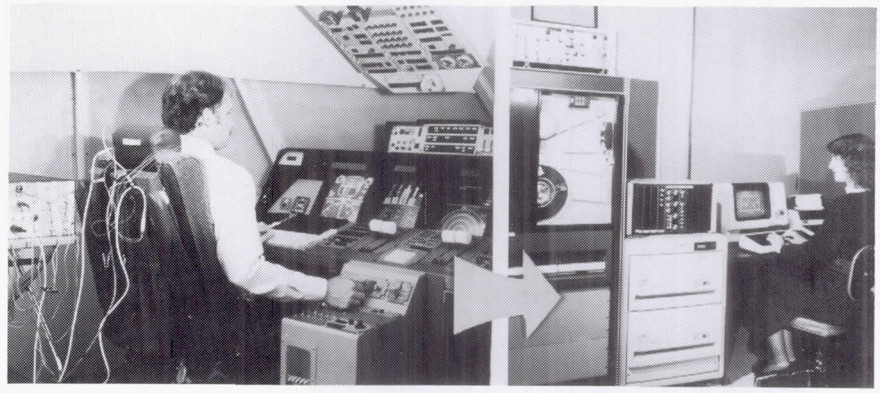

SIMULATOR WITH BIOINSTRUMENTATION

DATA ACQUISITION & ANALYSIS

Voice Measures of Mental Work Load

A series of studies was undertaken to determine the relationship between the acoustical properties of the voice and the work load demands placed on the speaker. Such measures of work load would be less obtrusive and better tolerated by pilots than present measures (which involve electrodes, such as the electrocardiogram, or which involve questionnaires). In the present study, subjects repeatedly spoke short, imperative sentences as pilots would do on an advanced flight deck employing voice recognition systems. This task elicited speech samples. A simultaneous loading task was used to manipulate work load. The time pressure of the loading task was great in a high-work-load condition and less in a low-work-load condition. The voice samples were subjected to a computer analysis used in previous studies of the mental state of psychiatric patients.

The results indicated that during both the high- and the low-work-load conditions, the amplitude of the voice fell over the course of the tasks. This drop-off occurred more quickly in the high-work-load condition. In the low-work-load condition, the amplitude recovered to earlier, higher levels following rest periods. In the high-work-load condition, this recovery did not occur. These results suggest that work load may not be best revealed by calculating the means of the acoustical parameters of the voice. Instead, it may be best to assess work load by the strain that it induces in the operator over time. Performing a high-work-load task over a period of time may cause strain, which in turn may reveal itself as a loss in the energy of the voice over time

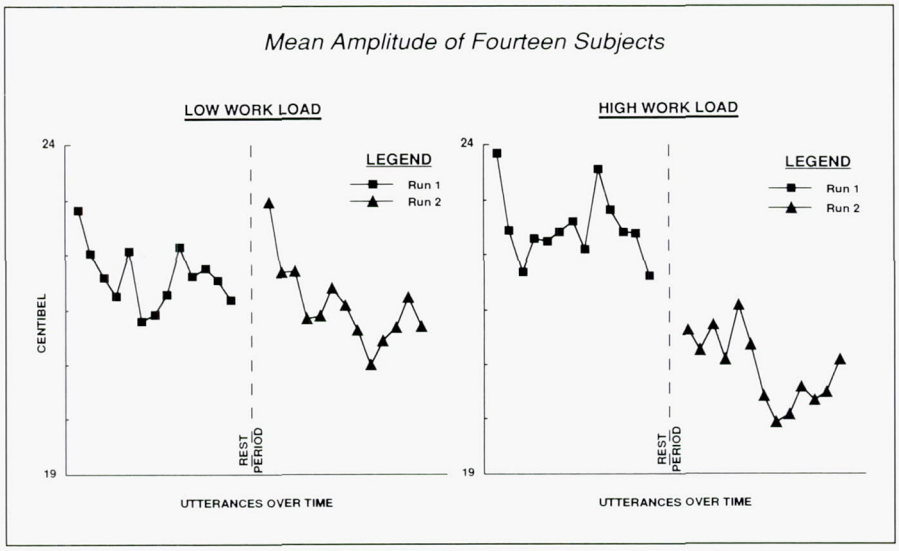

Relationship between voice amplitude over time and work load demands.

(that is, a reduction in loudness). Increased strain makes it less likely that the voice would regain its energy following rest periods. These findings were essentially replicated in follow-on tests in the Transport Systems Research Vehicle Simulator.

The results suggest that voice measures of work load could play a role in assessing the demands placed by new technology on operators. However, as results with pilots revealed, that role is limited by the variability among operators, and even within a single operator, by the effects of task demands on the voice. Increased mean amplitude may reflect heightened effort devoted to a task. Faster drop-offs in amplitude may reflect the fatigue resulting from sustained effort. In this way, the acoustical parameters of the voice may reveal the strategy that an operator uses for allocating effort during demanding situations.
(Alan T. Pope, 46642)

Indication of Lower Pilot Stress by Heart-Rate Measures for Stereo Pictorial Landing Approach Displays

Advances in technology have brought about numerous possibilities for the display of information to pilots in new, integrated display formats with the potential to improve situational awareness and pilot/vehicle performance. One potential advance in piloted displays is the presentation of pictorial information using stereopsis cueing. The objective of this research effort, undertaken as part of a larger piloted study on pilot/vehicle performance effects, was to determine if the use of stereopsis in a pictorial landing approach display would result in a reduction of pilot stress.

The study was designed to show the effects of stereopsis cueing upon heart-rate measures, because these measures have been demonstrated by Langley Research Center personnel and others to be indicative of pilot stress. Six U.S. Air Force pilots flew 24 transport aircraft landing approaches each in the Visual/Motion Simulator. The display presented a landing scene in stereo or nonstereo modes. The pictorial display offered guidance information in one of three curved-pathway formats, coupled with a lead aircraft that was to be followed in order to maintain the proper speed in the approach. The

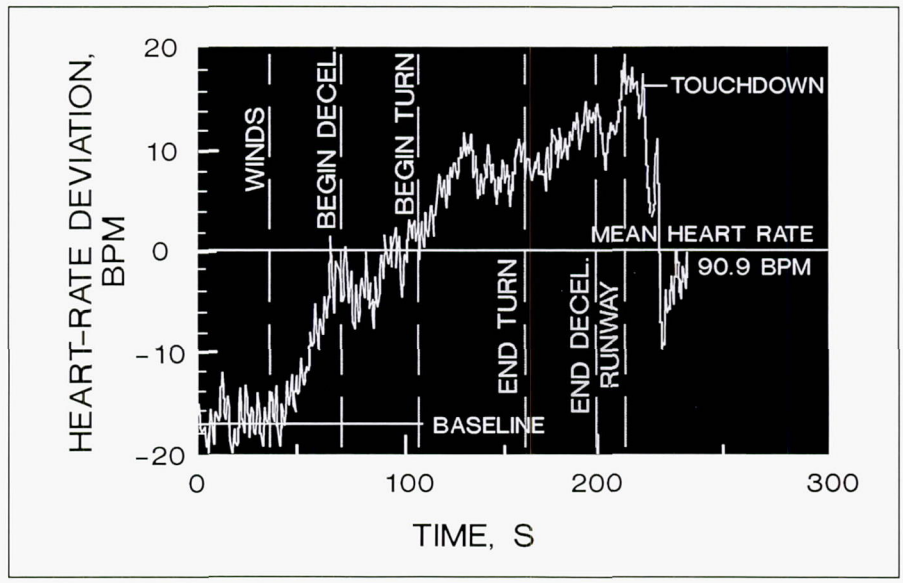

Typical heart-rate time history.

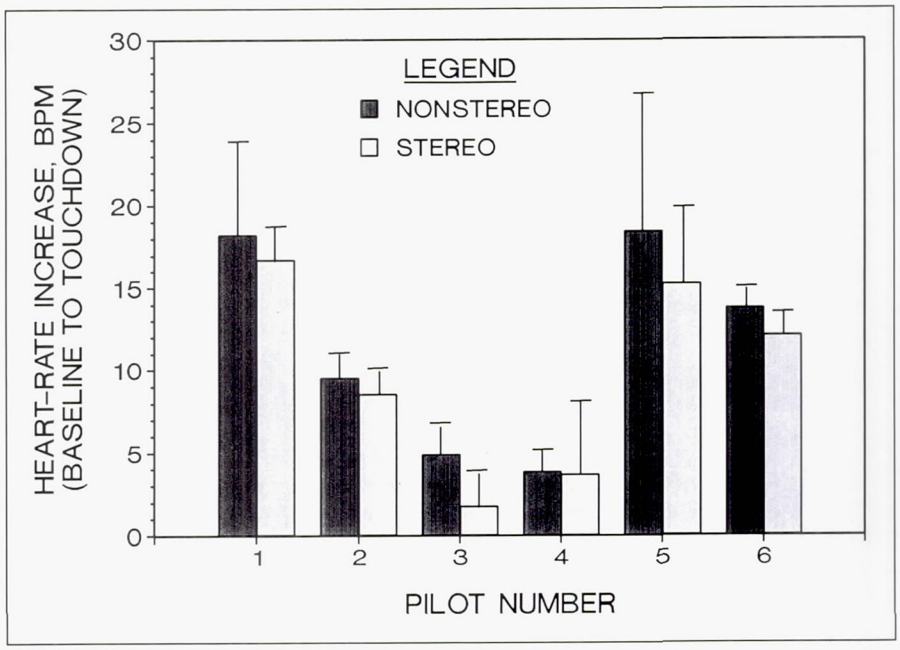

Comparison of pilot heart-rate responses to nonstereo landing approach display.

landing approach consisted of a curved, decelerating path to touchdown on the runway. The pilots were instrumented with electrocardiogram electrodes to record their inter-beat intervals. These data were sampled and stored for conversion to heart-rate data.

At the beginning of the run, the pilot had a level heart rate until the introduction of winds 36 s into the approach. This heart rate was taken as the baseline heart rate. The heart rate typically increased throughout the approach because of the increased amount of stress caused by the winds, then the curved, descending, decelerating approach, and then the flare-to-landing on the runway. The peak heart rate was measured at touchdown. The heart-rate measure used to indicate the level of stress of the run was the difference in the touchdown heart rate and the baseline heart rate. The difference between the average heart-rate increases with and without stereopsis cues is statistically significant at the 0.01 level. The average heart-rate increase for all pilots was 11.4 beats/min (BPM) for nonstereo presentations, but only 9.7 BPM for stereo presentations. These results indicate that stereopsis cues can reduce the amount of stress imposed upon pilots when using a pictorial display for the tasks involved in a curved, decelerating landing approach. Further, the results show that the increase in heart rate (between baseline and touchdown) is a far better physiological measure to use than heart rate at touchdown, because the increase in heart-rate measure is more tolerant of the variability between subjects.

(Randall L. Harris, Sr. and Mark Nataupsky, 46641)

General-Aviation Simulator

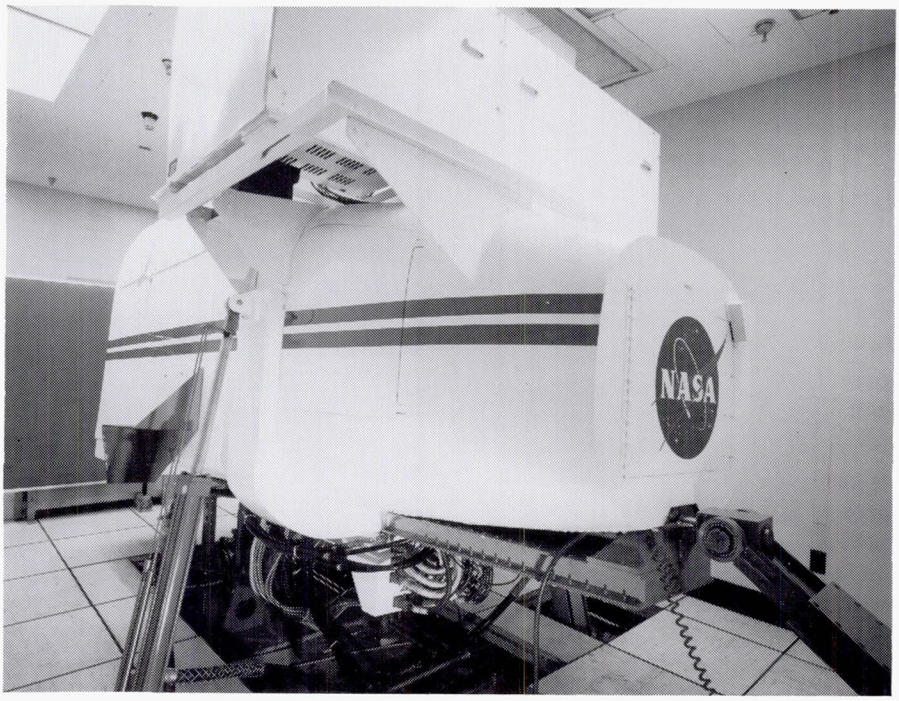

The General-Aviation Simulator (GAS) consists of a general-aviation aircraft cockpit mounted on a three-degree-of-freedom motion platform. The cockpit is a reproduction of a twin-engine propeller-driven general-aviation aircraft with a full complement of instruments, controls, and switches, including radio navigation equipment. Programmable control force feel is provided by a "through-the-panel" two-axis controller that can be removed and replaced with a two-axis side-stick controller that can be mounted in the pilot's left-hand, center, or right-hand position. A variable-force-feel system is also provided for the rudder pedals. The pilot's instrument panel can be configured with various combinations of cathode-ray tube (CRT) displays and conventional instruments to represent aircraft such as the Cessna 172, Cherokee 180, and Cessna 402B. A collimated-image visual system provides a 60° field-of-view out-the-window color display. The visual system can accept inputs from a terrain model board system and a computer-generated graphics system. The simulator is flown in real time with a CDC CYBER 175 computer to simulate aircraft dynamics.

Research has been conducted to improve the ride quality of GA aircraft by developing gust alleviation control laws to reduce the aircraft response to turbulence while still maintaining generally good flying characteristics. Research studies that are in progress are the GA Easy Fly, a program to investigate ways of making general-aviation airplanes easier to fly, especially for low-time or nonpilots, and a piloted simulation study to address handling qualities issues of advanced commuter-type turboprop configurations.

Easy-to-Fly General-Aviation Airplanes

New control and display concepts for the novice pilot are being developed and studied on the GAS. These systems are intended to reduce the initial training and recurring practice requirements for low-time or beginning pilots and thus make general aviation a safer and more practical transportation system. Two advanced systems are being simulated: a fly-by-wire automatic control system (Ez-Fly) and a head-up display (Highway in the Sky or HITS). The Ez-Fly control system is designed to decouple conventional airplane responses and provide responses to control inputs more similar to those of an automobile. The HITS display is designed to resemble a road marked with lane stripes as shown in the figure. In the top center of the display is a box in which commands are displayed to the pilot. Flight director arrows that guide the pilot to the center of the "highway" are displayed in the box most of the time. However, higher priority messages, such as those shown above the display, can temporarily displace the flight director arrows whenever the situation demands it.

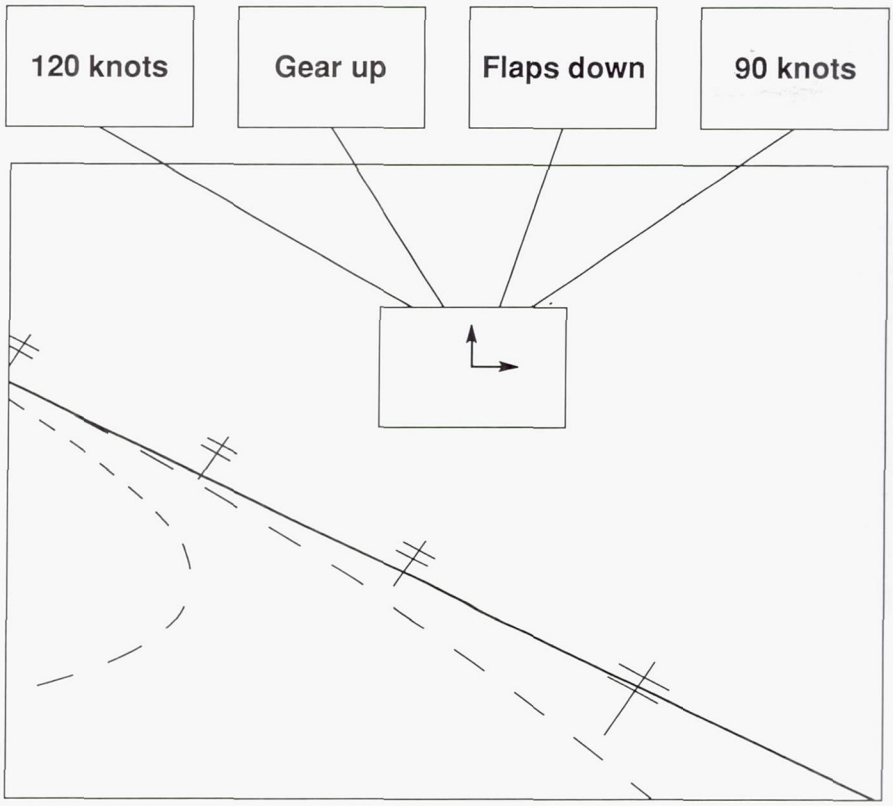

Highway-in-the-Sky display format.

In order to evaluate the instinctive reactions of the test subjects, no practice or training runs are given to the simulation test subjects, and only two runs are made with an individual test subject. Test subjects range from NASA research pilots to novice nonpilots, with an emphasis on the nonpilots. The first run is made with both the Ez-Fly control system and the HITS display. The second run is made with the HITS display and the conventional control system of the airplane. Many of the novice test subjects can fly a complete maneuver from takeoff to landing with the combined systems, but only a few can complete the maneuver with only the HITS display.

(Eric C. Stewart, 43939)

Differential Maneuvering Simulator

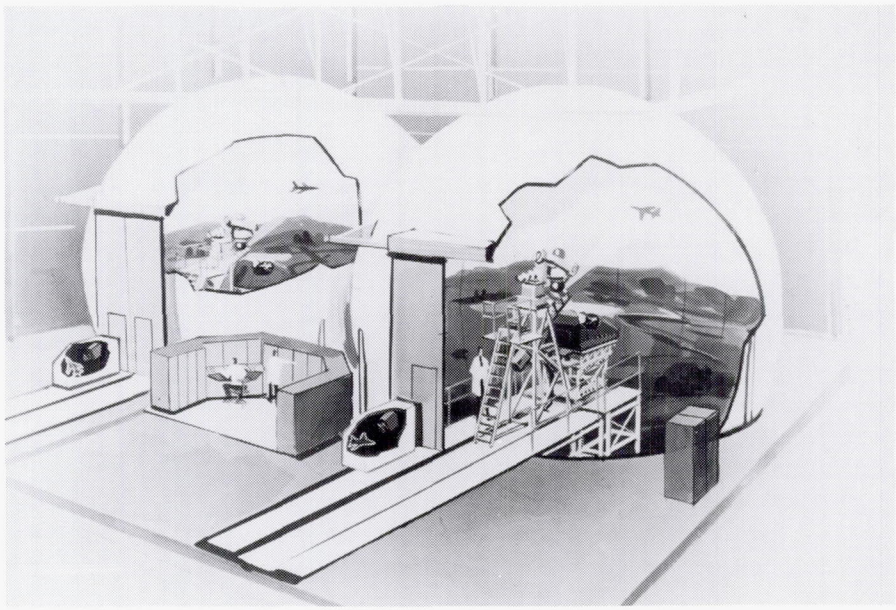

The Langley Differential Maneuvering Simulator (DMS) provides a means of simulating two piloted aircraft operating in a differential mode with a realistic cockpit environment and a wide-angle external visual scene for each of the two pilots. The system consists of two identical fixed-base cockpits and projection systems, each based in a 40-ft-diameter projection sphere. Each projection system consists of two terrain projectors to provide a realistic terrain scene and a system for target image generation and projection. The terrain scene driven by a Computer-Generated Image (CGI) system provides reference in all six degrees of freedom in a manner that allows unrestricted aircraft motions. The resulting sky/Earth scene provides full translational and rotational cues. The internal visual scene also provides continuous rotational and bounded (300 ft to 45,000 ft) translational reference to one or two other (target) vehicles in six degrees of freedom.

The target image presented to each pilot represents aircraft being flown by the other pilot in this two-aircraft simulator. This dual simulator can be tied to a third dome and can provide three aircraft interactions when required. Each cockpit provides three color displays with a 6.5-in. square viewing area and a wide-angle head-up display. Kinesthetic cues in the form of a g-suit pressurization system, helmet loader system, g-seat system, cockpit buffet, and programmable control forces are provided to the pilots consistent with the motions of their aircraft. Other controls include a side arm controller, dual throttles, and a rotorcraft collective. Research applications include studies of high-angle-of-attack flight control laws, evaluation of evasive maneuvers for various aircraft and rotorcraft, and evaluations of the effect of parameter changes on the performance of several baseline aircraft.

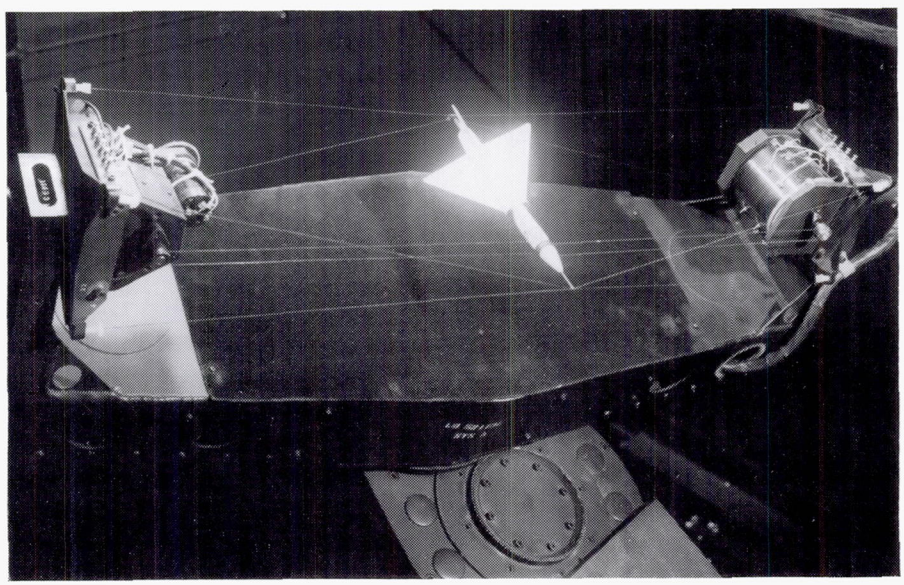

Target model. L-71-2579

Fighter Agility Research

Numerous studies have shown that enhanced high-angle-of-attack agility can significantly improve effectiveness in close-in air combat. A broad research program is under way at Langley Research Center to develop technologies that will provide future fighter aircraft with greatly enhanced agility at high-angle-of-attack flight conditions. This capability can be achieved through the use of advanced control concepts such as vectoring of the engine thrust and unconventional aerodynamic devices. Design requirements and guidelines are needed to implement most effectively this enhanced capability. Studies are under way to define and quantify enhanced agility/handling qualities related to improved high-angle-of-attack capability; develop the design requirements for agility/handling qualities, including tradeoffs; and develop the design tools/methodologies to enable these requirements to be met. The investigations include wind tunnel testing, analytical studies, and simulation investigations.

View of cockpit and visual display. L-88-7175

Piloted simulation studies on the Differential Maneuvering Simulator (DMS) are being conducted to investigate and quantify the high-angle-of-attack agility enhancements provided by thrust-vectoring controls. A full-envelope simulation model of the F-18 airplane incorporating a representative thrust-vectoring control system is being used in these investigations. A set of evaluation maneuvers was developed to serve as the basis for the study and for quantification of the agility characteristics of the F-18 with and without thrust-vectoring controls. The results show that thrust-vectoring controls can provide greatly enhanced high-angle-of-attack agility over the baseline airplane with only aerodynamic controls. However, proper design of the control laws is vital to maximize these benefits in air combat. An initial correlation of these results with full-scale flight data was obtained by flying the same evaluation maneuvers on the NASA F-18 High-Alpha Research Vehicle (HARV). The motions seen in flight agree well with those predicted in the simulation. These tests will be repeated in further tests of the HARV with thrust-vectoring controls that are currently being implemented on the airplane.

(Marilyn E. Ogburn, 41175)

Visual/Motion Simulator

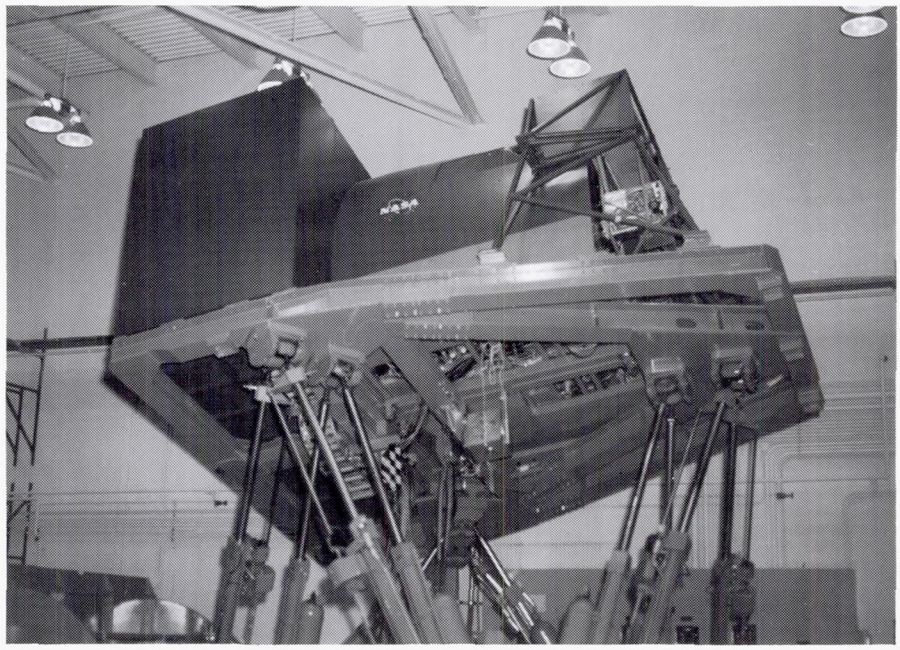

The Visual/Motion Simulator (VMS) is a general-purpose simulator consisting of a two-person cockpit mounted on a six-degree-of-freedom synergistic motion base. A collimated visual display provides 60° out-the-window color display for both left and right seats. The visual display can accept inputs from several sources of image generation. A programmable hydraulic-control loading system is provided for column, wheel, and rudder in the left seat. A second programmable hydraulic-control loading system for the right seat provides roll and pitch controls for either a fighter-type control stick or a helicopter cyclic controller. Right-side rudder control is an extension of the left-side rudder control system. A friction-type collective control is provided for both the left and the right seats. An observer's seat was installed in 1986 to allow a third person to be in the cockpit during motion operation.

A realistic center control stand was installed in 1983 which, in addition to providing transport-type control features, provides auto-throttle capability for both the forward and reverse thrust modes. Motion cues are provided in the VMS by the relative extension or retraction of the six hydraulic actuators of the motion base. Washout techniques are used to return the motion base to the neutral point once the onset motion cues have been commanded. In addition, a g-seat is provided which can be interchanged between the left and right seats to augment the motion cues from the base.

Research applications have included studies for transport, fighter, and helicopter aircraft as well as for the National Aero-Space Plane (NASP). These studies addressed phenomena associated with wake vortices, high-speed turnoffs, microwave landing systems, energy management,

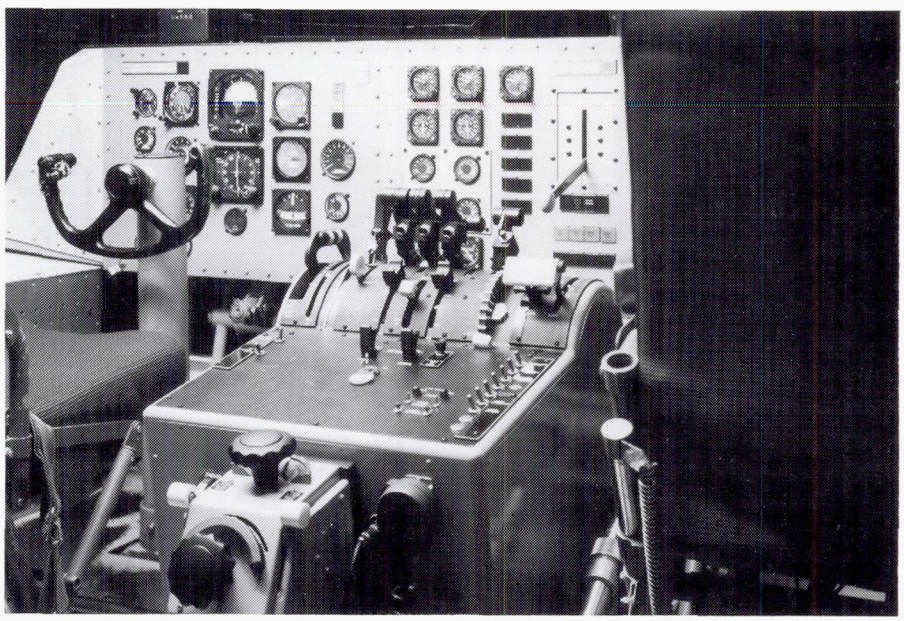

Visual/Motion Simulator cockpit. L-84-1079

multibody transports, maneuvering stability flight characteristics, wind shear recovery guidance, vortex flaps, and stereographic displays. Numerous simulation technology studies have also been conducted to evaluate the generation and usefulness of motion cues.

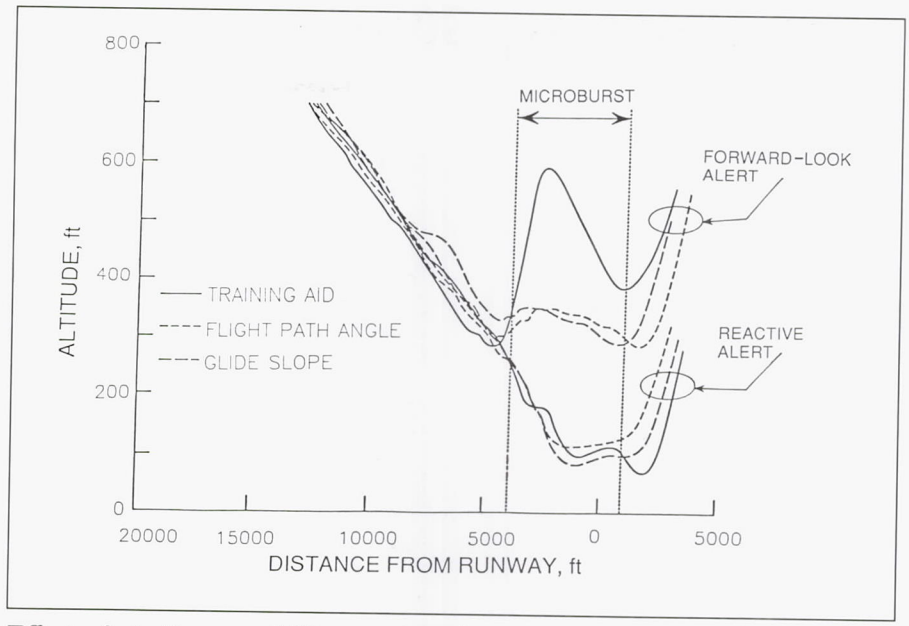

Effect of alerting capability on aircraft trajectory during wind shear encounter.

Evaluated Benefits of Forward-Look Wind Shear Detection During Landing Approach

Microburst wind shear poses a significant threat to transport aircraft during takeoff and landing. Among the issues concerning the aviation industry are how to recover from an inadvertent microburst encounter, what safety benefits can be achieved from forward-look wind shear sensing, and how far ahead of an airplane must a sensor see to ensure successful escape from a microburst. The objective of this research was to provide answers to these questions in a piloted-simulation environment.

Batch simulations of airplane recoveries from microbursts were conducted to evaluate candidate recovery strategies and the effect of varying the point at which the recovery was initiated. Three recovery strategies were chosen and implemented as flight director guidance in the VMS and programmed with a Boeing 737-100 math model. Both reactive and forward-look wind shear detection capabilities were simulated. Two wind shear models, a numeric model of the Dallas-Fort Worth microburst and a simple analytical model, were implemented. A total of 455 microburst encounters were made by 7 pilots, including research and air carrier pilots.

The three recovery strategies that were chosen for implementation were to rotate to an initial pitch of 15°, then control sink rate; track the glide slope to a preset altitude at full thrust to preserve airspeed, then fly level until exiting the wind shear; and manage the flight path angle to avoid obstacles and unnecessary climb and airspeed loss. The first strategy, which was used as a baseline, is an industry-accepted technique being taught to airline crews. The results showed that the factor that caused the greatest improvement in recovery performance was the time at which the recovery was initiated. When given only a reactive wind shear alert, the difference in recovery performance between the three strategies was not statistically significant. When given a forward-look alert, the advanced strategies showed improved characteristics over the baseline, but they had similar minimum altitudes. With the forward-look detection looking only 10 s ahead of the airplane, however, the improvement in recovery performance was very significant compared to receiving only a reactive alert. The figure shows examples of recovery trajectories with the three strategies and two alerts. All pilots provided very positive comments about the forward-look alerting capability.

The results provide the first quantification of the benefits of a forward-look alerting in a piloted simulation environment and have implications for near-term decisions being made by researchers and manufacturers in the field of remote sensing and by air carriers in the procurement of wind shear systems.
(David A. Hinton, 42040)

Active Flexible-Wing Simulator

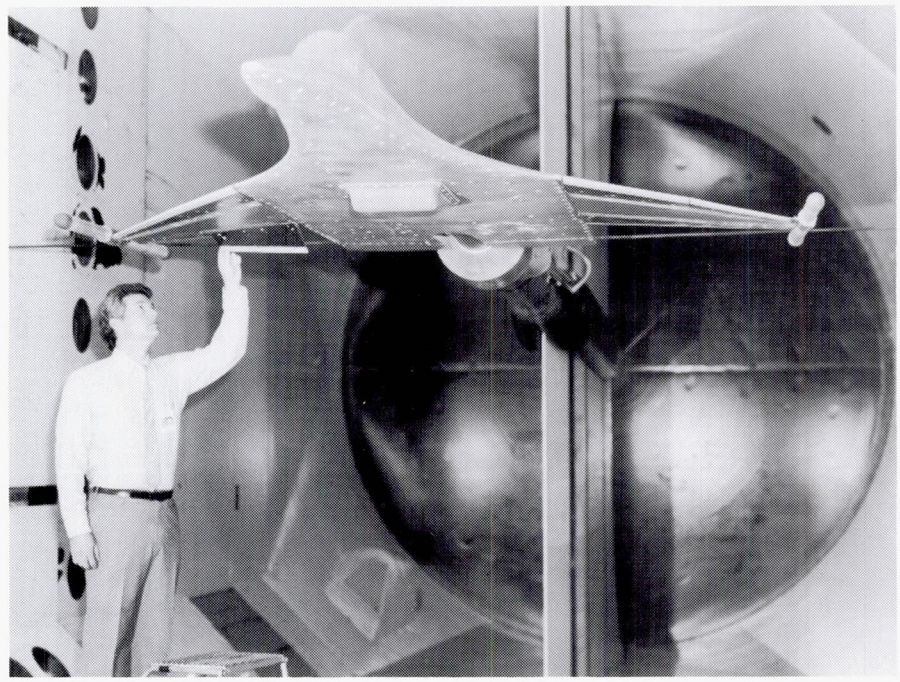

Most flight simulations at Langley Research Center are concerned with man-in-the-loop research aircraft; however, occasionally the real-time simulation facilities are used to study other dynamic systems (for example, the Active Flexible-Wing (AFW) wind tunnel model and its control computer). This simulation is configured with a CYBER 175 computer, a real-time control console, an engineer's console, an ADAGE Graphics Computer System, a CAMAC interface site, and the AFW control computer. The AFW wind tunnel model is programmed and simulated on the CYBER 175 in synchronized slow time with an integration time step of 1/2000 s and a clock step of 1/80 s when both symmetric and antisymmetric math models are simulated together. This procedure results in a synchronized slow time of 1/25 real time.

The control console is used to operate the simulation through the use of its touch panel, which can be programmed to represent various control switches. In addition, the programmer has available various readouts on the control console to monitor the simulation. The engineer's console provides various digital readouts and displays for monitoring the AFW experiment and a number of switches and potentiometers to allow parameter changes and inputs during the experiment. An ADAGE Graphics Computer, which is interfaced directly to the CYBER 175, displays a color-coded, three-dimensional wireframe outline of the AFW model. The display presents aircraft pitch, roll, and yaw angles, control surface deflections, and up to 10 modes of vibration. The CAMAC interface site converts CYBER 175 digital signals to analog signals that are sent to the AFW control computer through the wind tunnel interface unit. In addition, the CAMAC site converts analog signals coming from the AFW control computer to digital signals to be sent to the CYBER 175. The AFW control computer, which is programmed with the various control laws, runs during the simulation experiments with a clock step of 1/8 s for both symmetric and antisymmetric models running together, and an integration time step of 1/200 s. This process maintains the same synchronization between the AFW control computer and the real-time computer as would exist between the AFW control computer and the wind tunnel model during wind tunnel tests.

Hot-Bench Testing of Control Computer Used in Active Flexible-Wing Wind Tunnel Test Program

The purpose of this work, which took place in the Active Flexible-Wing Simulator, was to develop a simulation tool to validate the implementation of digital control laws being used to actively control the elastic deformation of a wind tunnel model. The wind tunnel model is a dynamically scaled model of an advanced tailless fighter being tested in the Transonic Dynamics Tunnel as part of the Active Flexible Wing

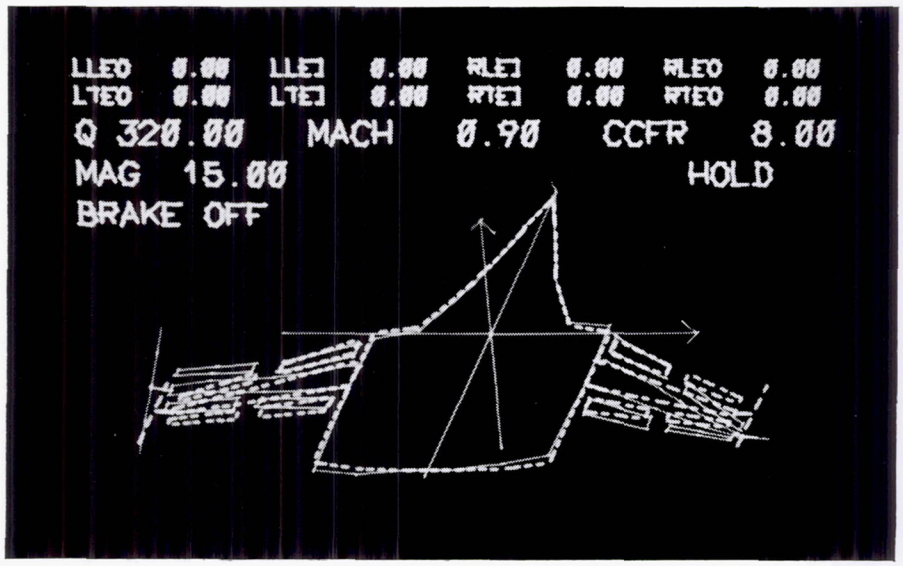

ADAGE graphics display of simulated AFW wind tunnel model. L-89-10758

(AFW) Program. Real-time simulation using rigid-body aircraft dynamic models is a frequently employed, well-understood step in the validation of flight control laws. The implementation of the more complex, aeroelastic vehicle equations is a challenging application of real-time simulation technology.

Prior to wind tunnel entry, end-to-end validation testing of the digital controller was accomplished using a real-time Hot-Bench Simulation (HBS) of the AFW wind tunnel model. The HBS computer program was developed to use data generated with existing aeroservoelastic analysis tools and implemented on the Analysis and Computation Division's advanced real-time simulation system. The simulation dynamic model included symmetric and antisymmetric elastic modes, third-order actuator models, unsteady aerodynamic "lag" states, symmetric and antisymmetric turbulence models, and first-order antialiasing filters on the feedback signals. An integration step size of 1/2000 s was used in combination with an update clock rate of 80 frames per second, the maximum update rate possible without losing time synchronization. While the HBS runs 25:1 "slow," dynamic validity is maintained by clocking the digital controller at 8 frames per second during HBS testing instead of 200 frames per second as used in the wind tunnel. While future work will attempt to reduce the slow to real-time ratio, a benefit of running in slow motion is that the critical model dynamics, which occur at 9 to 11 cycles per second in real time, may be more easily observed on the graphics display. To assist in understanding the AFW model dynamic behavior, a real-time display on the ADAGE Graphics Computers was developed as shown in the figure. The graphic uses the finite-element structural model of the vehicle, highlighting the main body and wings and the eight control surfaces. The dashed line represents the undeformed configuration. The deformations shown are exaggerated by a factor of 15.

The HBS was essential in debugging and validating the digital controller prior to tunnel entry. The implementation of appropriate real-time simulation models is an enabling technology for the design of active structural control for highly integrated airplanes.

(Carey S. Buttrill, 44016)

DC-9 Full-Work-Load Simulator

L-84-224

The DC-9 Full-Work-Load Simulator consists of a fixed-base McDonnell Douglas DC-9-30 cockpit, a test console, and electronics cabinets. This cockpit was formerly a DC-8 cockpit, but it was recently upgraded to provide the capability for dedicated DC-9 full-work-load simulations. Stations are available in the cockpit for a captain and a first officer. Flight control responses for elevator, aileron, and rudder are simulated by forces from hydraulic servo systems. Manual throttle control for two engines is provided on the center console. The forward electronics panel of the center console is outfitted with a 9-in. color cathode ray tube (CRT) which can be used to display computer-generated graphic presentations, such as Cockpit Display of Traffic Information (CDTI) or Area Navigation (RNAV). A transparent touch panel superimposed over the face of the CRT provides a discrete input to the computer when any point on the surface is touched. Work is progressing toward improvement of this simulator through retrofit of a modified aircraft center console with autothrottle capability and through the installation of a collimated visual display system to provide an out-the-window color display for both the captain and the first officer.

Full-work-load studies can be performed in this simulator because the capacity exists to simulate all aircraft instruments, annunciators, switches, and alarms. Three very-high-frequency (VHF) communication receivers are simulated for VOR/ILS (VHF Omnidirectional Range/Instrument Landing System). One ADF (Airborne Direction Finder) radio receiver and three marker beacon receivers are simulated in this cockpit. In 1986, a visual display system was installed to display out-the-window scenes to the pilot and copilot. The visual display system was upgraded in 1989 for compatibility with the Computer-Generated Image system. In 1988, a Control Display Unit (CDU) was installed in place of the CDTI CRT.

Prior to initiating dedicated research in this simulator, it was necessary to evaluate the full-work-load aspects of the simulator, validate the fidelity of the aircraft and subsystem models, and obtain baseline data on airline procedures. Normal approach and departure operations in the Denver area were flown by five pilots from two different airlines. Baseline data concerning crew procedures, simulator performance, and subsystem modeling were obtained and have been incorporated in the overall simu-

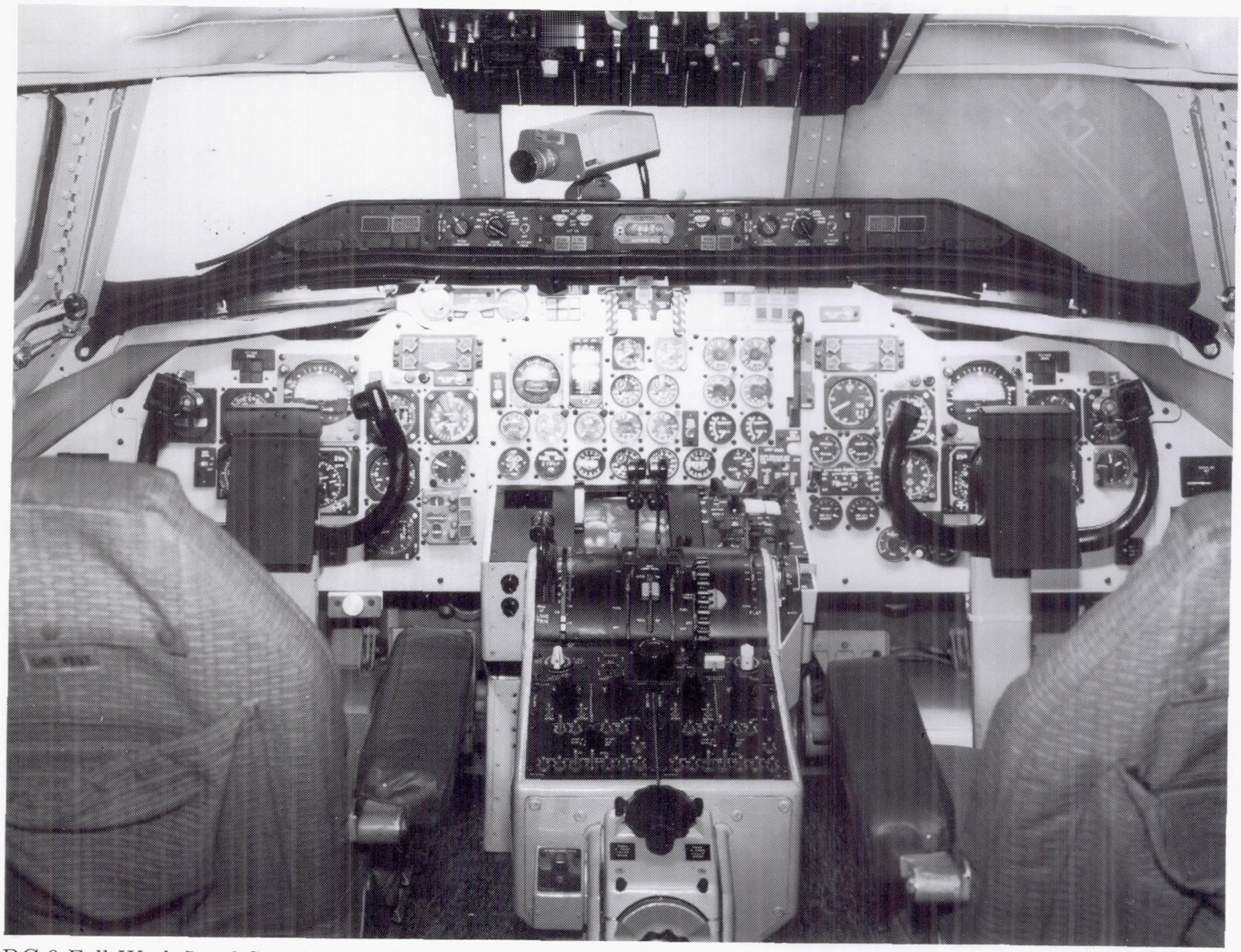

DC-9 Full-Work-Load Simulator cockpit.

L-84-1081

lation. Procedures for simulator Air Traffic Control (ATC) party-line communications were also developed and evaluated.

Studies have included a CDTI cockpit procedures study, a terminal time-based ATC delivery performance of conventional aircraft study, and a microwave landing system (MLS) study. An oculometer has been installed for studies to evaluate information transfer rate between instruments and pilots.

Space Simulation and Environmental Test Complex

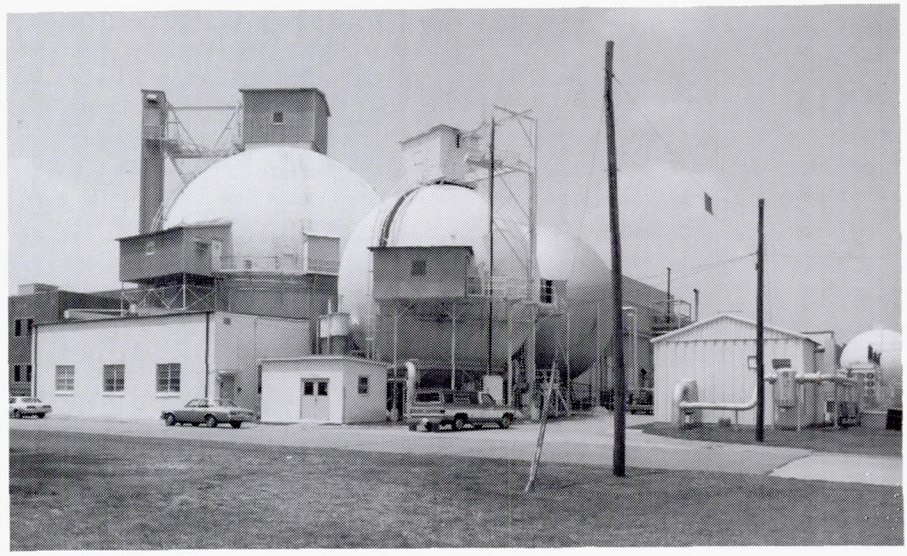

60-ft-diameter Space Simulation Sphere.

The 60-ft-diameter Space Simulation Sphere (Building 1295) can simulate an altitude of 320,000 ft (2×10^{-4} mm Hg). This vacuum level is attainable in 7 hours with a three-stage pumping system. The carbon steel sphere is accessible through a personnel door, a 12-ft-diameter specimen door, and a 4-ft maintenance door at the top. A 2-ton hoist located at the top enhances specimen handling inside the sphere. Sight ports are located both at the top and at the equator. Two closed-circuit television cameras, a videocassette recorder, and an oscillograph are available. Firing circuitry and a programmer are available for the use of pyrotechnics, and a system of flood lights is installed in the sphere to facilitate high-speed photography. The sphere is used primarily for dynamic testing of aerospace components and models at a near-space environment.

Thermal-vacuum testing has long been a prerequisite to the active deployment of space experiments. A series of experiments, which optically sense characteristics of the Earth's atmosphere from outer space, necessitated the creation of an ultra-high-cleanliness thermal facility. The optical components of these experiments would be severely degraded by contamination by oils or other vaporous materials commonly found in thermal chambers and vacuum pumping systems. Langley Research Center upgraded the 8- by 15-Foot Thermal-Vacuum Chamber (in Building 1250) by repeated vacuum bakeout and solvent wipedown. Two 35-in. cryogenic pumps were installed, and cold traps were inserted in the roughing pump lines to eliminate back contamination from the pumps. The chamber is capable of –300° F to +1000° F temperatures and has glass ports for solar illumination simulation.

A 5- by 5-Foot Thermal-Vacuum Chamber (also in Building 1250) augments the thermal testing capability. The smaller stainless-steel chamber is used for subsystem and component testing. A completely enclosed liquid-nitrogen cryopanel with sight ports that have externally adjustable irises can cool the ambient temperature to –300° F. Removable heater banks are used for precise temperature control and high ambient temperature applications. The chamber uses a 570 ft^3/min roughing pump and a 32-in. diffusion pump to reach its capacity of 1×10^{-7} torr. The pumping capability is high relative to the chamber volume; therefore, the 1×10^{-7} torr level can be attained in 1.5 hours.

Structural integrity of aerospace hardware is essential for both performance and safety. The Engineering Vibration Test Facility in Building 1250 is used to perform environmental vibration tests on aerospace flight systems and components to demonstrate that the flight equipment will maintain structural integrity when exposed to a mission environment. The facility includes two shaker units and centralized equipment for control, data acquisition, and signal processing. One unit is an Unholtz-Dickie T-1000 shaker with a 24,000-lbf peak force and a 1-in. armature stroke. The second shaker, a recent addition, is an Unholtz-Dickie T-4000 unit with a 40,000-lbf peak force and a 1-in. stroke (1.75-in. stroke for shock testing). The vibration control room houses a GenRad 2514 vibration control system for shaker control and signal processing plus signal conditioning and analog data recording equipment for 12 channels of data. Through auxiliary equipment, the data capacity can be expanded. Tests are con-

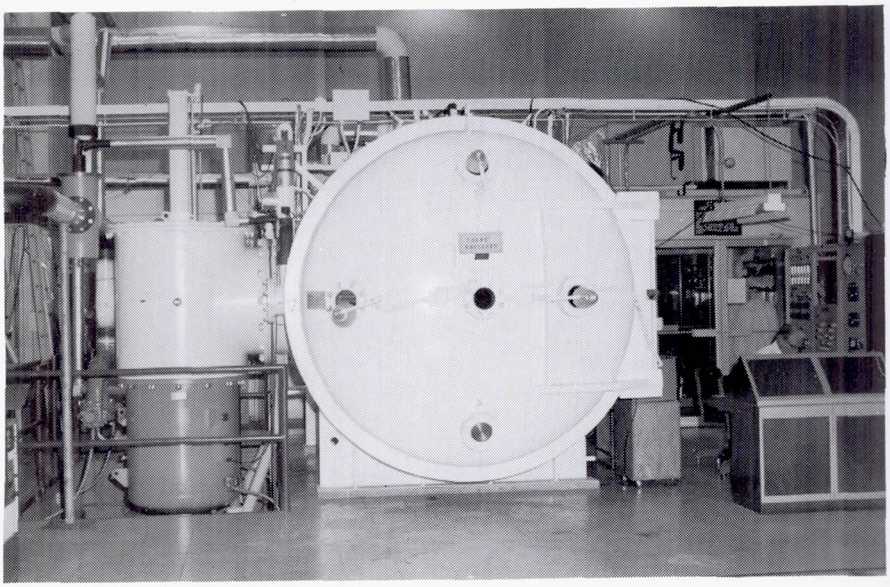

8- by 15-Foot Thermal-Vacuum Chamber. L-82-9672

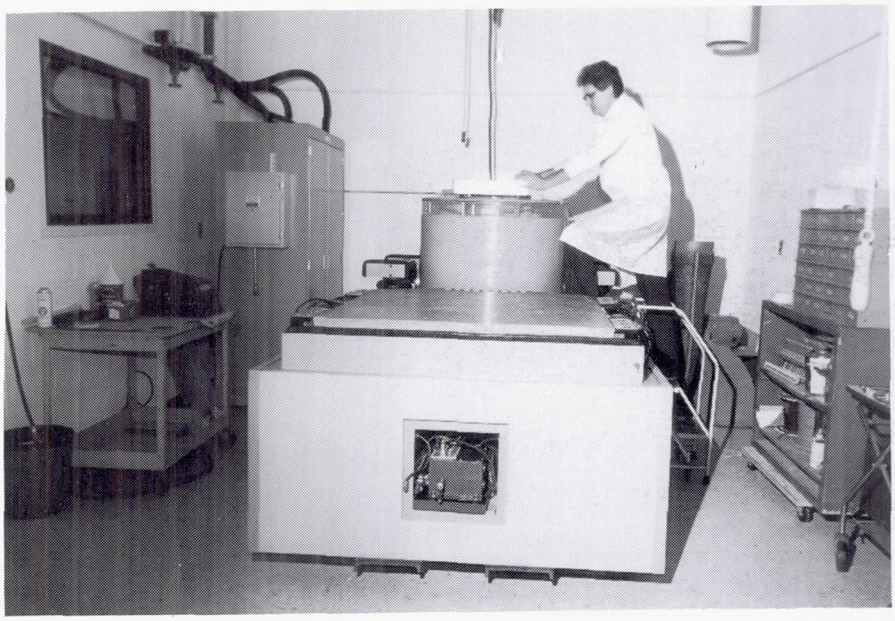

Unholtz-Dickie T-1000 shaker. L-85-10833

ducted with great care given to equipment, test article, and personnel safety. Closed-circuit television coverage is used to safely monitor the test article during all tests.

HALOE Gas Response Test

The Haloe Occultation Experiment (HALOE) will globally monitor the vertical distribution of key gases in the ozone chemistry by measuring the extinction of solar radiation (in the 2.5-μm to 10.0-μm range) which passes through the atmosphere of the Earth during solar occultation. The HALOE is one of 10 instruments on the Upper Atmosphere Research Satellite (UARS), which is scheduled for a late 1991 launch.

The HALOE Gas Response Test was performed in Building 1250 in the 8- by 15-Foot Thermal-Vacuum Chamber to assess understanding of the HALOE instrument end-to-end response under carefully controlled, known laboratory stimuli at three instrument temperatures (10°C, 20°C, and 30°C). The scientific test objectives were to demonstrate the ability to predict HALOE response to simulated orbital exposure to known gas mixtures, pressures, and temperatures of HF, HCl, NO, CH_4, CO_2, NO_2, O_3, and H_2O; to demonstrate adequacy of data reduction methods; to assess the adequacy of spectral parameters in each HALOE channel; and to characterize the instantaneous field of view (IFOV) as a function of temperature, the instrument balance versus signal intensity, the broadband polarization sensitivity, and the instrument drift stability and predictability.

The test concept was to insert known test gases into the collimated beam of a temperature-controlled blackbody source and direct the modulated radiation into the telescope of the HALOE instrument. The radiation path

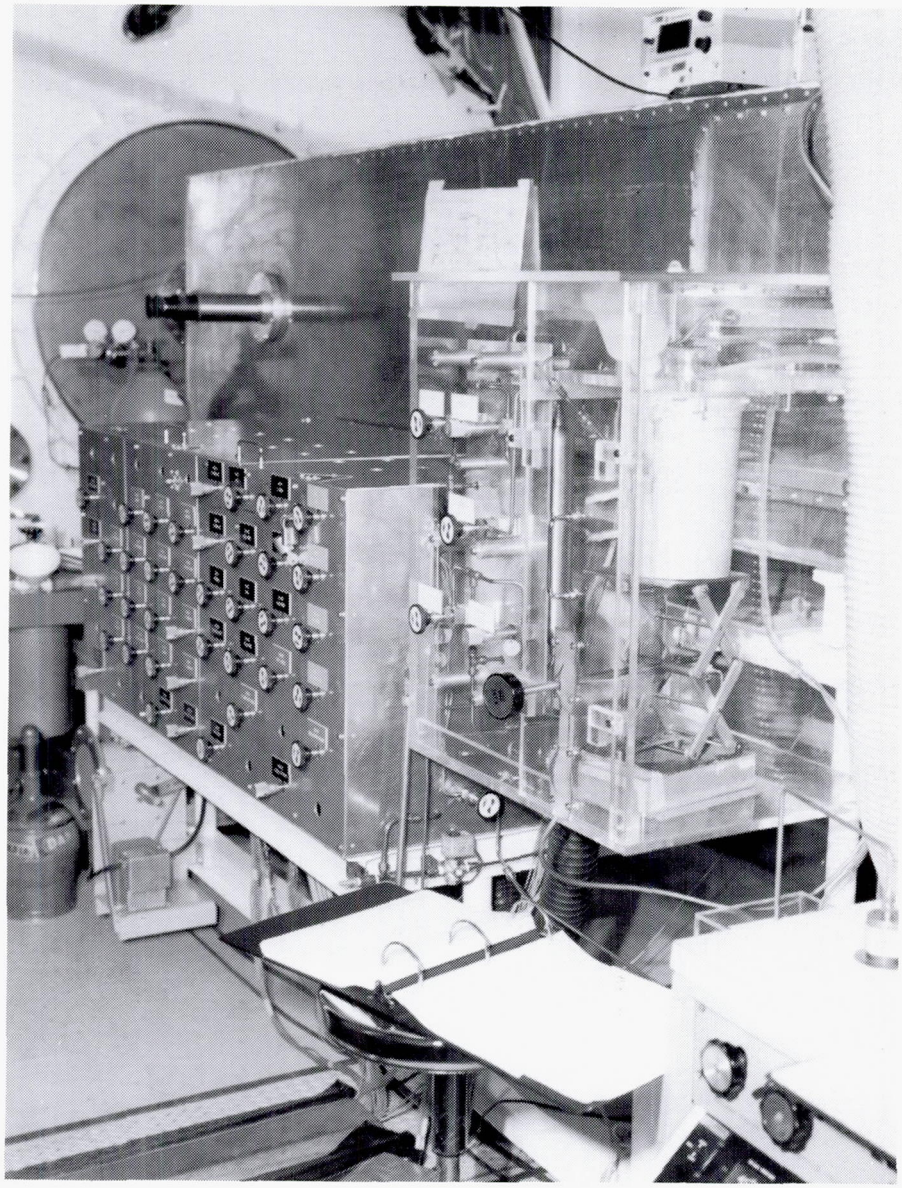

Gas Response Test Gas Fill Station and Purge Chamber. L-89-3992

up to the 8- by 15-Foot Thermal-Vacuum Chamber window was purged with gaseous nitrogen to maintain the dew point to less than –30°C. The figure shows the Gas Fill Station and Purge Chamber installed in front of the 8- by 15-Foot Thermal-Vacuum Chamber. All test objectives were accomplished. Additional tests are planned in 1990 prior to the UARS launch.

(N. A. Holmberg, 46970)

NTF Fan Blade Dynamic Properties Characterization

The recent repair of the National Transonic Facility (NTF) required engineering measurements and tests in the Space Simulation and Environmental Test Complex. Replacement fan blades for the NTF were balanced individually and then geometrically located on the hubs to minimize static and dynamic imbalance of the fan assembly. Each of the 25 blades was suspended from support fixtures that allowed for unrestricted motion in any of three perpendicular axes (X, Y, Z). Initial measurements of weight and linear displacement from the normal centerline were made to determine the actual center of gravity or *c.g.* These measurements were very precise, making use of calibrated load cells, a surveying transit, and a personal computer for calculating corrective ballast weight and location coordinates. These data were required to effect a shift of the *c.g.* to a point coincident with the normal centerline of each axis. Ballast weights were installed and measurements repeated to ensure that the blades were in static balance.

Additionally, a modal survey was performed on each blade to determine resonant frequencies (first, second, and torsional) and damping characteristics. Blades were rigidly attached to a support fixture. Surfaces were instrumented with accelerometers, and a vibrating force was induced using a small shaker. Signals were evaluated using a spectrum analyzer, and nodal plots were recorded. All operational procedures and weight,

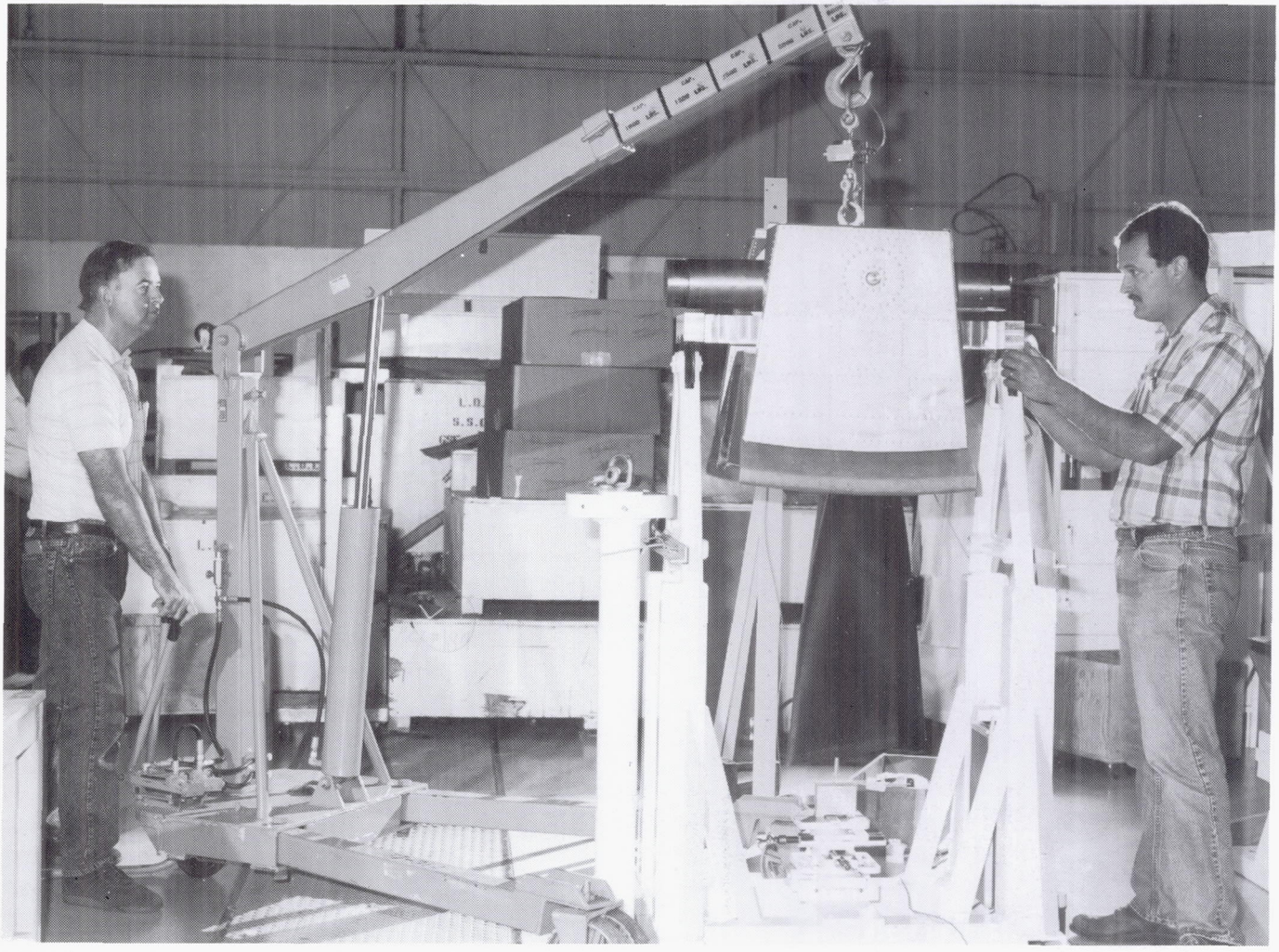

NTF fan blade being prepared for c.g. determination. L-89-07371

c.g., and modal survey data were retained in archival logs for possible future reference. In addition, a video recording of fixture attachment and assembly techniques was made.

The figure depicts an NTF fan blade being prepared for *c.g.* determination.
(Thomas J. Lash, 45644)

Aerospace Component Environmental Test Facilities

Experimental hardware currently under development for advanced aircraft and spacecraft sensors requires environmental testing for development, evaluation, characterization, qualification, and acceptance purposes.

The Lidar Atmospheric Sensing Experiment (LASE), which is an aircraft-borne instrument designed for the accurate remote measurement of tropospheric water vapor, is currently scheduled for flight on the Ames Research Center ER-2 aircraft in the summer of 1991. Recent LASE environmental testing has included vibration testing of the first- and second-stage etalon chambers, tape recorder and tray, encoder, converter, and precursor box.

The Lidar In-Space Technology Experiment (LITE) is a spaceborne instrument designed for an accurate remote determination of cloud top heights, planetary boundary-layer heights, tropospheric aerosols, stratospheric aerosols, and temperature and density. The experiment is to operate from the Space Transportation System (STS) cargo bay in the mid-1990's. Recent LITE component testing has included crystal oven develop-

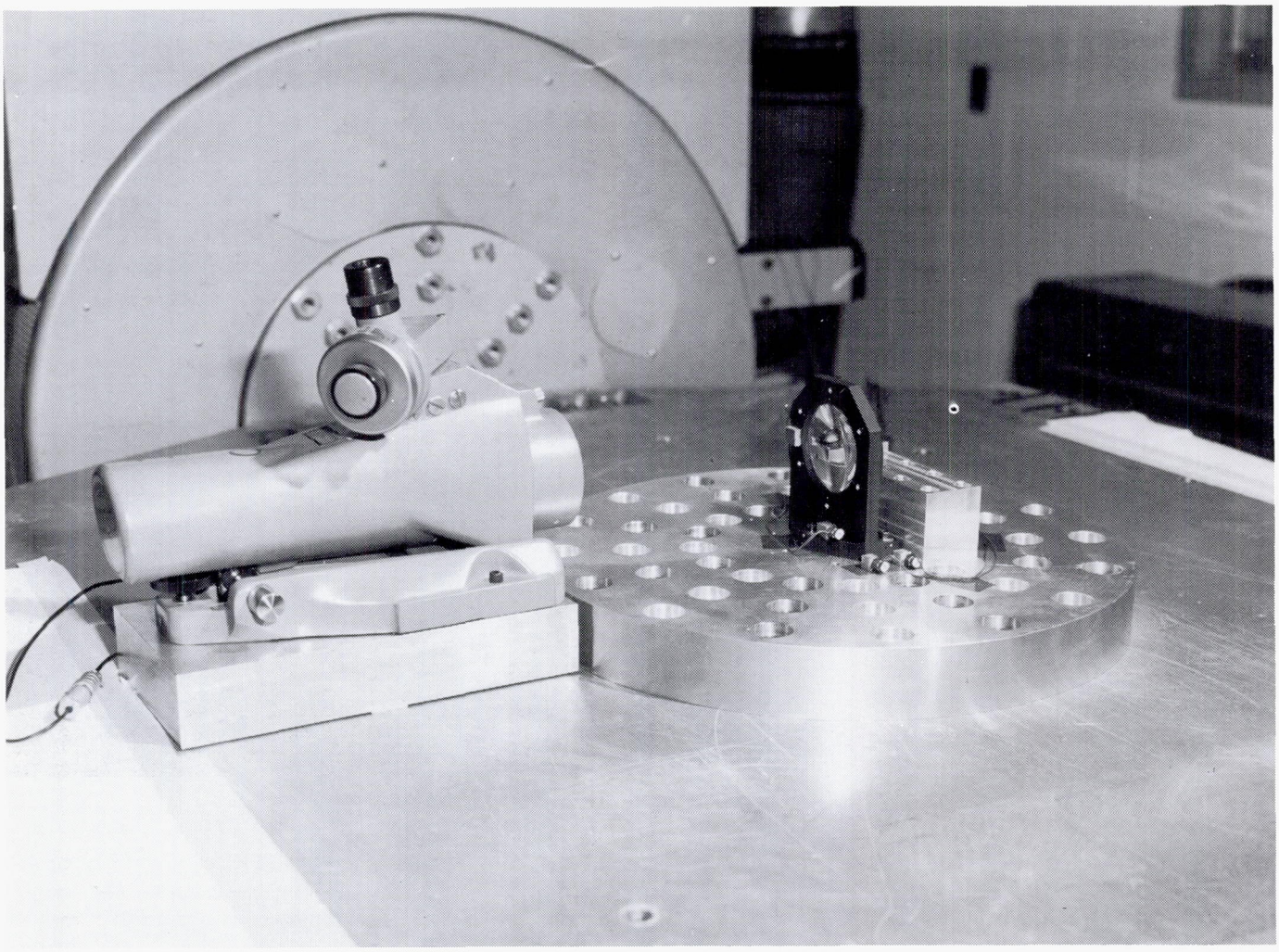

LITE optics mount assembly vibration test setup. L-89-3288

mental thermal-vacuum testing, qualification vibration testing of optical component mounts and electronic enclosures, and thermal-vacuum testing of optical mounts and interference filters.

The Aeroassist Flight Experiment (AFE) is a space-borne experiment designed for the evaluation and characterization of aerobraking. The experiment package is to be deployed by the STS and propelled toward Earth by a solid rocket motor. The Pressure Distribution/Air Data System (PD/ADS), which is one of 11 AFE experiments, is designed to measure the pressure distribution on the aerobrake by the utilization of a system of transducers attached to aerobrake orifices.

Recent AFE (PD/ADS) testing has included the evaluation of the performance of candidate transducers while subjected to flight-type vibration and thermal-vacuum environments.

Typical of this component testing is the LITE optics mount assembly vibration test setup shown in the figure.
(Robert T. Sherrill, 47085)

Advanced Technology Research Laboratory

The Advanced Technology Research Laboratory was dedicated in early 1989 in support of the NASA Space Energy Conversion Research and Technology Program. The laboratory houses multidisciplinary research activities assessing the feasibility of spacecraft-to-spacecraft laser power transmission for propulsion and for electric power distribution, conducting theoretical studies on galactic and solar cosmic ray exposure and shielding, and developing ultra-high vacuum gas-surface interaction technology. Major facilities include three solar simulators that consist of a single-lamp unit of 50-kW input power, a dual-lamp unit of 100-kW input power, and a state-of-the-art single-lamp unit of 160-kW input power. These simulators provide a range of solar irradiance conditions for the multifaceted research into the direct conversion of solar energy to laser power. The research includes investigations using solid, liquid, and gas lasers powered by simulated sunlight; electrically driven diode lasers; and the conversion of laser power back into electricity.

Theoretical research is supported by a computational capability that includes the latest computer technology. In addition, the facility is fully integrated into the Center's high-speed data network. A group of laboratories house ultra-high vacuum equipment that simulates the space environment and specialized conditions associated with advanced spacecraft.

The laboratory also contains a large, multikilojoule capacitor bank that is the energy source for the development of laser-power beaming technology.

High-Temperature Surface Analysis

The adsorption of hydrogen into the bulk of materials may form hydrides or unwanted phases that severely degrade the mechanical properties of the material. Titanium aluminides, for example, are very sensitive to the effects of hydrogen, especially above 600° C. Because the surface oxides, carbides, nitrides, and other barrier layers can substantially affect the rate of adsorption and dissolution of hydrogen into the bulk, it is important to determine the composition, thickness, and rate of formation of these barriers as a function of temperature.

The figure shows a surface system with a sample preparation chamber and high-temperature analysis capability. Samples can be introduced into the preparation chamber, heated up to 1000° C in a selected gas environment (10^{-9} torr to 760 torr), and then transferred to the analysis chamber ($<10^{-11}$ torr). The sample then can be studied with Auger electron spectroscopy, secondary-ion-mass spectroscopy, ion-scattering spectroscopy, electron-stimulated desorption, and temperature-programmed desorption. During any diagnostic study, the sample can be heated to a temperature of up to 1000° C, thus permitting multiple

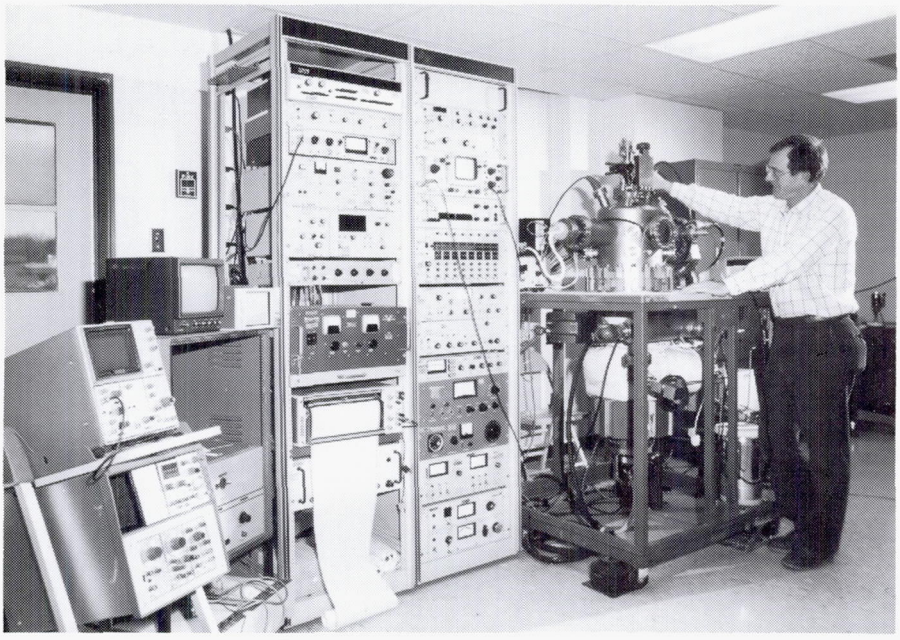

Surface analysis system with sample preparation chamber and high-temperature analysis capability (≈1000°C). L-88-01281

analyses at high temperatures. The sample also can be simultaneously sputtered for depth profiling using differentially pumped ion guns.
(R. A. Outlaw, 41433)

2-m Master-Oscillator Power-Amplifier System for Space Laser Power Transmission

A novel concept that involves focusing sunlight directly into a high-power laser for power distribution in space is under technological development. Potential applications may require the laser to provide 1 MW of power and operate over transmission distances of thousands of kilometers. One laser system feasible for scaling to such a power level is a master-oscillator power-amplifier (MOPA) system based on the iodide photodissociation laser. In this configuration, the master oscillator need only provide a low-power, high-quality beam, while the power amplifier provides increased power and preserves the beam quality that is required for long-distance transmission. Preliminary tests conducted earlier with the iodide n-C_3F_7I showed power amplifications of 1.7 and 5 for single and triple passes, respectively, traversing an amplifying region only 0.15 m long. These results encouraged further experimentation with longer amplifier tubes.

In 1989, a 2-m-long amplifier system was designed, fabricated, and installed for characterization of a long amplifier similar to one conceived for space operations, as shown in the first figure. Because a broad-optical-band (continuously emitting a light source 2 m long) which could provide the equivalent of solar spectral irradiance above the atmosphere was not available, a series of two 1-m-long flashlamps, which could be energized by a short electrical pulse, were used as the solar simulator. The flashlamps were placed on the focal line of a parabolic trough to produce parallel light

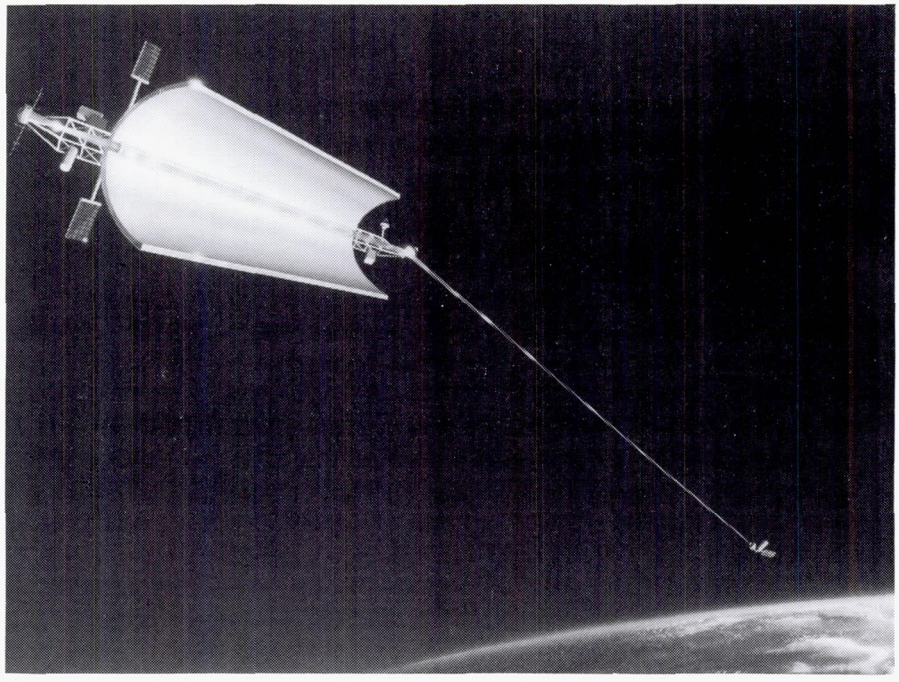

Conceptual MOPA system for space operations.

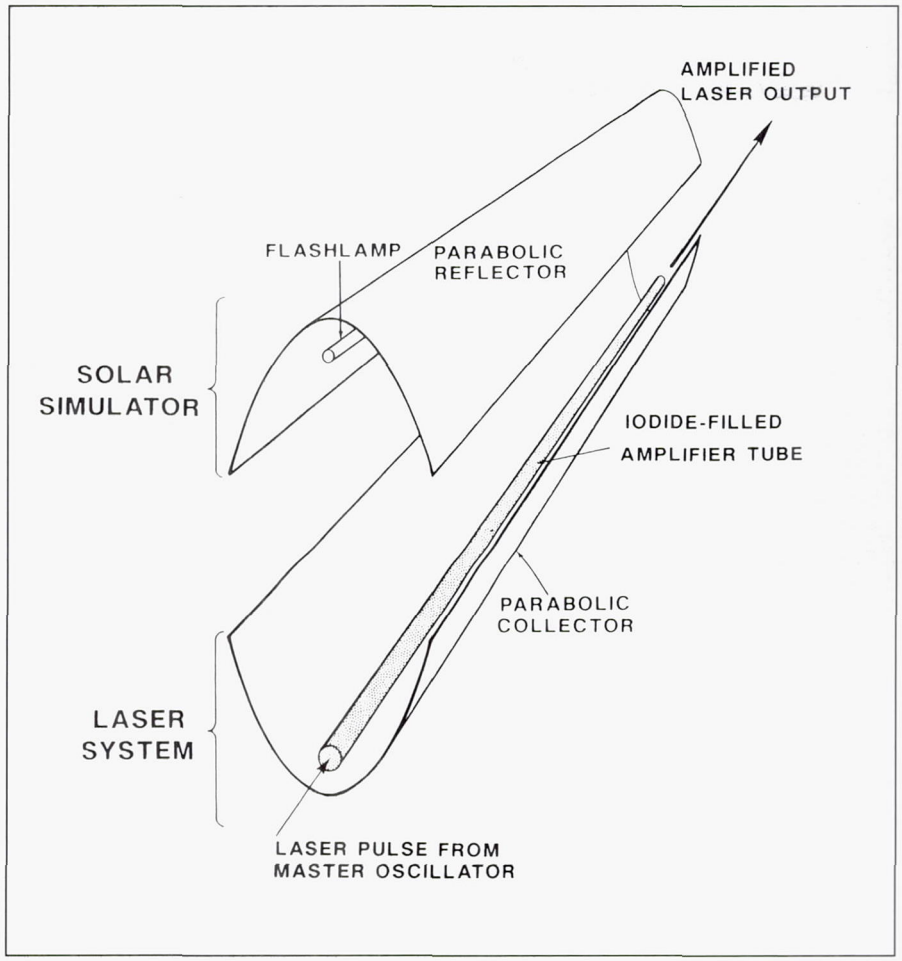

Basic arrangement of laser amplifier of 2-m MOPA system. The flashlamp-driving pulse-forming network, master oscillator, iodide vapor filling/evacuating unit, and laser power/energy beam profile diagnostics are not shown for clarity.

after reflection from the inner surface of the trough (see the second figure). The amplifier tube was placed on the focal line of a second parabolic trough (second figure), which collects and focuses the pump-beam from the flashlamps onto the amplifier tube. The irradiance on the amplifier tube could be varied with the electrical pulse energy. The amplifier tube was made of long, thin-walled quartz tubing. A XeCl-laser-pumped iodine laser (not shown in the second figure) was aligned with the amplifier tube as the master oscillator of the MOPA system. The output of the oscillator was 1 mJ. Other accessories of the MOPA system, such as the iodide-filling-evacuating unit, the XeCl-gas handling/cleaning unit, and the power/energy meters, have been installed and operated.

A test plan for characterization and evaluation of the MOPA system has been developed. The test parameters to be varied are iodide lasant pressure, pump-beam irradiance, the iodide species (n-C_3F_7I, i-C_3F_7I, and t-C_4F_9I), and the injection power/energy from the master oscillator. The effects of these parameters on the energy storage, the gain saturation, the amplification factor, and the beam quality will be studied carefully. **(J. H. Lee, 41473)**

Structural Dynamics Research Laboratory

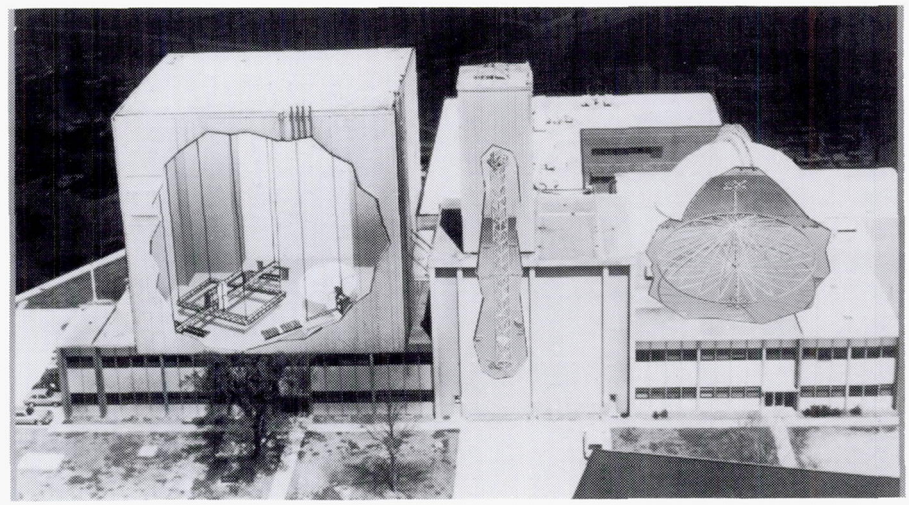

The Structural Dynamics Research Laboratory (SDRL) is designed to conduct research on the dynamics and controls behavior of spacecraft and aircraft structures, equipment, and materials. The SDRL offers a variety of environmental simulation capabilities, including acceleration, vacuum, and thermal radiation. Improvements are under way which will benefit controls and structures interaction research.

The newest feature of the SDRL is the 5200 ft^2 Space Structures Research Laboratory, which has a 68-ft high suspension platform from which large space structures may be suspended over any portion of the work area. This laboratory will house a 1/10-subscale Space Station Freedom model and a controls-structures interaction model for performing structural dynamics and controls research of large space structures. The SDRL also contains a 12-ft by 12-ft backstop area for cantilevered structural tests. A control room houses a state-of-the-art data acquisition capability, which is provided by a 128-channel GenRad 2515/CYTEC scanner and by a 16-channel Zonic system. A CAMAC crate connected via a fiber optic line to the real-time CYBER 175 computer provides computational capability necessary for closed-loop active vibration suppression. The crate has the capacity to handle up to 42 input and 42 output channels.

The dominant feature of the main laboratory is a 38-ft-high backstop of I-beam construction. Test areas available around this facility are 15 ft by 35 ft by 38 ft high and a 12 ft by 12 ft that is 95 ft high. The tower presently houses a 66-ft-high space truss. Spiral stairs, ladders, and platforms provide access over the entire main laboratory.

Another feature of the SDRL is the 16-Meter Thermal-Vacuum Chamber, which presently houses a 15-m-diameter hoop/column antenna. It has a 55-ft-diameter hemispherical dome with a removable 5-ton crane, a 64-ft-high dome peak, a flat floor, and an option for a large centrifuge or a rotating platform. Access is by an airlock door and an 18-ft-high by 20-ft-wide test specimen door. Ten 10-in.-diameter view ports are randomly spaced for visually monitoring tests. A vacuum level of 10 torr can be achieved within 120 min and, with diffusion pumps, 10^{-4} torr vacuum can be achieved in 160 min. The centrifuge attached to the floor of the chamber is rated to 100 g, with a 50,000-lbf capacity and a maximum allowable specimen weight of 2000 lb. Six-ft mounting faces for test articles are available at 16.5-ft and 20.5-ft radii. The tables can accommodate electromagnetic and hydraulic excitation devices. A temperature range of 100°F is obtained from 250 ft^2 of portable radiant heaters and liquid-nitrogen-cooled plates.

A control room for the main laboratory, the tower, and the 16-Meter Thermal-Vacuum Chamber houses state-of-the-art capability for up to 220 channels of signal conditioning and analog and digital data recording. A 128-channel GenRad 2515/CYTEC scanner provides digital signal processing. A VAX 11-780/EAI 2000 hybrid computer system for simulation and on-line test control is also available. A CAMAC crate similar to the one in the Space Structures Research Laboratory part of the SDRL is available for closed-loop active vibration suppression testing.

Available excitation equipment includes several types of small

shakers. The largest shaker is hydraulic with a maximum of 1200-lbf, a 6-in. stroke, and a 0-Hz to 170-Hz range. All areas are monitored by closed-circuit television cameras.

Mini-Mast CSI Test Bed Facility

Actively controlled vibration suppression of flexible large space structures is required for precision pointing of antennas and optical instruments and for assembly of the Freedom space station and space exploratory vehicles. Because these are low-frequency structures, precision control tends to lead to controls-structures interaction (CSI). The objective of the Mini-Mast development is to provide a ground-based test bed facility in which active controller designs can be tested and studied in a CSI environment, thus leading to operational designs.

A photograph of the Mini-Mast mounted in the Structural Dynamics Research Laboratory is shown in the figure. The Mini-Mast is an 18-bay, foldable, 65-ft-long, three-longeron, flight-like cantilever truss. The truss structure has characteristics associated with future large space structures, namely, low frequencies (starting at 0.8 Hz), closely spaced modes (e.g., 108 local member modes between 15 Hz and 22 Hz), and joints that introduce nonlinearity into the truss dynamics. Displacement, velocity, and acceleration sensors have been installed on the truss. A total of 36 channels of sensor measurements on the structure itself are available for feedback to the controller. Fifty-one noncontacting displacement transducers are distributed along the truss length. The complete set is used for dynamics characterization, and 16 of these transducers are used to provide feedback signals for control. Additional instrumentation pallets are located at mid-length and at the free end, or tip. Mounted to the tip pallet are three angular rate sensors and four accelerometers. The mid-length pallet has two accelerometers for measuring motion in the plane of the pallet. Excitation of the truss is provided by three 50-lbf shakers located immediately below the mid-length pallet and/or by three 50-ft·lb-output torque

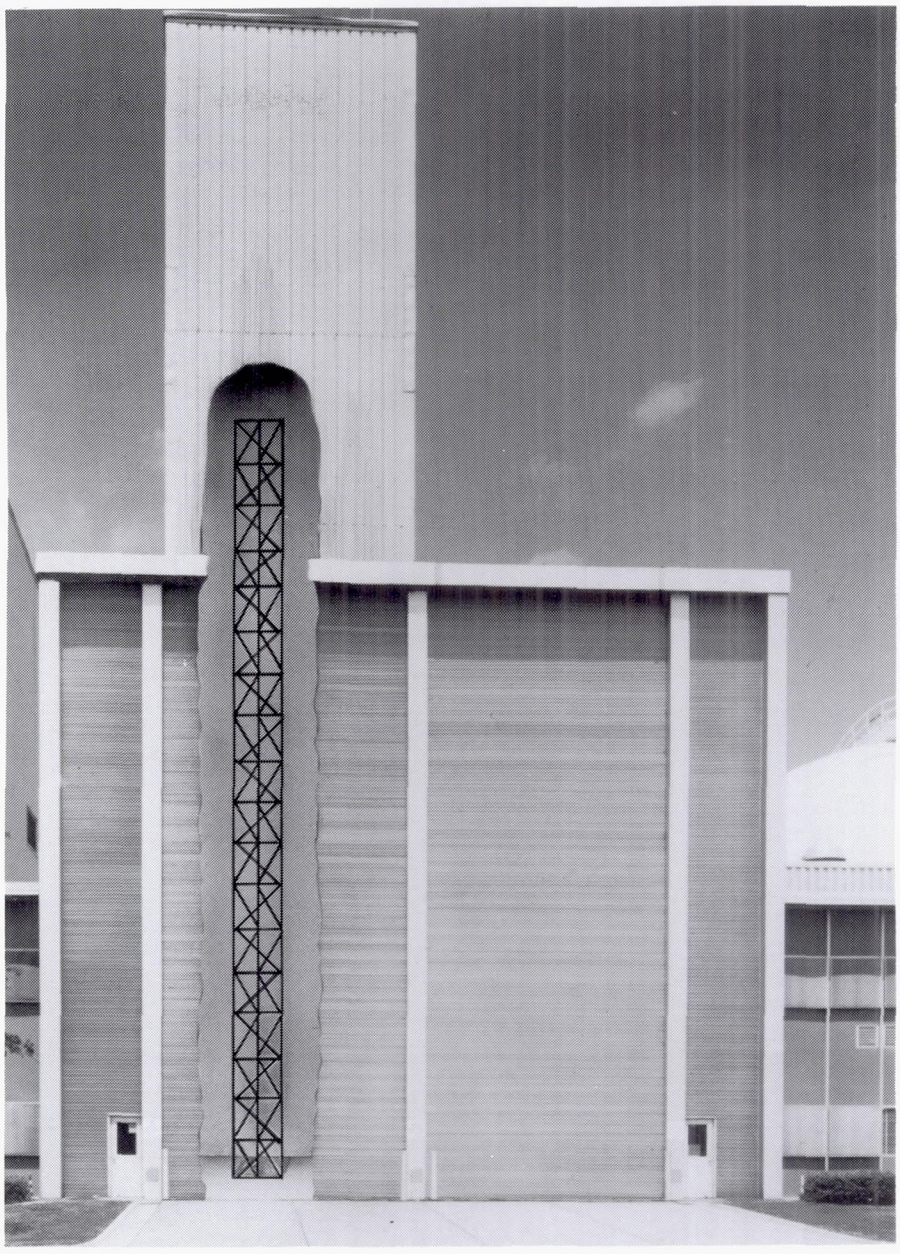

Mini-Mast mounted in Structural Dynamics Research Laboratory.

L-86-10105

wheels located on the tip pallet. The torque wheels also act as actuators to control the truss vibrations.

(J. M. Housner, 44325, R. S. Pappa, S. E. Perez, R. Miserentino, K. B. Elliott, J. L. Sulla, and B. L. Williams, Jr.)

Control System Design for Mini-Mast

The value of the Mini-Mast as a research facility has been confirmed by using it to develop and validate a procedure for control system design. The procedure began with a series of open-loop tests to generate an empirical model that was then used in the control system design. The design method selected was optimal multi-input/output linear quadratic Gaussian control theory. The design was examined by simulation before its implementation on the Mini-Mast. A time history of tip displacement for the first-mode open-loop test and corresponding closed-loop simulation is shown on the bottom half of the figure. After simulation, the control system was tested on the facility. Time histories of actual torque wheel command and the corresponding tip displacement history for active control of the first mode are shown on the top half of the figure. A comparison of tip displacement time histories between simulation and ground test (second plot from top and the bottom plot) shows close agreement. Significantly, substantial improvement in the damping of the mode is seen.

Checkout of the Mini-Mast system is now complete and well-documented for future use by researchers from government, industry, and academia.

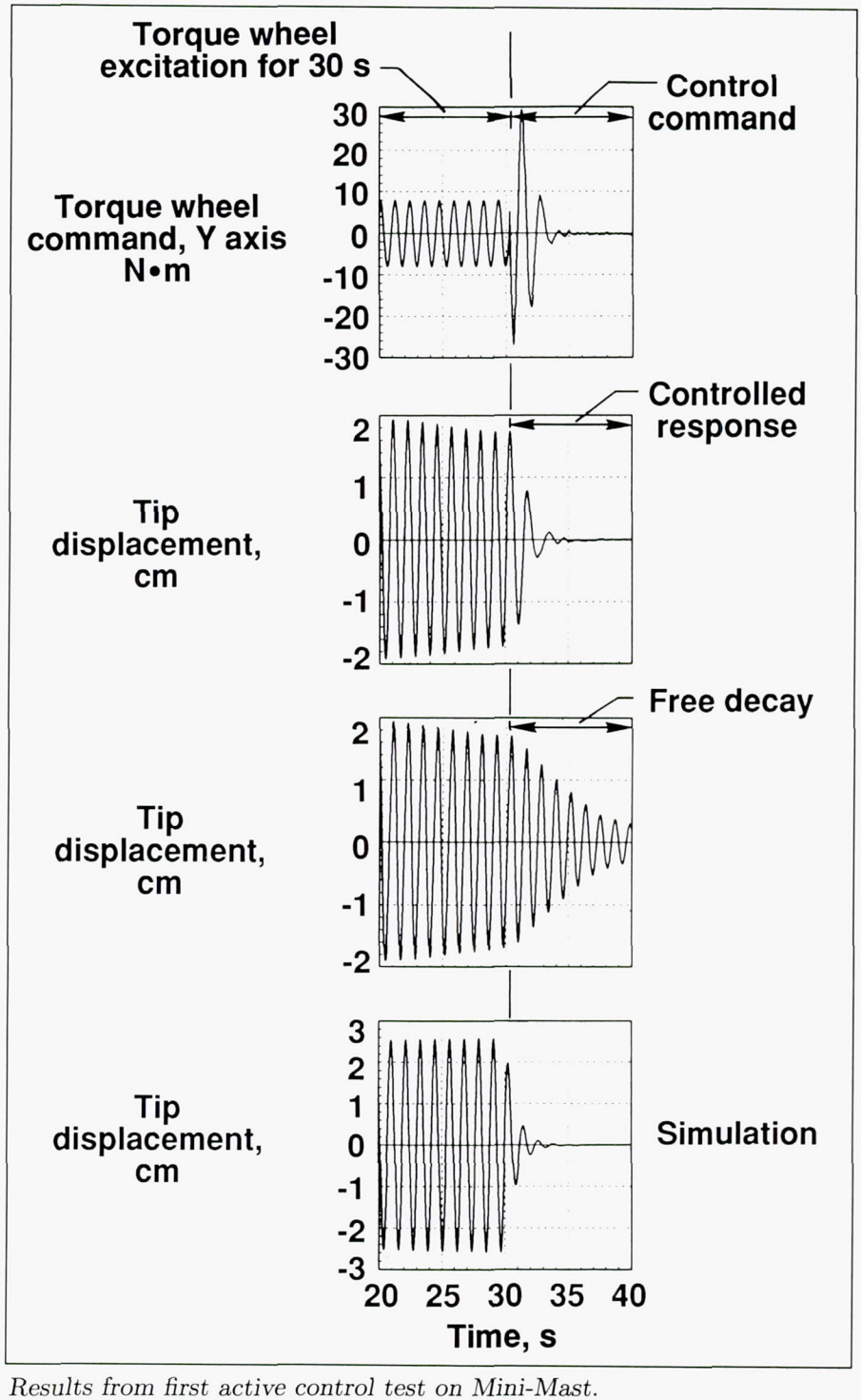

Results from first active control test on Mini-Mast.

Checkout of the Mini-Mast system is now complete and well-documented for future use by researchers from government, industry, and academia.

(D. Ghosh, 46616, and R. C. Montgomery)

Controls-Structures Interaction Ground Test Methodology

Spacecraft structural behavior and controller behavior can become interactive when the frequency response of the controller overlaps structural resonances. This controls-structures interaction (CSI) can be detrimental to spacecraft performance, cost, and system mass. Hence, CSI technology is being developed to design and validate spacecraft in which the structure and controller interact beneficially to meet the requirements of twenty-first-century NASA missions.

The ground test methodology needed to validate CSI designs is being studied using an evolutionary model test bed shown in the figure. The test bed permits the evolution of multi-input multioutput controllers, integrated structure/controller design, and realistic sensor and actuator systems. The test bed structure consists of 77 truss bays (each 10 in. long) and a radial-rib reflector. Linear acceleration and angular rate sensors are used for feedback control. Sixteen air jet thrusters are used to actively dampen vibrations of the structure and to maintain line-of-site (LOS) pointing. The LOS pointing is monitored using a structure-mounted laser. The laser beam is reflected by a mirror onto an inertially mounted photo-diode detector.

System identification tests of the initial test bed configuration have recently been completed. The results provided insight for modifying the cable suspension system to enhance ground-based test simulations of the on-orbit 0-g environment and vibration behavior of Earth-observing platforms. The system identification tests also identified the noise floor of the accelerometer and rate sensors. These test findings will strongly influence the control system design. Frequency response characteristics of the air jet thrusters are currently being measured. Subsequent to completion of finite-element model refinement and the thruster tests, the test bed will be actively controlled to augment vibration damping and to improve LOS pointing.

The ground test methodology developed through closed-loop testing of the evolutionary model will involve algorithms designed to ensure system safety, gravity compensation suspension modeling, and sensor/actuator modeling and filter design. This methodology will help develop CSI technology for future on-orbit implementation.

(W. K. Belvin, 44319)

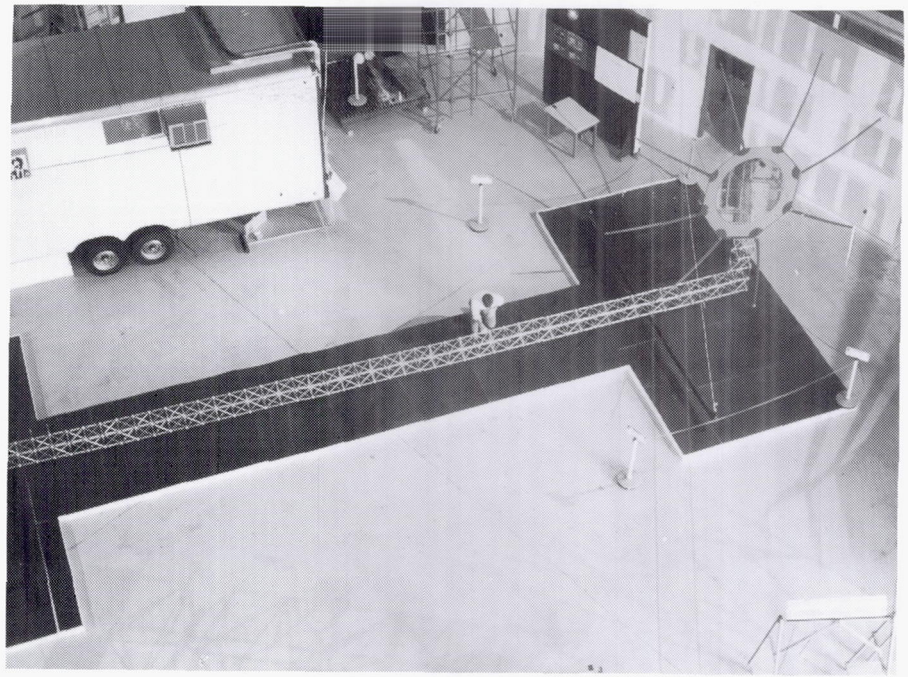

CSI test bed model. L-89-13575

Large-Scale Antenna Surface Optimization Tests

Langley Research Center has been a leader in technology development for large-scale microwave and millimeter wave antennas. In 1985, a 15-m hoop/column antenna that was designed and developed by Langley and the Harris Corporation was completed. This antenna was tested at Martin Marietta Denver Corporation (NAS1-178059) to determine its antenna pattern characteristics and at Langley in the 16-Meter Thermal-Vacuum Chamber to determine its vibration characteristics. One lesson learned from these tests is that a large-scale antenna will generally require post-deployment adjustment to obtain the surface figure required for most microwave applications.

Currently, testing is under way to evaluate a computer-controlled actuator system to adjust the

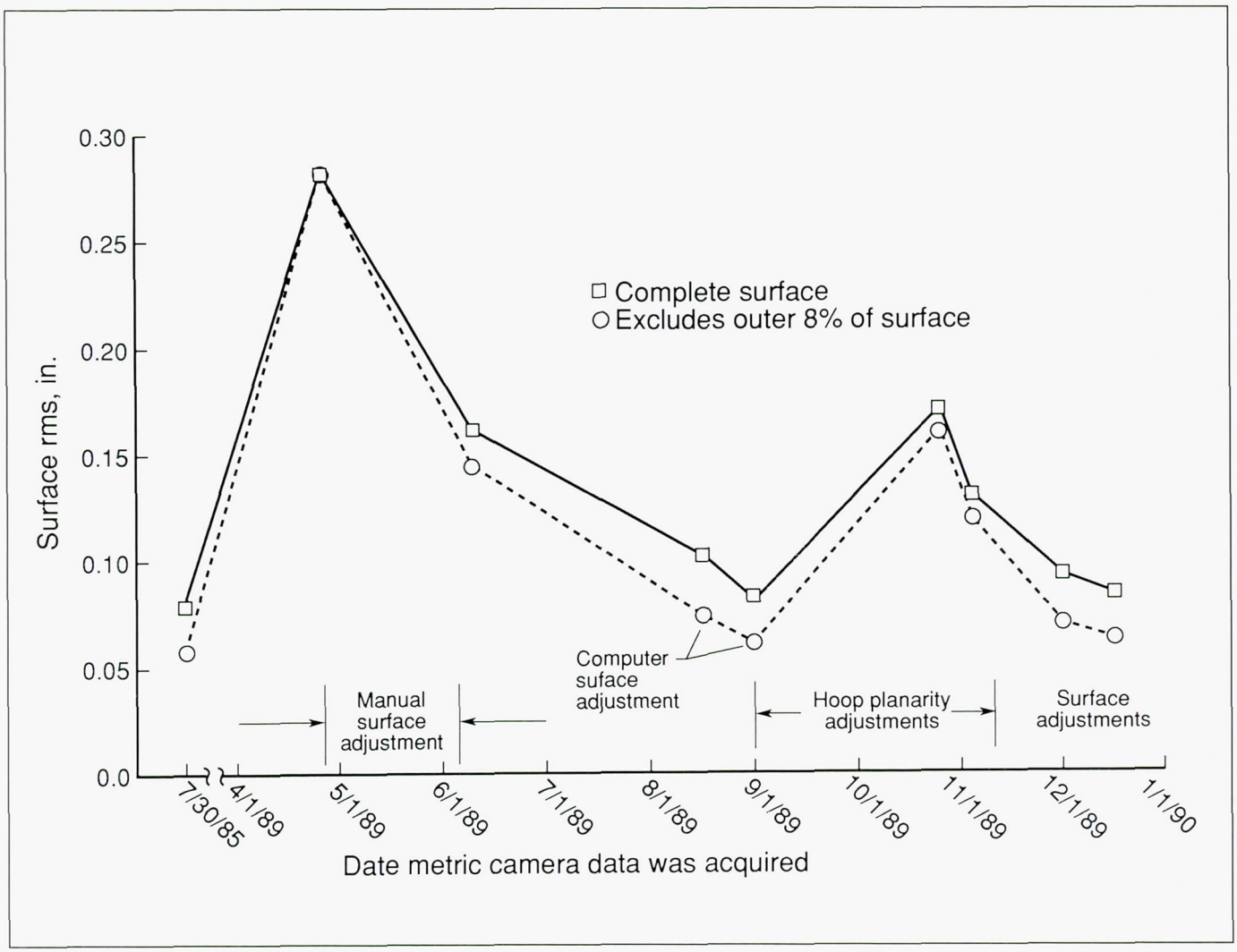

Measured root mean square (rms) roughness of 15-m hoop/column quadrant IV.

reflector surface roughness for the 15-m hoop/column antenna. One quadrant of this antenna was retrofitted with control/actuator motors to allow adjustment of the set of 28 rear control cords which, in turn, provided limited adjustment of the reflector surface.

A computer was used to implement required adjustments to the control/actuator motors, accurate to within 0.001 in. The system is employed by first using an optical sensor (in this case, stereo photography) to determine the offset at retroeffecting targets relative to a best-fit paraboloid. A code then is employed which calculates the optimum control cord adjustments necessary to optimally reduce the surface roughness, and the computer/actuator system adjusts the surface to the new positions. The cycle is repeated if necessary.

In the past year, the installation of the control/actuator system was completed and debugged. A preliminary set of tests indicated that planarity of the hoop structure may have been limiting optimum surface roughness. After reducing hoop planarity residuals by approximately a factor of 3, tests have been resumed and are still under way. Preliminary indications are that the limit in surface roughness is approximately 0.060 in. This limit is reached in one to three iterations, which in concept could be achieved very rapidly in space if a suitable optical sensor and computer were available.

The results of these surface optimization tests will be used as input test data for a method to reduce effects of surface distortion on electromagnetic (EM) signals. Analytical methods will be used to compensate the phase of signals for distortions caused by surface roughness. Prior

studies have shown that the effects of surface distortion can be greatly reduced by using multiple antenna feeds. By using these feeds, the effective surface roughness can be reduced by as much as one half.
(Lyle C. Schroeder, 41832)

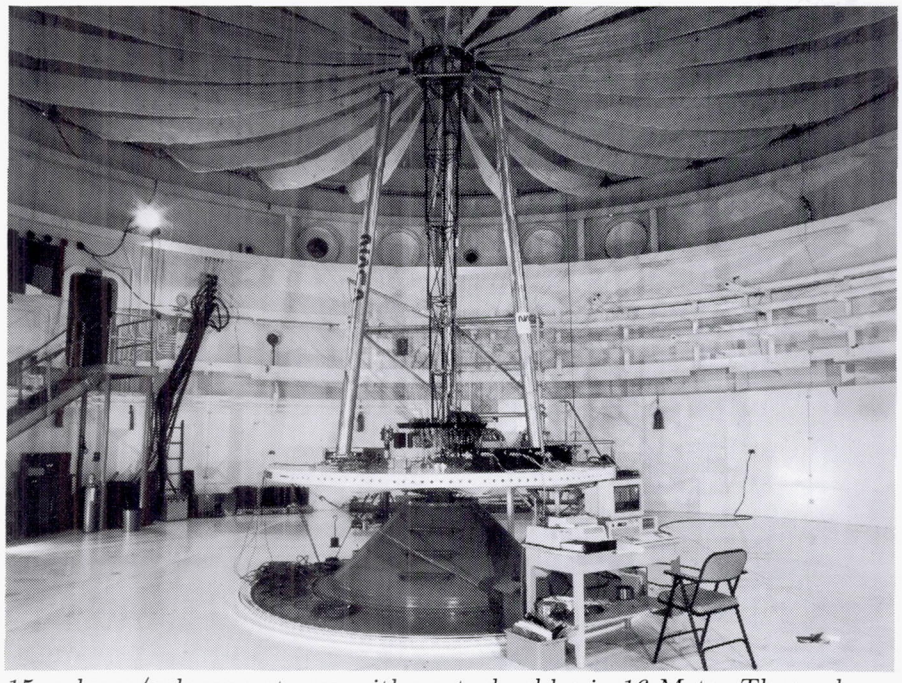

15-m hoop/column antenna with control cables in 16-Meter Thermal-Vacuum Chamber. L-89-08647

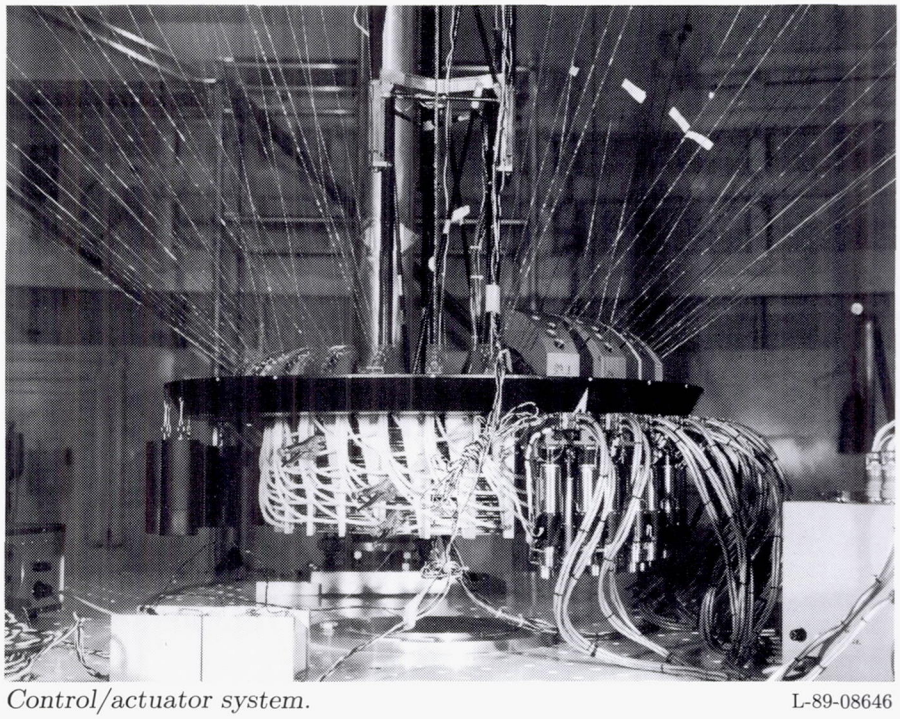

Control/actuator system. L-89-08646

Mechanics of Materials Laboratory

The Mechanics of Materials Laboratory houses experimental facilities for conducting a wide range of research to characterize the behavior of structural materials under the application of mechanical and thermal loads. Mechanics of materials research encompasses the study of the deformation characteristics of new materials leading to the development of nonlinear constitutive relationships and the study of damage mechanics leading to the development of strength criteria and fracture-mechanics-based damage tolerance criteria. The facility, which opened in 1968, provides approximately 25,000 ft^2 of laboratory space. The laboratory area rests on a heavy-duty steel-reinforced concrete floor with special isolation pads to support the high-capacity load frames. A high bay area, with a 20-ft clear height and a 7.5-ton traveling overhead crane, houses 9 multipurpose 20-kip to 100-kip servohydraulic systems for coupon testing and 3 high-load capacity systems for testing large panels. Enclosed laboratories around the perimeter of the high bay area are dedicated to specialized research. These laboratories house an additional 18 servohydraulic testing systems, a scanning electron microscope, 3 X-ray radiography systems, 13 high-temperature creep frames, 3 multiparameter test facilities, and 11 load frames for long-term environmental exposure testing.

The 27 servohydraulic testing systems are used for monotonic and cyclic loading of material level coupons under tension, compression, combined tension-torsion, and mechanical loading at both cryogenic and elevated temperatures. The load capacities range from 1 kip to 100 kips. A special cryostat and a 100-kip load frame allow testing to approximately –450°F in a liquid-helium environment. Liquid nitrogen is also used when lower cryogenic temperatures are not required. Combined thermal and mechanical loading conditions can be achieved by a variety of methods including convection furnaces (600°F), induction heaters (2000+°F), and quartz lamp heaters (1500+°F). Large specimens and panels can be tested under uniaxial monotonic or cyclic loadings in the 300-kip and 400-kip test facilities. A special biaxial system allows for the testing of flat cruxiform panels under monotonic or cyclic in-plane loads up to 175 kips. Two tension-torsion testing systems allow for the testing of tubular specimens to investigate the effects of multiaxial stress states. A special multiparameter test facility allows for the simultaneous testing of up to six specimens under combined temperature, cyclic mechanical loads, and partial pressures.

The scanning electron microscope is equipped with a loading stage to permit examination of a growing fatigue crack while the specimen is under load. The crack-tip process zone can also be investigated while the specimen is under load. Basic fracture morphology studies are also conducted in an environmental fatigue laboratory. A vacuum chamber allows for the control of moisture, temperature, and gaseous environment. Fatigue tests also can be conducted in salt water environments. In addition, nine load frames are located outside the building for conducting long-term durability tests in real atmospheric conditions. These hydraulic load frames are electronically controlled to permit mechanical loadings to simulate actual vehicular mission profiles. While not housed in the

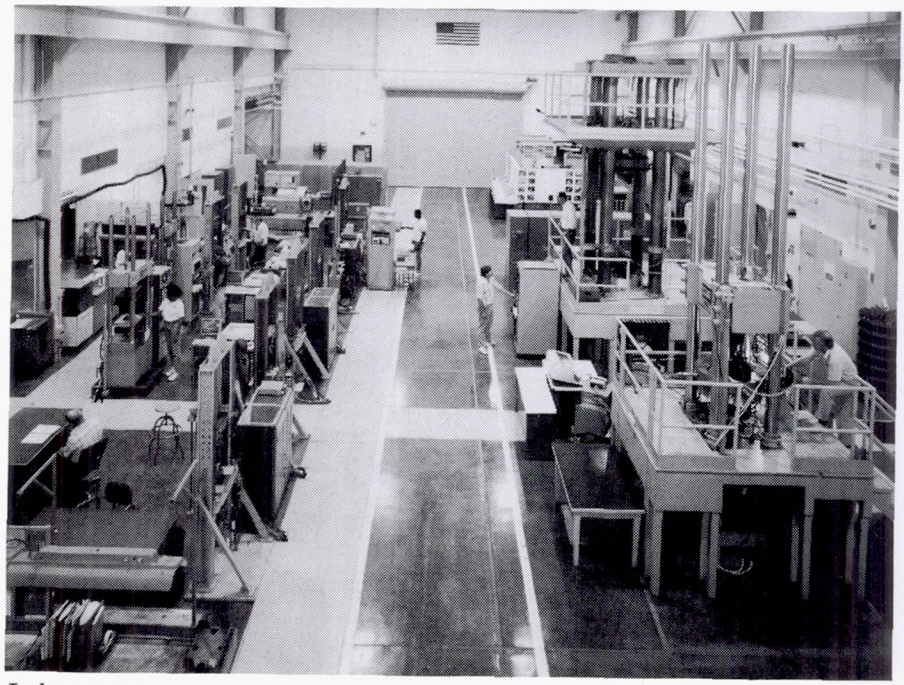

Laboratory area. L-88-6247

Mechanics of Materials Laboratory, a central analysis laboratory in the Materials Division provides a full range of fractographic and chemical analysis support for postmortem evaluations of all test specimens.

test facility built and housed in the Mechanics of Materials Laboratory, shown in the figure. This 1/4-scale test facility simulated the launch conditions of temperature, low-frequency vibrations, gap openings, and rapid pressurizations. The sealing characteristics of the O-ring joint were evaluated for the effects of temperature, gland surface finish, and contamination.

Under the simulated launch conditions, the Viton elastomeric O-ring sealed the joint for temperatures between 50°F and 120°F and for all surface finishes between 32 Ra (roughness average) and 250 Ra. Thin-gauge wires with diameters ranging from 0.0005 in. to 0.004 in. were used to simulate contaminants from human hair and fibrous debris. Wires as small as 0.001 in. were found to produce leaks. At 75°F and 120°F, the leak-check procedure was verified as capable of detecting contaminants >0.0016 in. in diameter. A clean-room environment has subsequently been established for the installation of the O-ring seals. **(Cynthia L. Lach, 43485)**

Evaluation of Redesigned SRM Field Joint Sealing Characteristics

As part of the redesign of the Space Shuttle solid rocket motor (SRM), the field joint was changed to minimize the relative joint motion caused by internal motor pressurization during ignition. The O-ring and seals for the field joint were also redesigned to accommodate structural deflections and to promote pressure-assisted sealing. The sealing characteristics of the redesigned O-ring joint were evaluated in a special

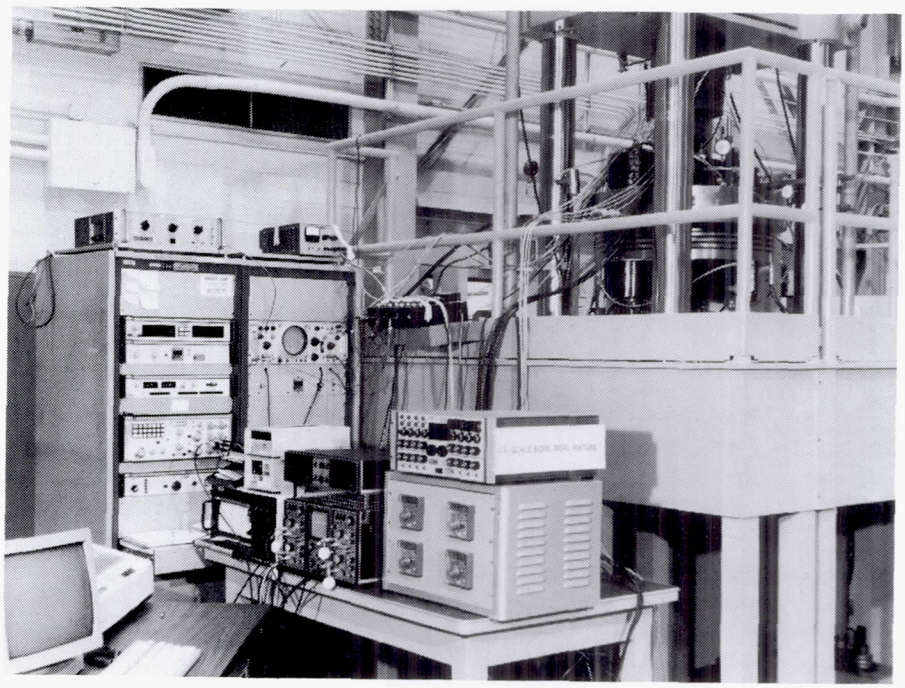

Test facility for evaluating sealing characteristics of redesigned O-ring joint. L-87-03434

Evaluation of Fracture-Critical SRM Components

The fatigue crack growth and fracture characteristics of the newly designed O-ring joint leak-check-port of the Space Shuttle SRM were experimentally investigated in the Mechanics of Materials Laboratory. The purpose of this investigation was to address several issues considered critical to the Space Shuttle Recovery Program. These issues included fracture toughness of D6AC steel between –30°F and 130°F, fatigue life of the leak-check-port, and critical crack sizes for this and other crack configurations. An experimental program was developed in which the fatigue life and critical crack sizes were determined from test specimens of the actual component configuration. A leak-check-port specimen is shown in the figure.

The test results confirmed the damage tolerance integrity of the redesigned SRM. A special eddy-current inspection probe that will reliably detect cracks > 0.035 in. deep at the root of the port threads was developed for the leak-check-port. At this crack size, the fatigue life of the leak-check-port specimens was >2000 cycles at the proof test load. The plane-strain fracture toughness of D6AC steel was found to be above the fracture toughness requirements for the motor at temperatures above approximately –10°F. Furthermore, it was verified that linear elastic fracture mechanics could be reliably used to predict the fracture loads and critical crack sizes for a wide variety of crack configurations including corner cracks at pin-loaded holes.

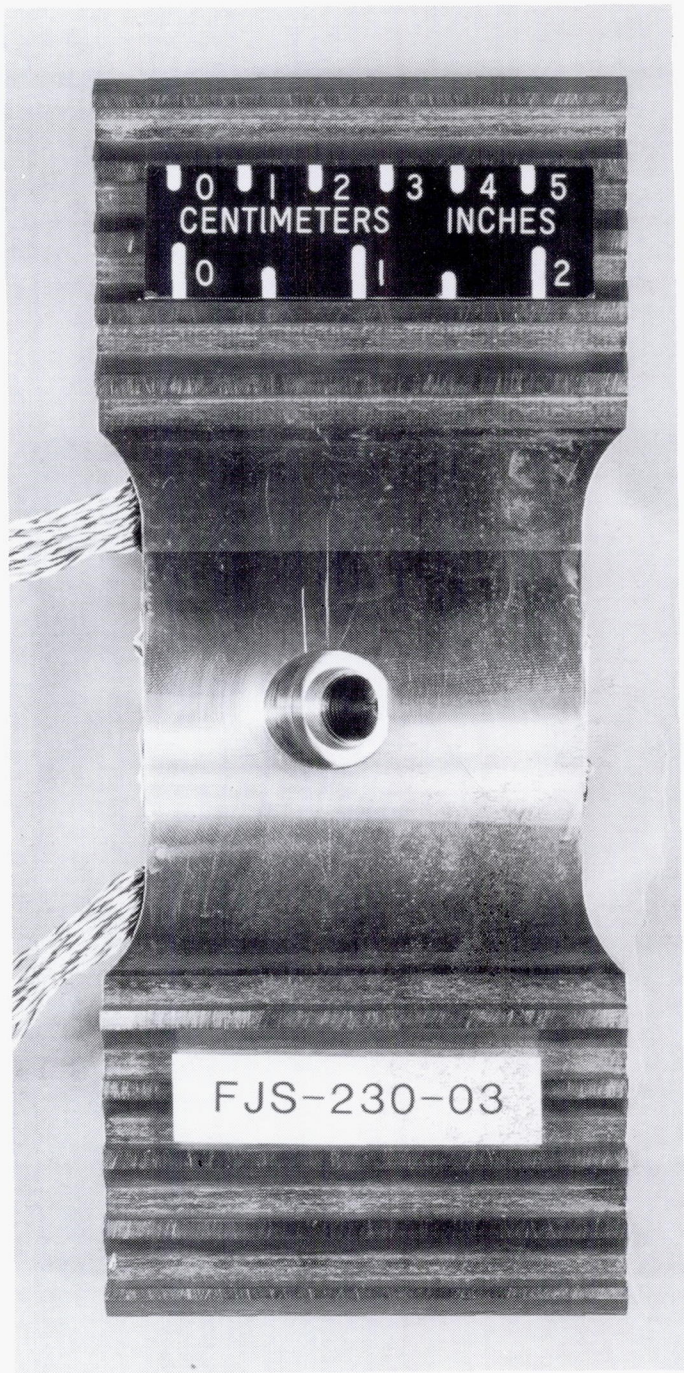

Leak-check-port specimen. L-89-9187

(James C. Newman, Jr., 43487)

Structures and Materials Research Laboratory

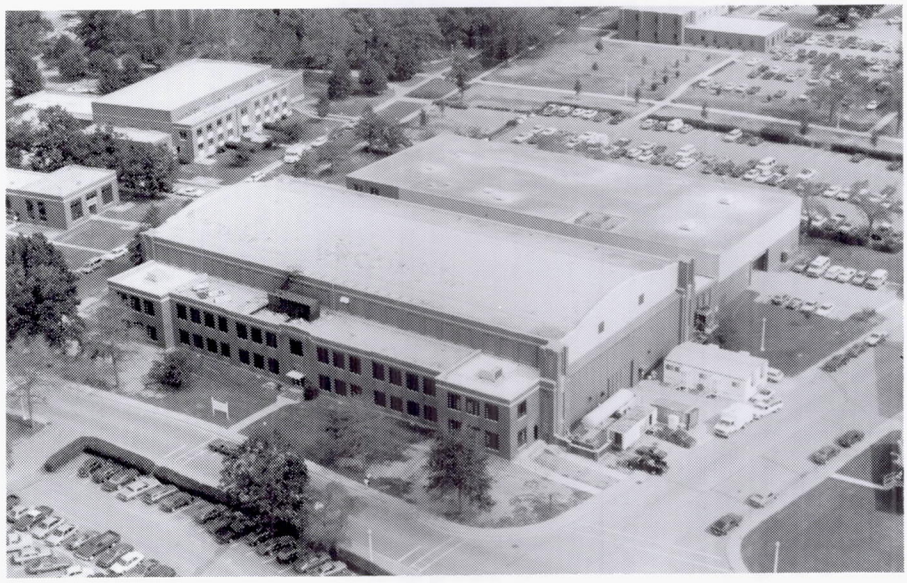

Built in 1939 to contribute to the development and validation of aircraft structural designs during World War II, this laboratory currently supports a broad range of structural and materials development activities for advanced aircraft, aerospace vehicles, and space platform and antenna structures. Research conducted in this laboratory includes the development, fabrication, and characterization of advanced materials and the development of novel structural concepts. Static testing, environmental testing, and material fabrication and analysis are performed using the unique capabilities of this laboratory. Research results are directly applicable to the development of structures and materials technologies required for future advanced subsonic aircraft, high-speed transports, high-performance military aircraft, advanced hypersonic and aerospace vehicles, and large space structures and antennas. Emphasis is on the development of structural mechanics technology and advanced structural concepts enabling the verified design of efficient, cost-effective, damage-tolerant advanced composite airframe structural components subjected to complex loading and demanding environmental conditions. This research also emphasizes advanced space-durable materials and structural designs for future large space systems affording significant improvements in performance and economy.

A significant feature of the laboratory is its static testing equipment. A 1,200,000-lb-capacity testing machine is used for tensile and compressive tests of specimens up to 6 ft wide by 18 ft long. Lower capacity testing machines of 300,000-, 120,000-, 100,000-, and 10,000-lb capacity also are used for smaller specimens. Capability also exists for assembling and testing large structural specimens and components such as the trusses used for Space Station Freedom development and future large space structures.

This complex also houses the Langley Research Center state-of-the-art analytical and metallurgical laboratory featuring all aspects of material specimen preparation and examination. Complete, automated metallographic preparation equipment is available for research on light alloys as well as metal matrix and resin matrix composites. Optical microscopy includes quantitative image analysis in addition to regular microscopy. Current technology electron microscopy is available including scanning electron microscopy, scanning transmission electron microscopy, and electron microprobe X-ray analysis.

Environmental testing for materials also is performed in this laboratory. Environmental exposure and characterization facilities for space materials research include two thermal cycling chambers ($\pm 250^{\circ}$F), three electron irradiation chambers capable of pressures to 10^{-8} torr and energy levels to 85 keV, and four laser interferometers for measuring coefficients of thermal expansion (to 0.05 parts per million (p/m) strain) and surface accuracy (to 0.2 μm rms) for elements of precision space structures. A hypersonic materials environmental system is capable of continuous test operation at Mach 5 to a 150,000-ft altitude to simulate operating conditions for future high-speed and hypersonic aircraft. The system is used

to study the effects of environment on the materials used for future high-speed and hypersonic aircraft applications.

Carbon-carbon composite materials development for advanced hypersonic vehicles also is conducted. Experimental test materials are fabricated using two high-temperature ovens (1300°F), a vacuum/pressure impregnator with capability to 500°F at 300 psig, and two inert-atmosphere pyrolysis furnaces (2200°F). Test specimens are heat treated, and oxidation-resistant coatings are applied in a 4500°F inert-atmosphere furnace.

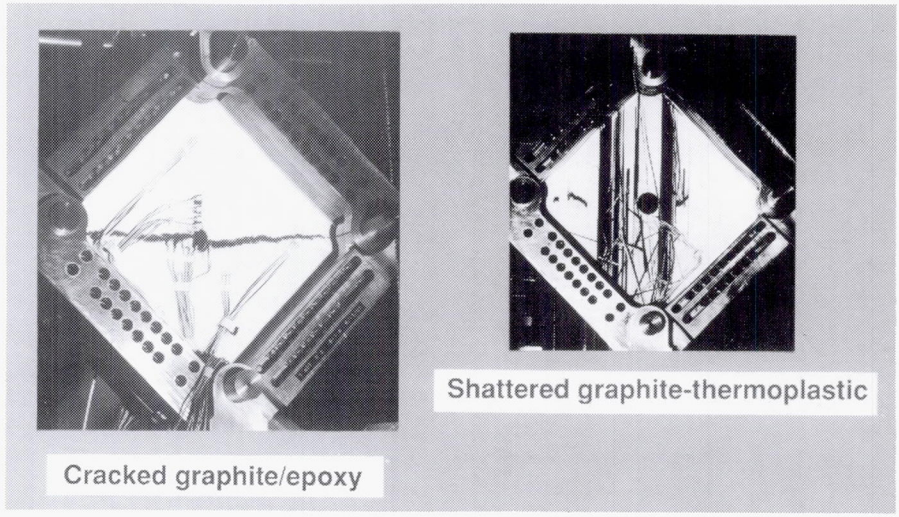

Failure mode comparison for buckled shear webs.

Postbuckling of Composite Shear Webs

The test specimens shown in the figure were tested in the Structures and Materials Laboratory to quantify the effects of circular cutouts on the buckling, postbuckling, and failure characteristics of composite shear webs. The graphite/epoxy and graphite/thermoplastic shear webs had 12 in. by 12 in. test sections and were tested using a picture frame fixture. The cutout diameters ranged from 0 in. to 3 in. Quasi-isotropic 24-ply laminates were studied. The graphite/thermoplastic specimens were fabricated by The Boeing Company. Moiré interferometry was used to observe out-of-plane displacements, and a high-speed data acquisition system was used to record displacements, strain, and applied loads.

The experimental results provide useful insights to the behavior of composite shear webs. The graphite/thermoplastic shear webs had approximately the same initial buckling mode shapes as similar graphite/epoxy shear webs. The graphite/thermoplastic shear webs had higher buckling and failure strains and a different failure mode when compared to results for similar graphite/epoxy shear webs. The graphite/thermoplastic shear webs were characterized by a shattering-type failure mode, and the graphite/epoxy shear webs were characterized by a tearing-type failure mode. A nonlinear finite-element analysis is currently being conducted for comparison with the experimental results.

(Marshall Rouse, 43182)

Precision Segmented Reflector Support Truss Test Bed

The efficient use of precision segmented reflectors (PSR) in space requires erecting them upon accurate supporting structures that will maintain reflective surface precision. Similarly, testing various reflector concepts also requires an accurate test bed support structure. Such an accurate, doubly curved erectable truss for use as a test bed in support of PSR activities at the Jet Propulsion Laboratory was designed and fabricated at Langley Research Center.

The resulting configuration contained 150 graphite/epoxy struts, 300 aluminum joints, and 45 aluminum nodes to form a doubly curved tetrahedral truss 4 m in diameter. This configuration was designed to support a segmented surface having a focal length of 2.4 m. The 0.77-m to 0.92-m struts were commercially manufactured with Langley-provided aluminum fittings bonded in each end to accept threaded aluminum joints. The root mean square (rms) surface accuracy achieved was

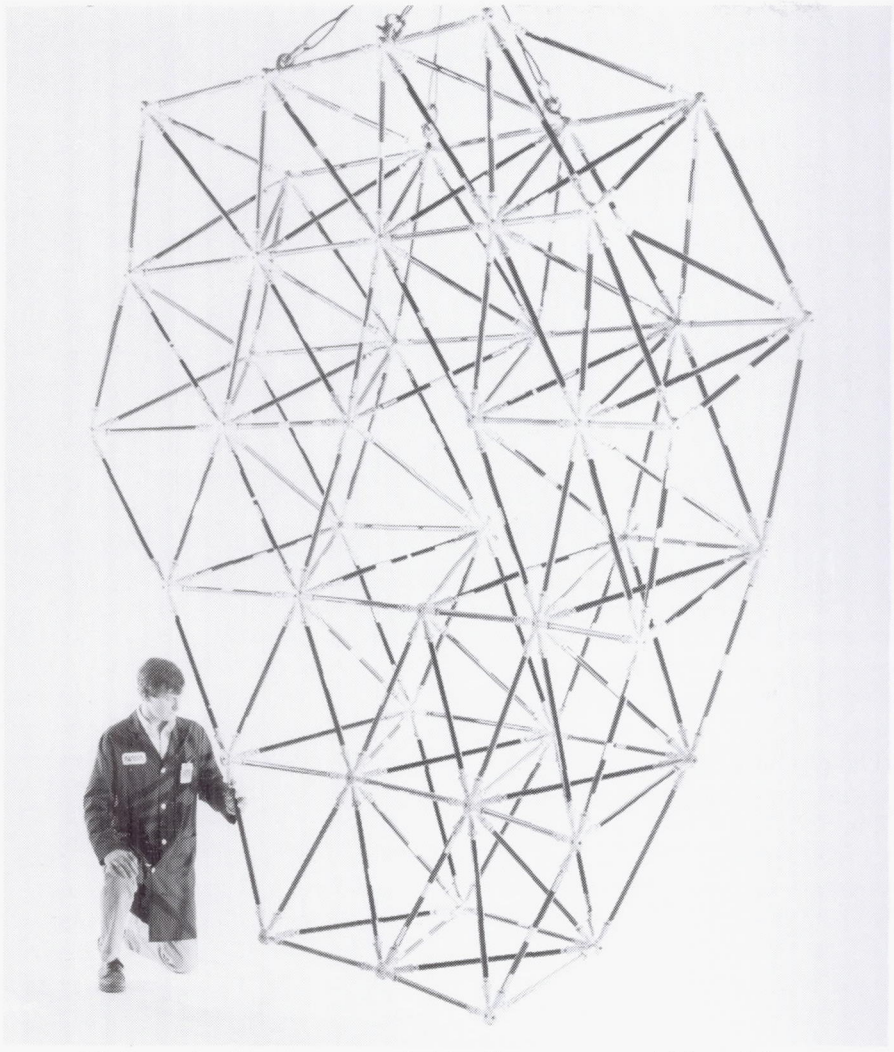

Assembled test bed truss suspended in Structures and Materials Research Laboratory to show double curvature. L-89-7527

approximately 0.005 cm as determined by photogrammetry. The assembled test bed establishes a baseline start-to-finish design and fabrication capability for erectable reflector support structures at Langley.

(Harold G. Bush, 43124, Catherine L. Herstrom, Richard E. Walsom, and James E. Phelps)

Effects of Thermal Cycling on Composite Tubes for Space Truss Structures

Graphite-fiber-reinforced composite tubes will be the primary structural elements for Space Station *Freedom* because of their low coefficient of thermal expansion (CTE) and high specific stiffness. Changes in these properties due to prolonged orbital thermal cycling are significant considerations in the design of these structures. A study to determine the effects of long-term thermal cycling on representative candidate composite tubes has been conducted.

Three types of composite tubes with the same layups were selected for study in this program. The $[+15/0/\pm10/0\text{–}15]_S$ layup was selected to provide resistance to microcracking, a CTE of $< 1 \times 10^{-6}$ in/in., and sufficient hoop strength to resist handling damage. Two fibers (a high-strength, moderate modulus T-300 and a moderately high-modulus P75S) were selected for study along with two resin systems: Fiberite 934 and American Cyanamid BP907. Two-mil-thick

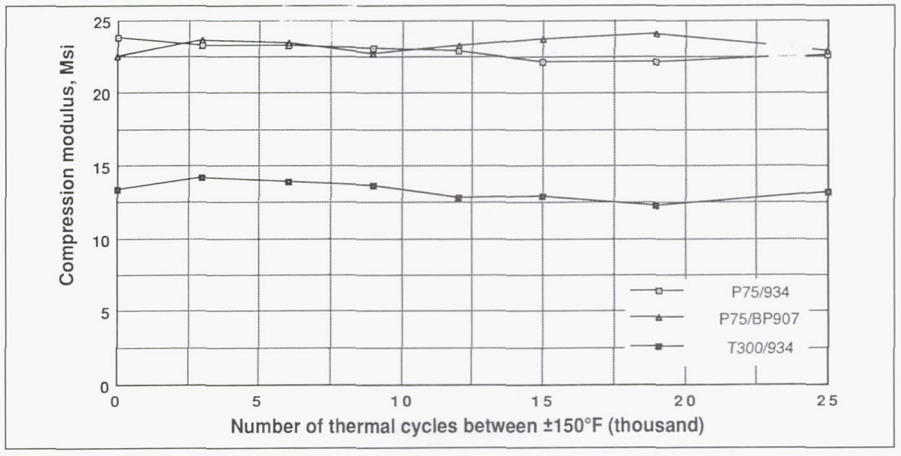

Effects of thermal cycling on compression modulus of composite tube ($[+15/0/\pm10/0\text{–}15]_S$ with 2 mil Al foil inside diameter and outside diameter).

anodized aluminum foil was co-cured onto the inside and outside of most of these tubes to provide thermal control and atomic oxygen protection.

Ten-ft-long by 2-in. ID (inner diameter) × 0.065-in. wall thickness tubes were fabricated and cut into 10-in.-long sections for thermal cycling testing. A compressive modulus at 2000 lb load was used to check for changes in the modulus due to thermal cycling. Test data indicate that no significant changes in modulus occurred for 25,000 thermal cycles between ±150°F.

(W. S. Slemp, 41334)

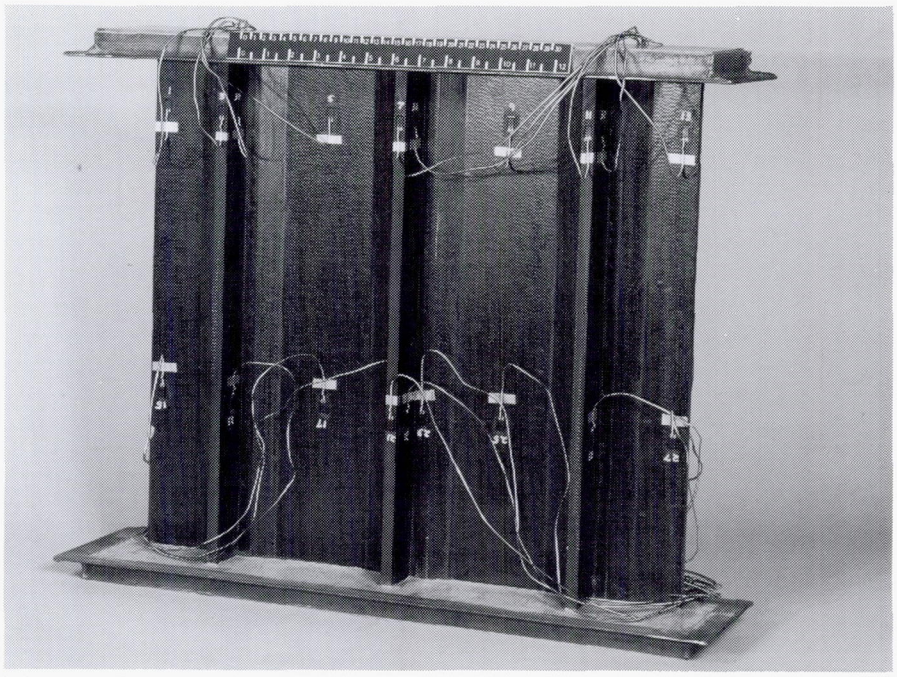

Blade-stiffened carbon/epoxy wing panel. L-89-2129

Evaluation of Stitched, Resin-Transfer-Molded Carbon/Epoxy Wing Panel

Fabrication concepts that are cost effective and are also suitable for producing efficient composite structures are being studied for application to future aircraft. Resin transfer molding (RTM) of stitched carbon fabrics is a promising concept for exploiting the structural efficiency of composite materials. Stitching layers of dry carbon fabric with closely spaced threads provides through-the-thickness reinforcement and greatly improves damage tolerance. The dry carbon preform is then filled with a low-viscosity epoxy resin and cured to complete fabrication. The stitched panel (approximately 2 ft wide by 2 ft long) shown in the figure has three blade stiffeners and has been designed for a transport aircraft wing box with in-plane loadings of $N_x = 22,000$ lb/in. in compression and $N_{xy} = 3000$ lb/in. in shear. The panel was made in a four-step process. First, the skin preform was laid up using dry carbon fabric plies and stitched with strong thread. Second, the blade stringer preforms were laid up and lightly stitched in the web areas. Third, the stringer flanges were folded out and stitched to the skin preform with strong thread. Finally, the entire stitched preform was placed in a tool, filled using an inexpensive epoxy resin, and cured at 350°F. For compression testing at Langley Research Center, the panel ends were potted in metal frames and ground flat, and then numerous strain gauges were attached. The panel was subjected to low-speed impact damage at a critical location opposite the edge of one center stiffener flange. Panel failure occurred at 157 percent of design ultimate load. These test results indicate that stitching provided excellent damage tolerance and that the RTM process can be used to fabricate usable heavily loaded carbon/epoxy aircraft structures.

(M. B. Dow, 43090)

Improved Performance of Titanium Alloys by Thermal Control Coatings

Titanium alloys are candidate materials for hot structures and heat shields of hypersonic vehicles because of their high structural efficiency. However, the range of conditions in which they can be used may be limited by their reactivity to oxygen and loss in mechanical properties at high temperatures. Protective thermal control coatings that shield the materials from oxidation will enable their use at higher temperatures. Further, coatings that provide a high emittance and low-catalytic efficiency surface can significantly

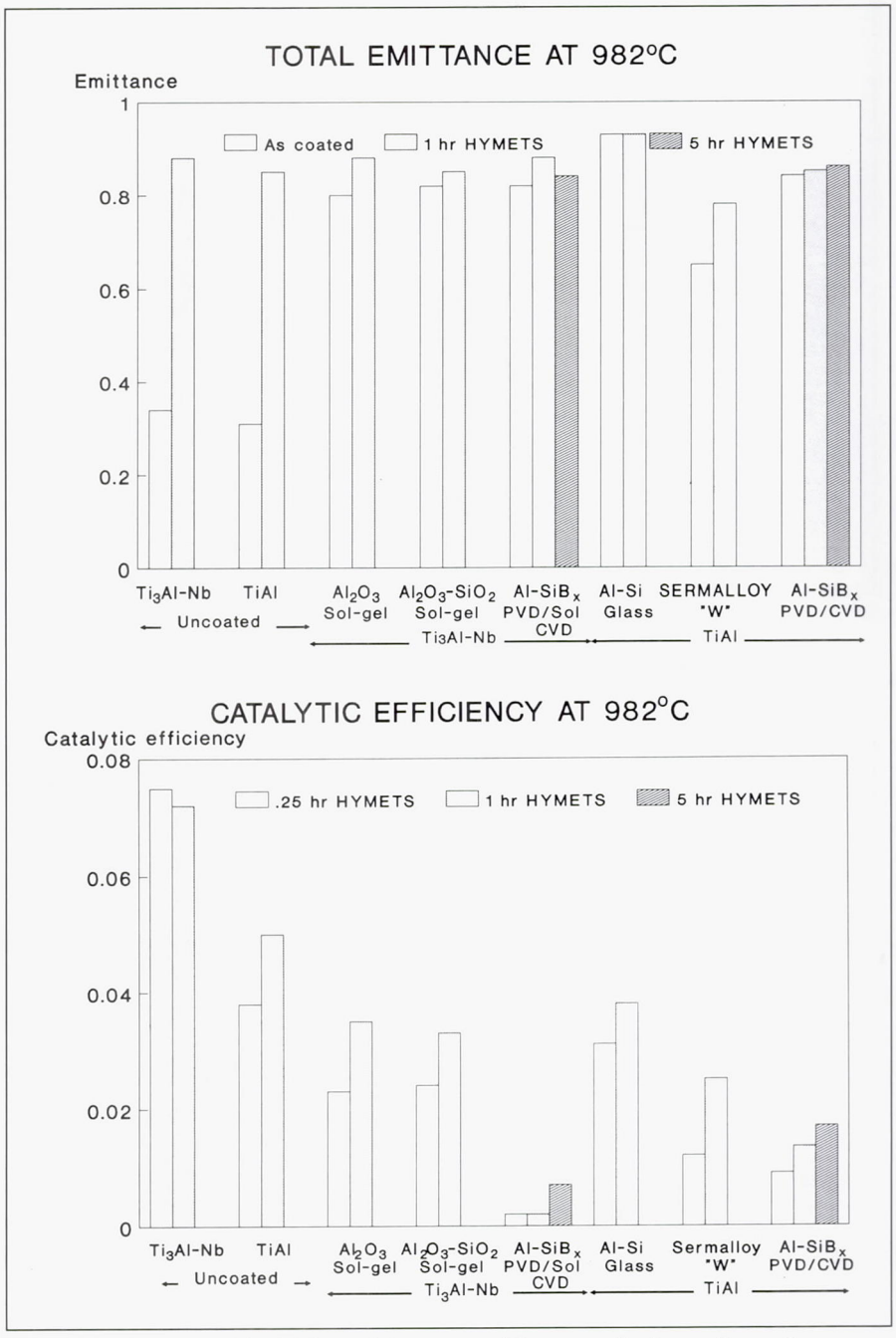

Coatings that provide high emittance and low-catalysis surfaces for titanium-aluminide alloys.

extend the applicability of these materials by reducing the net heating to the vehicle surfaces in hypersonic flight environments that contain dissociated species. The low-catalytic efficiency reduces heat input from recombination of dissociated species in the environment, and the high emittance rejects a significant portion of the convective heat flux from the surface by radiation.

A coatings development program has produced a lightweight coating that significantly reduces the surface temperature of titanium-aluminide alloys tested under simulated hypersonic flight conditions. Coatings are tested in the Hypersonic Materials Environmental Test System (HYMETS Facility), which is a 100-kW arc-heated wind tunnel capable of testing 2.5-cm-diameter specimens in a stagnation configuration at a Mach number of 3.5 to 4 with surface temperatures to 1650°C (3000°F). The catalytic efficiency of coatings is determined from aerothermal heating analysis of specimens during HYMETS exposure. The emittance of coatings is determined before and after HYMETS exposure using a room-temperature spectral reflectance apparatus.

The figure shows emittance and catalysis data for a variety of coatings on titanium-aluminide alloys: Al_2O_3 and Al_2O_3-SiO_2 applied by sol-gel, Al-Si glass applied as a slurry, Sermalloy W, and Al-SiB_x applied by either a three-step physical-vapor-deposition/solution-spray/chemical-vapor-deposition process or by a two-step physical-vapor-deposition/chemical-vapor-deposition process. The emittance of uncoated alloys after testing is significantly higher than before testing because of the heavy oxidation during exposure to the HYMETS environment. The Sermalloy W coated specimen had a lower emittance than the remaining coatings. The catalytic efficiency of each of the coatings is somewhat lower than the catalytic efficiency of the uncoated alloys. The lowest catalytic efficiencies measured were for the Al-SiB_x. The Al-SiB_x coating is being developed by Lockheed Missiles and Space Corporation under contract to NASA.

(R. K. Clark, 43513)

CETA Structural Verification Test

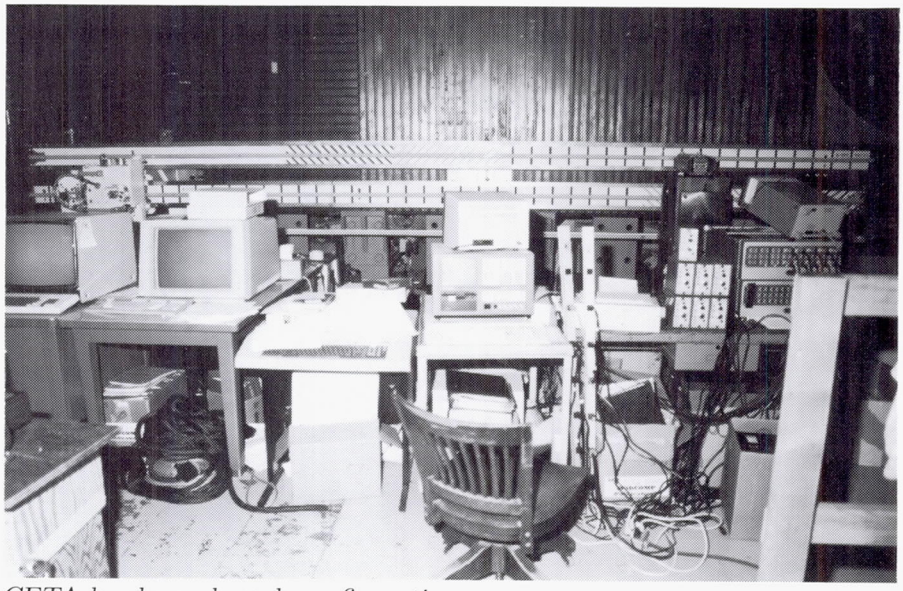

CETA hardware launch configuration. L-89-14051

The Crew and Equipment Translation Aid (CETA) flight experiment will fly on the STS-37 Gamma Ray Observatory Mission in the mid-1990 time frame. In order to satisfy the payload verification requirements of the National Space Transportation System (NSTS) 14046 document, *Payload Verification Requirements*, a certification hardware assembly must be structurally tested to demonstrate the minimum required safety factor of 1.4. A test-verified payload structural dynamic math model must be provided for a Space Transportation System (STS) coupled load analysis; therefore, the mode frequencies and shapes must be determined from a modal survey of the certification assembly.

The figure shows the CETA hardware launch configuration mounted to a backstop during the modal survey. This configuration includes two rail sections and one outrigger (each approximately 24 ft long), one truck/cart, and one tether shuttle assembly. Also shown is the random input shaker attached to the fixed track. All mode shapes and frequencies below 35 Hz were determined. Design limit loads for launch and landing are 15 g in three axes. Orbit loads are 187 lb for handrails and 200 lb/200 ft·lb tether loads to the cart. The deployed track with the truck/cart/tether shuttle assembled was tested to a 21 g load by statically loading the rail with lead shot bags and concentrated loads at the truck/tether shuttle. Because gravity loading was utilized, the assembly had to be mounted to the backstop via rigid adapter blocks to provide gravity loads in multiple directions. Ground support equipment (GSE) support hardware provided the handrail loads for the track and outrigger as well as the orbit loads to the cart.

Testing was completed without component failure or permanent deformation of the certification flight hardware.

(Richard W. Faison, 47083)

NDE Research Laboratory

The reliability and safety of materials and structures are of paramount importance to NASA. The assurance of reliability must be based on a quantitative measurement science capability that is nondestructive. The Langley Research Center NDE Research Laboratory has as its prime focus the development of new measurement technologies that can be directly applied to ensuring material integrity. Furthermore, the laboratory activity is strongly directed toward developing physical properties required for structural performance.

A new facility has been constructed which added 16,000 ft^2 of laboratory space to the existing nondestructive evaluation (NDE) research area. This new facility was furnished and occupied in January 1989 and will allow for some expansion of NDE efforts over the coming years.

The NDE Research Laboratory is a combination of research facilities providing advanced NDE capabilities for NASA and is an important resource for government and industry technology transfer. The laboratory is the Agency's focal point for NDE and combines basic research with technology development and transfer. The activity concentrates on NDE materials measurement science for composites and metals with emphasis in materials characterization as well as impact damage, fatigue, applied and residual stress, and structural NDE with smart sensors/materials. A particular new focus highlights NDE requirements for Space Station Freedom on-orbit NDE and national problems of aging aircraft.

The facility is a state-of-the-science measurement laboratory linking 16 separate operations to a central computer consisting of a VAX-750 with 10 megabytes of internal memory and more than 500 megabytes of fast storage tied to staff desktop microcomputers. The system interfaces with a real-time video input-output so that NDE images can be obtained, processed, and analyzed on-line. The major laboratory operations include a 55-kip and a 100-kip load system for stress/fatigue NDE research, a magnetics laboratory for residual stress, three computer-controlled ultrasonic scanners for imaging material properties, a technology transfer laboratory, an electromagnetic impedance characterization laboratory for composite fiber integrity, and a composite cure monitoring laboratory for process control sensor development. Other major laboratory operations include a nonlinear acoustics laboratory for advanced NDE research, a laser modulation applications laboratory for remote sensing and smart materials, a pressure and temperature derivative laboratory for higher order elastic constant measurements, a thermal NDE laboratory, and a signal processing laboratory for improved image resolution and information transfer. An X-ray tomography system is under construction to provide the first view of material or structural failure under load and will be on-line in 1990.

Scanning Electron Acoustic Microscopy

The capability to assess microstructural features of materials is important not only in fundamental studies of material properties but also in identifying those microstructural features that most directly influence nondestructive measurements. Traditionally, the primary tools

for microstructural studies have been optical and electron microscopes. Except for transmission microscopes, which require extensive and often elaborate specimen preparation, most microstructural images are topographical. Thus, while the images reveal important surface features, they are generally incapable of revealing significant subsurface information. During the last decade, a number of novel microscopic imaging techniques have been developed; these techniques provide new information about materials which was previously unattainable in microscopic images. Among the more significant of these new microscopies is scanning electron acoustic microscopy (SEAM).

SEAM is based on a modification of traditional scanning electron microscopy (SEM) in that the electron beam, normally continuous in SEM, is chopped or modulated in SEAM at some frequency ranging from roughly 20 kHz to 5 MHz. Upon penetrating the specimen surface, the chopped electron beam loses its energy in a series of random atomic collision processes. Part of the electron energy loss results in the generation of acoustic waves having a frequency equal to that of the beam chopping frequency. The acoustic signal propagates through the specimen and is detected by a piezoelectric transducer attached to the opposite side of the specimen. As the electron beam rasters the specimen surface, an electron-acoustic image is generated and displayed on a phosphored screen.

Extensive three-dimensional theoretical modeling of the electron-acoustic signal generation process reveals that the microscopic image contrast depends upon the local variations in the thermal and elastic properties of the specimen as well as local variations in the electron attenuation coefficient. Subsurface as well as surface features can be imaged with a spatial resolution of less than 1 μm under optimum conditions. The imaging capability is illustrated in the figure where the same area of an alumina specimen is examined both by SEM (panel (a)) and SEAM (panel (b)). The SEM micrograph clearly shows a surface-breaking crack. The SEAM micrograph, however, reveals not only the surface-breaking crack but also a subsurface crack at right angles to the surface-breaking one. The basic features of the SEAM image shown in the figure are predicted by the mathematical model. Further applications and modeling of the SEAM signal generation on a variety of materials are in progress.

(J. H. Cantrell, 44989)

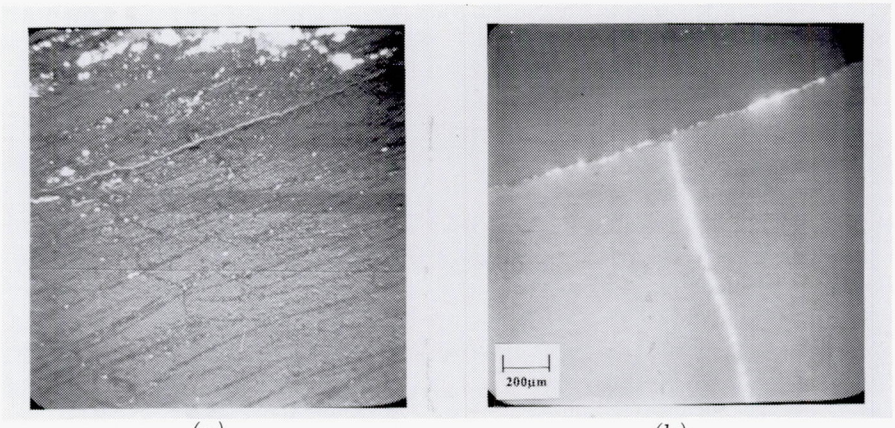

(a) (b)

Micrographs of alumina. Panel (a) shows SEM secondary electron, and panel (b) shows SEAM at a chopping frequency of 305.43 kHz.

Evaluation of Aerospace Structural Adhesive Joints Using Ultrasonic Techniques

The reliability of bonded joints in critical structures goes well beyond the need to be able to quickly and reliably determine disbonds. Quantitative evaluation of bonded joint strength is also of high importance to the safety/reliability and cost effectiveness of aerospace systems. One of the more perplexing issues is the evaluation procedures of bonded joints for reliability and characteristic strength. Though significant advances in the state of the art of ultrasonic inspection of adhesive bond lines have been made, much work still remains in order to develop a complete bond flaw prediction algorithm.

During the past year research efforts were investigated using a quadrature phase detection technique to monitor the amplitude and phase of a toneburst ultrasonic wave, reflected from an adhesively bonded steel/rubber interface that simulates the solid rocket motor (SRM). A theoretical model of the interface is shown in the first figure and is

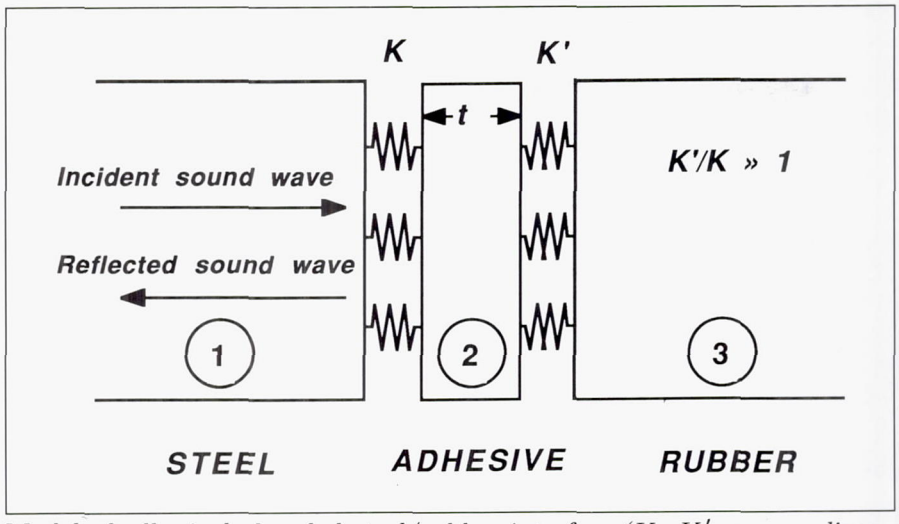

Model of adhesively bonded steel/rubber interface (K, K' are coupling constants).

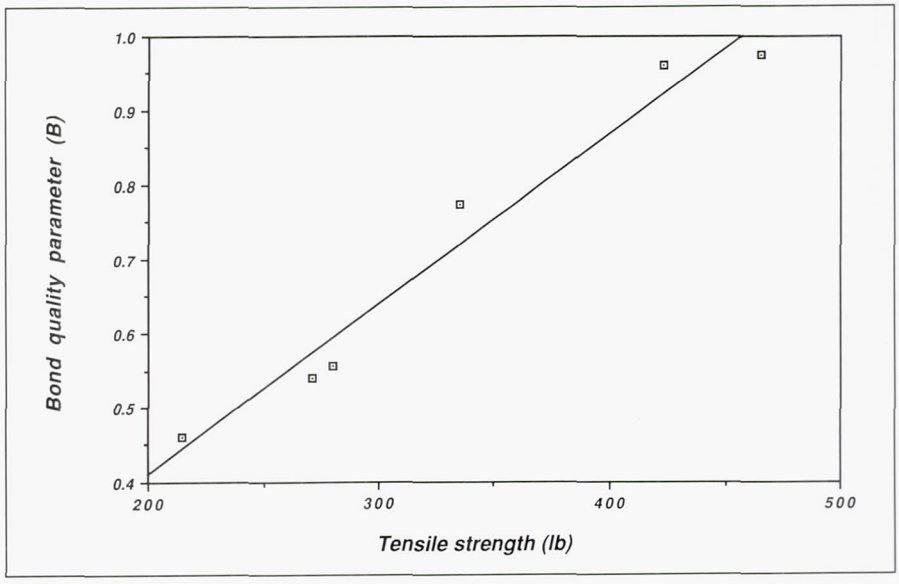

Plot of bond quality parameter versus measured tensile strength.

used to calculate sound wave propagation in a multilayered elastic medium. A bond quality parameter deduced from experimental data is correlated with tensile strength. Results of the data in the second figure show the structural strength variations to be correlated with strength.

The application of this technique to bond line evaluations has been shown to add significantly to a body of knowledge in this critical and important area. Continued efforts will be maintained for the development of experimental and theoretical models to help enhance NASA's ability for future applications to bond line problems.

(A. Smith, 44961)

Evaluation of Acoustic Emission Signals in Gr/Ep Space Station Freedom Truss Tubes

Graphite/epoxy composite materials, because of their high strength and light weight, have been chosen as the material for the Space Station *Freedom* (SSF) truss structure. However, during the 30-year expected life of SSF, these tubes will be exposed to an extremely harsh environment that will include large temperature variations, hypervelocity micrometeroid impacts, and atomic oxygen attack, in addition to the normal operating stresses of the structure itself. Thus, for the safety of SSF and its inhabitants, it will be important to nondestructively monitor the integrity of these tubes.

One proposed method for doing this is by the use of the acoustic emission (AE) technique. This technique places acoustic sensors on the structure to detect noise from impact damage and the propagation of cracks. This technique has several advantages in that it allows the monitoring of a large area, requires no extravehicular activity by the astronauts, and can yield the location of damage. However, current state-of-the-art AE leaves much to be desired in quantifying the amount of damage which will be important for this application. To avoid unnecessary extravehicular activity for maintenance, it will be necessary to know the amount of damage in a particular tube.

One problem with current AE techniques is the use of narrowband acoustic sensors. These sensors mask the true characteristics of the acoustic signal and thus limit information available

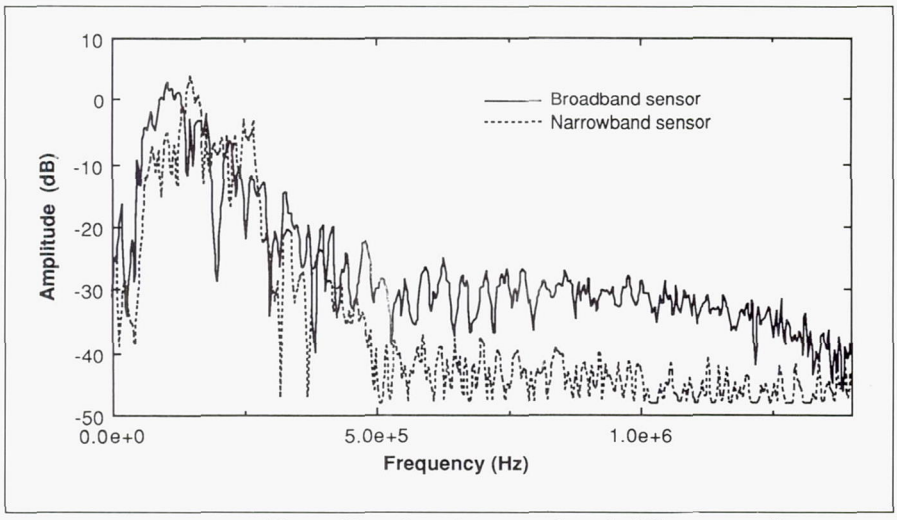

Frequency response of broadband and narrowband AE sensors for simulated AE event on Space Station Freedom truss tube.

concerning damage. Current research involves characterizing newly developed broader band sensors that may make damage assessment more accurate. The figure compares the frequency response of a conventional acoustic emission narrowband sensor to that of a new class of broadband sensors for a simulated acoustic emission event created by a lead pencil break on a full-scale Space Station *Freedom* tube. The plot shows that although the sensors have similar amplitude responses for the lower frequencies, the narrowband sensor loses significant information at the higher frequencies. This high-frequency information is important in constructing the time characteristics of the source which yield information concerning the type and quantity of damage.

(W. H. Prosser, 44960)

Ultrasonic Monitoring of Pultrusion Process

Pultrusion is an attractive technique for quick, inexpensive production of a continuous stream of composite parts by curing in a short heated die. However, the pultrusion process currently lacks instrumentation that is capable of continuously monitoring the integrity of the composite during processing. Postprocessing inspection of the composite is time consuming, and the time delay in feedback to the pultruder could result in the fabrication of large quantities of defective material. Currently, on-line quality control is left to the eyes and experience of the operator to ensure a continuous quality product.

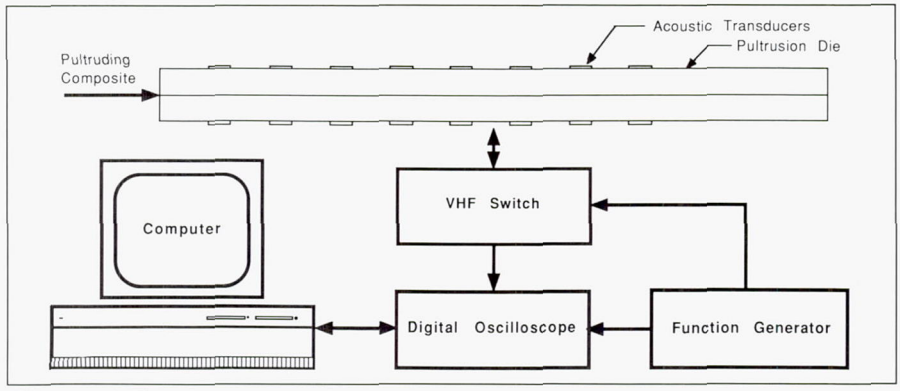

Ultrasonic instrumentation of pultrusion die.

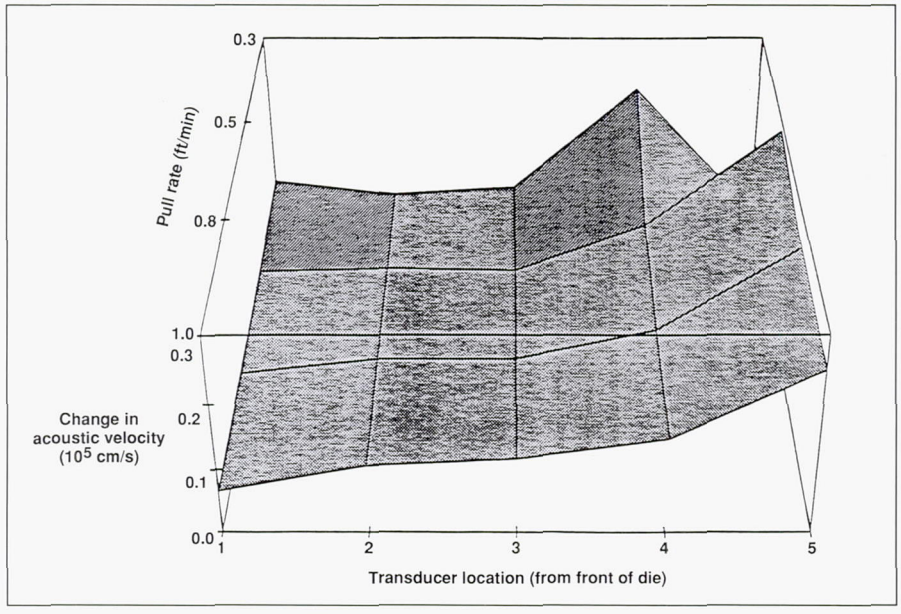

Effect of pull rate on change in acoustic velocity.

A nondestructive measurement technique that is well suited for quality control in the pultrusion process is ultrasonics inspection; it is a nonintrusive technique that can be used to continuously monitor properties of the composite as it is being pultruded. Ultrasonics inspection is particularly well suited for monitoring the pultrusion process because ultrasonic properties have been shown to vary during composite cure and to be related to resin viscosity and the degree of cure.

To measure the ultrasonic properties of the composite as it moves through the die, several pairs of high-temperature ultrasonic transducers are mounted at a series of positions on opposite sides of the die (as shown in the first figure). The transducers act as both stimuli and sensors for characterizing the acoustic response of the system. By activating different pairs of transducers, the measurement system continuously scans the ultrasonic properties along the die during the cure.

This method provides a means for continuous and nonintrusive measurements of a pultruding composite at select positions along the pultrusion die. The second figure shows a spatial representation of the acoustically determined change in cure state as the resin moves through the die. Because these ultrasonic measurements are related to the important processing parameters of viscosity and degree of cure, ultrasonic monitoring of the pultrusion process has potential as an input into a quality control feedback loop, therefore enhancing quality control of the pultrusion process.

(F. Raymond Parker, 44965)

Thermographic Detection of Disbonds in Aging Aircraft

The detection of the degradation of bonding in lap joints of aging aircraft is essential to ensure their safety and reliability. Thermographic techniques have a possible application to detect the degradation of bonding in such structures. The thermographic techniques are particularly useful because they are able to scan large areas in a short period of time. They also require no couplant because the object may be both heated radiometrically and the subsequent temperature profiles measured radiometrically. For these reasons, thermographic techniques are both quick and easy to use.

Research performed at Langley Research Center has shown it is

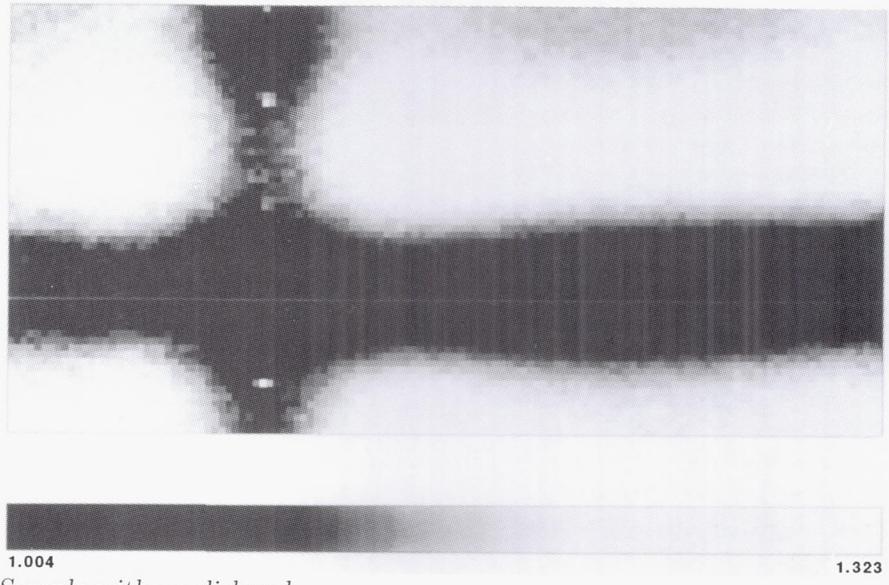

Sample with no disbond.

Sample with disbond.

possible to detect the disbonds in samples typical of the structures found in aging aircraft. This technique uses quartz lamps to radiometrically heat the structure and an infrared camera to measure the resulting temperature profiles. A comparison of the temperature profiles during and after the heating gives a clear image of the extent of the bonding in the structure. The first figure shows a thermographic image of a region of the structure where the bonding of a subsurface tear strap is still present. In contrast, the second figure is a thermographic image of a region of the structure where the tear strap is unbonded. The time required for data acquisition for this case was 15 s. Similar tests have shown it is possible to image simultaneously with reasonable resolution areas up to 1 m^2.

(W. Winfree, 44963)

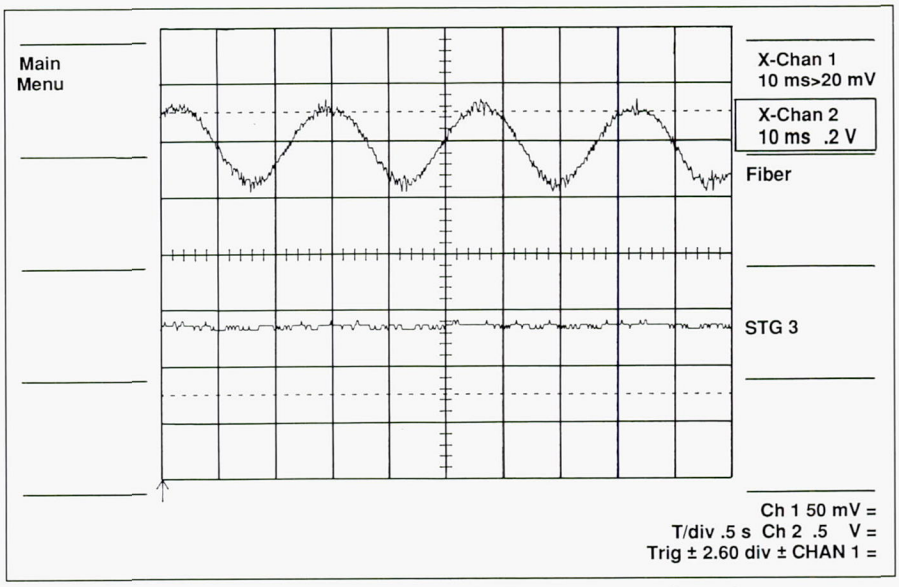

Comparison of strain gauge and optical fiber response for vibrating cantilever beam.

Smart Materials and Structures

Materials with internal sensors are being developed for "health monitoring" of structures during use. The smart structures laboratory is focusing on techniques that take advantage of the unique properties of fiber optic sensors. These sensors are lightweight and highly sensitive, have wide bandwidth, and are immune to electromagnetic interference.

Several methods for interrogating the fiber sensor are under investigation. Reported here are some results that were obtained with a fiber optic strain and vibration sensor that indicates the degree of strain by interference effects of two or three modes propagating in a fiber (a modal domain sensor). The light exiting the end of the fiber is detected, and the intensity indicates the strain in the fiber.

The results shown in the figure compare the signals from an optical fiber and a strain gauge (STG 3) attached to a cantilever beam. The beam is a model developed for control experiments simulating Space Station *Freedom* vibrational frequencies. The beam is instrumented with three strain gauges and a single fiber running nearly the full length of the beam. Because the fiber is a distributed sensor, which integrates the strain over the fiber length, it does not have the limitations of point sensors. The figure indicates that a single fiber sensor can track all the vibrational modes, whereas for certain modes, one or more strain gauges may be at a node producing no signal.

The program for smart structures development includes research on sensors for strain, temperature, acoustic emission, impact damage assessment, and aging and corrosion of composite materials and structures.

(Robert S. Rogowski, 44990)

Vehicle Antenna Test Facility

The Vehicle Antenna Test Facility (VATF) is a research facility used to obtain data for new antenna performance and electromagnetic scattering data in support of various research programs. The VATF consists of two indoor radio frequency anechoic test chambers and an outdoor antenna range system. The anechoic chambers provide simulated free-space conditions for measurements from 100 MHz to >40 GHz. The anechoic chambers, which are shaped like pyramidal horns to reduce specular reflections of the walls, are more than 100 ft long and have test area cross sections approximately 30 ft by 30 ft.

A spherical near-field (SNF) measurement capability was added to the low-frequency anechoic chamber. A precision antenna positioning system, an antenna source tower, and an optical alignment system designed for SNF measurements were installed in the low-frequency anechoic chamber, and the capability now exists for automatic performance of precision SNF measurements up to at least 18 GHz. Antennas with diameters up to 12 ft can be measured if their electrical size is no greater than 100 wavelengths (i.e., diameter/wavelength $\leq$100). This limitation is imposed by the SNF system software, which transforms the near-field data to obtain the desired far-field data. Measured data stored on disk can be processed to provide antenna directivity, polar or rectangular plots of the radiation patterns, and three-dimensional contour

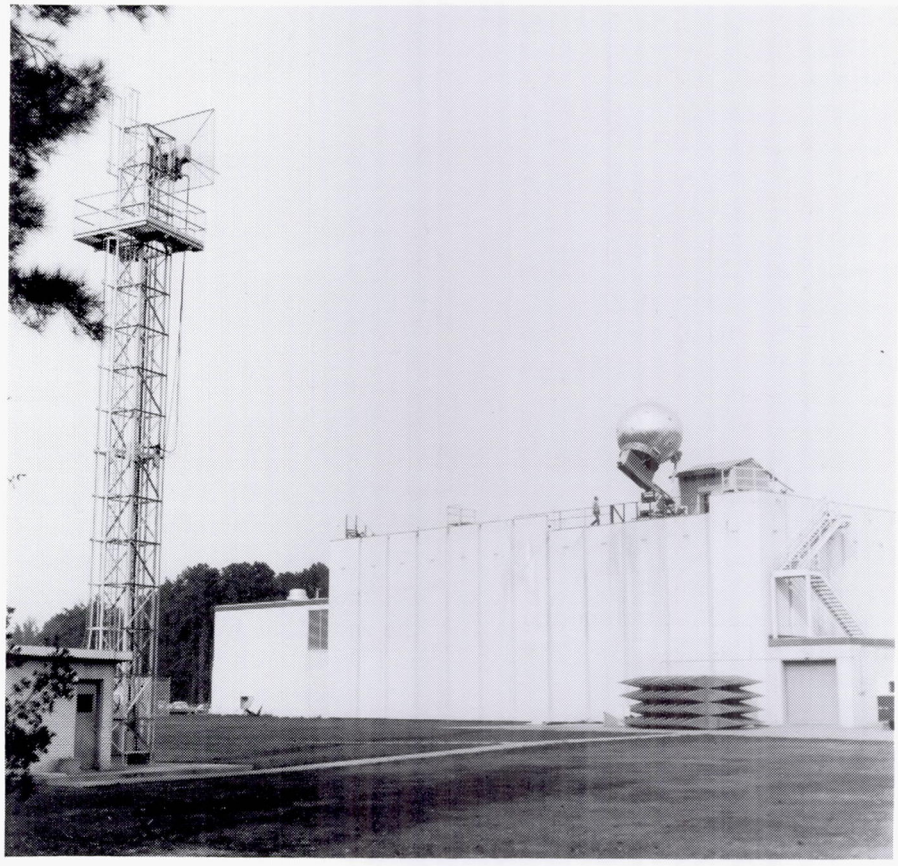

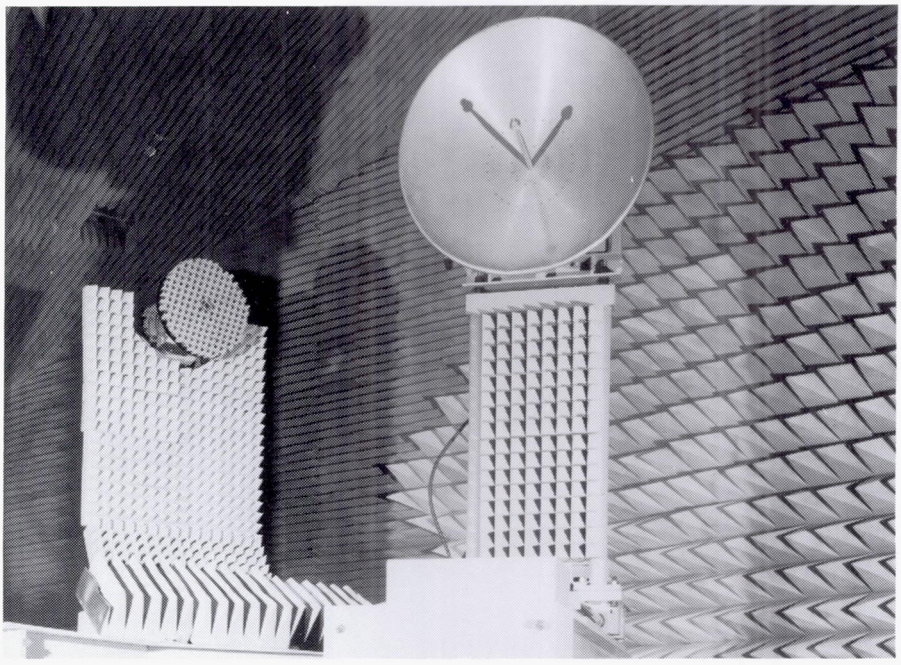

Spherical near-field equipment. L-85-2143

plots of the antenna radiation characteristics.

The high-frequency anechoic chamber was used to establish a Compact Range Facility. The compact range is an electromagnetic measurement system used to simulate a plane wave illuminating an antenna or scattering body. The plane wave is necessary to represent the actual use of the antenna or scattering from a target in a real-world situation. The compact range utilizes an offset-fed parabolic reflector to create the simulated plane wave test conditions. The standard commercially available compact range is limited to the measurement of antennas or models with maximum dimensions of 4 ft over the frequency range of 4 GHz to 100 GHz.

The outdoor antenna range system is available for use when the antenna or test model size or frequency precludes the use of the anechoic chambers. The outdoor range consists of two remote transmitting towers that are spaced 150 ft and 350 ft from the test positioner mounted on the VATF roof. The VATF has several electronic laboratories with the extensive measurement capability needed to support the design of unique antennas prior to their evaluation in the antenna chambers or on the outdoor antenna range system.

Space Station Freedom Antenna Pattern Measurements

Antenna pattern measurements were made at 60 GHz in the Compact Range Facility for both broad and narrow beam antennas mounted on a precision 1/30-scale model of the middle section of Space Station *Freedom* (shown in the first figure). This testing of the 1/30-scale model at 60 GHz simulates a 2-GHz frequency on the full-scale *Freedom* station. The measurement objective was to obtain experimental data that could be used for verification of analytical results obtained with a recently developed computer program. The computer program, the Numerical Electromagnetic Code–Basic Scattering Code (NEC-BSC, Version 1), was used to calculate the far-field radiation patterns for a broad beam slot

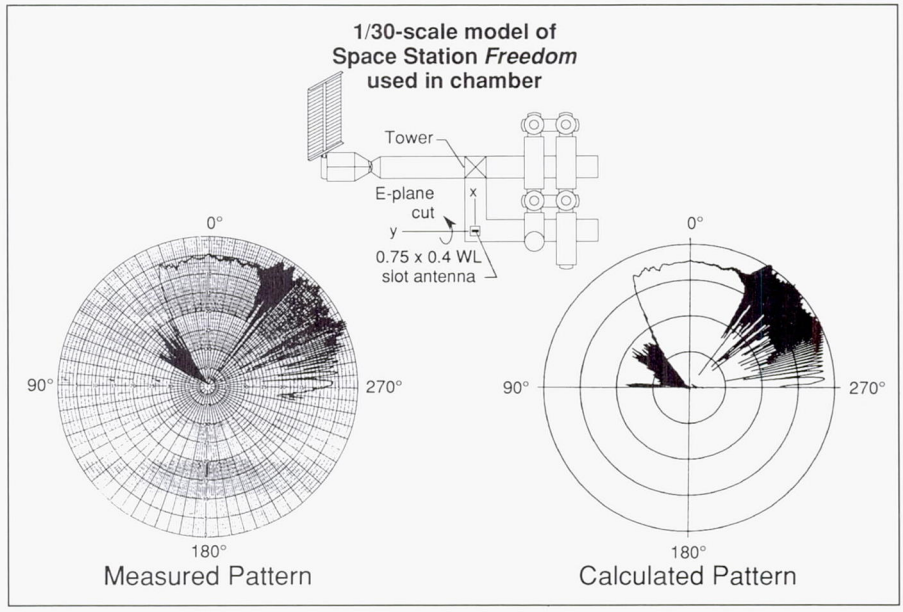

Predicted and measured antenna patterns for Space Station Freedom model.

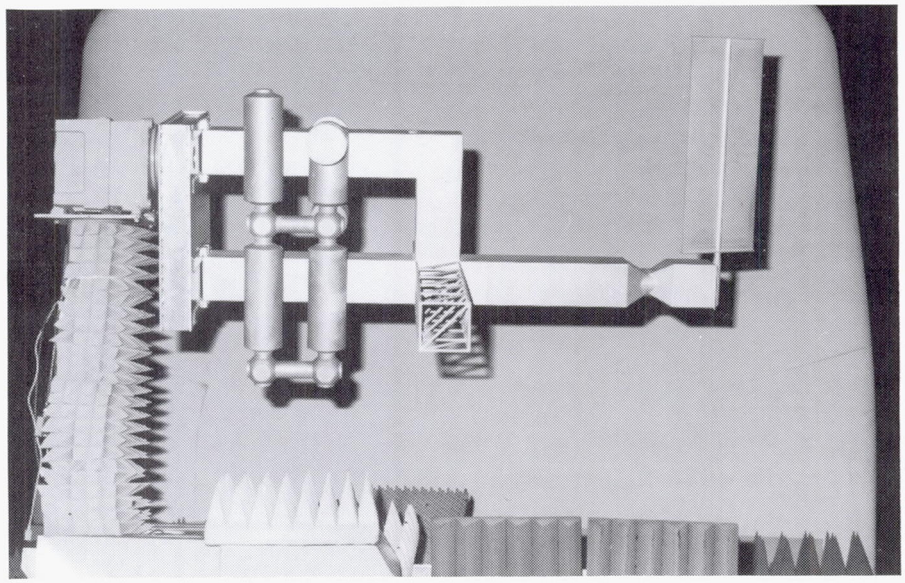

Space Station Freedom model during testing in Compact Range Facility.

L-89-06235

antenna mounted on Space Station *Freedom* as shown in the second figure. Excellent agreement was obtained between the calculated and measured principal E-plane patterns as shown. Several other model configurations and antenna orientations were evaluated. Excellent agreement also was achieved between measured and calculated results, thus providing further verification of the capability of the computer program for predicting antenna performance on large complex Space Station *Freedom* configurations. The computer program has the capability to predict both near- and far-field antenna performance for a wide range of antenna types.

(Melvin C. Gilreath, 41817, and Emedio M. Bracalente)

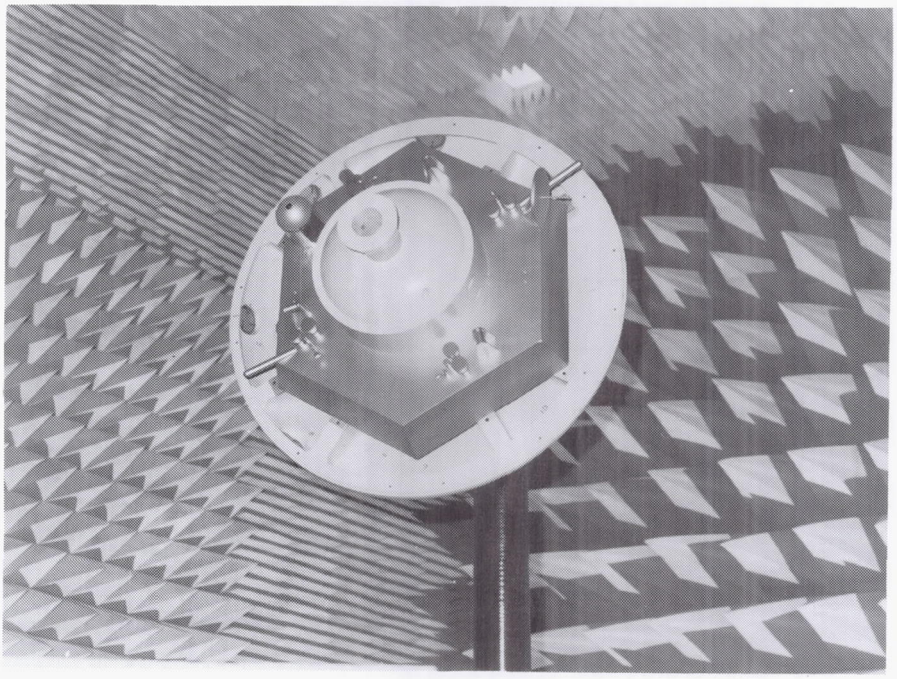

0.4-scale model of AFE in anechoic chamber. L-89-3055

Communication Antenna Pattern Measurements on Aeroassist Flight Experiment

The 0.4-scale Aeroassist Flight Experiment (AFE) model (shown in the first figure) was used to predict antenna radiation patterns for many configurations and verify pattern prediction computer codes written at Ohio State University (OSU). The antennas will be used to establish communications with the Tracking and Data Relay Satellite System (TDRSS) during the actual AFE launch in the mid-1990's. Patterns were made using a circularly polarized microstrip patch near the scaled frequency of operation for TDRSS S-band communications.

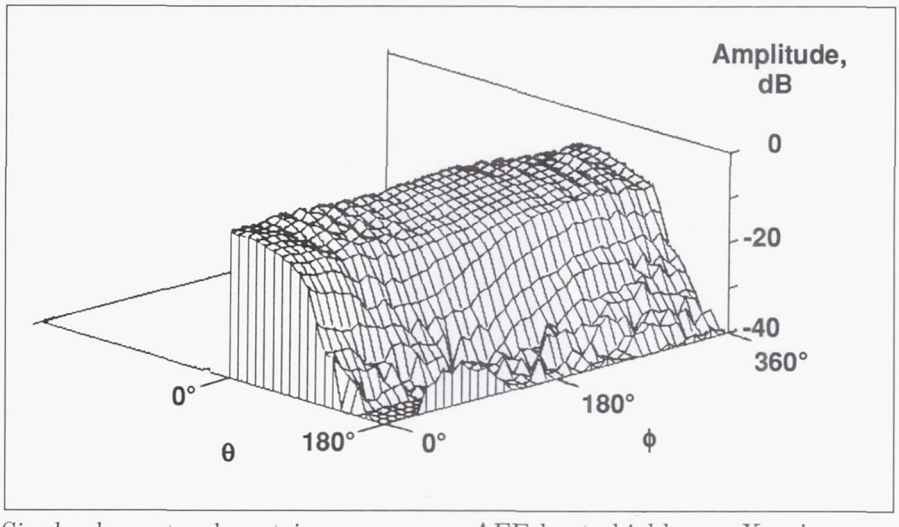

Single-element volumetric coverage on AFE heat shield near X axis.

Two major tradeoffs were considered in choosing an appropriate configuration; these tradeoffs include a high-gain system requiring single antenna elements and a switching network, or a low-gain system using an array for broad coverage. A lower transmit power level is needed for the high-gain system, but it needs accurate and timely switching to remain in contact with the TDRSS. Constraints in the power link budget led officials at Marshall Space Flight Center to choose a three-element switching network.

Volumetric pattern tests of the three prime candidate locations and other locations of interest were made in the low-frequency anechoic chamber at two orthogonal polarizations.

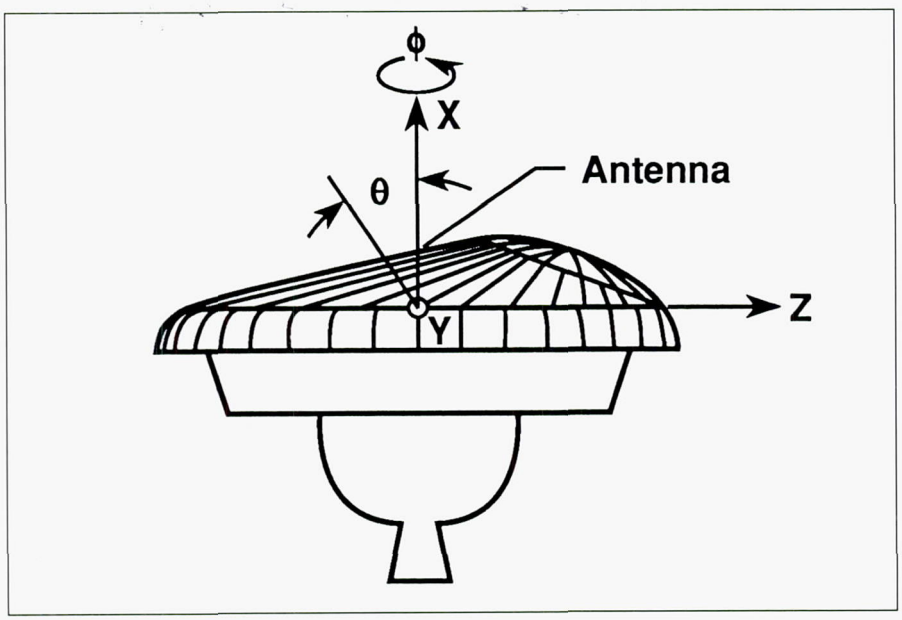

Antenna element location on AFE spacecraft.

The second figure shows the volumetric coverage of a single element located on the heat shield near the X axis as shown in the third figure. The transmit polarization is parallel to the Y axis, with the microstrip element in the receive mode (as can be seen in the second figure). Nearly uniform coverage can be seen out to $\theta = 70°$, symmetric with respect to ϕ, where θ and ϕ are the pitch and roll angles, respectively. Results show that coverage of at least 3 dB is obtainable everywhere outside of a 90° cone around the solid rocket motor plume.

Results of the comparison between the OSU code-predicted patterns and the measured patterns were presented at an IEEE conference in May 1990. Future measurements must be made with actual heat shield tiles to determine their effect on radiation patterns and impedance.

(Erik Vedeler, 41825)

Impact Dynamics Research Facility

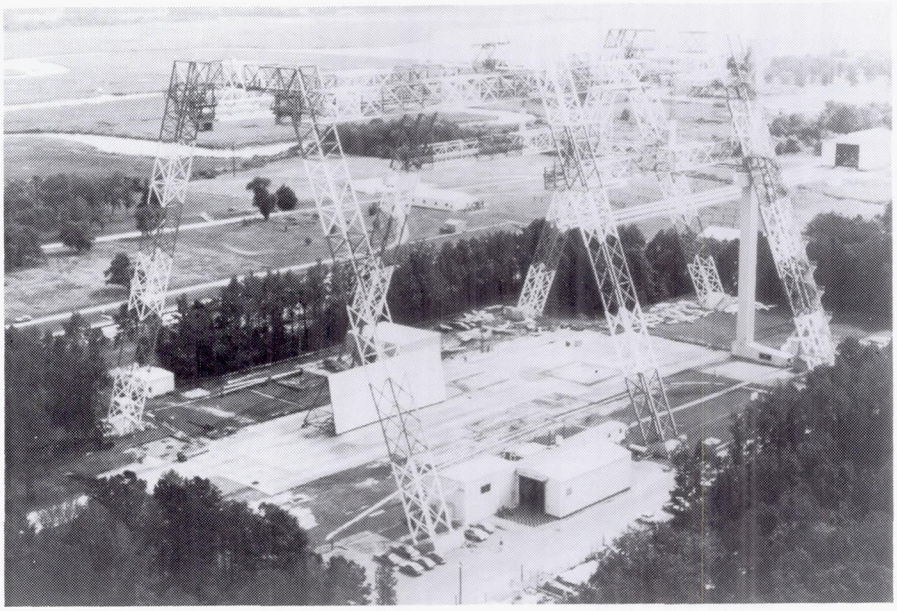

This facility, which was originally used by the astronauts during the Apollo Program for simulation of lunar landings, has been modified to simulate crashes of full-scale aircraft under controlled conditions. The aircraft are swung by cables, pendulum-style, into the concrete impact runway from an A-frame structure approximately 400 ft long and 230 ft high. The impact runway can be modified to simulate other ground crash environments, such as packed dirt, to meet a specific test requirement.

Each aircraft is suspended by swing cables from two pivot points 217 ft off the ground. It is then pulled back along an arc to a predetermined height by a pullback cable from a movable bridge on top of the A-frame, released from the pullback cable, and allowed to swing, pendulum-style, into the ground. An instant before impact, the swing cables are separated from the aircraft by pyrotechnics. The length of the swing cables regulates the aircraft impact angle from 0° (level) to approximately 60°. Impact velocity can be varied to approximately 65 mph (governed by the pullback height) and to 90 mph with rocket assist. Variations of aircraft pitch, roll, and yaw can be obtained by changes in the aircraft suspension harness attached to the swing cables. Onboard instrumentation data are obtained through an umbilical cable attached to the top of the A-frame. Data are transmitted by hard wire to the control room at the base of the A-frame. Photographic data are obtained by onboard cameras, ground-mounted cameras, and cameras mounted on top of the A-frame. The maximum allowable weight of the aircraft is 30,000 lb.

Analytical Prediction Correlation With Large-Deflection Static Failures

As part of a research study to determine the effectiveness of scale model testing in studying the energy absorption and dynamic response capabilities of aircraft subcomponents subjected to impact or crash-type loads, a combined experimental and analytical program has been developed to investigate scaling effects on the large-deflection response and failure behavior of graphite/epoxy composite beams.

Static tests were conducted on several scale model beams of AS4/3502 graphite/epoxy composite material having unidirectional, angle-ply, cross-ply, and quasi-isotropic laminate stacking sequences. The beams were tested under an eccentric axial load to failure by using the loading mechanism shown in the sketch in the figure. This testing arrangement produces large bending deformations and global failure of the beam away from the hinged end support. To correlate with the experimental results and to assist in providing a fundamental understanding of the loading and failure mechanisms, two methods of analysis were used. One method was a one-dimensional large rotation "elastica"-type beam solution that incorporated the exact expression relating moment and curvature, thus allowing the solu-

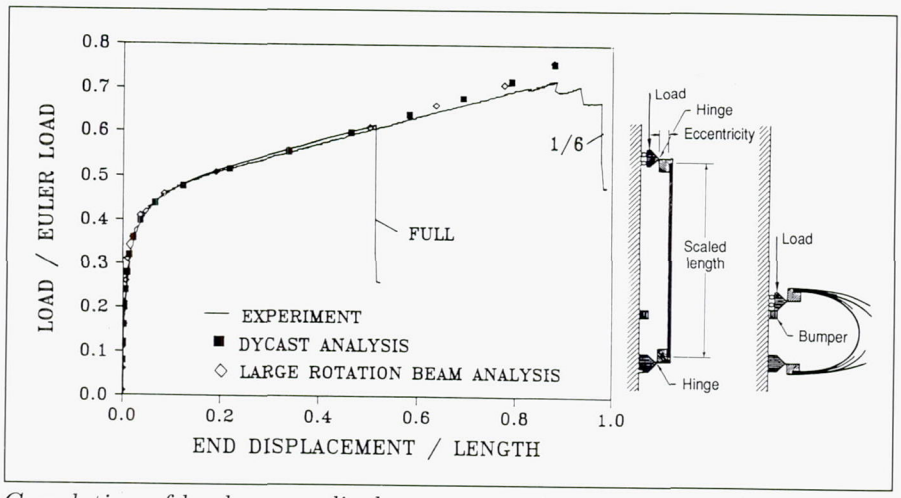

Correlation of load versus displacement results with sketch showing test setup.

tion to predict the large-rotation responses of composite beams. The other method was a nonlinear finite-element structural analysis code applicable to composite beam-column structures.

The illustrative normalized loads (the ratios of applied loads to Euler buckling loads) versus normalized displacements (the ratios of end deformations to the length of test specimens) for the 1/6-scale and full-scale quasi-isotropic laminate beams are shown in the figure with the predictions obtained by using the two analysis methods. Note the good agreement between the experimental and analytical results. During the study, it was learned that to obtain the agreement (as shown in the figure) between theory and experiment, it was necessary to actually measure the beam bending stiffness rather than rely on classical lamination theory predictions using properties of the AS4/3502 system determined from material characterization tests.

(Karen E. Jackson and Edwin L. Fasanella, 44147)

Experimental Verification of Unidirectional Composite Beam Scaling

As part of a research program to determine the effectiveness of utilizing results obtained by using scale models to predict the dynamic large-deflection response and failure of full-size composite beams subjected to impact loads, a series of tests have been conducted using 1/2-, 2/3-, 3/4-, 5/6-, and full-scale (prototype) replica model beams of AS4/3502 graphite/epoxy composite material. Beams having unidirectional, angle-ply, cross-ply, and quasi-isotropic layups were tested under an eccentric axial compressive load to failure. The load was applied impulsively by a free-falling weight using the drop tower illustrated in the figure. This testing configuration was chosen because it promotes large bending deformations and global beam failures that are typical of the loading environment seen by aircraft structures during a crash.

Some illustrative results for the 1/2-scale and full-scale unidirectional test specimens are shown in the figure as the variation of load in thousands of pounds with time. Impact conditions for each test were scaled according to a scale law derived for the experiments.

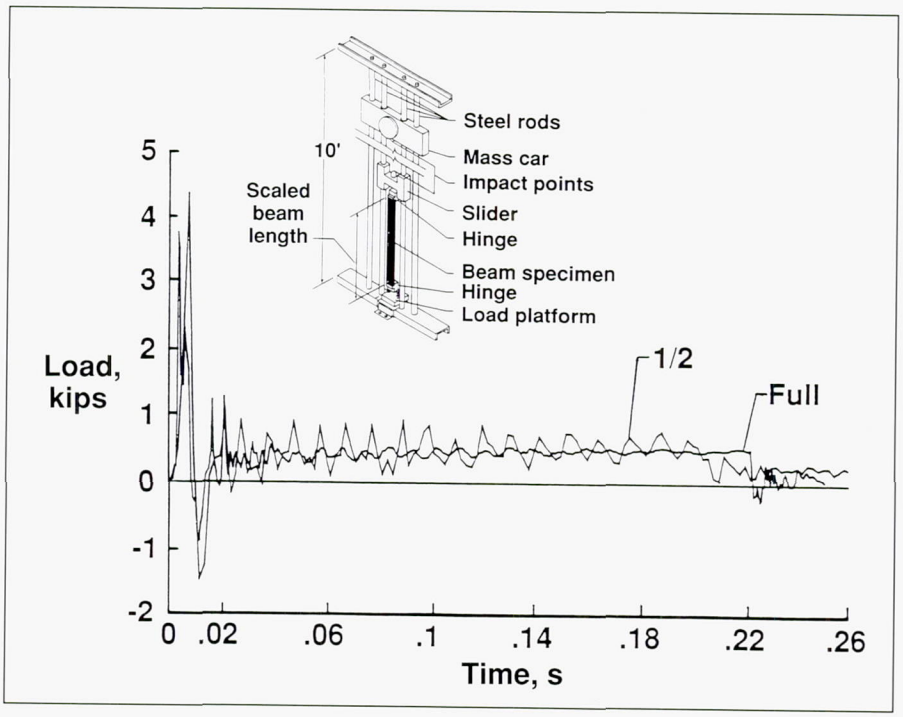

Correlation of load time histories with sketch showing test setup.

Failure of the beams occurred by fiber fracture at the beam midpoint, which is the location of maximum moment, and by longitudinal splitting. Both the 1/2-scale and full-scale beams exhibited this failure mode, thus indicating that failure mechanisms are not a function of specimen size. A comparison of the two dynamic response time histories shown in the figure indicates that the 1/2-scale beam results can be used to accurately predict the peak load, pulse duration, and sustained load of the full-scale beam. In general, all the unidirectional scaled model beams provided an excellent comparison with the prototype when scaled to full-scale values by using the appropriate scaling law.

Tests such as these are an important first step in ensuring that relatively inexpensive model tests can be used with confidence to predict impact response characteristics of full-size structures.
(Karen E. Jackson, 44147)

Aircraft Landing Dynamics Facility

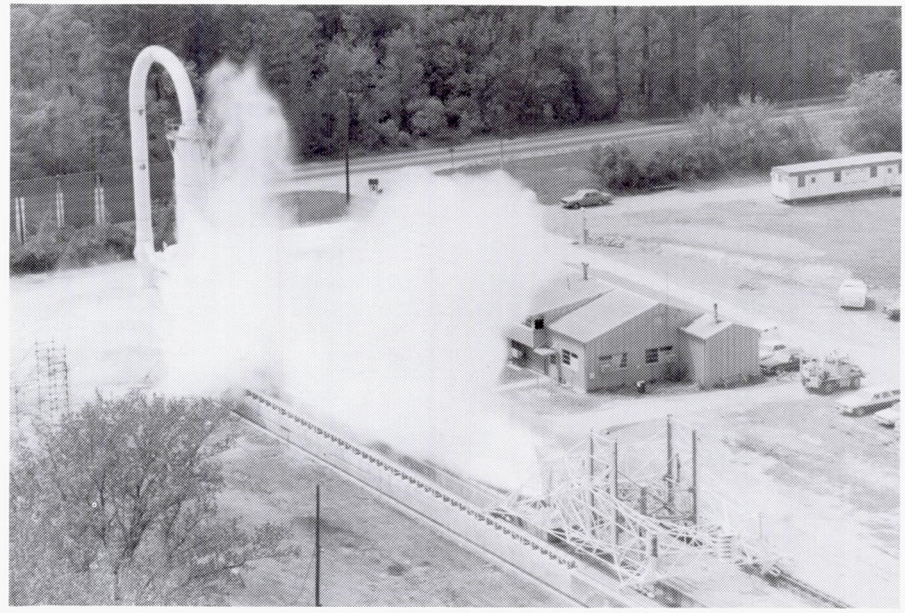

In 1985, Langley Research Center updated the landing loads track to the Aircraft Landing Dynamics Facility (ALDF) to improve the capability for low-cost testing of wheels, tires, and advanced landing systems. The main features of the updated facility are the propulsion system, the arresting gear system, the high-speed carriage, and the track extension. In 1988, the capability of ALDF was enhanced by the addition of a Rain Simulation System (RSS). The ALDF-RSS is a 500-ft-long, 44-ft-wide overhead distribution system comprised of three parallel 10-in.-diameter irrigation pipes aligned lengthwise along the track and supported every 100 ft at a height of 42 ft above the track. The RSS can be configured with as many as 1590 nozzles and can simulate rainfall intensities as high as 40 in/hr.

The ALDF uses a high-pressure water jet system to propel the test carriage along the 2800-ft track. The propulsion system consists of an L-shaped vessel that holds 28,000 gal of water pressurized to 3150 lb/in^2 by an air supply system. A timed quick-opening shutter valve is mounted on the end of the "L" vessel and releases a high-energy water jet, which catapults the carriage to the desired speed. The propulsion system produces a thrust of 2×10^6 lb force, which is capable of accelerating the 108,550-lb test carriage to 220 knots within 400 ft. This thrust creates a peak acceleration of approximately 20 g. The carriage coasts through the 1800-ft test section and decelerates to a velocity of 175 knots or less when it intercepts the five arresting cables that span the track at the end of the test section. The arresting system brings the test carriage to a stop in 600 ft or less. Essentially any landing gear can be mounted on the test carriage, including those exhibiting new concepts, and any runway surface and weather condition can be duplicated on the track.

Since 1985, ALDF has been extensively used to evaluate the friction and wear characteristics of the Space Shuttle orbiter main- and nose-gear tires, define modifications to the runway at the John F. Kennedy Space Center Shuttle Landing Facility, and demonstrate the ability of the orbiter to safely complete a landing following tire and wheel failures. During 1989, initial testing was completed on the Radial Tire Program and the Heavy Rain Simulation Program.

Automated Wetness System

With the implementation of the joint NASA/FAA Radial Tire Program on ALDF, facility operation time is in great demand. The test schedule for ALDF is completely filled over the next 5 years, and considerable backlog of research programs for the facility exists. Consequently, it is very desirable to improve the operational efficiency of the facility. One improvement that has been made is the installation of a test runway wetting system using 45 sprinkler heads to wet the entire 1800-ft length of the runway. This system is shown in the figure. The newly installed runway wetting system not only reduces the time needed to set up for wet-runway tests and to maintain a wet runway test under hot day conditions, but also provides for better test data because it maintains a more consistent wetness condition (i.e., water depth) than the old man-

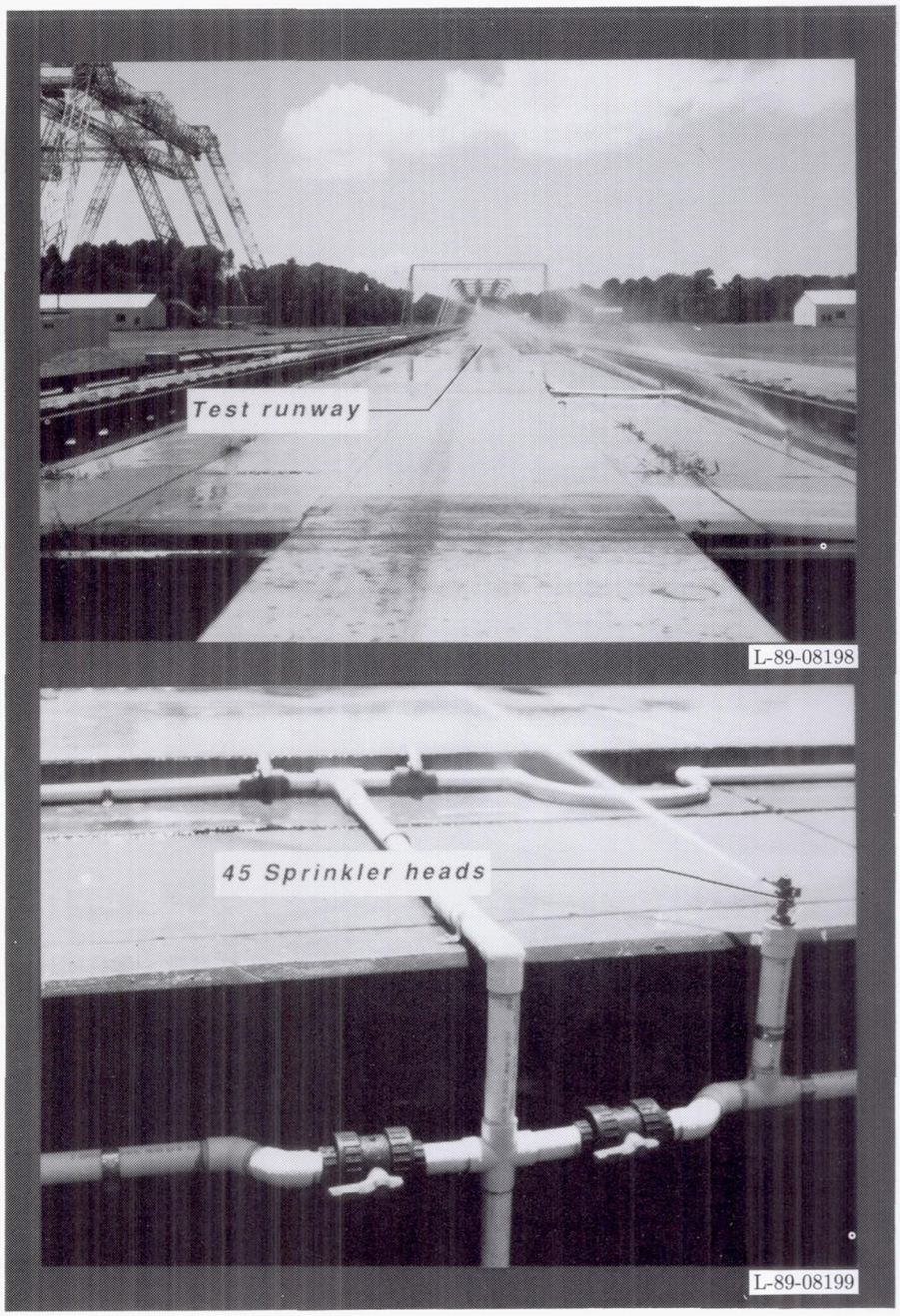

Wetting system components.

ual system. This same wetting system can be used in combination with a system of rubber dams to maintain a flooded runway test condition. This ALDF modification will greatly enhance the productivity of this unique national facility and significantly accelerate the development of the data base on radial-belted aircraft tires.

(Robert H. Daugherty and Sandy M. Stubbs, 41309)

Definition of Mechanical and Friction Characteristics of Bias-Ply, Radial-Belted, and H-Type Tires

The objective of the joint NASA/FAA Radial Tire Program is to develop a data base of tire mechanical properties and friction characteristics for radial-belted and H-type aircraft tires and to compare these characteristics with those of comparable bias-ply aircraft tires. Static and dynamic testing of several bias-ply, radial-belted, and H-type aircraft tires representing the full range of tire sizes and strength capabilities is being carried out to define the stiffness, damping, and friction properties of these tires over a range of operational loads and runway wetness conditions.

A photograph of three of the test tires is shown in the first figure. These 40 × 14 aircraft tires are the size used on many versions of the Boeing B-737 an McDonnell Douglas DC-9 transport aircraft. Some vertical load-deflection characteristics of the three tires are shown by the data in the second figure. Both the bias-ply and H-type tires exhibit higher stiffness values than the radial-belted tire when all three tires are inflated to 170 lb/in^2. Some additional results for the radial-belted tire and the bias-ply tire, not shown in the figure, show that for dry runway operations the radial-belted tire produces larger cornering forces than the bias-ply tire over the entire range of yaw angles tested.

The data obtained from this study are essential to establish the compatibility of radial-belted aircraft tires with such landing

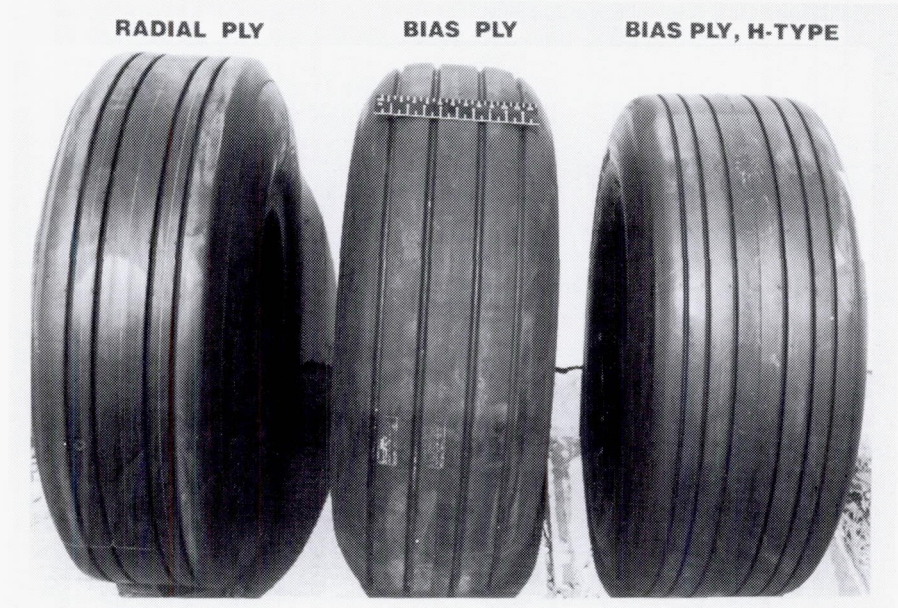

Three 40 × 14 test tires. L-89-8192

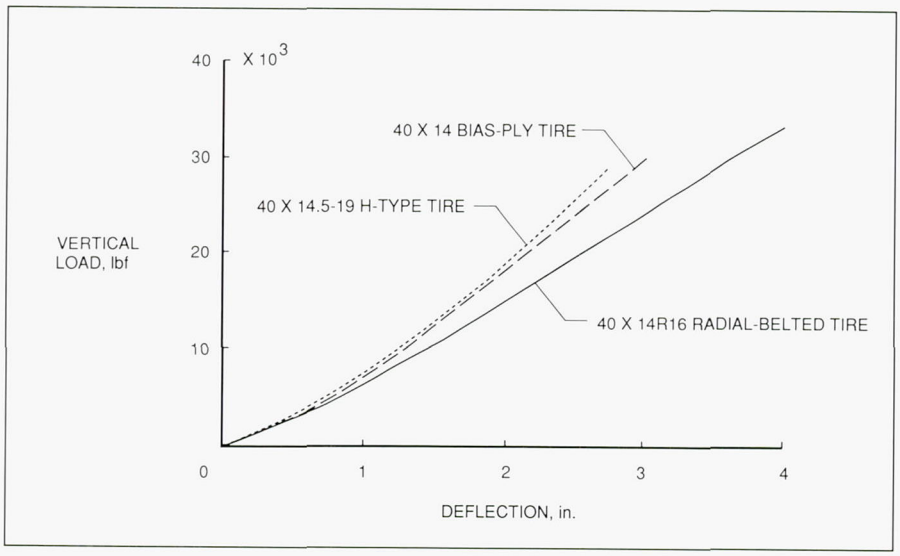

Load versus deflection results for three types of tires.

gear components as the antiskid braking system, the nose-gear steering system, and the shimmy damping system. Furthermore, these data will be used to ensure the ground-handling safety of future aircraft equipped with radial-belted tires.

(Pamela A. Davis, Sandy M. Stubbs, and Thomas J. Yager, 41307)

Large-Scale Testing of Transport Wing Section in Simulated Heavy Rain

Since 1982, NASA has been studying the influence of heavy rain on airfoil aerodynamic performance. Small-scale wind tunnel studies show that a high-intensity rainfall does adversely affect airfoil performance. A test was recently conducted at the ALDF to determine if the wind tunnel rain simulation properly modeled the rain environment effects on large wing sections. A 10-ft-chord NACA 64-210 wing section (equipped with a leading-edge slat and a double-slotted trailing-edge flap deflected to simulate a landing configuration) was mounted on the test carriage (as shown in the first figure). Aerodynamic lift data were obtained with (wet data) and without (dry data) the rain simulation system operating for an angle-of-attack range of 7.5° to 19.5° and for simulated rainfall rates of 9 in/hr and 40 in/hr. The results obtained at the 40 in/hr rainfall rate show a 15- to 20-percent reduction in observed maximum lift and a reduction in the dry air stall angle of approximately 6°. There appears to be a small reduction in maximum lift and only a slight reduction in the stall angle of attack at the 9 in/hr rainfall rate; however, only a limited amount of data were taken, and these results are inconclusive.

Although the ALDF wing section and the wind tunnel model have the same airfoil section and model configurations, their respective testing environments have dictated different end plate geometries and aspect ratios. In order to make meaningful comparisons of the wind tunnel data and the ALDT data, the wind tunnel data were corrected for differences in aspect ratio and end plate geometry between the two model configurations. A comparison of lift coefficient versus angle of attack for the ALDF and wind tunnel configurations is shown in the second figure at similar test conditions. The ALDF dry data measured show excellent correlation to the wind tunnel dry lift perfor-

Wing section exiting rain simulation system. L-88-11370

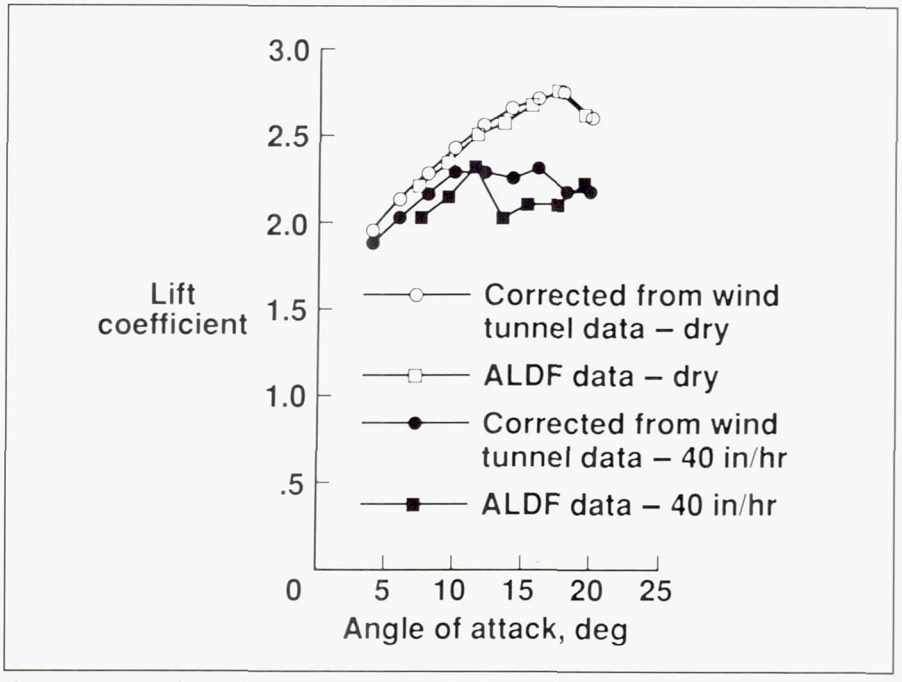

Comparison of wind-tunnel-corrected lift coefficient data for ALDF large-scale configuration and ALDF large-scale data acquired at similar test conditions.

mance. There also appears to be a reasonable degree of correlation between the two sets of wet data for the 40 in/hr rainfall rate. Hence, it appears that to a first order, the rain scale effects are not large and that the wind tunnel research technique can be used to predict rain effects on airplane performance.

(Dana J. Dunham and Gaudy M. Bezos, 45055)

Flight Research Facility

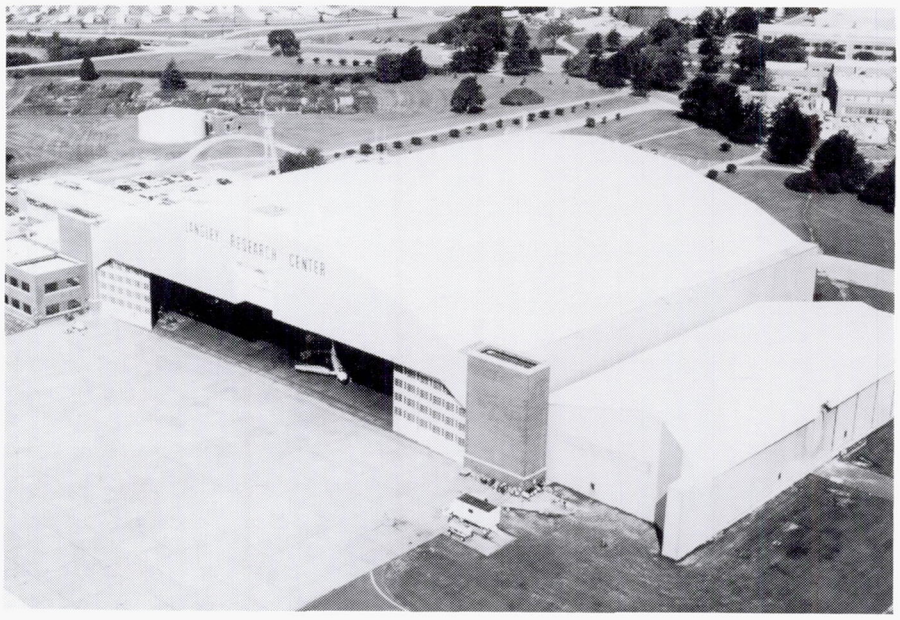

The truss-supported roof of the huge hangar of the Flight Research Facility provides a clear floor space with nearly 300 ft in each direction (over 87,000 ft^2).

Door dimensions will allow entry of a Boeing 747. Features such as floor air and electrical power services, radiant floor heating to eliminate corrosion-causing moisture, a modern deluge fire suppression system, energy-saving lighting, modern maintenance spaces, and entry doors and taxiways on either side of the building make this structure equal or superior to any hangar in the country. Extensive and modern maintenance equipment makes it possible to maintain, repair, and modify aircraft ranging in sophistication from modern metal and composite airliners, fighters, and helicopters to fabric-covered light airplanes. Surrounding the hangar are ramp areas with load-bearing capacity sufficient to handle the largest current wide-body jet. The high-power turnup area can also handle a wide variety of aircraft.

The present array of research and research support aircraft includes an airliner, military fighters, trainers, experimental one-of-a-kind designs, helicopters, and single and multiengine light airplanes. This variety enables research to be carried out over a wide range of flight conditions, from hover to Mach 2 and from the surface to 60,000 ft. Research pilot currency in this wide spectrum of aircraft is important in conducting credible in-flight experiments as well as in-flight simulator assessments. A variety of research can be conducted in such areas as terminal traffic flow, microwave landing system (MLS) approach optimization, airfoil properties, handling qualities, performance, engine noise, turbulence research, natural laminar flow, winglet studies, stall/spin, and severe storm hazards.

One of the support helicopters is used to drop unpowered remotely controlled models of high-performance airplanes to study high-angle-of-attack control characteristics. The Radio-Controlled Drop Model Facility is used to

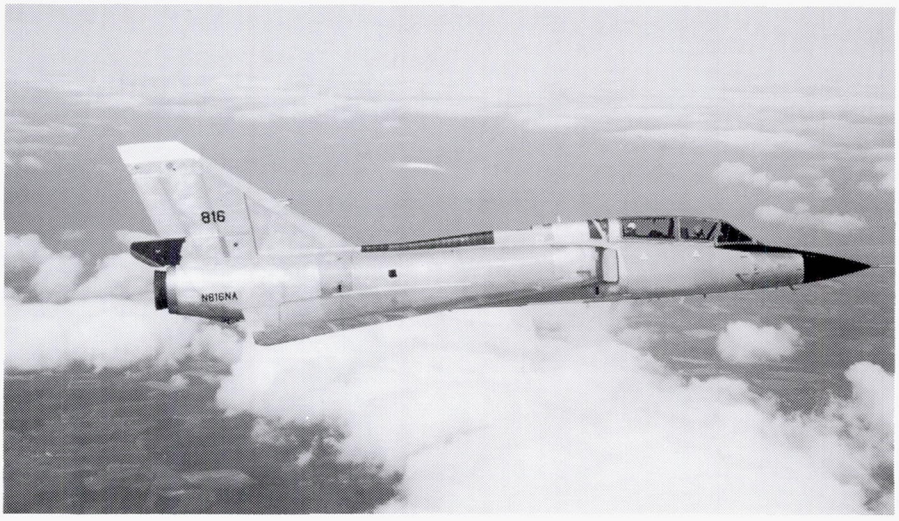

Convair F-106B configured for Storm Hazards Program. L-83-2747

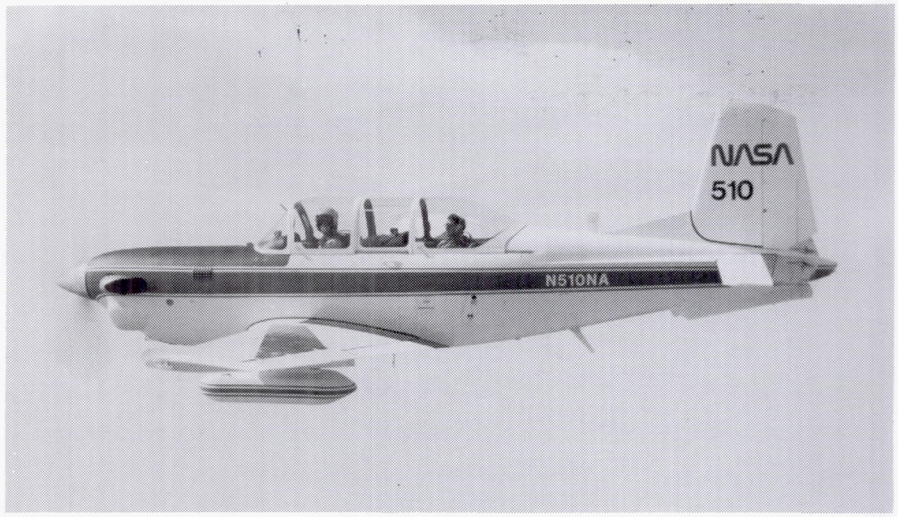

Beech T34C used for flight support. L-80-3923

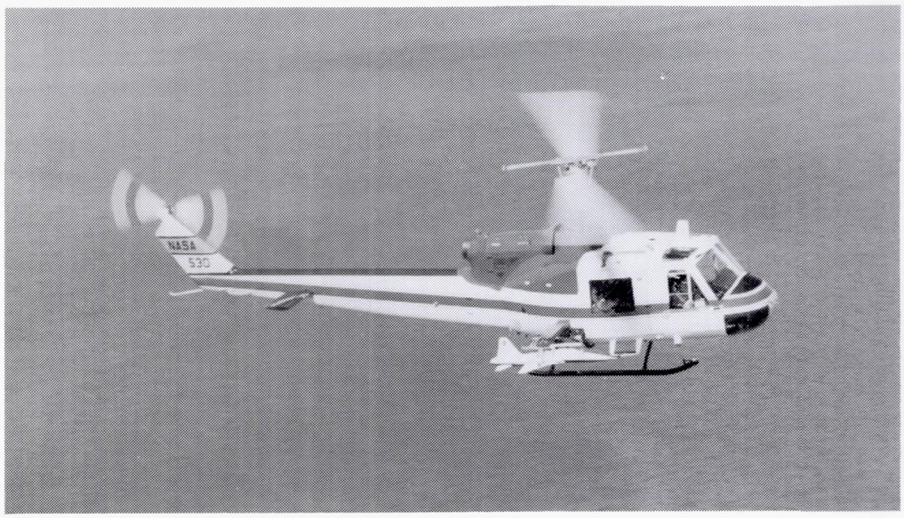

Bell 204B configured for model drop mission. L-76-6425

Radio-Controlled Drop Model Facility. L-83-11167

study the low-speed flight dynamic behavior of aerospace vehicles with particular emphasis on high-angle-of-attack characteristics of combat aircraft. The technique consists of launching an unpowered, dynamically scaled, radio-controlled model into gliding flight from the support helicopter, controlling the flight of the model from the ground, and recovering the model with a parachute.

The models are constructed primarily of molded fiberglass and are typically approximately 10-ft long with weights in the range of 200 lb to 300 lb. A comprehensive onboard instrumentation system provides measurements of key flight dynamics parameters that are transmitted to the ground via telemetry and recorded for analysis. The model control loop involves a combination of ground-based and onboard equipment and the required communication links. The heart of the system is a ground-based digital computer into which the control laws are programmed. The processor accepts downlinked feedback signals from the model and commands from the pilot and computes the control surface commands that are then transmitted to the model. Very-high bandwidth electromechanical servoactuators are used to drive the model control surfaces. The pilot flies the model from a ground station that provides the required information on a number of displays. These displays include a high-resolution video image of the model, a map display showing model ground track, and conventional analog instruments presenting key parameters such as angle of attack and airspeed.

The tests are conducted at the Plum Tree Test Site located ap-

proximately 5 miles from Langley Research Center. The test site is a marsh approximately 2 miles long and 1 mile wide.

Wing Leading-Edge Vortex Flap

Flight tests of a Langley Research Center developed wing leading-edge vortex flap concept have continued during 1989. The flap is being flown on an F-106B research aircraft instrumented to measure wing and flap surface pressures, strain, structural accelerations, and other pertinent information. Acquisition of aerodynamic, performance, structural, and stability and control data has been completed for the flap configuration of 40°, shown installed on the research airplane, over a flight test envelope that encompassed speeds up to Mach 1, altitudes up to 40,000 ft, and maneuver loadings just over 4 *g*'s. Results are being processed and analyzed for comparison with data from flight tests of the unmodified wing and results from wind tunnel and computational models of the same F-106B configuration.

The next series of flight tests will be conducted using a vapor-screen system to visualize the flow field above the wing of the aircraft as an aid in understanding the vortex flow aerodynamics with and without the leading-edge flaps. The vapor-screen technique used to provide this information is the same developed for an earlier study except that the light sheet direction can be rotated to illuminate various wing stations. After documenting the flow field associated with the vortex flap set at 40°, similar data and flow visualization flights will be repeated for a vortex flap setting of 30°.

(D. J. DiCarlo, 43870, and J. B. Hallissy)

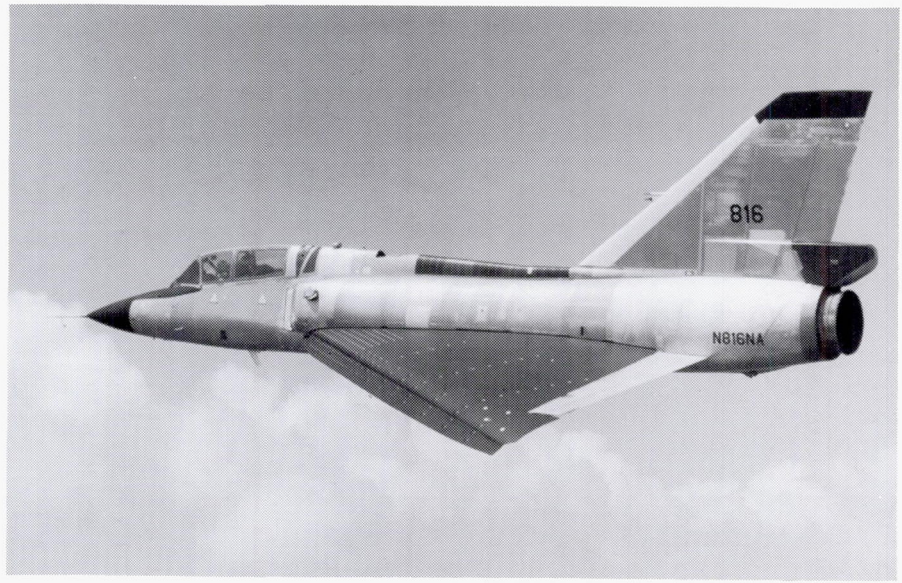

F-106B research aircraft with vortex flap. L-88-8180

Tumble Research Using X-29 Drop Model

In support of the current high-angle-of-attack tests being conducted on the X-29 airplane at the Hugh L. Dryden Flight Research Facility, drop-model flight tests have been conducted at Langley Research Center on a 22-percent dynamically scaled model of the configuration. The first series of tests focused on documenting the flight dynamics of the configuration throughout its angle-of-attack envelope. In addition, control law concepts were developed, successfully tested, and subsequently adopted for use on the full-scale X-29.

The tests in 1989 focused on tumble susceptibility. Earlier wind tunnel investigations had shown that under certain conditions the X-29 configuration exhibits a pitch autorotation characteristic that could lead to a very dangerous out-of-control tumble condition. It was not known, however, if the airplane could enter this condition from controlled flight. The drop-model tests provided the only safe and effective method for addressing this issue. In the tests, the model was flown to a very high-angle-of-attack, low-speed condition in which full nose-down controls were applied and held in an attempt to drive the model into a tumble. Earlier analysis had shown that this maneuver would represent a very stringent test of the tumble susceptibility of the configuration. The results from the drop flights showed that although very severe pitch departures were obtained, in which negative angles of attack as large as −130° were reached, the model did not enter a sustained tumble motion. These data show that the X-29 configuration is fairly resistant to tumbling.

X-29 drop model.

L-87-3588

Because the tumble phenomenon is a concern for future advanced aircraft designs with relaxed static stability, a generic research program has been initiated which will build on the results obtained on the X-29. **(David J. Fratello and Mark A. Croom, 41146)**

Transition Physics Flight Research Experiments

Current laminar-flow research conducted by NASA is focused on understanding the dominant instability modes responsible for initiating the transition process from laminar to turbulent flow. Recently, flight experiments were conducted on a gloved surface of a Lear Model 28/29 airplane (as shown in the figure) to study in detail the growth of Tollmien-Schlichting (T-S) instability in the laminar boundary layer. The purpose of these experiments was to help validate computational fluid dynamics (CFD) compressible linear stability theory through measurement of the instability mechanisms. These experiments incorporated a fiberglass and foam, 6-ft-span, gloved section attached to the wing surface. Using the existing wing airfoil shape that was already conducive to long runs of laminar flow, the glove had a thickness of 0.25 in. to incorporate subsurface wiring in order to provide streamwise located instrumentation for measuring the streamwise growth of T-S instability frequencies (via hot-film and microphone sensors), temperature distributions, and pressure distributions.

These experiments were the first of their kind to measure

Lear Model 28/29 airplane with instrumented natural laminar-flow glove. L-89-2828

streamwise growth patterns along the wing chord at a specific spanwise location. Previous experiments using sensors staggered across the span could not accurately study the growth of disturbances at a specific span station in the streamwise direction. In addition, these were the first experiments to obtain temperature distribution information that can be used as input to the compressible CFD codes. This research will provide information on disturbance growth and transition mode which is essential to the understanding of design limits for applications of laminar-flow technology.

(Cynthia C. Lee, 43865)

Space Shuttle Exhaust Particle Experiment (SEPEX) STS-34

At the request of the National Space Transportation System (NSTS) Office, Langley Research Center personnel developed a method of airborne collection and measurement of aluminum oxide particulates exhausted from the Space Shuttle solid rocket boosters. This study will enable environmental planners to make more accurate assessments of the impact that these particles may have on the atmosphere.

Two Langley aircraft, a Cessna 402B and a Beechcraft T-34C, were equipped with atmospheric sampling equipment designed by personnel from the Atmospheric Sciences Division (ASD), Atmospheric Studies Branch. Approximately 4 min after launch of STS-34 on October 18, 1989, the test aircraft made several passes through particulates for study. The Cessna 402B sample was obtained at an altitude of 8000 ft, and the T-34C sample was taken at 24,000 ft. Filters from the sampling apparatus were returned to Langley for analysis.

Using an electron microscope, ASD personnel visually grouped the aluminum oxide particles by size in order to determine the particulate size distribution at each test condition. By determining the particle-size distributions of samples obtained from different altitudes, the researchers can ascertain the effect, if any, of altitude on the size of the exhausted particles. Variances in the particulate size distributions can have a significant effect on the environmental impact of introducing these particles into the atmosphere.

(W. R. Coffer III, 45835, G. C. Purgold, M. R. Phillips, and H. A. Verstynen)

Cessna 402B used for SEPEX. L-89-11509

Image Processing Laboratory

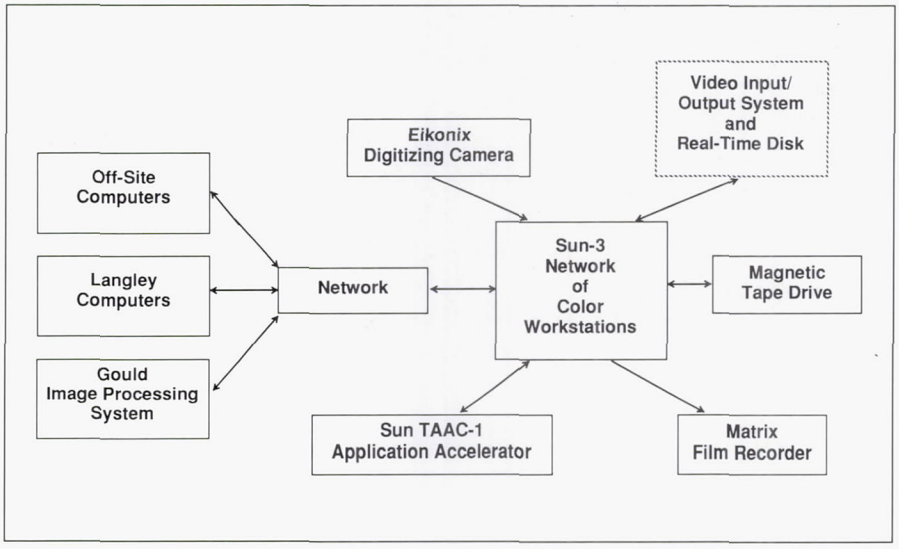

The Image Processing Laboratory (IPL) is a versatile image processing system that allows researchers to enhance and analyze digital images. These images arise from a wide range of applications including wind tunnel flow field experiments, computational fluid dynamics solutions obtained on the Cray supercomputer, nonintrusive aerodynamic heat-transfer measurements, radioscopic techniques, and satellite imaging systems. The IPL provides researchers with analysis tools that allow enhanced images and accurate results to be generated in minutes.

The IPL is a Sun-based image processing network (as shown in the figure). An important feature of the system is the Sun TAAC-1 application accelerator, which is designed for improved imaging and visualization performance. The TAAC-1 handles the processing of large arrays of image data fast enough to support interactive work. The system is supported by a number of input/output peripherals in the laboratory. For instance, images on photographic media are input to the Sun using the Eikonix digitizing camera, which converts visual information into a digital array of numbers (digital image) that can be quantitatively processed by the system. Also, data on any computer in the Center's local area network may be transferred to the system, and a nine-track magnetic tape unit can read digital images created at remote locations. The digital images then are analyzed and interactively enhanced on the Sun network using either the capabilities of the TAAC-1 or any of the various image processing software packages that exist on the Sun. The matrix film recorder converts the enhanced digital images into photographic media for a hard copy of results.

The IPL was originally based on a Gould IP8500 image processing system prior to upgrading to the Sun-based image processing network. The Gould system supports the input of individual frames on videotape using the color videotape recorder. Simple enhancements on a sequence of images can be performed in real time and recorded back onto videotape or used to produce a sequence of photographic images. A planned upgrade to the Sun-based image processing network will allow this capability to be supported directly on the Sun.

The IPL provides researchers with enhanced images that increase their ability to accurately interpret image data in a wide variety of applications. The interactive nature of the system allows researchers to use their experience and judgment to analyze and process quickly their image data. The enhanced images provide an effective means of presenting research results for analysis, publication, and presentation. The IPL provides a practical and interactive environment for users to process image data quickly and to obtain a variety of outputs to meet their needs.

Enhancement of Infrared Thermographic Images of Transpiration-Cooled Fuel Jet

Spatial filtering, two-dimensional surface contouring, and construction of directional temperature profiles were performed in the IPL as a postpro-

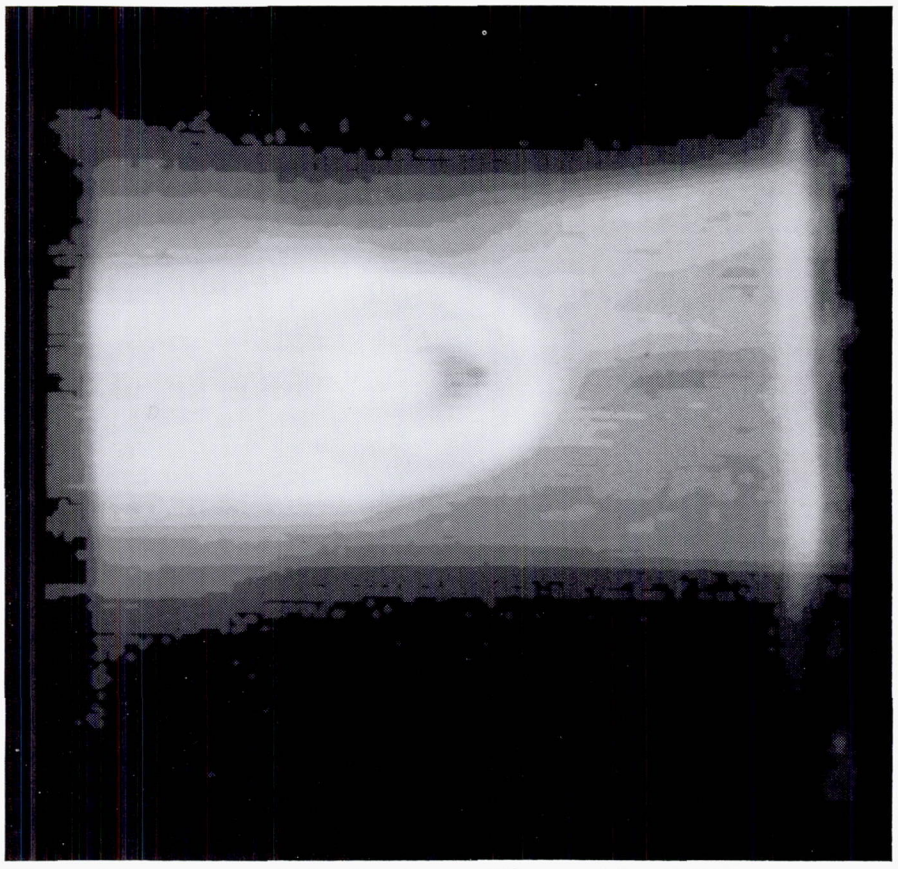

Thermal image generated using Agema Thermovision 880 System.

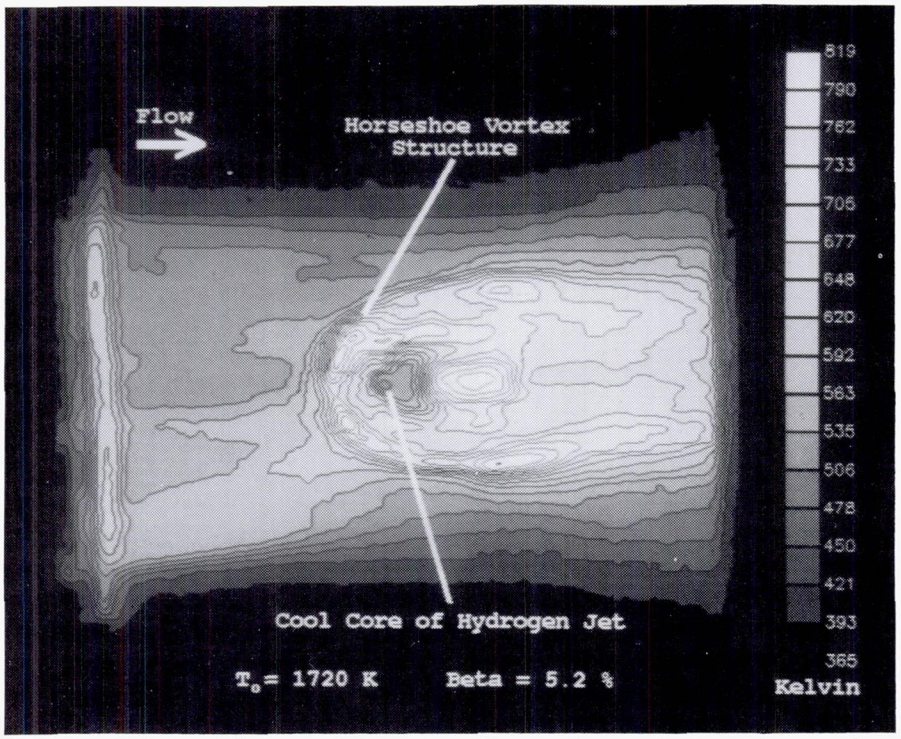

Enhanced thermal image with contour lines and gray temperature scale using PV-WAVE.

cessing technique of infrared thermographic data. Infrared thermography, a technique which, with inversion software, resolves the temperature of a surface of a known emissivity from electromagnetic intensity measurements in the infrared band, was used in conjunction with a series of open-jet tests in the Test Cell #2 facility of the Scramjet Test Complex. With these data produced over a range of experimental conditions, Precision Visuals Workstation Analysis and Visualization Environment (PV-WAVE) software has been used to filter spatially the output data files and quantify the streamwise and lateral temperature gradients along the surface of the injector model.

The experimental investigation was performed to examine the effectiveness of transpiration cooling at relieving the local heating rates in the region of a sonic, perpendicular, fuel jet of gaseous hydrogen in a Mach 3 cross stream. The heat release due to combustion in the vortical mixing region surrounding the injector results in a high-temperature boundary layer, which convects large amounts of thermal energy onto the surface. Room temperature hydrogen gas was blown through discrete orifices to reduce the boundary-layer temperature and act as a thermal blanket to protect the surface.

The surface temperatures, shown in the first figure as a thermal map, were processed in near real time from the Agema Thermovision 880 System. The high-enthalpy, vitiated airflow is from left to right, and the main fuel injector is the cold region in approximately the center of the figure. The transpiration orifices surround the main injector

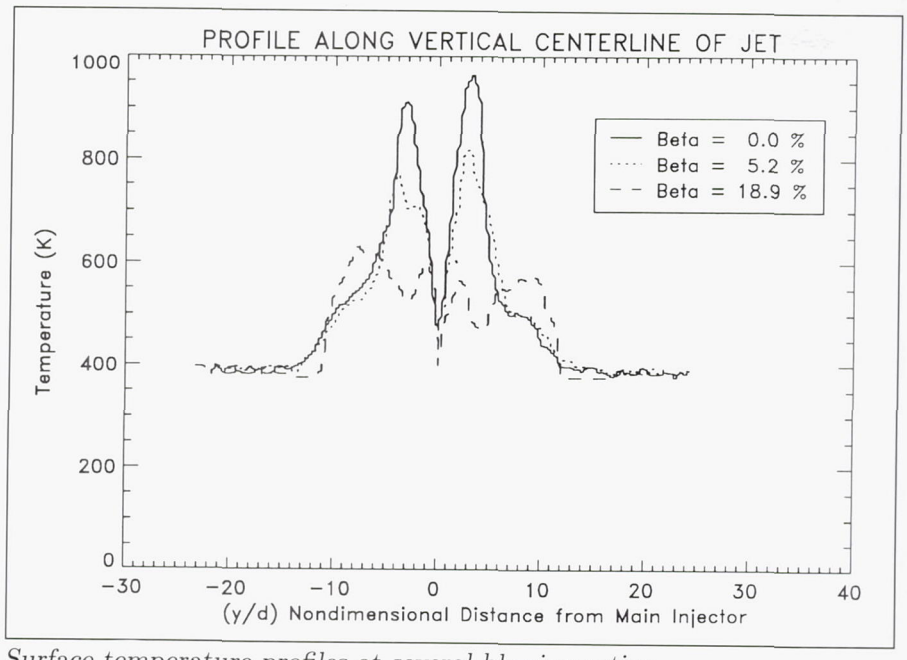

Surface temperature profiles at several blowing ratios.

but are too small to be discerned in the figure. The Agema Thermovision 880 System is an effective tool for data acquisition, but currently it is not capable of performing qualitative image enhancement or quantitative graphical presentation of the measured signal.

In order to achieve publication-quality thermal images with surface contouring and temperature profiles along the plate, the raw data were processed into matrix files and transferred to the IPL. The second figure illustrates the ability of the PV-WAVE software to filter noise from the data and contour the surface temperatures to illustrate surface heating patterns. This method enhances the distinguishing features of the cool, inner core of the gaseous jet and the surrounding hot spots generated in the combustion region. Images such as this one represent qualitative illustrations of local heating patterns and the effect of the coolant on these patterns. For a quantitative demonstration of the effectiveness of various amounts of coolant injection at reducing the surface temperature, profiles of the surface temperature (see the third figure) also were constructed using PV-WAVE. This figure depicts the reduction in temperature along the centerline of the jet due to an increase in the amount of coolant blown through the orifices. These results demonstrate the applicability of transpiration cooling as a leading cooling technique for supersonic combustors.

(Carl S. Byington, 46266)

16- by 24-Inch Water Tunnel

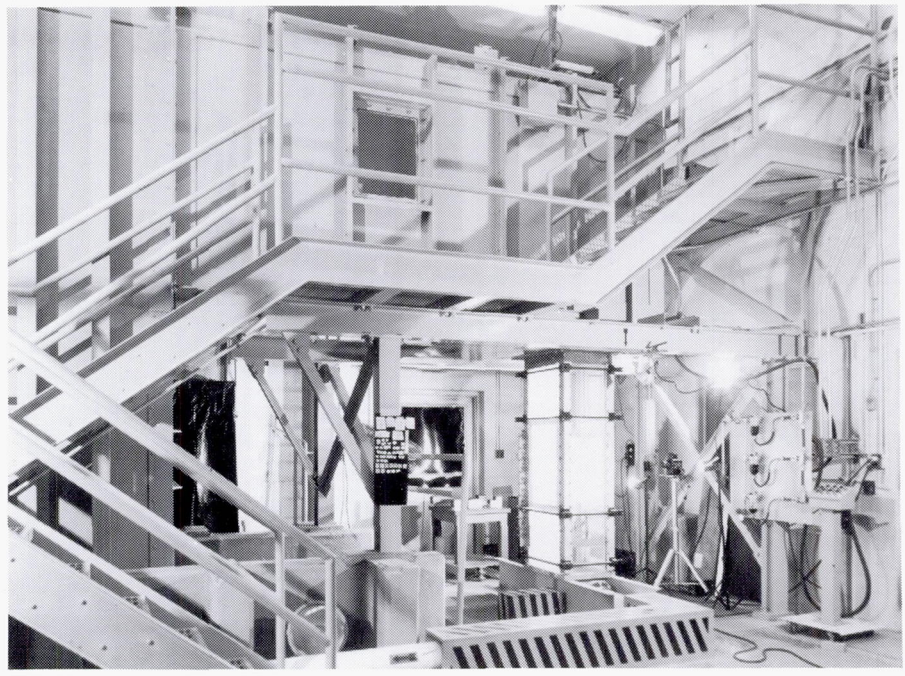

The Langley 16- by 24-Inch Water Tunnel is used for flow visualization studies at low Reynolds numbers. The tunnel has a vertical test section with an effective working length of approximately 4.5 ft. The test section is 16 in. high by 24 in. wide. All four sidewalls are plexiglass to provide optical access. A pump transfers the water from the test section exit to the reservoir upstream of the test section. The test section velocity can be varied from 0 ft/s to 0.75 ft/s. The unit Reynolds number range for water at 78°F for this velocity range is 0 to 7.7×10^4/ft. The normal test velocity that produces smooth flow is 0.25 ft/s.

A sting-type model support system positions the model. The model attitude can be varied in two planes over angle ranges of ± 33° and ± 15°. Operator-controlled electric motors are mounted outside of the test section to control the model position. The model position is read by the operator on a protractor mounted to the model support. Semispan models are mounted on a splitter plate supported by a sting with a lateral offset.

Ordinary food coloring is used as a dye to visualize the flow. The dye is supplied by three reservoirs under pressure so that up to three dye colors may be used. Dye may be ejected from small orifices on the model surface or injected upstream of the test section. The water tunnel was placed in operation in 1987 and has been used to study flows over delta wings and over a rectangular wing with a Gurney flap.

Forebody Strake Vortex Study

Because of the strong vortex generated by a strake mounted on an aircraft forebody when at high angles of attack, it has been suggested that a deployable strake may be used to augment aircraft control, especially at high angles of attack where conventional aerodynamic controls become ineffective. To investigate the effects of strake geometry and orientation on vortex strength, a water tunnel study was conducted on an axisymmetric forebody having the same area distribution as the F-18 aircraft forebody. A typical strake configuration and the resulting vortex (made visible by the use of colored dye streams) are shown in the figure. Tests were conducted at angles of attack from 0° to 30° and angles of sideslip from –5° to 5°. Orientation of the strake relative to the model top was varied from 0° to 70°. Strake variables included planform, chord (length), span (width), camber, incidence, and position relative to the nose tip.

Results from this study indicated that vortex strength was increased by increasing strake chord, increasing strake incidence, or moving the strake closer to the nose tip. Based on these results, a limited number of strake configurations have been

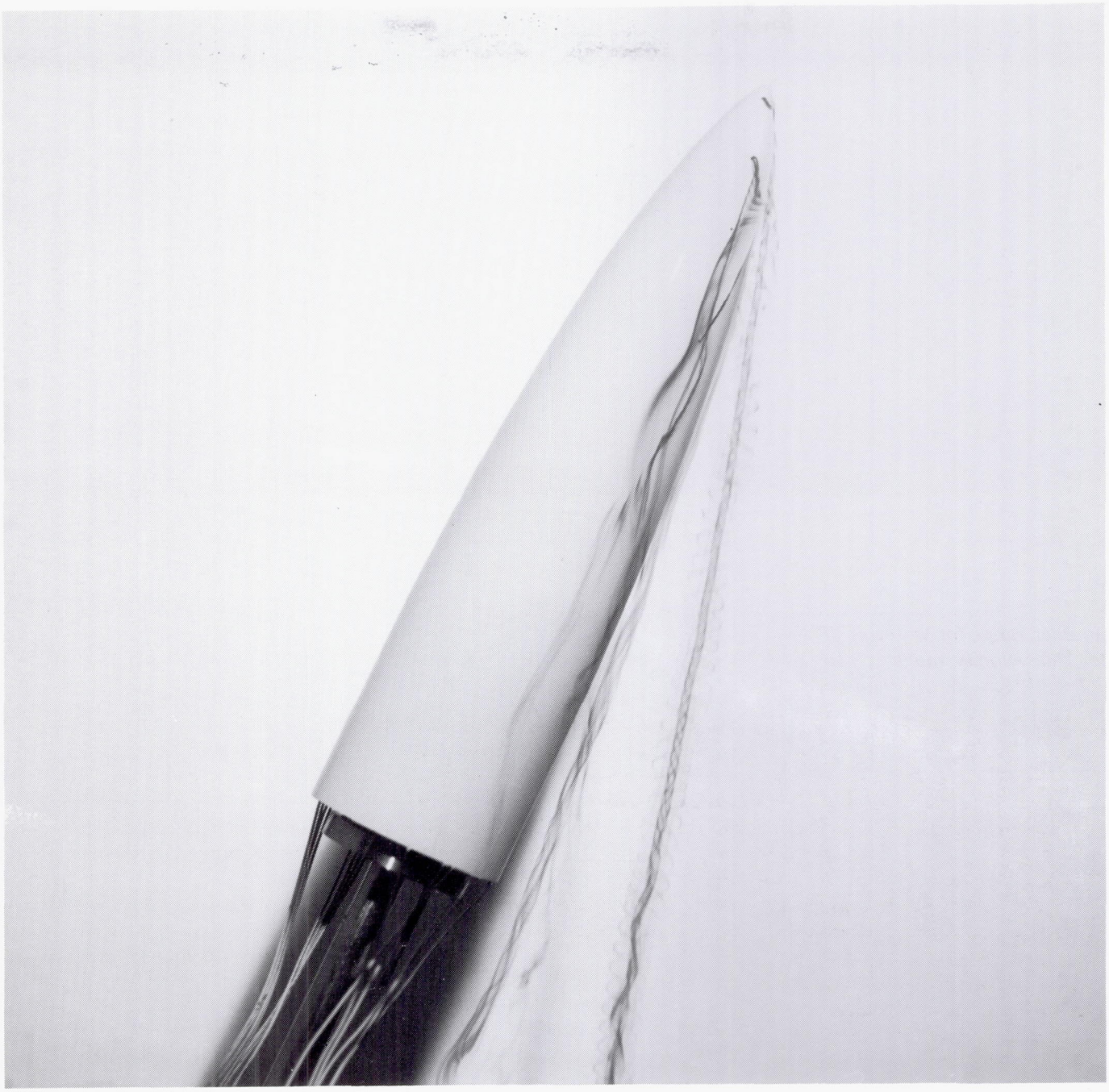

Baseline strake configuration at angle of attack of 25°.

selected for a more detailed study in the 16-Foot Transonic Tunnel. **(Dan Neuhart, 43012, and Bobby L. Berrier)**

Concepts for Alleviation of Adverse Inlet Spillage Interactions on External Stores

The spillage flow around inlets on fighter-type aircraft at reduced engine throttle settings has the potential to adversely interact with external stores. The resultant effect on store aerodynamic surfaces due to the interaction with the vortical spillage flows can be structural damage due to severe buffeting and release of the stores into an unsteady flow environment. As a first step in addressing this problem, a test was conducted

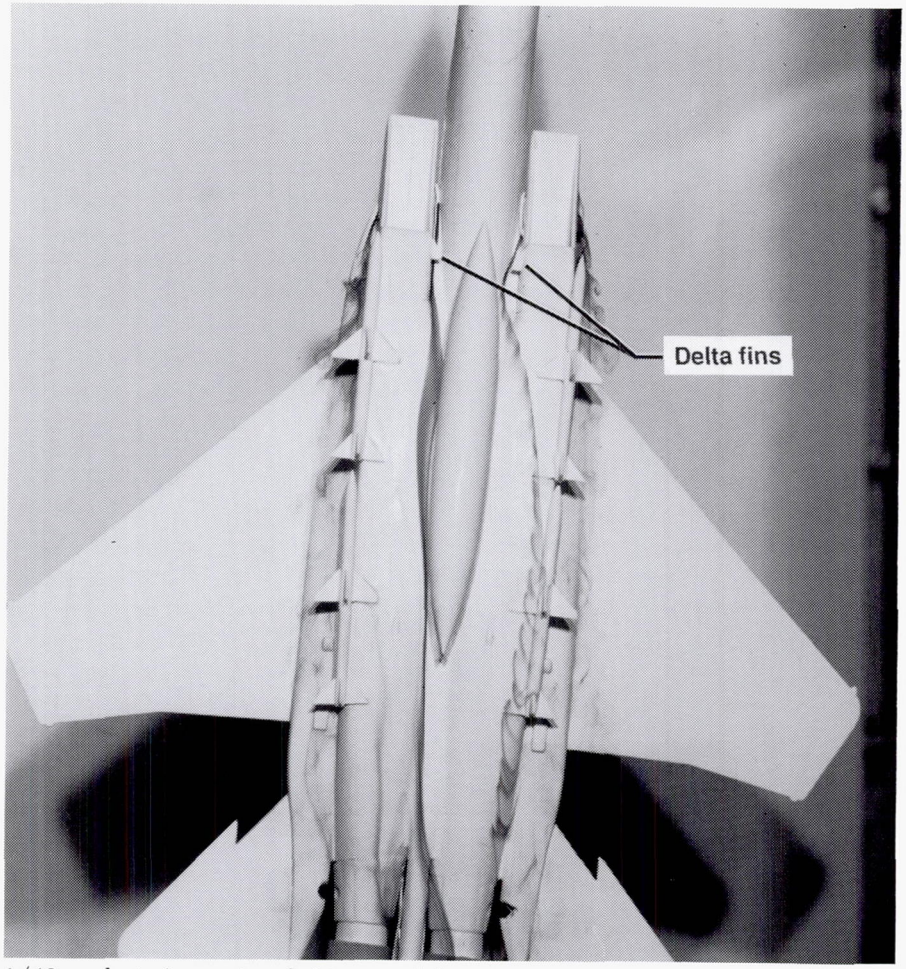

1/48-scale twin-engine fighter model.

in the Langley 16- by 24-Inch Water Tunnel on a 1/48-scale twin-engine fighter model at a Reynolds number based on a mean geometric chord of 8400. The model had flowing inlets that were connected to a series of valves and flowmeters so that the inlet flow rates could be varied. Flow visualization using colored dye indicated the path of the vortical spillage flows.

A series of flow control devices was studied for manipulating the spillage flows. Two approaches were taken to the solution of the problem. First, devices for deflecting the spillage flows were tested. These devices were small fins attached to the bottom of the fuselage and placed to deflect the spillage flow away from the external stores. The second approach was based on the creation of auxiliary vortex flows to interact with the vortical spillage flows and alleviate their adverse interaction with the external stores. The devices that created these auxiliary vortex flows were also fins placed at various locations on the fuselage. The tip vortices from these devices were used to neutralize ("unwind") the spillage vortices, induce the spillage vortices away from the stores, or deflect and deform the spillage vortices.

The results of the study showed that the devices that created auxiliary vortices worked more effectively than the flow-deflecting devices. In particular, the fins that neutralized the spillage vortex and those that deflected and deformed it appeared most successful. The delta fins for neutralizing the spillage flow are shown in the figure. These fins are located near the source of the vortical spillage flow and immediately neutralize the flow and slightly overcompensate by reversing the direction of rotation. This flow rotation reversal is not observable in the figure, but it was verified during testing and recorded on videotape. The potential for effective utilization of devices for alleviation of adverse interactions of inlet spillage flows with external stores has been shown by the results of this test.

(D. H. Neuhart, 43012, and M. N. Rhode)

Computer-Generated Animation System

A rack-mounted portable video system has been assembled for use in making tape recordings of computer-generated graphics of dynamic physical phenomena such as fluid flows and structural vibrations. The video system can be used with any computer that outputs RS170A RGB (red/green/blue) color signals and a sync signal and has an RS232 port.

A photograph of the video system in use next to a graphics workstation is shown in the upper right figure. The principal components of the system are sketched in the schematic drawing that shows the system being used with an IRIS workstation.

The animation software executing on the IRIS includes a device driver that communicates with the animation controller through an RS232 port. The animation controller regulates the frame-by-frame recording of graphics drawn on the system console monitor. By recording each frame only after it is fully drawn, the process of actually rendering the scene, however time consuming, is not reproduced on tape, and smooth animations can be achieved of even complicated color images. The transcoder conditions the RGB signals for input to the tape recorders. A sync generator is included for use with workstations that do not provide the proper sync signals themselves.

A high-quality 1/2-in. Betacam recorder/player for producing the master tape and a U-matic

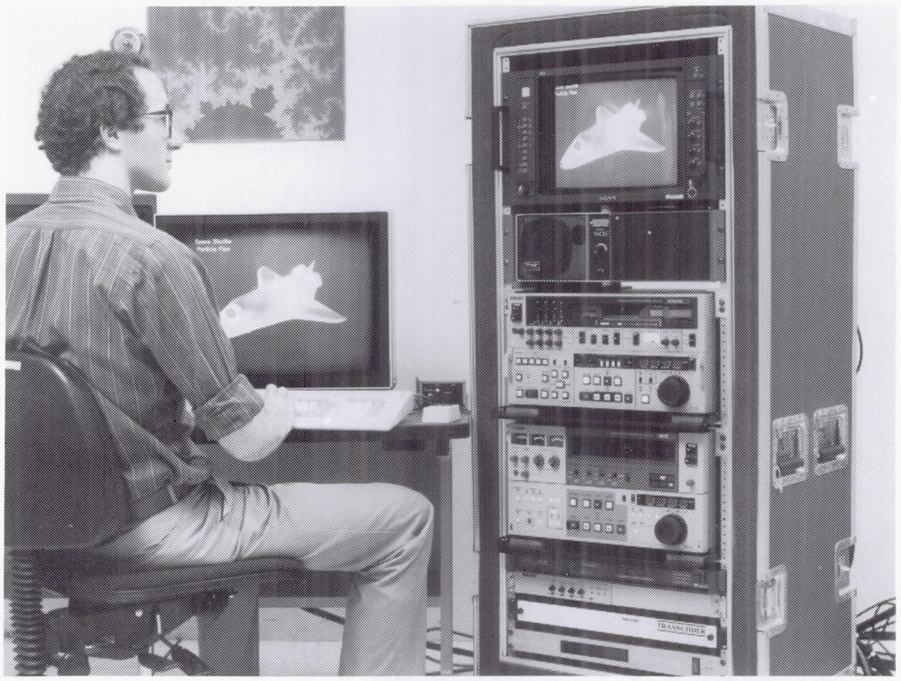

Video system in use at graphics workstation.

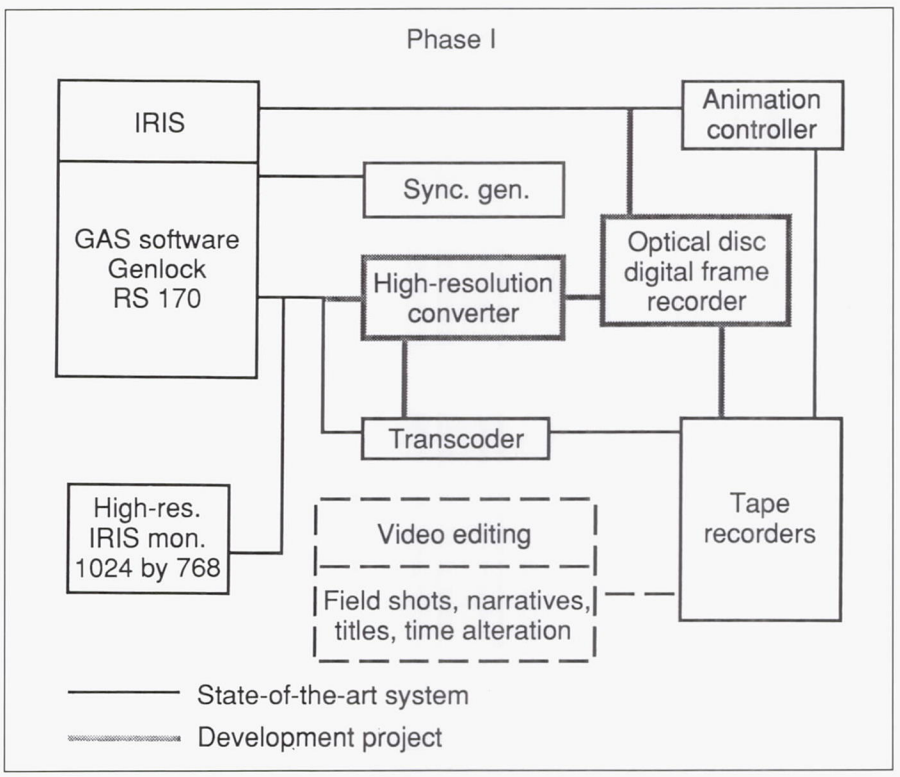

Schematic of video system attached to IRIS workstation.

SP 3/4-in. recorder for making distribution copies are available. A scan converter, configured for 1024- by 768-pixel screen resolution, has been added to the system. This device antialiases high-resolution graphics in real time to provide good-quality standard video resolution signals for the recorders with no time penalty. A videodisc player/recorder capable of holding up to 1 hour of video is being integrated into the system. This videodisc will eliminate some tape handling and provide more flexible user access to recorded video frames. These components form an integrated system designed to work as a unit. The system has been configured to operate successfully with Silicon Graphics IRIS 3030 and 4-D workstations, a Lexidata Solidview raster workstation, and an Evans and Sutherland PS 300 color graphics system.

The Betacam recorder is capable of simple manual editing of original rough videos. For professional editing, the videotapes obtained with this system may be processed through the Langley Research Center Research Information and Applications Division Video Section.

This system has been used to produce videotapes of hypersonic inlet flows, boundary-layer transition, grid generation, and pressure distributions on flexible bodies. Groups in the Aeronautics, Structures, Electronics, and Space Directorates have found videotaping useful to convey the results of their computer simulations to a wide audience in the research community.

Video Recording System

The open-shop Graphics Laboratory supports computer-generated video tape recordings that simulate dynamic physical processes or time-dependent experimental data. The equipment, which consists of several high-resolution tape recorders, an optical disc recorder, and hardware, interfaces with a variety of

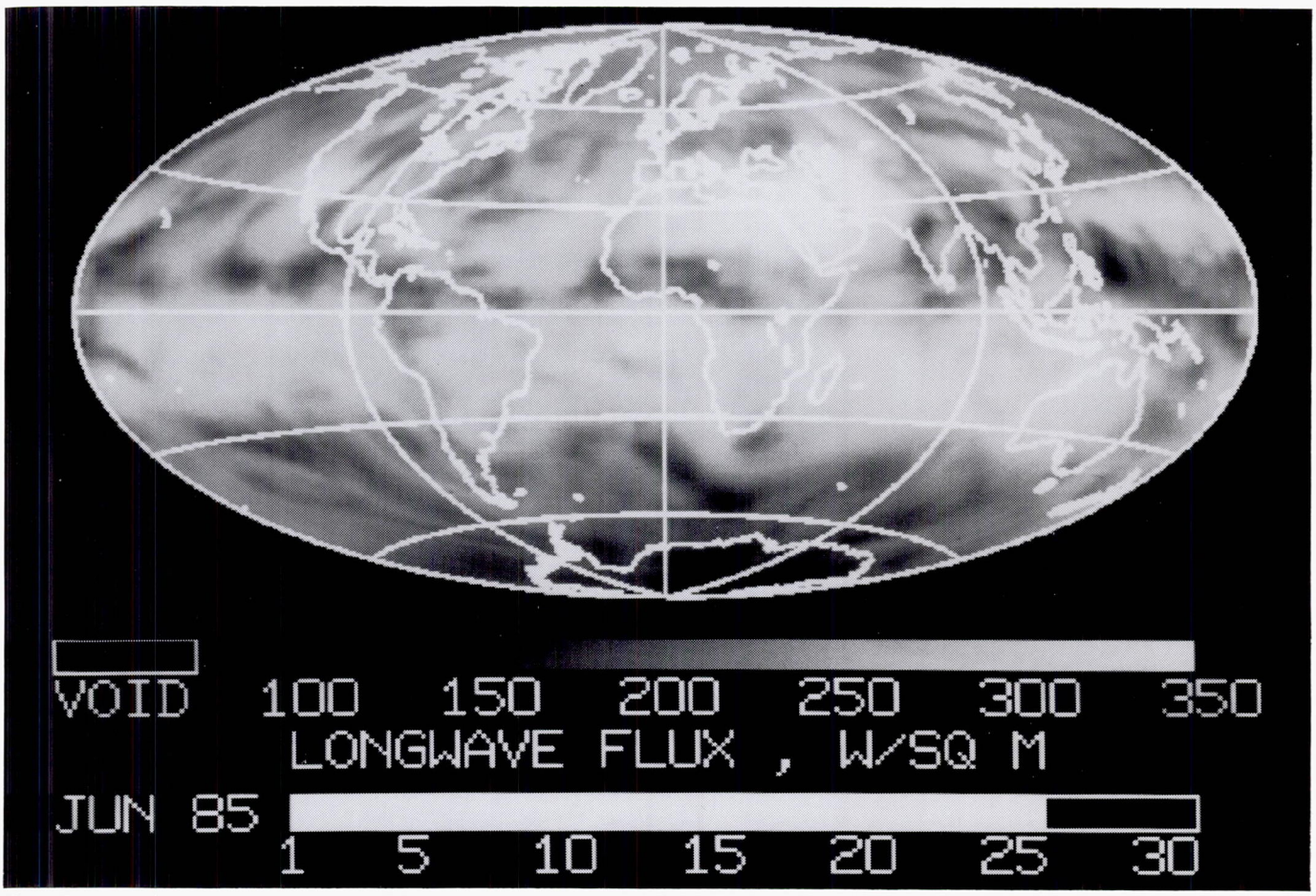

One frame of computer-generated image representing global heat radiation detected by ERBE.

color workstations and enables software control of the recorders. Recordings may be made in the Graphics Laboratory or at a researcher's graphics workstation.

In the Graphics Laboratory, recordings may be made using the IRIS workstation running the Graphics Animation System (GAS), MOVIE.BYU, or customized software. The UltraNet frame buffer and high-speed network connection to the Cray-2 also support video recordings. A sequence of precomputed images in the Langley Research Center raster metafile (RM) format may be used to generate an animation on the UltraNet frame buffer. Software is available to generate images in UltraNet format directly from a computed data base. The video hardware has been interfaced to a Tektronix 4115, IRIS 4D and 3030 models, an Evans and Sutherland PS 390, a Sun 3/280 with TAAC-1 application accelerator board, and a Macintosh with a card to drive a high-resolution RGB monitor.

Recordings have been made by Langley researchers in the Structures, Electronics, Space, and Aeronautics directorates. The subjects of these recordings have ranged from time-dependent flow fields, computer simulation (shown widely on TV network news) of the Space Shuttle recovery of the Long-Duration Exposure Facility (LDEF), actual temperature distribution on Space Shuttle orbiter surfaces, grid generation for computational fluid dynamics, and oil-flow development on aerodynamic surfaces. Other subjects included buckling behavior of shells and stiffened flat panels, global heating and cooling, spacecraft mission planning, and changes in helicopter disk loading with forward speed. Video is the medium of choice to show the evolving dynamics of complex, three-dimensional events for which several still photos or sketches are totally inadequate.

As an example of the use of this equipment, video recordings are being used to examine data from the Earth Radiation Budget Experiment (ERBE). One frame from such a color video is shown in the figure. The raw data for the animation were first retrieved from archived magnetic tapes containing the original satellite readings. Using software on the Convex computers, this information was fitted and interpolated onto two-dimensional images depicting the surface of the Earth. A Langley standard RM file containing a legend and a time scale then was rendered for each set of ERBE data. Using software on the IRIS workstation, these images were recorded onto videodisc and subsequently placed onto U-matic and VHS videotapes. These tapes provide an unprecedented insight into the dynamic ERBE data and can be distributed to researchers around the world.
(Kurt Severance, 46715)

Color Film Recording System

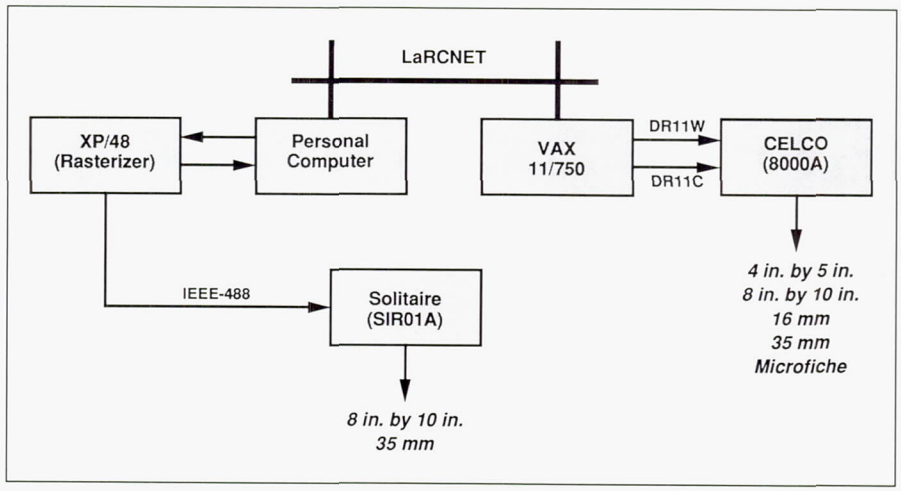

The Color Film Recording System (CFRS) in the Central Computing Complex provides the researcher with film output of computer-generated graphics using state-of-the-art high-resolution image recording devices. The film output aids the researcher in the investigation, interpretation, and presentation of complex data results. Support is provided over a wide range of disciplines, including wind tunnel flow field experiments, computational fluid dynamics, atmospheric sciences, remote sensing, and information sciences. The CFRS is comprised of two film recorders (a Celco 8000A and a Solitaire SIR01A), a Superset XP/48 hardware rasterizer, a VAX 11/750, and a personal computer.

Because of the design of the optical systems, the film transports, and the camera control electronics, a variety of formats can be imaged on the film recorders. The Celco 8000A can produce 16-mm movies, 35-mm slides, 8-in. by 10-in. viewgraphs, microfiche, and 70-mm and 4-in. by 5-in. negatives for photoprocessing. Software for controlling the operation of the Celco 8000A resides on the VAX 11/750. Command codes and data are sent via the DR11-W and DR11-C interfaces. The Solitaire SIR01A film recorder can produce 35-mm slides and 8-in. by 10-in. viewgraphs. Command codes and data are sent to the recorder via the IEEE-488 interace on the rasterizer. Each film recorder is capable of producing images up to 8 K line resolution.

Image data sent to the film recorders must be in raster format. Data in nonraster format are preprocessed on the XP/48 rasterizer. The rasterizer is a high-speed device capable of rasterizing a complex image of at least 40,000 vectors at 7500 line resolution in less than 60 s. Data from the rasterizer can be in a variety of formats,

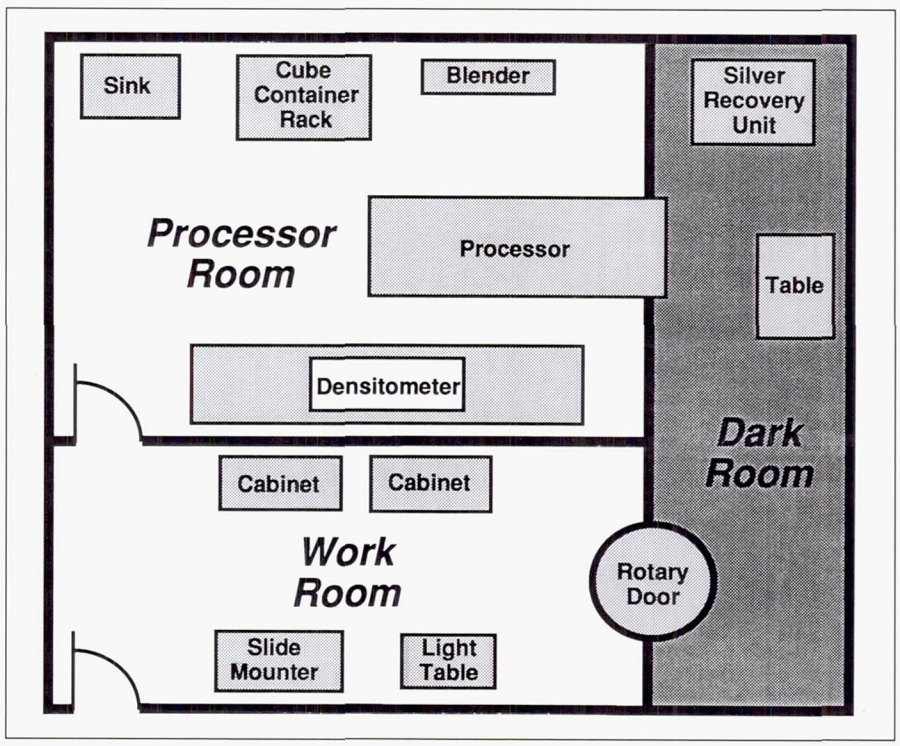

E-6 Film Processing System.

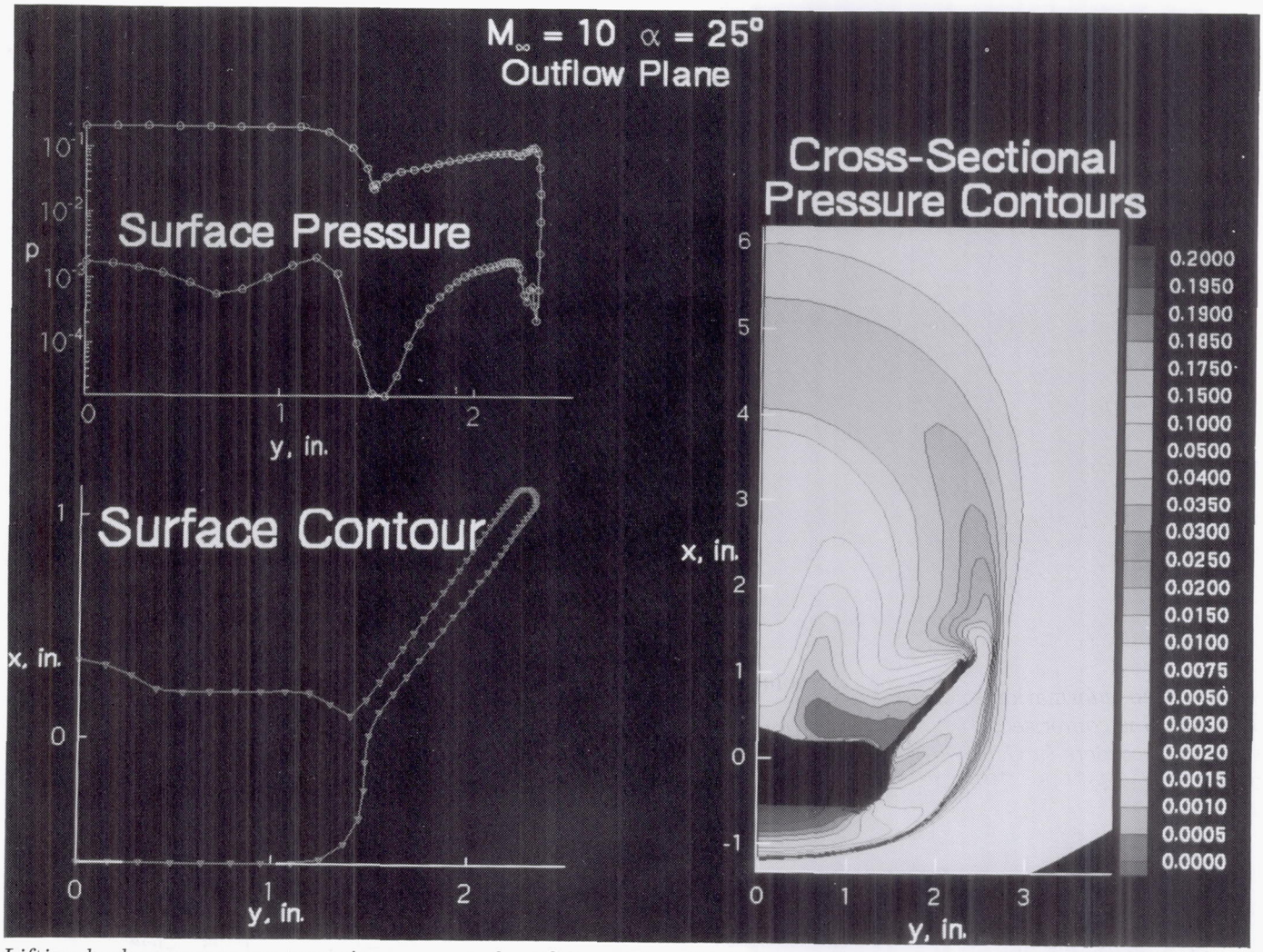

Lifting body pressure contours image created on Silicon Graphics IRIS workstation using AMTEC Engineering Incorporated TECPLOT software.

including Celco, Solitaire, and Targa formats. The Targa output format allows preview capability. The personal computer in the CFRS has hardware and software for controlling the Superset XP/48 rasterizer. Both the personal computer and the VAX are nodes on LaRCNET. This provides easy access to the CFRS from all mainframes in the complex and other systems using XNS or TCP/IP communications protocol. The CFRS supports the output formats from a variety of graphics programs including DI-3000, DI-3000 XPM, CGM interpreter, NCAR, RASLIB, PV-WAVE, and the Langley Research Center defined raster metafile (RM) format.

The most recent addition to the CFRS is the Automatic E-6 Film Processing System. This system is comprised of a Hope processor and an Automatic Chemical Management System. The Hope processor is a leaderless, random access, roller transport processor capable of processing roll film from 16 mm wide to 11 in. wide up to 400 ft and sheet film from 4 in. by 5. in to 11 in. by 14 in. The Automatic Chemical Management System is designed such that chemicals can be mixed and supplied to the processor from cube containers of concentrates. This system has been used to produce movies, slides, viewgraphs, and negatives to support research and presentation of graphics by persons in all directorates. The graphics output has been used locally, at national and international conferences, and in many scientific journals.

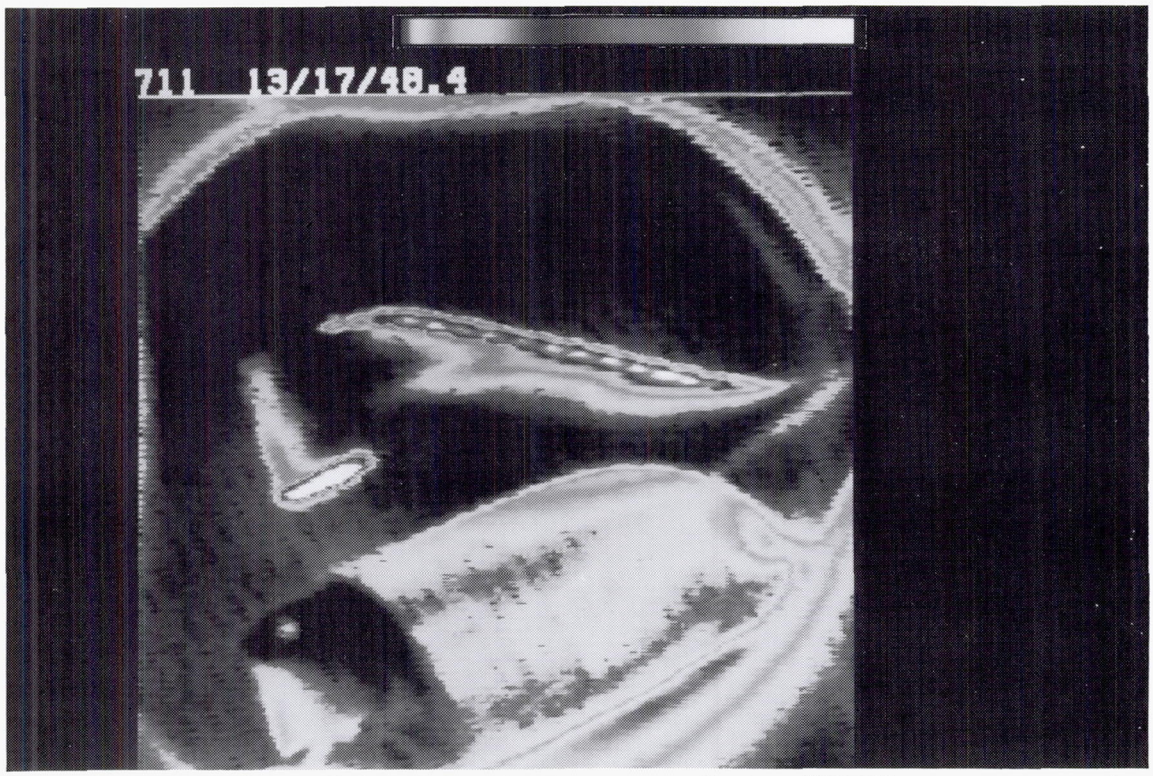

Image frame from Shuttle Infrared Leeside Temperature Sensing (SILTS) experiment on mission STS-28. Recorded analog data were converted to digital form. Logarithmic algorithms were used to convert data to color using programs on the CYBER computer.

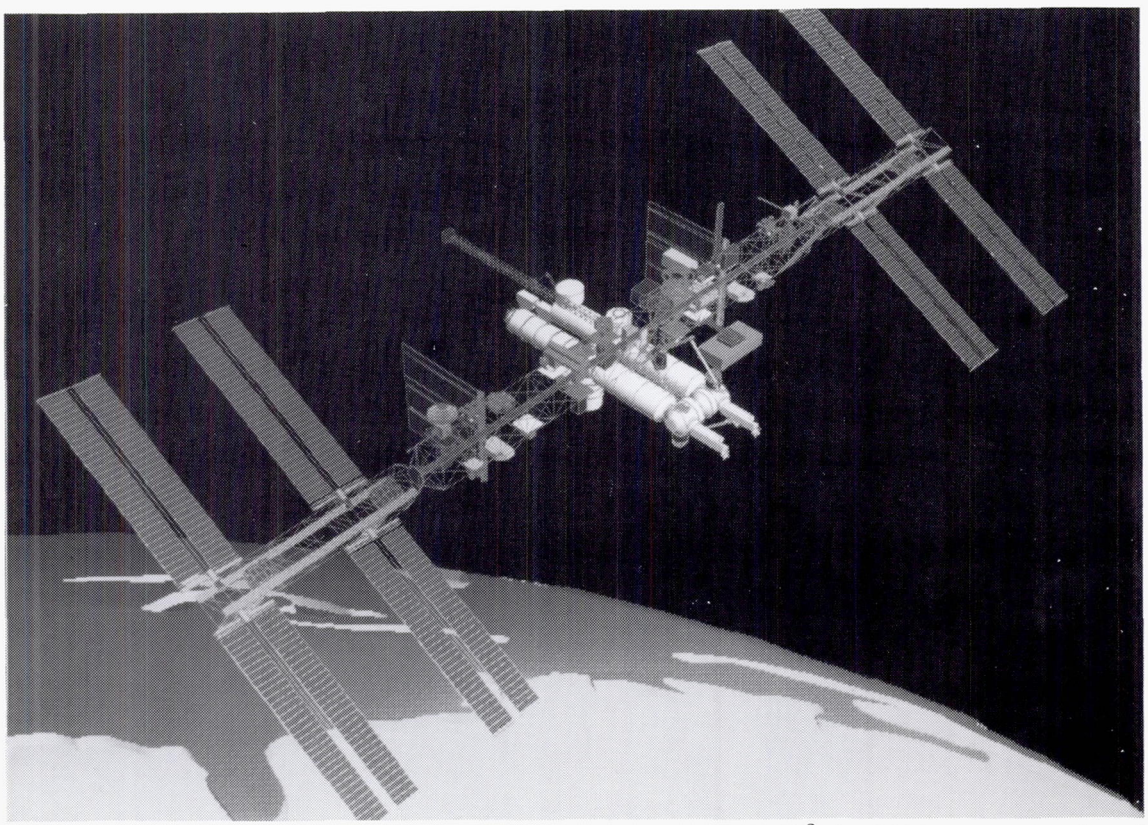

Space Station Freedom image created on VAX 6230 using IDEAS^2 (a CAE system developed jointly by NASA and Structural Dynamics Research Corporation).

13-Inch Magnetic Suspension and Balance System

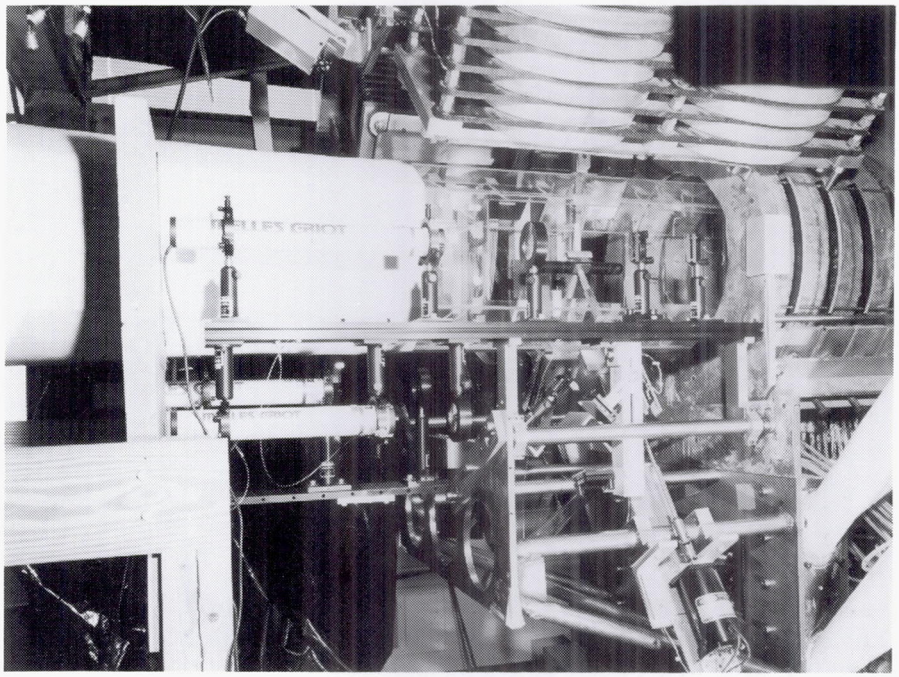

The Langley 13-Inch Magnetic Suspension and Balance System (MSBS) is a laboratory established to develop technology required for wind tunnel testing that is free of model-support interference. In 1984, the laboratory began operation as a combination of a magnetic suspension and balance system.

For this system, four electromagnets (arranged in a "V" configuration) above the wind tunnel test section provide the lift force, pitching moment, side force, and yawing moment. A drag electromagnet opposes the drag force. Motion is controlled in these five degrees of freedom with no provision for generation of controlled magnetic roll torque on the model. The 13-Inch MSBS has a lift force capability of approximately 6 lb depending on the size and shape of the iron core in the model. The test section passes through the drag electromagnet.

The tunnel is a continuous-flow, closed-throat, open-circuit design. Ambient air enters the tunnel from the outside through a large bellmouth intake protected from outside contaminants by a screen enclosure. At the end of the tunnel, the flow exhausts to the outdoors. The tunnel is capable of speeds up to Mach 0.5. The transparent test section measures approximately 12.6 in. high and 10.7 in. wide.

The tunnel has not been in operation during 1989, but it is scheduled to resume research studies in mid-1990.

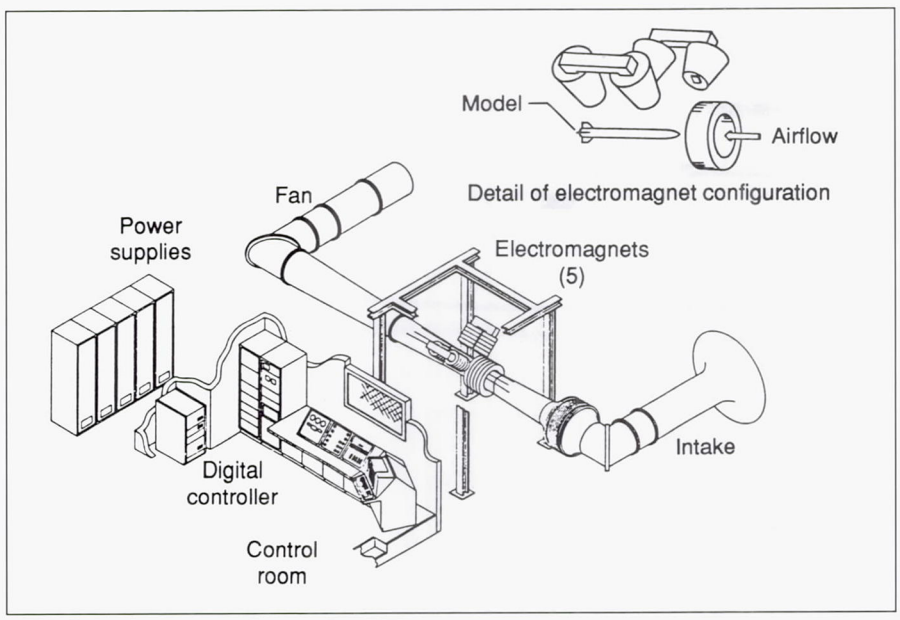

MSBS laboratory schematic.

Supersonic Low-Disturbance Pilot Tunnel

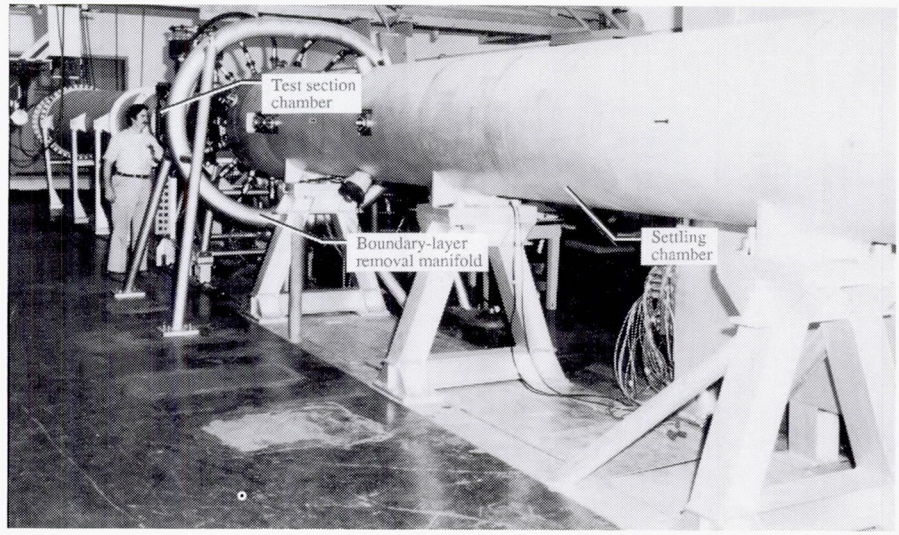

The Supersonic Low-Disturbance Pilot Tunnel (formerly called the Langley Mach 3.5 Low-Disturbance Pilot Tunnel) has been in operation since 1981. The tunnel, which is located in the Gas Dynamics Laboratory, uses high-pressure air from a 4200-psi tank field that is dehydrated to a dew point temperature of –52° F, reduced in pressure by control valves located upstream of the settling chamber, and filtered to remove all particles larger than 1 μm in size.

The predicted locations of transition from laminar-to-turbulent flow in the boundary layers of high-speed, high-altitude flight vehicles are critical design considerations because both friction drag and aerodynamic heating may be greatly affected by uncertainties in these predictions. Unfortunately, transition phenomena are extremely sensitive to noise, which is a known contaminant in conventional high-speed wind tunnels. For Mach numbers >2.5, the predominant sources of this wind tunnel noise are acoustic disturbances radiated into the free stream from the supersonic turbulent boundary layers on the tunnel walls. Other sources of noise in blow-down wind tunnels are pressure-reducing control valves that regulate the settling chamber pressure. The tunnel is a part of an ongoing Langley Research Center program to develop and test methods for eliminating or reducing severe noise problems.

The main figure above shows the settling chamber (visible on the right-hand side) and the open-jet test section chamber (visible on the left-hand side). The tunnel flow exhausts to a vacuum sphere complex that provides up to approximately 1-hr run times for stagnation pressures from 25 psia to 100 psia. At higher pressures, the flow is exhausted to the atmosphere. The settling chamber contains seven antiturbulence screens along with a number of dense porous plates that function as acoustic baffles to attenuate the high-level noise from the control valves and the piping system. These porous plates reduce the incoming noise from approximately 0.2 percent of stagnation pressure to approximately 0.01 percent. The antiturbulence screens reduce the normalized rms velocity fluctuations to approximately 1 percent.

With the input disturbances reduced to these low levels, research has shown that the most successful technique to eliminate the radiated noise is to laminarize the nozzle wall boundary layers by using boundary-layer removal slots just upstream of the nozzle throat and properly tailored expansion nozzles with highly polished walls. The large circular manifold shown in the figure is connected to a vacuum sphere and is used to remove the nozzle inlet boundary layer through a series of 1-in.-diameter pipes. By the use of these techniques, all disturbances have been practically eliminated in three different nozzles for Mach numbers of 3 and 3.5.

Supersonic Free-Shear Layer Transition

Free-shear layer transition at supersonic speeds is critical to scramjet combustor design and performance due to its strong influence on the fuel/air mixing process. The influence

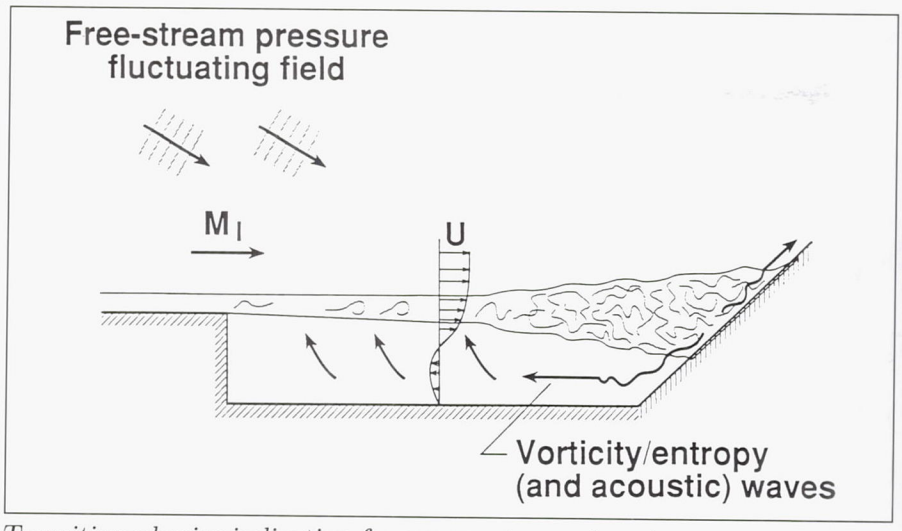

Transition physics indication from present experiment.

of free-stream disturbances on the location of transition in free-shear layers is not well known and the Supersonic Low-Disturbance Pilot Tunnel provides a unique test facility capable of varying the level of incident noise on a free-shear layer generated by an aft-facing, step-wedge combination, as shown in the figure. The adjacent surface downstream of the step simulates a geometry common in combustor design, and the downstream wedge is used to balance the pressure across the shear layer.

Measurements of the transition process were made at Mach 3.5 using both hot wires in the flow field and hot-film gauges on the cavity floor. The hot-wire data revealed that the incident free-stream noise had little or no influence on the location of transition in the free-shear layer. The hot-film gauges indicated that the transition process was dominated by slow-moving, upstream-feeding disturbances through the subsonic cavity region. The most amplified disturbances leading to transition of the shear layer were much lower than those predicted from linear stability theory.

These results reveal that the free-shear layer transition process for cavity-type flows with turbulent reattachment downstream is dominated by upstream feeding disturbances, as illustrated by the figure. This process is an example of transition bypass and is not predicted by linear stability theory.

(R. A. King, 45727)

Advances in Quiet Nozzle Development

Laminar nozzle-wall boundary layers are required for low-disturbance wind tunnels to avoid the adverse effects of radiated noise on supersonic transition studies. The size of the quiet test core in the nozzle is a direct function of the length of laminar flow on the nozzle walls. New nozzle designs are required to maximize the length of the quiet test core for tests with large models.

Current laminar-flow nozzles use upstream boundary-layer bleed to remove the oncoming turbulent boundary layer and a rapid downstream expansion that produces a strong favorable pressure gradient to maintain laminar flow. Such nozzles are strongly inflected and generate Görtler vortices along the concave portion of the nozzle walls. These vortices eventually lead to transition of the laminar boundary layer. A new concept based on linear stability theory has been

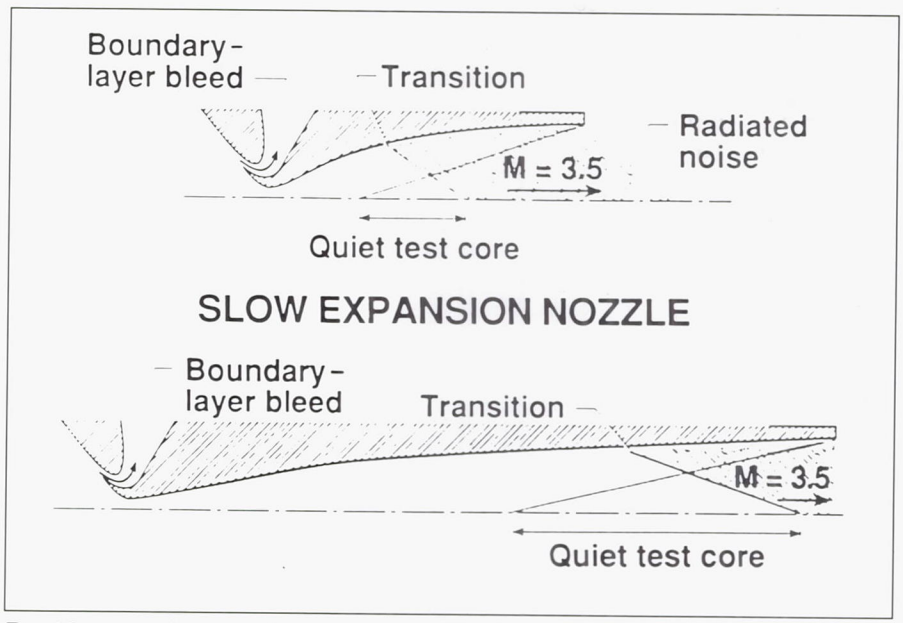

Rapid expansion nozzle.

used to design slower expansion nozzles (less inflected) that reduce the growth of the Görtler vortices, but still retain some of the favorable pressure gradient effect that minimizes the growth of other disturbances. This new design technique has been verified by recent tests of a Mach 3.5 nozzle fabricated using this method. The figure shows that the quiet test core for the new design is three times larger than that obtained with the rapid expansion design.

These results provide full confirmation of the theory and provide confidence in the technique for new nozzle designs. Significantly larger, more complex models can now be tested under quiet conditions, thus allowing more detailed studies of the factors affecting boundary-layer transition. **(S. P. Wilkinson, 45733)**

Pyrotechnic Test Facility

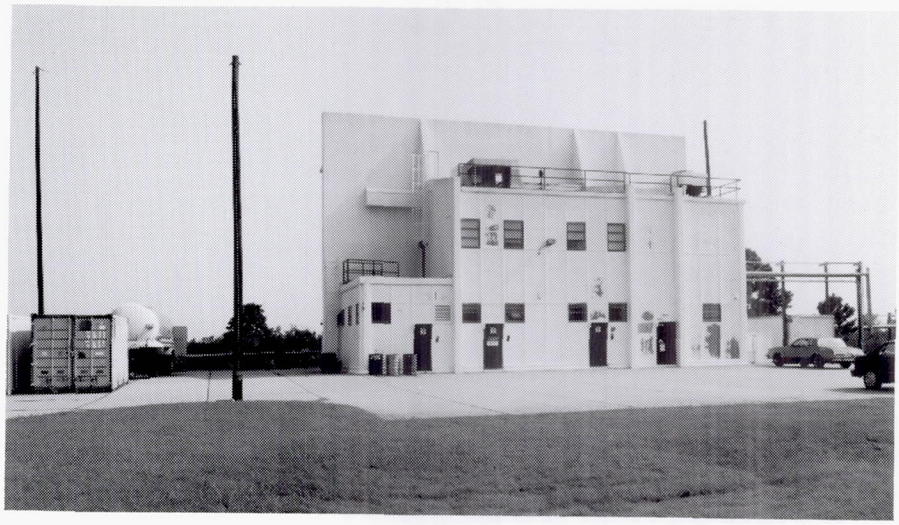

The Pyrotechnic Test Facility (Building 1159) contains the Langley Research Center space simulation environmental and functional test equipment used for the handling and testing of small-scale potentially hazardous materials. This facility includes three test cells and a general-purpose work area.

The environmental test equipment includes a 2000 lbf vibration machine, a thermal-vacuum chamber, which is 35 in. in diameter and 48 in. long and is capable of pressures to 1×10^{-7} torr at temperatures of −320°F to +200°F, and a mechanical shock apparatus, which is capable of producing up to a 30,000 g pulse for 0.2 ms. This facility also includes thermal chambers with a capability of −320°F to +600°F, a centrifuge with a capability of 200 g's, a 25,000-V electrostatic discharge apparatus, and a high-pressure pump with a capability of 40,000 lb/in^2. The functional test capabilities are programmable electrical firing circuits, measurements of acceleration, force, pressure, and temperature, and a variety of explosive performance monitoring systems. A high-frequency (40-kHz) analog recording/playback system is used for dynamic measurements.

The general-purpose open work area has a 30-ft by 60-ft floor space with a vertical working height of 35 ft. Two explosion-proof pneumatic gantry cranes are available to handle the heavier loads. The three reinforced concrete test cells are designed with lightweight external walls to relieve overpressures in an outboard manner. These test cells serve three separate functions. Environmental testing is performed in cell one, and temporary storage of potentially hazardous materials and test article assembly and checkout are performed in cell two. Cell three is used for explosives functional testing because this cell contains an exhaust fan, which is used for the purge of smoke or other caustic products, and a mobile steel containment box, which is used for testing and may produce explosive fragments.

Pyrotechnic Component Testing

Langley Research Center has unique facilities for testing pyrotechnic (explosive, propellant-actuated) systems to determine functional performance and environmental stability and to accomplish research. Because pyrotechnics contain potentially hazardous materials, these facilities are designed to contain the total reaction under any test condition. During 1989, three major programs were conducted in these facilities. These programs include the Halogen Occultation Experiment (HALOE) pin puller failure investigation, Scout spin rocket motor service life extension, and ignitability test method development.

Personnel in the HALOE program, which utilizes two NASA Standard Initiator (NSI)-powered pin pullers to release telescope gimbals, became aware of two functional failures of similar pin pullers on the Magellan program. The Langley failure investigation quantified all functional aspects of the design, including the energy required to function the pin puller compared to the energy delivered by the NASA Standard Initiator. Several weaknesses were discovered in the basic design of the pin puller, as well as the NSI.

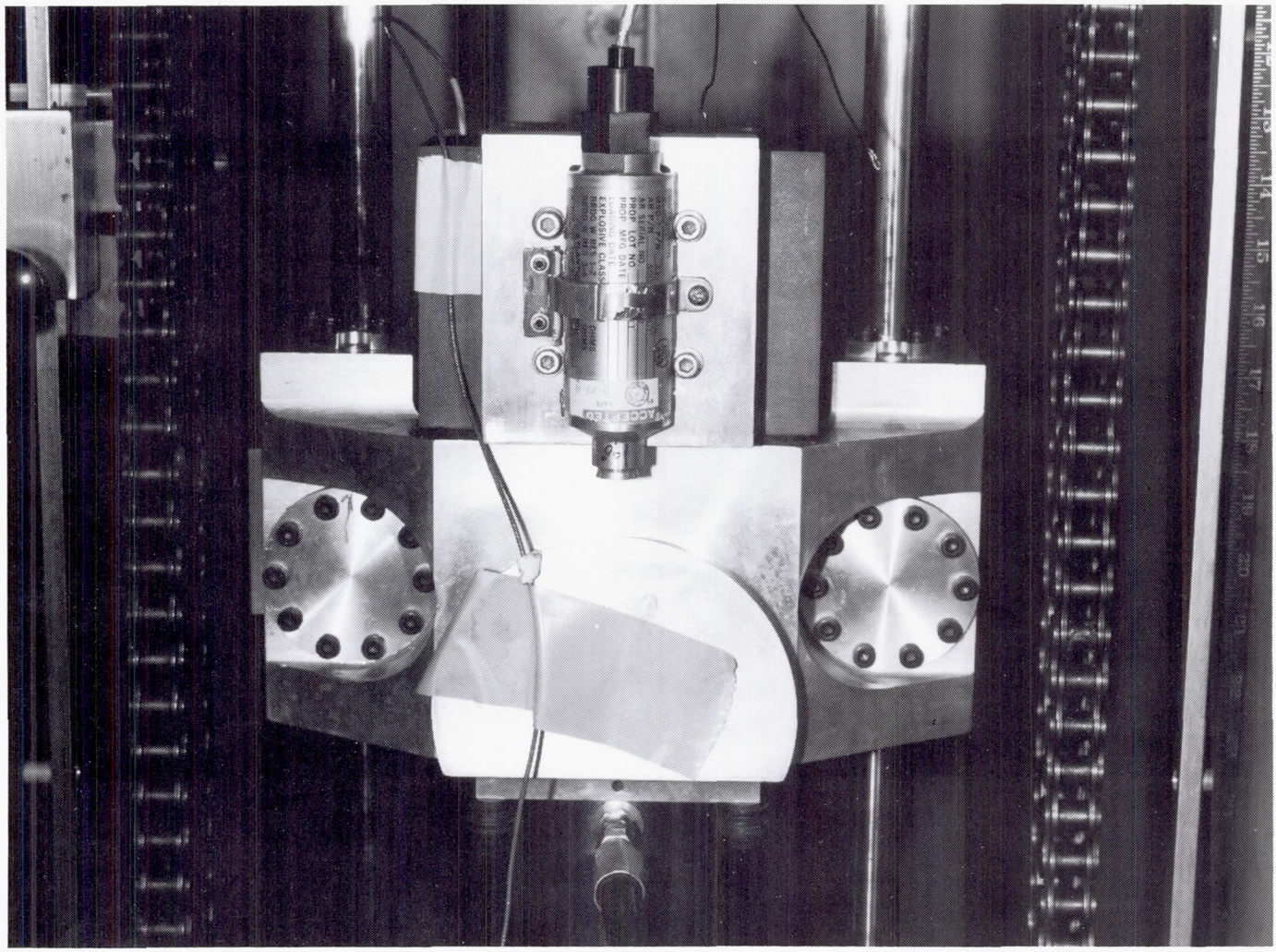

Scout spin motor mounted on mechanical shock test machine. L-90-00731

The Scout Project Office sponsored a program to extend the service of a 40-lb thrust solid rocket motor from 14.5 to 20 years. Three motors with ages of 18.3 years each were subjected to environmental tests that duplicated their original qualification and test fired to provide the necessary justification. The environments were electrical inspection, mechanical shock, vibration, and constant acceleration.

The U.S. Air Force is sponsoring a service life extension program at Langley on the B-1B aircraft escape system pyrotechnic components. To quantify the effects of service, functional test methods are needed to compare the performance of all components before and after service. Unfortunately, no test method existed to measure the output of percussion primers, the critical system initiation component. A unique test method was developed in which the output of the primer was directed into a bed of ignition material, while monitoring how this material ignited and burned.

(Laurence J. Bement, 47084)

NASA
National Aeronautics and Space Administration

Report Documentation Page

1. Report No.	2. Government Accession No.	3. Recipient's Catalog No.
NASA TM-102631		

4. Title and Subtitle	5. Report Date
Langley Aerospace Test Highlights—1989	May 1990
	6. Performing Organization Code
7. Author(s)	8. Performing Organization Report No.
9. Performing Organization Name and Address NASA Langley Research Center Hampton, VA 23665-5225	10. Work Unit No.
	11. Contract or Grant No.
12. Sponsoring Agency Name and Address National Aeronautics and Space Administration Washington, DC 20546-0001	13. Type of Report and Period Covered Technical Memorandum
	14. Sponsoring Agency Code

15. Supplementary Notes

16. Abstract

The role of the NASA Langley Research Center is to perform basic and applied research necessary for the advancement of aeronautics and spaceflight, to generate new and advanced concepts for the accomplishment of related national goals, and to provide research advice, technological support, and assistance to other NASA installations, other government agencies, and industry. This report highlights some of the significant tests that were performed during calendar year 1989 in the NASA Langley Research Center test facilities, a number of which are unique in the world. The report illustrates both the broad range of the research and technology activities at the NASA Langley Research Center and the contributions of this work toward maintaining United States leadership in aeronautics and space research. Other highlights of Langley research and technology for 1989 are described in *Research and Technology 1989—Langley Research Center.* Further information concerning both reports is available from the Office of the Chief Scientist, Mail Stop 105-A, NASA Langley Research Center, Hampton, Virginia 23665 (804-864-6062).

17. Key Words (Suggested by Authors(s))	18. Distribution Statement
Research Technology Wind tunnels Simulators Laboratories Facilities Aeronautics	Unclassified—Unlimited Subject Category 99

19. Security Classif. (of this report)	20. Security Classif. (of this page)	21. No. of Pages	22. Price
Unclassified	Unclassified	173	A08

For sale by the National Technical Information Service, Springfield, Virginia 22161-2171